Dissertation
submitted to the
Combined Faculties for the Natural Sciences and for Mathematics
of the Ruperto-Carola University of Heidelberg, Germany
for the degree of
Doctor of Natural Sciences

presented by

MSc. Octavian Postavaru
born in Tulcea, Romania

Oral examination: 8$^{\text{th}}$ December 2010

To Dan, Raica and Silviu Postavaru.
This thesis is for you.

STRONG-FIELD RELATIVISTIC PROCESSES IN HIGHLY CHARGED IONS

Referees: **Prof. Dr. Christoph H. Keitel**
Prof. Dr. Sandra P. Klevansky

ZUSAMMENFASSUNG

In der vorliegenden Arbeit untersuchen wir durch starke Felder hervorgerufene relativistische Prozesse in hochgeladenen Ionen. Im ersten Teil der Arbeit studieren wir die Resonanzfluoreszenz von Laser-getriebenen Ionen im relativistischen Bereich, indem wir die zeitabhängige Master-Gleichung in einem Mehrniveaumodell lösen. Unser ab initio Ansatz, basierend auf der Dirac-Gleichung, ermöglicht es hochrelativistische Ionen zu untersuchen und liefert folglich eine präzise Methode, um korrelierte relativistische Dynamik, Phänomene der Quantenelektrodynamik gebundener Zustände und Kerneffekte durch die Anwendung von kohärentem Röntgenlicht zu überprüfen. Atomare Dipol- oder Multipolmomente können bis zu nie da gewesener Genauigkeit bestimmt werden, indem das durch Interferenz verschmälerte Fluoreszenzspektrum gemessen wird. Desweiteren untersuchen wir die Niveaustruktur von schweren Wasserstoff-ähnlichen Ionen in Laserfeldern. Die Wechselwirkung mit dem Lichtfeld führt zu dynamischen Verschiebungen der elektrischen Energieniveaus, was relevant ist für Spektroskopieexperimente. Die elektrischen Zustände werden vollständig relativistisch behandelt durch die Dirac-Gleichung. Unser Formalismus geht über die Dipolapproximation hinaus und berücksichtigt Nicht-Dipoleffekte wie Retardierung und die Wechselwirkung mit den Magnetfeldkomponenten des Laserfeldes. Wir konnten Wirkungsquerschnitte für die zwischen-Schalen trielektrische Rekombination (TR) und den quadruelektrischen Rekombinationsprozess vorhersagen, welche experimentell mit Hilfe von Elektronenstrahl-Ionenfallen bestätigt wurden, hauptsächlich für C-artige Ionen von Ar, Fe und Kr. Für Kr^{30+} wurden Zwischen-Schalen TR-Beiträge von nahezu 6% zur gesamten resonanten Photorekombinationsrate gefunden.

ABSTRACT

In this thesis we investigate strong-field relativistic processes in highly charged ions. In the first part, we study resonance fluorescence of laser-driven highly charged ions in the relativistic regime by solving the time-dependent master equation in a multi-level model. Our ab initio approach based on the Dirac equation allows for investigating highly relativistic ions, and, consequently, provides a sensitive means to test correlated relativistic dynamics, bound-state quantum electrodynamic phenomena and nuclear effects by applying coherent light with x-ray frequencies. Atomic dipole or multipole moments may be determined to unprecedented accuracy by measuring the interference-narrowed fluorescence spectrum. Furthermore, we investigate the level structure of heavy hydrogenlike ions in laser beams. Interaction with the light field leads to dynamic shifts of the electronic energy levels, which is relevant for spectroscopic experiments. We apply a fully relativistic description of the electronic states by means of the Dirac equation. Our formalism goes beyond the dipole approximation and takes into account non-dipole effects of retardation and interaction with the magnetic field components of the laser beam. We predicted cross sections for the inter-shell trielectronic recombination (TR) and quadruelectronic recombination processes which have been experimentally confirmed in electron beam ion trap measurements, mainly for C-like ions, of Ar, Fe and Kr. For Kr^{30+}, inter-shell TR contributions of nearly 6% to the total resonant photorecombination rate were found.

In connection with the work performed during the thesis, the following paper was published or accepted in refereed journals:

- C. Beilmann, O. Postavaru, L. H. Arntzen, R. Ginzel, C. H. Keitel, V. Mäckel, P. H. Mokler, M. C. Simon, H. Tawara, I. I. Tupitsyn, J. Ullrich, J. R. Crespo López-Urrutia, and Z. Harman, *Intershell trielectronic recombination with K-shell excitation in* Kr^{30+}, Phys. Rev. A 80, 050702(R) (2009)
- C. Beilmann, P. H. Mokler, S. Bernitt, Z. Harman, C. H. Keitel, O. Postavaru, J. Ullrich, and J. R. Crespo López-Urrutia, *Resonant high-order electronic recombination in medium-Z highly charged ions*, J. Phys: Conf. Ser., accepted (2010)

The following paper is submitted:

- O. Postavaru, Z. Harman, C. H. Keitel , *High-precision metrology of highly charged ions via relativistic resonance fluorescence*

Results from work on the thesis currently in preparation:

- O. Postavaru, Z. Harman, C. H. Keitel , *Relativistic light-shifts in hydrogen-like ions*
- O. Postavaru, Z. Harman, C. H. Keitel , *Relativistic theory of resonance fluorescence in three-level systems*

DECLARATION

The work in this thesis is based on research carried out at the Max Planck Institute for Nuclear Physics (MPIK) in Heidelberg, Germany, within the Theory Division of Prof. Dr. Christoph H. Keitel, *Theoretical Quantum Dynamics in Intense Laser Fields*. No part of this thesis has been submitted elsewhere for any other degree or qualification and it is all my own work unless referenced to the contrary in the text.

Contents

List of Figures

–I–

INTRODUCTION

In the present thesis, we theoretically investigate strong-field dynamical processes in highly charged ions. Highly charged ions (HCI) are atomic ions in very high charge states due to the loss of many or most of their bound electrons by energetic collisions or high-energy photon absorption. An example of a highly charged ion is e.g. carbonlike (C-like) krypton (see Fig. 1.1), which was also studied in this work and in our experimental collaboration (see Chapter 4). Research with these exotic ions is motivated by several areas of science. The strong Coulomb field of the nucleus allows tests of quantum electrodynamics in the strongest electromagnetic fields accessible. Due to the large overlap of the electronic probability density with the nuclear matter, nuclear effects on the electronic shell can also be effectively investigated in such species, and nuclear properties can be inferred through experiments with ions in high charge states. Furthermore, such ions are found in astrophysical objects such as stellar coronae, in active galactic nuclei, in supernova remnants, and in accretion disks. Most of the visible matter found in the universe consists of highly charged ions. High-temperature Tokamak plasmas used for nuclear fusion energy research also contain ions in high charges generated by the plasma-wall interaction. In the laboratory, highly charged ions are investigated by means of heavy ion particle accelerators or storage rings, and by the use of electron beam ion traps (EBITs).

Quantum electrodynamics (QED) is the best confirmed field theory in physics. QED has an enormous success in predicting the electron properties in weak fields. Approximately 50 years ago, Lamb and Rutherford observed for the first time a shift, the Lamb shift, in the atomic structure scheme of the hydrogen atom. Since than, more and more precise Lamb-shift measurements have been performed determining QED effects in light atomic systems to high accuracies. Now, a precise test in the strong-field limit where novel phenomena might show up, is still pending. The atomic structure of an ion is primarily determined by the strength of the nuclear Coulomb field which increases with the atomic number Z. Thus, a primary goal of research with HCI is to explore the behavior of electrons in the strongest electromagnetic fields accessible to experimental investigation. Precision measurements of electron binding energies are best suited to deduce characteristic QED phenomena in intense fields. Therefore, the comparison of predicted with experimentally determined level energies of strongly bound electrons provides a critical test of QED in strong fields. This also requires an extention of QED as known from, e.g., particle physics: the strong Coulomb nuclear field of HCI can not be treated perturbatively, since its magnitude, characterized by the dimensionless product of the nuclear charge number and the fine structure constant, i.e., $Z\alpha$, is comparable to unity. Therefore, one needs to turn to a non-perturbative treatment and apply the exact wave functions and propagators corresponding to the strong central nuclear field. Also, the appearance of poles in the Green's functions due to bound states and the presence of the negative Dirac continuum introduces further issues that need to be accounted for in a rigorous theoretical

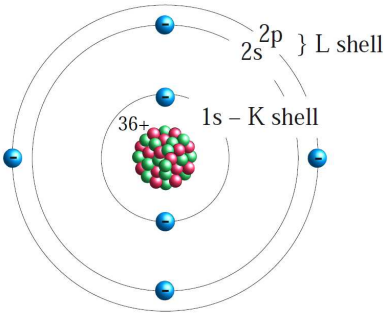

Figure 1.1: An example of a highly charged atomic ion: carbon-like krypton. Its charge number is Z=36, just like that of the neutral krypton atom, and its shell consists of six electrons just like in the case of the carbon atom. The ions net charge is therefore $q = +30e$, with e being the elementary charge, and the ion is denoted as Kr^{30+}.

treatment of such systems.

Uranium is the heaviest element in which QED effects can be studied in the laboratory: the transuranium elements are radioactive and usually short lived, forbidding a conclusive experimental study of the electron shell. For the case of hydrogen-like uranium, where the ground-state binding energy amounts to 132 keV, a measurement of the $1s$ Lamb shift (465.8 eV) with an accuracy of 1 eV and below still remains one of the most important tests of QED in strong fields. In addition, the development and understanding of bound-state QED in strong fields can be improved significantly for many-body systems by measuring, e.g., the $2s_{1/2} - 2p_{1/2}$ splitting in lithium-like uranium. Heavy lithium-like ions are particularly well suites because the electron-electron interaction contributions can be calculated reliably and the relatively low atomic excitation energies are strongly influenced by QED effects.

HCI are naturally rare on earth, but they are very common in the universe, because stars and other massive bodies are in most cases at extreme temperatures. This motivates to investigate HCI from an astrophysical point of view. Those elements of the periodic table heavier than hydrogen are born under nuclear fusion conditions at extreme temperatures. Supernova explosions are believed to be the main mechanism for the production of elements heavier as iron (Fe, Z=26). As new nuclei are formed, they are bare, and may remain so for extended periods of time. Their radiation emission is strongly affected by the ionic charge state. As their environment cools down, ions gradually recombine by capturing free electrons, eventually becoming neutral atoms. But other energetic processes, as those occurring in active galactic nuclei, stellar cores and coronae, accretion disks and shocks can cause again ionization up to very high stages. Since heavy atoms tend to emit more radiation than light atoms, and highly charged ions even more so, the radiation from these exotic ions is very strong and therefore may even be observed on the Earth or in space laboratories. As an example, the most intense line in the solar corona is produced by 13-fold ionized iron, Fe^{13+}. The radiation produced by HCI at different energy ranges of the electromagnetic spectrum can be used to diagnose and thus to better understand such astrophysical processes.

Research with HCI is also motivated by its interest for controlled nuclear fusion, which may be the dominant source of energy used by mankind in the future. In Tokamak plasmas, atoms from the wall of the chamber are constantly ionized to high charge states. Also, gases such as argon and krypton are artifically injected into the plasma: through energetic collisions within the electron beam, they lose most of their shell electrons, and become highly charged. During this process, and through photorecombination, x rays are emitted, which works to cool the plasma. This gives one an additional degree of freedom to control

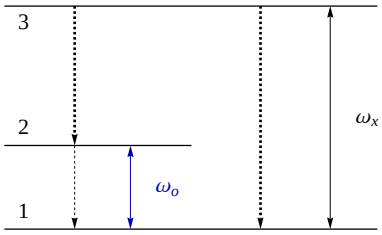

Figure 1.2: Level scheme of an atomic three-level system driven by two different laser fields. In the relativistic ionic systems studied in our work, the transition between the uppermost level 3 and the ground state 1 has energies in the keV range and is driven by an x-ray laser (frequency ω_x). Level 1 and 2 are hyperfine-split ground state sublevels with transition energies in the eV range, and are connected by an optical laser (frequency ω_o). The thick arrows represent fast (electric dipole) spontaneous decay channels and the thin arrows represent slow (magnetic dipole) decay transitions.

the thermodynamics of the hot plasma. Furthermore, the emission lines originating from HCI provide an important plasma diagnostic tool. In the case when HCI are embedded in a plasma environment, the balance between collisional excitation and ionization on the one hand and radiative and collisional de-excitation and recombination on the other hand strongly depends on the composition, density and temperature of the host plasma. Such a situation can only very approximately be described by plasma models and is nowadays treated by involved numerical simulations, for which respective precise atomic data from theoretical calculations or experiments is a prerequisite.

The discovery of the parity non-conservation (PNC) in the beta decay of ^{60}Co by Wu and co-workers about forty years ago marked an important landmark in the history of physics. This phenomenon which suggests the lack of left-right mirror symmetry has now been observed in several physical systems. An important case in this field is parity non-conservation in atomic systems. Indeed, parity non-conservation has now been observed in several heavy atoms. The latest measurement on cesium has yielded a result of unprecedented accuracy (0.35%) and has lead to the discovery of the nuclear anapole moment. It appears that the atomic parity non-conservation can serve as an important probe of physics beyond the standard model of particle physics if the present accuracy of the atomic theory is improved, or the uncertainties associated with it can be removed by comparing very accurate parity non-conservation measurements on several isotopes of the same element. A further increase in sensitivity to PNC phenomena are expected from theoretical and experimental studies involving highly charged ions: the inner-shell electrons mostly influenced by PNC effects can be most effectively addressed in heavy few-electron systems. Experiments with highly charged uranium ions to explore this field are currently planned at FAIR to be constructed as an extension of the GSI facility at Darmstadt, Germany.

After this general overview about the relevance of HCI in physics, in the following we give a more detailed summary of the topics discussed in this thesis:

In Chapter 2, we develop a fully relativistic theory of resonance fluorescence. The phenomenon of resonance fluorescence provides an interesting manifestation of the quantum theory of light. In this process, a multi-level atomic system is driven by a resonant continuous-wave laser field and the spectral and quantum statistical properties of the fluorescent light emitted by the atom are measured. If the driving field is monochromatic, at low excitation intensity the atom or ion absorbs and reemits it at the same frequency as a consequence of conservation of energy. The situation, however, is considerably more complicated when the excitation intensity increases and the Rabi frequency associated with the driving field becomes comparable to, or larger than, the atomic linewidth. At such intensity levels, the Rabi

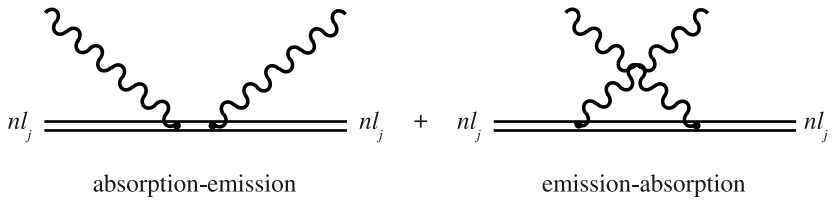

Figure 1.3: Diagrams illustrating the second-order light shift effect with bound relativistic electrons. The double lines represent Furry-picture electronic wave functions and propagators, i.e. solutions of the Dirac equation with the Coulomb nuclear potential. The wavy lines represent emitted or absorbed real photons from the laser field.

oscillations show up as a modulation of the quantum transition moment and sidebands start emerging in the spectrum of emitted radiation (dynamic Stark splitting).

In the case of atomic systems with higher nuclear charges or in the case of certain transitions, the usual non-relativistic treatment is not valid. Not only do the electronic wave functions differ significantly from the Schrödinger wave functions, but also the interaction with the light field is modified. Therefore, we formulate an ab initio description that is inherently relativistic, i.e. it is based on the Dirac equation. Such a formalism is especially needed in the case of inner-shell transitions of highly charged ions. These transitions can nowadays or in the near future be driven by x-ray lasers or coherent x-ray light created by high harmonic generation schemes, therefore, the understanding of the relativistic resonance fluorescence spectrum is mandatory.

The theoretical description of resonance fluorescence is not only interesting on its own but it also lays the foundation of laser spectroscopic methods. High-precision optical laser spectroscopy is a versatile tool to investigate correlated relativistic quantum dynamics, the testing of fundamental theories like quantum electrodynamics (QED) [BCTT05, GSB$^+$05] or parity non-conservation in atomic systems, as summarized previously. In the regime of heavy few-electron systems, however, the accuracy of optical spectroscopy can seldom be exploited due to the scarcity of low-frequency transitions. With the advent of modern short-wavelength laser systems, the accuracy and versatility of laser spectroscopy may be combined with the increased sensitivity to relativistic and QED effects and nuclear properties at higher nuclear charges and for inner-shell transitions. Brilliant x-ray light has recently enabled to study transitions in the x-ray regime. Coherent light with photon energies over 10 keV becomes experimentally accessible in the near future [XFE, LCL], allowing for an extension to heavier systems and the exploitation of coherence properties.

We study resonance fluorescence of laser-driven highly charged ions in the relativistic regime by solving the time-dependent master equation in a multi-level model. Our ab initio approach may provide a sensitive spectroscopic tool by applying coherent light with x-ray frequencies. In the scheme we put forward, atomic dipole or multipole moments may be determined to unprecedented accuracy by measuring the interference-narrowed fluorescence spectrum. To this end, we develop a theoretical formalism for relativistic resonance fluorescence of a three-level atomic configuration driven by two fields, namely, a short-wavelength laser and a long-wavelength light source in the optical regime. This scheme is illustrated in Fig. 1.2. In such a three-level setting, the linewidth of the spontaneous transition of interest may be rendered much narrower than the natural linewidth, with the simultaneous increase of the total emitted intensity by orders of magnitude. Due to this effect, the determination of atomic multipole moments by means of the detection of the fluorescence spectrum is anticipated to largely increase in accuracy.

Furthermore, we investigate in Chapter 3 the level structure of heavy hydrogenlike ions in laser beams

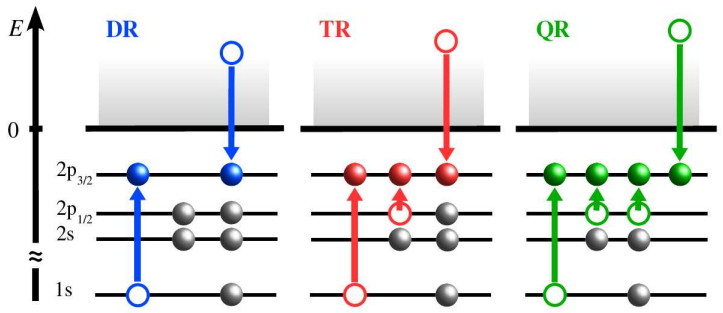

Figure 1.4: Scheme of resonant electron recombination processes in a six-electron ion: In DR (blue diagram) one bound electron is excited by the captured electron, in TR (red diagram) two and in QR (green diagram) three electrons are promoted by the captured electron.

with off-resonant frequencies. In heavy ions, the electrons are tightly bound by the Coulomb potential of the nucleus, which prohibits ionization even by strong lasers. However, interaction with the light field leads to dynamic shifts of the electronic energy levels. The dominant diagrams are illustrated in Fig. 1.3. Here we again apply a relativistic description of the electronic states by means of the Dirac equation. Theoretical investigation so far apply non-relativistic approaches and are restricted to electric dipole transitions. Our relativistic generalization allows one to extend the field of investigations to stronger laser fields, higher frequencies – e.g., x-ray lasers [ECB$^+$07] –, and to the highest nuclear charges. Interaction with the monofrequent laser field is treated by time-dependent perturbation theory. Our formalism goes beyond the Stark long-wavelength dipole approximation and takes into account non-dipole effects of retardation and interaction with the magnetic field components of the laser beam. The resulting level shifts are relevant for experiments at present and near-future laser facilities.

In Chapter 4, we develop a relativistic theoretical formalism and summarize the computational scheme used for the description of resonant many-body recombination processes. Such processes provide a viable alternative to laser spectroscopy: the ions are excited by beams of electrons rather than photons, which allows the experimental study of transitions with keV energies even without the use of large-scale x-ray sources such as synchrotrons or free electron lasers. The most fundamental resonant recombination process is dielectronic recombination (DR). In this two-step process, a free electron is captured into a bound state of the ion with the simultaneous excitation of a second, bound electron. This inverse Auger process is followed by a radiative de-excitation of the so-formed state, completing the photorecombination process. This process is illustrated in the first panel of Fig. 1.4. DR often represents the dominant pathway for populating excited states in plasmas and, consequently, for inducing easily observable x-ray emission lines which are used as diagnostic tools for fusion plasmas (whereby Kr as well as Ar were chosen as ideal candidates) [CCH$^+$90, WBD$^+$95], triggering a range of DR studies with highly charged Kr ions [BHB$^+$93, FBR98, RBF$^+$00]. From a more fundamental point of view, the selectivity of DR [BKM$^+$03] allows testing stringently sophisticated atomic structure and dynamics calculations, in particular of relativistic and QED effects in strong electromagnetic fields.

Beyond the well-known DR, resonant recombination processes involving higher-order correlations are relevant, too. Here, as displayed in Fig. 1.4, two or even three bound electrons can be simultaneously excited by the resonantly captured electron in trielectronic or even quadruelectronic recombination (TR and QR, respectively). It is important to mention that in general TR and QR offer new photorecombination channels and their contribution to the radiative cooling of Tokamak and astrophysical plasmas needs to be considered in the theoretical modeling. We calculated TR and QR resonance energies and cross

sections in the framework of the multiconfiguration Dirac-Fock (MCDF) method, which can be regarded as a relativistic generalization of the Hartree-Fock scheme and will be also briefly described in Chapter 4.

We investigate trielectronic recombination with simultaneous excitation of a K-shell and a L-shell electron, hence involving three active electrons. Our theoretical prediction triggered experimental activities at the electron beam ion trap facility of the Max Planck Institute for Nuclear Physics. The TR process was identified in the x-ray emission spectrum of recombining highly charged Kr, Fe and Ar ions trapped in the EBIT. An energy resolution three times higher than any reported for this collision energy range around 10 keV resulted in the separation of the associated lines from the stronger dielectronic resonances. For Kr^{30+}, inter-shell TR contributions of nearly 6% to the total resonant photorecombination rate were found, and even higher contributions in the case of the lighter elements of Ar and Fe are deduced from both theoretical and experimental spectra.

In Chapter 5, conclusions and a brief outlook including proposals concerning possible future theoretical and experimental work are given. Some additional derivations and intermediate results are presented in the Appendix.

–II–

RELATIVISTIC THEORY OF RESONANCE FLUORESCENCE IN A TWO- AND THREE-LEVEL SYSTEM

2.1 Introduction

High-precision laser spectroscopy has resulted in crucial advancements in our understanding of nature. In particular, optical laser spectroscopy (OS) is a versatile tool to investigate correlated relativistic quantum dynamics, the testing of fundamental theories like quantum electrodynamics (QED) [BCTT05, GSB+05] or parity non-conservation in atomic systems. The determination of atomic dipole or multipole moments via lifetime measurements by means of, e.g., visible emission spectroscopy [LJC+05], approaching the accuracy of one per thousand, sheds light on QED effects like the electron anomalous magnetic moment. Isotope shifts (IS) in atomic spectra which has been providing valuable insight into the collective structure of nuclei: for example, recently, isotope shifts were determined two-photon Doppler-free spectroscopy and by collinear laser spectroscopy [SNE+06, GNA+08]. Beyond purely nuclear effects, the interaction of the correlated motion of electrons and that of the nucleus can be studied in IS measurements: recently, relativistic effects on nuclear recoil [Sha98] have been measured in visible forbidden transitions of the few-electron argon ions by a trapped-ion method [SHC+06].

In the regime of heavy few-electron systems, however, the accuracy of optical spectroscopy can seldom be exploited due to the scarcity of low-frequency transitions. Therefore, one has to apply other techniques. Measuring the $2s \leftrightarrow 2p$ x-ray emission lines of highly charged uranium ions confined in an electron beam ion trap allowed testing strong-field QED on the two-loop level [BCTT05] and delivered a new value for the radius of the radioactive isotope ^{235}U [EBC96]. Recently, a method based on the storage ring measurement of dielectronic recombination spectra has yielded the change of the mean square charge radius for Nd isotopes [BKH+08, cHSG04].

With the advent of modern short-wavelength laser systems, the accuracy and versatility of laser spectroscopy may be combined with the increased sensitivity to relativistic and QED effects and nuclear properties at higher nuclear charges and for inner-shell transitions. Brilliant x-ray light has recently enabled to study transitions in the soft x-ray regime in the intermediate range of nuclear charges [ECB+07]. Coherent light with photon energies over 10 keV becomes experimentally accessible in the near future [XFE], allowing for an extension to heavier systems and the exploitation of coherence properties. This would also ask for the validity of numerous quantum control schemes of resonance fluorescence [NSO+90, ZS96b, ZS96a, PK98, SZ98, Kei99] for concrete systems in the relativistic regime.

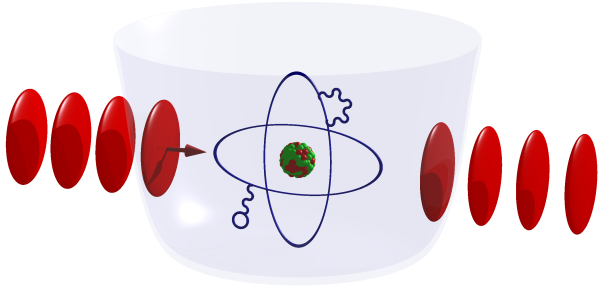

Figure 2.1: Schematic setup of a resonance fluorescence experiment with trapped highly charged ions: the ions are trapped in the electromagnetic potential of an EBIT, Paul trap or Penning trap, and a laser beam is directed through the ion cloud. Emitted photons (not shown) are registered with a detector or spectrometer.

In the present work, we investigate the possibility of measuring atomic transition dipole – or multipole – moments and transition energies via relativistic resonance fluorescence of a three-level atomic configuration driven by two fields, namely, a short-wavelength laser and a long-wavelength light source in the optical regime. In such a three-level setting, the linewidth of the spontaneous transition of interest may be rendered much narrower than the natural linewidth, with the simultaneous increase of the total emitted intensity by orders of magnitude. Due to this effect, the determination of atomic multipole moments by means of the detection of the fluorescence spectrum is anticipated to increase in accuracy by several orders of magnitude.

As relativistic effects on the bound electronic wave function increase rapidly with the nuclear charge number Z, one needs to formulate a fully relativistic theory of coherent laser-atom interaction based on the Dirac equation [Dir28]. Not only do the electronic wave functions differ significantly from the Schrödinger wave functions, but also the interaction with the laser light is modified. For example, magnetic dipole transitions, which are non-relativistically forbidden even in the visible range, can only be explained by a relativistic theory. An approach via the time-dependent numerical solution of the Dirac equation was recently employed to describe ionization phenomena [HK09]. For our purposes, one needs to go beyond this approach and incorporate radiative relaxation in bound-bound transitions. These transitions can nowadays or in the near future be driven by x-ray or soft x-ray lasers, therefore, the understanding of the relativistic resonance fluorescence spectrum is indispensable.

2.2 The spectrum of resonance fluorescence in two-level approximation

The phenomenon of resonance fluorescence provides an interesting manifestation of the quantum theory of light. In this process, a two- or many-level atomic system is driven by a resonant continuous-wave laser field and the spectral and quantum statistical properties of the fluorescent light emitted by the atom are measured. Experimentally this can be achieved by scattering a laser off a collimated beam or a trapped ensemble of atoms.

If the driving field is monochromatic, at low excitation intensity the atom or ion absorbs and reemits it

at the same frequency as a consequence of conservation of energy. The spectral width of the fluorescent light is given by the natural decay width of the upper state. The situation, however, is considerably more complicated when the excitation intensity increases and the Rabi frequency associated with the driving field becomes comparable to, or larger than, the transition linewidth. At such intensity levels, the Rabi oscillations show up as a modulation of the quantum dipole – or multipole – moment and sidebands start emerging in the spectrum of emitted radiation. This so-called dynamic Stark splitting is an interesting feature of the atom-light field interaction.

2.2.1 Description of the model and equations of motion

In this section, we are interested in the evolution of a two-level system driven by an incident field of arbitrary strength whose carrier frequency ω is resonant or nearly resonant with the atomic transition. The aim is to calculate the complete power spectrum of the radiation spontaneously emitted by the atomic system ('atom'). The atom is assumed to be isolated and fixed in position.

Consider the interaction of a single-mode radiation field of frequency ω with a two-level atom. Let $|a\rangle$ and $|b\rangle$ represent the upper and lower levels of the atom, i.e., they are eigenstates of the unperturbed part of the Hamiltonian $\mathscr{H}_0$ with the eigenvalues $\hbar\omega_a$ and $\hbar\omega_b$, respectively. The wave function of a two-level system can be written in the form

$$|\Psi(t)\rangle = C_a(t)|a\rangle + C_b(t)|b\rangle\,, \tag{2.1}$$

where C_a and C_b are the probability amplitudes of finding the atom in states $|a\rangle$ and $|b\rangle$, respectively. The corresponding Hamiltonian is $\mathscr{H} = \mathscr{H}_0 + \mathscr{H}_1$, where $\mathscr{H}_0$ and $\mathscr{H}_1$ represent the unperturbed and the interaction parts, respectively. By using the closure property $|a\rangle\langle a| + |b\rangle\langle b| = 1$, we can write $\mathscr{H}_0$ as

$$\begin{aligned} \mathscr{H}_0 &= (|a\rangle\langle a| + |b\rangle\langle b|)\mathscr{H}_0(|a\rangle\langle a| + |b\rangle\langle b|) \\ &= \hbar\omega_a|a\rangle\langle a| + \hbar\omega_b|b\rangle\langle b|\,, \end{aligned} \tag{2.2}$$

where we use $\mathscr{H}_0|a\rangle = \hbar\omega_a|a\rangle$ and $\mathscr{H}_0|b\rangle = \hbar\omega_b|b\rangle$. Similarly, the part of the Hamiltonian $\mathscr{H}_1$ that represents the interaction of the atom with the radiation field can be written as

$$\begin{aligned} \mathscr{H}_1 &= -exE(t) \\ &= -e(|a\rangle\langle a| + |b\rangle\langle b|)x(|a\rangle\langle a| + |b\rangle\langle b|)E(t) \\ &= -(\gamma_{ab}|a\rangle\langle b|e^{-i\omega t} + \gamma_{ba}|b\rangle\langle a|e^{-i\omega t})\mathscr{E}\,, \end{aligned} \tag{2.3}$$

where $\gamma_{ab} = e\langle a|x|b\rangle$ is the matrix element of the transition and $E(t) = \mathscr{E}(e^{-i\omega t} + e^{i\omega t})$ is the field at the location of the atom. We kept just the conservative terms, all other being neglected in the rotating wave approximation. Here, we assume that the electric field is linearly polarized along the x-axis. Thus, the Hamiltonian of two-level system interacting with one classical field is given by

$$\mathscr{H} = \sum_{i=1}^{2} \varepsilon_i|i\rangle\langle i| + \Omega_R(e^{-i\omega t}|2\rangle\langle 1| + e^{i\omega t}|1\rangle\langle 2|)\,, \tag{2.4}$$

where ε_i (i=1,2) are the energies of the two stationary states of the atom, and Ω_R is the Rabi frequency of the driving field.

There exists a state vector $|\Psi\rangle$ which contains all possible information about the given physical system. If we want to extract a piece of the system's information, we have to calculate the quantum mechanical (QM) expectation value of the corresponding operator O,

$$\langle O\rangle_{\mathrm{QM}} = \langle\Psi|O|\Psi\rangle\,. \tag{2.5}$$

In many situations we may not know $|\Psi\rangle$; we may only know the probability P_Ψ that the system is in the state $|\Psi\rangle$. For such a situation, we not only need to take the quantum mechanical average but also the ensemble average over many identical systems that have been similarly prepared. Instead of Eq. (2.5), we now have

$$\langle\langle O\rangle_{\rm QM}\rangle_{\rm ensemble} = {\rm Tr}(O\rho)\,, \tag{2.6}$$

where the density operator ρ is defined by

$$\rho = \sum_\Psi P_\Psi |\Psi\rangle\langle\Psi|\,. \tag{2.7}$$

It can be seen that ${\rm Tr}(O\rho) = {\rm Tr}(\rho O)$. In the particular case where all P_Ψ are zero except the one for a state $|\Psi_0\rangle$, then $\rho = |\Psi_0\rangle\langle\Psi_0|$, and the state is called a pure state. It follows from the conservation of probability that ${\rm Tr}(\rho) = 1$. Also, for a pure state, ${\rm Tr}(\rho^2) = 1$.

We can obtain the equation of motion for the density matrix from the Schrödinger equation,

$$|\dot\Psi\rangle = -\frac{i}{\hbar}\mathscr{H}|\Psi\rangle\,. \tag{2.8}$$

Taking the time derivative of ρ (Eq. (2.7)) we have

$$\dot\rho = \sum_\Psi P_\Psi(|\dot\Psi\rangle\langle\Psi| + |\Psi\rangle\langle\dot\Psi|)\,, \tag{2.9}$$

where P_Ψ is time independent. Using Eq. (2.8) to replace $|\dot\Psi\rangle$ and $\langle\dot\Psi|$ in Eq.(2.9) we get

$$\dot\rho = -\frac{i}{\hbar}[\mathscr{H},\rho]\,. \tag{2.10}$$

Equation Eq. (2.10) is often called the reversible part of the Liouville or von Neumann equation of motion for the density matrix. It is more general than the Schrödinger equation since it uses the density operator instead of a specific state vector and can therefore give statistical as well as quantum mechanical information.

Consider first the reversible part of the Liouville equation in the interaction representation:

$$\dot\rho' = -\frac{i}{\hbar}[\mathscr{H}_1',\rho']\,, \tag{2.11}$$

where

$$\mathscr{H}_1' = \hbar\Omega_R(|2\rangle\langle 1|e^{i\Delta t} + |1\rangle\langle 2|e^{-i\Delta t})\,, \tag{2.12}$$

and $\Delta = \omega_{21} - \omega$. The prime denotes the interaction representation and ω_{21} is the atomic transition frequency. The matrix elements of ρ' according to Eq. (2.12) satisfy linear coupled equations of motion containing explicit time-dependent factors of the complex exponential type. These can be removed with the transformation

$$R_{ii} = \rho_{ii}\,(i = 1, 2), \quad R_{12} = \rho_{12}e^{i\Delta t}\,, \tag{2.13}$$

whose effect is to produce autonomous equations for matrix elements R_{ij}; we would like to stress that the absence of explicit time dependence in the equations of motion plays an important role for the implementation of the procedure. Next we consider the irreversible part of the atomic dynamics. This is described by the master equation for the arbitrary multilevel system [NSO$^+$90, MDLMNO91]

$$\dot\rho'_{irrev} \equiv \Lambda\rho' = \sum_{i,j}[|i\rangle\langle j|\rho'|j\rangle\langle i|(A_{jiij} + A^*_{jiij}) - |j\rangle\langle j|\rho' A_{jiij} - \rho'|j\rangle\langle j|A^*_{jiij}]\,, \tag{2.14}$$

where A_{jiij} are complex rate constants related to the decay rates Γ_{ij}, polarization decay rates μ_{ij}, and the frequency shifts $\Delta\Omega_{ij}$ given by

$$\begin{aligned} \Gamma_{ij} &= A_{jiij} + A^*_{jiij}\,, \\ \mu_{ij} &= \sum_k \Re(A_{ikki} + A^*_{jkkj}) = \frac{1}{2}\sum_k (\Gamma_{ik} + \Gamma_{jk})\,, \\ \Delta\Omega_{ij} &= -\sum_k \Im(A_{jkkj} + A^*_{ikki})\,. \end{aligned} \tag{2.15}$$

In the following we shall ignore both level shifts and pure phase relaxation effects due to elastic collisions (i.e., we assume $A_{iiii} = 0$). Note in addition that

$$\Re A_{ijji} = \Re A_{jiij} \exp\left(\frac{\hbar\omega_{ij}}{kT}\right)\,, \tag{2.16}$$

where ω_{ij} is the transition frequency between the levels i and j and T is the absolute temperature. From the above equation it follows that the rates of excitation from a lower to a higher level due to (incoherent) collisional effects can be safely ignored as long as the energy separation between the levels is much larger than kT. Because one may encounter situations where this condition is not fulfilled, for completeness we continue to include the rate coefficient Γ_{ij} with $i < j$. The full master equation is

$$\dot{\rho}' = -\frac{i}{\hbar}[\mathscr{H}_1', \rho'] + \Lambda\rho'\,. \tag{2.17}$$

In terms of the variable R_{ij}, Eq. (2.17) takes the explicit form

$$\begin{aligned} \frac{dR_{12}}{d\tau} &= (i\tilde{\Delta} - \tilde{\gamma}_{12})R_{12} + 2i\beta R_{22} - i\beta\,, \\ \frac{dR_{22}}{d\tau} &= -i\beta R_{12} + i\beta R_{21} - (1 + \tilde{\Gamma}_{12})R_{22} + 1\,, \end{aligned} \tag{2.18}$$

where

$$R_{11} = 1 - R_{22} \text{and} \quad R_{21} = R^*_{12}\,. \tag{2.19}$$

In arriving at Eqs. (2.18) we have introduced the dimensionless time $\tau = \Gamma_{21}t$ and the scaled Rabi frequency $\beta = \Omega_R/\Gamma_{21}$. The remaining rate constants are scaled to Γ_{21} and are labeled with a tilde. For the purpose of the following development it is convenient to represent the set of three linearly independent equations for the matrix R_{ij} in the compact form

$$\frac{d}{d\tau}\Psi = L\Psi + I\,, \tag{2.20}$$

where the three components of the vector Ψ are defined by

$$\Psi_1 = R_{12}\,, \quad \Psi_2 = R_{21}\,, \quad \Psi_3 = R_{22}\,, \tag{2.21}$$

and L is the (3×3) matrix

$$L = \begin{pmatrix} i\tilde{\Delta} - \tilde{\gamma}_{12} & 0 & 2i\beta \\ 0 & -i\tilde{\Delta} - \tilde{\gamma}_{21} & -2i\beta \\ -i\beta & i\beta & -(1 + \tilde{\Gamma}_{12}) \end{pmatrix}\,. \tag{2.22}$$

The vector I is an inhomogeneous term with components

$$I_1 = -i\beta\,, \quad I_2 = i\beta\,, \quad I_3 = 1\,. \tag{2.23}$$

Because our calculation of the quantities of interest involves the quantum regression theorem, we will need explicit expressions for the variables Ψ_i $(i = 1, 2, 3)$ in terms of their initial values. This is done conveniently in the Laplace space. Thus, if τ_0 denotes an arbitrary initial time, the Laplace transform of Eq. (2.20) yields

$$\hat{\Psi}(z) = M(z)\Psi(\tau_0) + \frac{1}{z}M(z)I\,, \tag{2.24}$$

or in component form

$$\hat{\Psi}_i(z) = \sum_j M_{ij}(z)\Psi_j(\tau_0) + \frac{1}{z}\sum_j M_{ij}(z)I_j\,, \tag{2.25}$$

where

$$M = (z - L)^{-1}\,. \tag{2.26}$$

For the steady state (Eq. (2.20)) we then have

$$\Psi(\infty) = -L^{-1}I\,, \tag{2.27}$$

or, explicitly, in component form

$$\Psi_i(\infty) = -\sum_j (L^{-1})_{ij}I_j\,. \tag{2.28}$$

2.2.2 Electric field operator for spontaneous emission from a single atom

We first discuss the interaction of the quantized radiation field with the two- or three-level atomic system described by a Hamiltonian in the dipole approximation. For a single-mode field it reduces to a particularly simple form. This Hamiltonian provides the simplest illustration of spontaneous emission and an explanation of effects of various kind.

The spontaneous decay of an atomic level is treated by considering the interaction of the atomic levels with the modes in the vacuum state. We examine the state of the field that is generated in the process of emission of a quantum of energy equal to the energy difference between the atomic levels. Such a state may be regarded as a single-photon state.

The interaction of the radiation field $\mathbf{E}$ with a single-electron atom can be described by the following Hamiltonian in the dipole approximation:

$$\mathscr{H} = \mathscr{H}_A + \mathscr{H}_F - e\mathbf{r}\mathbf{E}. \tag{2.29}$$

Here, $\mathscr{H}_A$ and $\mathscr{H}_F$ are the Hamiltonian operators of the atom and the radiation field, respectively, in the absence of interaction, and $\mathbf{r}$ is the position vector of the electron. For relativistic atomic systems, e.g. for a single-electron ion, the Hamiltonian is given by

$$\mathscr{H}_A = c\boldsymbol{\alpha}\boldsymbol{p} + \boldsymbol{\beta}m_0c^2 - \frac{Ze^2}{4\pi\epsilon_0 r}\,. \tag{2.30}$$

In the above equation, $\boldsymbol{\alpha}$ and $\boldsymbol{\beta}$ are the usual Dirac matrices and $\boldsymbol{p}$ is the three-momentum of the electron. We note here that the above treatment can be extended to many-electron atoms in a rather straightforward way.

The energy operator of the free field, $\mathscr{H}_F$, is given in terms of the creation and annihilation operator by

$$\mathscr{H}_F = \sum_{\mathrm{k}} \hbar\nu_{\mathrm{k}} \left(a_{\mathrm{k}}^\dagger a_{\mathrm{k}} + \frac{1}{2} \right) . \tag{2.31}$$

We can express $\mathscr{H}_A$ and $e\mathbf{r}$ in terms of the atomic transition operators

$$\sigma_{ij} = |i\rangle\langle j| . \tag{2.32}$$

The states $\{|i\rangle\}$ represent a complete set of atomic energy eigenstates, i.e. $\sum_i |i\rangle\langle i| = 1$. It then follows from the eigenvalue equation $\mathscr{H}_A|i\rangle = E_i|i\rangle$ that

$$\mathscr{H}_A = \sum_i E_i |i\rangle\langle i| = \sum_i E_i \sigma_{ii} . \tag{2.33}$$

In the dipole approximation, the field is assumed to be uniform over the whole atom. The dipole moment can be rewritten as

$$e\mathbf{r} = \sum_{i,j} e|i\rangle\langle i|\mathbf{r}|j\rangle\langle j| = \sum_{i,j} \gamma_{ij}\sigma_{ij} , \tag{2.34}$$

where $\gamma_{ij} = e\langle i|\mathbf{r}|j\rangle$ is the electric-dipole transition matrix element. The electric field operator is evaluated in the dipole approximation at the position of the point-like atom. For the atom at the origin, we have

$$\mathbf{E} = \sum_{\mathrm{k}} \hat{\epsilon}_{\mathrm{k}} \mathscr{E}_{\mathrm{k}} (a_{\mathrm{k}} + a_{\mathrm{k}}^\dagger) , \tag{2.35}$$

where $\mathscr{E}_{\mathrm{k}} = (\hbar\nu_{\mathrm{k}}/2\epsilon_0 V)^{1/2}$. Here, for simplicity, we have taken a linear polarization basis and the polarization vectors to be real.

It now follows by making some substitutions, that

$$\mathscr{H} = \sum_{\mathrm{k}} \hbar\nu_{\mathrm{k}} a_{\mathrm{k}}^\dagger a_{\mathrm{k}} + \sum_i E_i \sigma_{ii} + \hbar \sum_{i,j} \sum_{\mathrm{k}} g_{\mathrm{k}}^{ij} \sigma_{ij} (a_{\mathrm{k}} + a_{\mathrm{k}}^\dagger) , \tag{2.36}$$

where

$$g_{\mathbf{k}}^{ij} = -\frac{\gamma_{ij}\hat{\epsilon}_{\mathbf{k}}\mathscr{E}_{\mathbf{k}}}{\hbar} . \tag{2.37}$$

In Eq. (2.36), we have omitted the zero-point energy from the first term. For the sake of simplicity, we assume γ_{ij} to be real throughout.

We now proceed to the case of a two-level atomic system. For $\gamma_{ab} = \gamma_{ba}$ we write

$$g_{\mathrm{k}} = g_{\mathrm{k}}^{ab} = g_{\mathrm{k}}^{ba} . \tag{2.38}$$

The following form of the Hamiltonian is obtained:

$$\mathscr{H} = \sum_{\mathrm{k}} \hbar\nu_{\mathrm{k}} a_{\mathrm{k}}^\dagger a_{\mathrm{k}} + (E_a\sigma_{aa} + E_b\sigma_{bb}) + \hbar \sum_{\mathrm{k}} g_{\mathrm{k}} (\sigma_{ab} + \sigma_{ba})(a_{\mathrm{k}} + a_{\mathrm{k}}^\dagger) . \tag{2.39}$$

The second term in Eq. (2.39) can be rewritten as

$$E_a\sigma_{aa} + E_b\sigma_{bb} = \frac{1}{2}\hbar\omega(\sigma_{aa} - \sigma_{bb}) + \frac{1}{2}(E_a - E_b)\,, \tag{2.40}$$

where we use $(E_a - E_b) = \hbar\omega$ and $\sigma_{aa} + \sigma_{bb} = 1$. The constant energy term $(E_a + E_b)/2$ can be ignored. If we use the notation

$$\begin{aligned} \sigma_z &= \sigma_{aa} - \sigma_{bb} = |a\rangle\langle a| - |b\rangle\langle b|, \\ \sigma_+ &= \sigma_{ab} = |a\rangle\langle b|, \\ \sigma_- &= \sigma_{ba} = |b\rangle\langle a|\,, \end{aligned} \tag{2.41}$$

the Hamiltonian (2.39) takes the form

$$\mathscr{H} = \sum_{\mathrm{k}} \hbar\nu_{\mathrm{k}} a_{\mathrm{k}}^\dagger a_{\mathrm{k}} + \frac{1}{2}\hbar\omega\sigma_z + \hbar\sum_{\mathrm{k}} g_{\mathrm{k}}(\sigma_+ + \sigma_-)(a_{\mathrm{k}} + a_{\mathrm{k}}^\dagger)\,. \tag{2.42}$$

It follows from the identity

$$[\sigma_{ij}, \sigma_{kl}] = \sigma_{il}\delta_{jk} - \sigma_{kj}\delta_{il}, \tag{2.43}$$

that σ_+, σ_- and σ_z satisfy the spin-$1/2$ algebra of the Pauli matrices, i.e.,

$$\begin{aligned} [\sigma_-, \sigma+] &= -\sigma_z\,, \\ [\sigma_-, \sigma_z] &= 2\sigma_-\,, \\ [\sigma_+, \sigma_z] &= 2\sigma_+\,. \end{aligned} \tag{2.44}$$

In the matrix notation, σ_-, σ_+ and σ_z are given by

$$\sigma_- = \begin{pmatrix} 0 & 0 \\ 1 & 0 \end{pmatrix}, \qquad \begin{pmatrix} 0 & 1 \\ 0 & 0 \end{pmatrix}, \qquad \begin{pmatrix} 1 & 0 \\ 0 & -1 \end{pmatrix}\,. \tag{2.45}$$

The σ_- operator takes an atom in the upper state into a lower state whereas σ_+ promotes an atom in the lower state into the upper state.

The interaction energy in Eq. (2.42) consists of four terms. The term $a_{\mathrm{k}}^\dagger\sigma_-$ describes the process in which the atom is taken from the upper state into the lower state and a photon of mode k is created. The term $a_{\mathrm{k}}\sigma_+$ describes the opposite process. The term $a_{\mathrm{k}}\sigma_-$ describes the process in which the atom makes a transition from the upper to the lower level and a photon is annihilated, resulting in the loss of approximately $2\hbar\omega$ in energy. Similarly, $a_{\mathrm{k}}^\dagger\sigma_+$ results in the gain of $2\hbar\omega$. Dropping the energy non-conserving terms corresponds to the rotating-wave approximation. The resulting simplified Hamiltonian is

$$\mathscr{H} = \sum_{\mathrm{k}} \hbar\nu_{\mathrm{k}} a_{\mathrm{k}}^\dagger a_{\mathrm{k}} + \frac{1}{2}\hbar\omega\sigma_z + \hbar\sum_{\mathrm{k}} g_{\mathrm{k}}(\sigma_+ a_{\mathrm{k}} + a_{\mathrm{k}}^\dagger\sigma_-)\,. \tag{2.46}$$

Let us consider a two-level atom located at a point $\mathbf{r_0}$ which is driven by a strong continuous-wave (cw) laser field. The driven atom is excited to the higher energy state and then radiates spontaneously in all directions. The field operator at point $\mathbf{r}$, associated with this fluorescent radiation field is related to the appropriate atomic operator at retarded time in order to allow the field to propagate from the position $\mathbf{r_0}$ to $\mathbf{r}$.

The interaction of a two-level atomic system with the radiation field is described by the following rotating-wave approximation Hamiltonian (see Eq. 2.46):

$$\mathscr{H} = \frac{\hbar\omega}{2}\sigma_z + \sum_{\mathbf{k},\lambda}\hbar\nu_\kappa a^\dagger_{\mathbf{k},\lambda}a_{\mathbf{k},\lambda} + \sum_{\mathbf{k},\lambda}\hbar g_{\mathbf{k},\lambda}\left(a_{\mathbf{k},\lambda}\sigma_+ e^{i\mathbf{k}\mathbf{r}_0} + a^\dagger_{\mathbf{k},\lambda}\sigma_- e^{-i\mathbf{k}\mathbf{r}_0}\right). \tag{2.47}$$

Here we include the interaction between the atom and all the field modes characterized by the wave vector $\mathbf{k}$ and polarization λ. We proceed by introducing the slowly varying operators $\widetilde{a}_{\mathbf{k},\lambda}$ and $\widetilde{\sigma}_-$ such that

$$\begin{aligned} a_{\mathbf{k},\lambda}(t) &= \widetilde{a}_{\mathbf{k},\lambda}(t)e^{-i\nu_\kappa t}, \\ \sigma_-(t) &= \widetilde{\sigma}_-(t)e^{-i\omega t}. \end{aligned} \tag{2.48}$$

The Heisenberg equations of motion for these are

$$\begin{aligned} \dot{\widetilde{a}}_{\mathbf{k},\lambda}(t) &= -ig_{\mathbf{k},\lambda}\widetilde{\sigma}_-(t)e^{-i(\omega-\nu_\kappa)t-i\mathbf{k}\mathbf{r}_0}, \\ \dot{\widetilde{\sigma}}_-(t) &= \sum_{\mathbf{k},\lambda} ig_{\mathbf{k},\lambda}\sigma_z(t)\widetilde{a}_{\mathbf{k},\lambda}(t)e^{i(\omega-\nu_\kappa)t+i\mathbf{k}\mathbf{r}_0}. \end{aligned} \tag{2.49}$$

These equations can be formally integrated to yield

$$\begin{aligned} \widetilde{a}_{\mathbf{k},\lambda}(t) &= \widetilde{a}_{\mathbf{k},\lambda}(0) - ig_{\mathbf{k},\lambda}e^{-i(\omega-\nu_\kappa)t-i\mathbf{k}\mathbf{r}_0}\int_0^t dt'\widetilde{\sigma}_-(t')e^{i(\omega-\nu_\kappa)(t-t')}, \\ \widetilde{\sigma}_-(t) &= \widetilde{\sigma}_-(0) + \sum_{\mathbf{k},\lambda} ig_{\mathbf{k},\lambda}e^{i(\omega-\nu_\kappa)t+i\mathbf{k}\mathbf{r}_0}\int_0^t dt'\sigma_z(t')\widetilde{a}_{\mathbf{k},\lambda}(t')e^{-i(\omega-\nu_\kappa)(t-t')}. \end{aligned} \tag{2.50}$$

The first term in these equations represents the free evolution of the field and atomic operators in the absence of interaction. In the following, we shall focus on the contribution to the field due to its interactions with the atom. The positive frequency part of the electric field operator is

$$\mathbf{E}^{(+)}(\mathbf{r},t) = \sum_{\mathbf{k},\lambda}\mathscr{E}_{\mathbf{k}}\hat{\epsilon}^{(\lambda)}_{\mathbf{k}}a_{\mathbf{k},\lambda}(t)e^{i\mathbf{k}\mathbf{r}}, \tag{2.51}$$

where $\mathscr{E}_{\mathbf{k}} = (\hbar\nu_\kappa/2\epsilon_0 V)^{1/2}$. Substituting $a_{\mathbf{k},\lambda}(t)$ by Eqs. (2.48) and (2.50), we obtain

$$\mathbf{E}^{(+)}(\mathbf{r},t) = \left(\frac{i}{16\pi^3\epsilon_0}\right)e^{-i\omega t}\int d^3k\sum_\lambda \hat{\epsilon}^{(\lambda)}_{\mathbf{k}}[\hat{\epsilon}^{\lambda}_{\mathbf{k}}\cdot\ \hat{\gamma}]\nu_\kappa e^{i\mathbf{k}(\mathbf{r}-\mathbf{r}_0)} \tag{2.52}$$

$$\times \int_0^t dt'\widetilde{\sigma}_-(t')e^{i(\omega-\nu_\kappa)(t-t')}, \tag{2.53}$$

where we have recalled the definitions of $g_{\mathbf{k}}$ from Eq. (2.37) and replaced the sum by an integral via

$$\sum_{\mathbf{k}} \to \frac{V}{(2\pi)^3}\int d^3k. \tag{2.54}$$

It is very easy to show that

$$\sum_\lambda \hat{\epsilon}^{(\lambda)}_{\mathbf{k}}\hat{\epsilon}^{(\lambda)}_{\mathbf{k}} = 1 - \frac{\mathbf{k}\mathbf{k}}{k^2}, \tag{2.55}$$

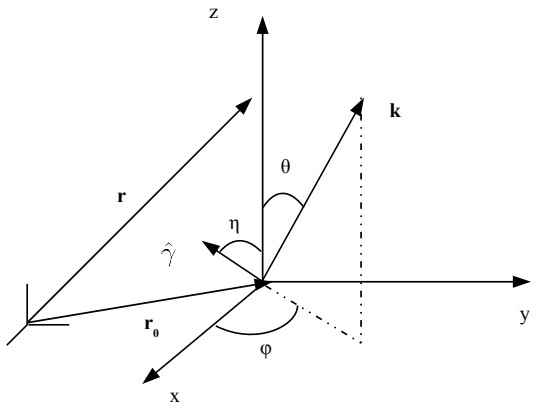

Figure 2.2: The atomic dipole γ and the $\mathbf{k}$-vector of the electric field in polar coordinates. η denotes the angle of the dipole with the z axis.

and thus we have the vector field operator in the useful form

$$\begin{aligned}\mathbf{E}^{(+)}(\mathbf{r},t) &= \left(\frac{i}{16\pi^3\epsilon_0}\right)e^{-i\omega t}\int dkd\theta d\varphi k^2\sin\theta\left[\hat{\gamma}-\frac{\mathbf{k}(\mathbf{k}\cdot\hat{\gamma})}{k^2}\right]\nu_\kappa e^{i\mathbf{k}(\mathbf{r}-\mathbf{r}_0)} \\ &\times \int_0^t dt'\widetilde{\sigma}_-(t')e^{i(\omega-\nu_\kappa)(t-t')}\,.\end{aligned} \tag{2.56}$$

Next we assume that the line joining the atom to the observation is along the z-axis, which is parallel to $\mathbf{r}-\mathbf{r}_0$, and the electric dipole is in the $x-z$ plane making an angle η with the z-axis, see Fig. 2.2. Then the vectors $\mathbf{k}$ and $\hat{\gamma}$ are defined in polar coordinates by

$$\begin{aligned}\mathbf{k} &= k(\hat{x}\sin\theta\cos\varphi+\hat{y}\sin\theta\sin\varphi+\hat{z}\cos\theta), \\ \hat{\gamma} &= \gamma(\hat{x}\sin\eta+\hat{z}\cos\eta).\end{aligned} \tag{2.57}$$

Consider first the angular integrations in Eq. (2.56). The φ-integration yields for the x-component

$$\begin{aligned}&\int_0^{2\pi}d\varphi\left[\hat{x}\cdot\hat{\gamma}-\frac{(\hat{x}\cdot\mathbf{k})(\mathbf{k}\cdot\hat{\gamma})}{k^2}\right]=\int_0^{2\pi}d\varphi\gamma[\sin\eta-\sin\theta\cos\varphi(\sin\eta\sin\theta\cos\varphi+\cos\eta\cos\theta)] \\ &=2\pi\gamma\sin\eta(1-\tfrac{1}{2}\sin^2\theta)\,,\end{aligned} \tag{2.58}$$

for the y-component

$$\int_0^{2\pi}d\varphi\left[\hat{y}\cdot\hat{\gamma}-\frac{(\hat{y}\cdot\mathbf{k})(\mathbf{k}\cdot\hat{\gamma})}{k^2}\right]=\int_0^{2\pi}d\varphi\gamma[0-\sin\theta\sin\varphi(\sin\eta\sin\theta\cos\varphi+\cos\eta\cos\theta)]=0\,, \tag{2.59}$$

and for the z-component

$$\begin{aligned}&\int_0^{2\pi}d\varphi\left[\hat{z}\cdot\hat{\gamma}-\frac{(\hat{z}\cdot\mathbf{k})(\mathbf{k}\cdot\hat{\gamma})}{k^2}\right]=\int_0^{2\pi}d\varphi\gamma[\cos\eta-\cos\theta(\sin\eta\sin\theta\cos\varphi+\cos\eta\cos\theta)] \\ &=2\pi\gamma\cos\eta(1-\cos^2\theta)=2\pi\gamma\cos\eta\sin^2\theta\,.\end{aligned} \tag{2.60}$$

Thus the y-component of the electric field vanishes. Next we consider the θ-integration in Eq. (2.56). By writing

$$e^{i\mathbf{k}(\mathbf{r}-\mathbf{r}_0)}=e^{ik|\mathbf{r}-\mathbf{r}_0|\cos\theta}\,, \tag{2.61}$$

and using $\cos\theta$ as a new variable $\mu = \cos\theta$, we obtain for the x-component

$$2\pi\gamma \sin\eta \int_0^\pi d\theta \sin\theta \left(1 - \tfrac{1}{2}\sin^2\theta\right) e^{i\mathbf{k}(\mathbf{r}-\mathbf{r}_0)} = 2\pi\gamma \sin\eta \int_{-1}^{1} d\mu \left[1 - \tfrac{1}{2}(1-\mu^2)\right] e^{ik|\mathbf{r}-\mathbf{r}_0|\mu}$$
$$= 2\pi\gamma \sin\eta \left[\frac{e^{ik|\mathbf{r}-\mathbf{r}_0|} - e^{-ik|\mathbf{r}-\mathbf{r}_0|}}{ik|\mathbf{r}-\mathbf{r}_0|} + O\left(\frac{1}{|\mathbf{r}-\mathbf{r}_0|^2}\right)\right], \tag{2.62}$$

and for the z-component

$$2\pi\gamma \cos\eta \int_0^\pi d\theta \sin^3\theta e^{i\mathbf{k}(\mathbf{r}-\mathbf{r}_0)} = 2\pi\gamma \cos\eta \int_{-1}^{1} d\mu (1-\mu^2) e^{ik|\mathbf{r}-\mathbf{r}_0|\mu} \sim O\left(\frac{1}{|\mathbf{r}-\mathbf{r}_0|^2}\right), \tag{2.63}$$

where we have used the results (2.58) and (2.60). In the far-field region, the terms proportional to $O(1/|\mathbf{r}-\mathbf{r}_0|^2)$ can be neglected, and the z-component of the electric field also vanishes. Combining Eqs. (2.56) and (2.62), we obtain

$$\begin{aligned} \mathbf{E}^{(+)}(\mathbf{r},t) &= \left(\frac{c\gamma \sin\eta\hat{x}}{8\pi^2\epsilon_0|\mathbf{r}-\mathbf{r}_0|}\right) e^{-i\omega t} \int_0^\infty dk k^2 \left(e^{ik|\mathbf{r}-\mathbf{r}_0|} - e^{-ik|\mathbf{r}-\mathbf{r}_0|}\right) \\ &\times \int_0^t dt' \tilde{\sigma}_-(t') e^{i(\omega-\nu_k)(t-t')}. \end{aligned} \tag{2.64}$$

We proceed by replacing $k^2 \to (\omega/c)^2$, extended the limit of k-integration to $-\infty$ and upon performing the k-integration, and obtain

$$\begin{aligned} \mathbf{E}^{(+)}(\mathbf{r},t) &= \left(\frac{\omega^2\gamma \sin\eta\hat{x}}{4\pi\epsilon_0 c^2|\mathbf{r}-\mathbf{r}_0|}\right) \left[e^{-i\omega(t-|\mathbf{r}-\mathbf{r}_0|/c)} \int_0^t dt' \tilde{\sigma}_-(t') \delta\left(t - t' - \frac{|\mathbf{r}-\mathbf{r}_0|}{c}\right)\right. \\ &- \left. e^{-i\omega(t+|\mathbf{r}-\mathbf{r}_0|/c)} \int_0^t dt' \tilde{\sigma}_-(t') \delta\left(t - t' + \frac{|\mathbf{r}-\mathbf{r}_0|}{c}\right)\right]. \end{aligned} \tag{2.65}$$

Ignoring the incoming wave contribution and going back to $\sigma_-(t)$, see Eq. (2.49), we find

$$E^{(+)}(\mathbf{r},t) = \frac{\omega^2\gamma sin(\eta)}{4\pi\epsilon_0 c^2|\mathbf{r}-\mathbf{r_0}|}\hat{x}\sigma_-\left(t - \frac{|\mathbf{r}-\mathbf{r_0}|}{c}\right) \tag{2.66}$$

with a similar expression for $E^{(-)}(\mathbf{r},t)$. Equation (2.66) indicates that the positive frequency part of the field operator is proportional to the atomic lowering operator at retarded time.

2.2.3 The spectrum of resonance fluorescence

In this section, we evaluate the complete power spectrum of radiation scattered by a two-level atom driven by an incident field of arbitrary strength. The atom is assumed to be isolated and fixed in position. We look for the field emitted along the x-axis. The field operator in Eq. (2.66) can therefore be treated as a scalar. The power spectrum $S(\mathbf{r},\omega_0)$ of the fluorescent light at some suitable chosen point $\mathbf{r}$ in the far field is obtained by taking the Fourier transform of the normally-ordered correlation function of the field $\langle E^{(-)}(\mathbf{r},t)E^{(+)}(\mathbf{r},t+\tau)\rangle$ with respect to τ. According to the Wiener-Khintchine theorem, the power spectrum $S(\omega_0)$ is given as

$$S(\omega_0) = \frac{1}{2\pi}\lim_{T\to\infty}\frac{1}{T}\int_0^T dt \int_0^T dt' \langle E^{(-)}(t)E^{(+)}(t')\rangle e^{-i\omega_0(t-t')}. \tag{2.67}$$

Under the stationary condition, the correlation function $\langle E^{(-)}(t)E^{(+)}(t')\rangle$ depends only on the time difference $\tau = t - t'$ and Eq. (2.67) becomes

$$\begin{aligned} S(\omega_0) &= \frac{1}{2\pi}\lim_{T\to\infty}\frac{1}{T}\int_0^T dt\left(\int_0^t dt' + \int_t^T dt'\right)\langle E^{(-)}(t)E^{(+)}(t')\rangle e^{-i\omega_0(t-t')} \qquad (2.68)\\ &= \frac{1}{2\pi}\lim_{T\to\infty}\frac{1}{T}\int_0^T dt\left[\int_0^t d\tau\langle E^{(-)}(\tau)E^{(+)}(0)\rangle e^{-i\omega_0(\tau)} + \int_0^{T-t} d\tau\langle E^{(-)}(0)E^{(+)}(\tau)\rangle e^{i\omega_0\tau}\right]. \end{aligned}$$

Provided that the field operators are correlated only over a short period of time, we can extend the upper limit of the τ-integrations to infinity with no significant change. Since we have

$$\langle E^{(-)}(\tau)E^{(+)}(0)\rangle = \langle E^{(-)}(0)E^{(+)}(\tau)\rangle^*, \qquad (2.69)$$

it follows from Eq. (2.68) that

$$S(\omega_0) = \frac{1}{\pi}\mathrm{Re}\int_0^\infty d\tau\langle E^{(-)}(0)E^{(+)}(\tau)\rangle e^{i\omega_0\tau}\,. \qquad (2.70)$$

It follows from Eq. (2.66) that

$$\langle E^{(-)}(\mathbf{r},t)E^{(+)}(\mathbf{r},t+\tau)\rangle = I_0(\mathbf{r})\langle\sigma_+(t)\sigma_-(t+\tau)\rangle, \qquad (2.71)$$

where we introduced the quantity

$$I_0(\mathbf{r}) = \left(\frac{\omega^2\gamma\sin\eta}{4\pi\epsilon_0 c^2|\mathbf{r}-\mathbf{r}_0|}\right)^2. \qquad (2.72)$$

2.2.4 Calculation of the fluorescence spectrum

The polarization operator of the two-level atom is given by

$$P(\tau) = \gamma_{12}(|1\rangle\langle 2| + |2\rangle\langle 1|)\,, \qquad (2.73)$$

where γ_{ij} are the moduli of the induced transition dipole (multipole) moments. The positive and negative parts of the polarization operator are given by

$$P^{(+)}(\tau) = \gamma_{12}|1\rangle\langle 2|\,, \quad P^{(-)}(\tau) = \gamma_{21}|2\rangle\langle 1|\,. \qquad (2.74)$$

The quantum regression theorem states that if M, Q and N are members of a complete set of system operators $\{S_\mu\}$, and if the one-time averages can be expressed in the form

$$\langle M(\tau)\rangle = \sum_\mu O_\mu(\tau,\tau')\langle S_\mu(\tau')\rangle\,, \quad \tau' < \tau\,, \qquad (2.75)$$

where $O_\mu(\tau,\tau')$ are c-number functions of time, than the two-time expectation values take the form

$$\langle Q(\tau')M(\tau)N(\tau')\rangle = \sum_\mu O_\mu(\tau,\tau')\langle Q(\tau')S_\mu(\tau')N(\tau')\rangle\,, \quad \tau' < \tau\,. \qquad (2.76)$$

In particular, Q or N can be identified with the identity operator. The starting point is the one-time average

$$\langle P^{(-)}(\tau_1)\rangle = Tr[\rho(\tau_1)\gamma_{12}|2\rangle\langle 1|]\,, \qquad (2.77)$$

which can be written in terms of Ψ_1 as follows:

$$\langle P^{(-)}(\tau_1)\rangle = \gamma_{12} e^{i\omega\tau_1}\Psi_1(\tau_1)\,. \tag{2.78}$$

At this point the essential step is to express each of the matrix elements $\Psi_i(\tau_1)$ that appear in Eq. (2.78) in terms of their initial values $\tau = \tau_0$. While this could be done beginning with the formal integration of Eq.(2.20), here we operate in the space of the Laplace transform. Thus, Eq. (2.78) yields

$$\langle \hat{P}^{(-)}(z)\rangle = \gamma_{12}\hat{\Psi}_1(z')\,, \tag{2.79}$$

where $z' = z - i\omega$. By the help of the Eq. (2.25), Eq. (2.79) can be cast into the required form

$$\langle \hat{P}^{(-)}(z)\rangle = \gamma_{12}\sum_j M_{1j}(z')\Psi_j(\tau_0) + \frac{\gamma_{12}}{z'}\sum_j M_{1j}(z')I_j\,. \tag{2.80}$$

Next we have to express $\Psi_j(\tau_0)$ and I_j in the form of expectation values of system operators at $\tau = \tau_0$. This can be done directly from the definition of $\Psi_j(\tau_0)$ as illustrated by the following example:

$$\Psi_1(\tau_0) = e^{-i\omega\tau_0}\rho_{12}(\tau_0) = e^{-i\omega\tau_0}\langle |2\rangle\langle 1|\rangle_{\tau_0}\,. \tag{2.81}$$

The regression theorem gives

$$\langle \hat{P}^{(-)}(z)P^{(+)}(\tau_0)\rangle_{\tau_0} = \gamma_{12}^2 M_{11}(z')\Psi_3(\tau_0)e^{-i\omega\tau_0} + \frac{\gamma_{12}^2}{z'}\sum_j M_{1j}(z')\Psi_2(\tau_0)I_j\,. \tag{2.82}$$

In the limiting case of $\tau_0 \to \infty$, the above expression becomes

$$\langle \hat{P}^{(-)}(z)P^{(+)}(\infty)\rangle = \gamma_{12}^2 M_{11}(z')\Psi_3(\infty) + \frac{\gamma_{12}^2}{z'}\sum_j M_{1j}(z')\Psi_2(\infty)I_j\,. \tag{2.83}$$

Eq. (2.83) shows that the spectrum of resonance fluorescence has a structure with a center located at ω, and a magnitude proportional to the atomic transition matrix element. The spectrum has the form

$$f(z) = \frac{A}{z} + g(z)\,, \tag{2.84}$$

where A is a constant and $g(z)$ is an analytic function of z for $\Re z \le 0$. The singularity reflects the existence of a coherent Rayleigh peak whose origin can be traced to the elastic scattering of the driving fields, while $g(z)$ describes the incoherent part of the spectrum of the emitted radiation. If we denote the full correlation function with

$$\hat{\Gamma}(z) \equiv \langle \hat{P}^{(-)}(z)P^{(+)}(\infty)\rangle\,, \tag{2.85}$$

the incoherent part can be determined according to the simple algorithm

$$\hat{\Gamma}_{\rm incoh}(z) = \hat{\Gamma}(z) - \frac{1}{z'}\lim_{z'\to 0} z'\hat{\Gamma}(z)\,. \tag{2.86}$$

Finally, the required emission spectrum is given by

$$S(\omega) = \Re\hat{\Gamma}_{incoh}(z)|_{z=i\omega}\,, \tag{2.87}$$

where

$$\hat{\Gamma}_{\rm incoh}(z) = \gamma_{12}^2 M_{11}(z')\Psi_3(\infty) + \gamma_{12}^2\sum_j N_{1j}(z')\Psi_2(\infty)I_j\,, \tag{2.88}$$

and

$$N_{ij}(z) = (L^{-1}(z-L)^{-1})_{ij}\,. \tag{2.89}$$

2.2.5 Analytic calculation of the spectra in the strong field approximation

In this section we show that a convenient set of dressed atomic states allows a much more natural description of the atomic dynamics and that, in the limit of a strong effective Rabi frequency, this allows the calculation of the required correlation functions and spectra in a closed analytic form. The benefit of this procedure is that explicit expressions for the line shapes, line widths, and peak heights become available.

We consider the following atomic states:

$$\begin{aligned} |s\rangle &= \frac{1}{\sqrt{1+(\Omega_R/2+\sqrt{1+(\Omega_R/2)^2})^2}}|1\rangle + \frac{\Omega_R/2+\sqrt{1+(\Omega_R/2)^2}}{\sqrt{1+(\Omega_R/2+\sqrt{1+(\Omega_R/2)^2})^2}}|2\rangle\,, \\ |t\rangle &= \frac{1}{\sqrt{1+(\Omega_R/2-\sqrt{1+(\Omega_R/2)^2})^2}}|1\rangle + \frac{\Omega_R/2-\sqrt{1+(\Omega_R/2)^2}}{\sqrt{1+(\Omega_R/2-\sqrt{1+(\Omega_R/2)^2})^2}}|2\rangle\,, \end{aligned} \tag{2.90}$$

where $\Delta_R \equiv \frac{\Delta}{\Omega_R}$. In order to minimize the algebraic effort we limit our considerations to the first order in Δ_R,

$$\begin{aligned} |s\rangle &= (1/\sqrt{2}-\Omega_R/\sqrt{32})|1\rangle + (1/\sqrt{2}+\Omega_R/\sqrt{32})|2\rangle\,, \\ |t\rangle &= (1/\sqrt{2}+\Omega_R/\sqrt{32})|1\rangle + (-1/\sqrt{2}+\Omega_R/\sqrt{32})|2\rangle\,. \end{aligned} \tag{2.91}$$

These states are eigenstates of $\mathscr{H}_1'$, i.e.,

$$\begin{aligned} \mathscr{H}_1'|s\rangle &= \hbar\sqrt{\Omega_R^2+\Delta^2/4}|s\rangle\,, \\ \mathscr{H}_1'|t\rangle &= -\hbar\sqrt{\Omega_R^2+\Delta^2/4}|t\rangle\,. \end{aligned} \tag{2.92}$$

Because of the diagonal nature of $\mathscr{H}_1'$ in this representation, the new matrix L, which is responsible for the atomic dynamics, contains the effective Rabi frequency along the main diagonal and is zero elsewhere. The irreversible decay process breaks this symmetry. However, if the effective Rabi frequency is sufficiently large, it is possible to introduce an accurate approximation that allows to calculate the spectral features analytically.

We consider again the master equation in the interaction picture

$$\dot{\rho}' = -\frac{i}{\hbar}[\mathscr{H}_1', \rho'] + \Lambda\rho'\,. \tag{2.93}$$

The reversible part of Eq. (2.93) in the dressed-state representation takes a very simple form owing to the fact that states (2.91) are exact eigenstates of $\mathscr{H}_1'$. Thus we have

$$\left(\frac{d}{dt}\right)_{rev}\begin{pmatrix}\rho_{st}'\\ \rho_{ss}'\\ \rho_{tt}'\end{pmatrix} = \begin{pmatrix}-2I\Omega_R\rho_{st}'\\ 0\\ 0\end{pmatrix}\,. \tag{2.94}$$

Again, the trace condition $\rho_{ss}' = 1-\rho_{tt}'$, and the Hermitian symmetry relation $\rho_{st}' = (\rho_{ts}')^*$ hold.

The penalty one pays for using this representations is that the irreversible part of the master equation becomes complicated. In fact, the original irreversible part of the master equation is

$$\left(\frac{d}{dt}\right)_{irrev}\rho_{ij}' = \sum_{pq}\Lambda_{ijpq}\rho_{pq}'\,, \tag{2.95}$$

where Λ_{ijpq} are the various decay rates that appear explicitly in Eq. (2.14). From the transformation equation between the two pictures $\rho'_{\mu\nu} = \sum_{ij}\langle\mu|i\rangle\rho'_{ij}\langle j|\nu\rangle$, it is easy to obtain

$$\left(\frac{d}{dt}\right)_{irrev}\rho'_{\mu\nu} = \sum_{\sigma\tau}\left(\sum_{ijpq}\langle\mu|i\rangle\langle j|\nu\rangle\langle p|\sigma\rangle\langle\tau|q\rangle\Lambda_{ijpq}\right)\rho'_{\sigma\tau} \equiv \sum_{\sigma\tau}\Gamma_{\mu\nu\sigma\tau}\rho'_{\sigma\tau}\,, \tag{2.96}$$

where the transformation matrix elements $\langle\mu|i\rangle$ can be read immediately from Eq. (2.91). We now consider the limit when the Rabi frequency is much larger than the relaxation rates. We focus on the derivation of an expression for resonance fluorescence for the response of the system around steady state with an accuracy of order $1/\Omega_R$. We introduce the vector Ψ with the components

$$\Psi_1 = \rho'_{st}\,, \quad \Psi_2 = \rho'_{ss}\,, \quad \Psi_3 = \rho'_{ts}\,. \tag{2.97}$$

This vector is a solution of the linear equation

$$\frac{d}{dt}\Psi = L\Psi + I\,, \tag{2.98}$$

with the matrix L defined as

$$L = \begin{pmatrix} \Gamma_{stst} - 2I\Omega_R & \Gamma_{stss} - \Gamma_{sttt} & \Gamma_{stts} \\ \Gamma_{ssst} & \Gamma_{ssss} - \Gamma_{sstt} & \Gamma_{ssts} \\ \Gamma_{tsst} & \Gamma_{tsss} - \Gamma_{tstt} & \Gamma_{tsts} + 2I\Omega_R \end{pmatrix}\,, \tag{2.99}$$

and the vector

$$I_1 = \Gamma_{sttt}\,, \quad I_2 = \Gamma_{sstt}\,, \quad I_3 = \Gamma_{tstt}\,. \tag{2.100}$$

In the steady state, it takes the form $\Psi(\infty) = -L^{-1}I$. It is not difficult to see that

$$L^{-1}(\mathscr{O}(1/\Omega_R)) = \begin{pmatrix} 0 & 0 & 0 \\ 0 & \frac{1}{\Gamma_{ssss}-\Gamma_{sstt}} & 0 \\ 0 & 0 & 0 \end{pmatrix}\,, \tag{2.101}$$

so the solution is

$$\Psi_1(\infty) = \Psi_3(\infty) = 0\,, \quad \Psi_2(\infty) = \frac{\Gamma_{sstt}}{\Gamma_{sstt} - \Gamma_{ssss}}\,. \tag{2.102}$$

We define the deviation from the steady state as

$$\delta\Psi = \Psi(t) - \Psi(\infty)\,, \tag{2.103}$$

which satisfies the equation

$$\frac{d}{dt}\delta\Psi = L\delta\Psi I\,. \tag{2.104}$$

In the asymptotic limit of interest, however, we replace the matrix L in the fluctuation equation Eq. (2.104) with a diagonal approximation L_0 witch is accurate up to corrections of order $1/\Omega_R$. In order to understand the nature of this approximation, let us consider the explicit form of equations for $\delta\rho'_{\mu\nu}$:

$$\begin{aligned} \frac{d}{dt}\delta\rho'_{st} &= (\Gamma_{stss} - \Gamma_{sttt})\delta\rho'_{ss} + (\Gamma_{stst} - 2I\Omega_R)\delta\rho'_{st} + \Gamma_{stts}\delta\rho'_{ts}\,, \\ \frac{d}{dt}\delta\rho'_{ss} &= (\Gamma_{ssss} - \Gamma_{sstt})\delta\rho'_{ss} + \Gamma_{ssst}\delta\rho'_{st} + \Gamma_{ssts}\delta\rho'_{ts}\,, \\ \frac{d}{dt}\delta\rho'_{ts} &= (\Gamma_{tsss} - \Gamma_{tstt})\delta\rho'_{ss} + \Gamma_{tsst}\delta\rho'_{st} + (\Gamma_{tsts} + 2I\Omega_R)\delta\rho'_{ts}\,. \end{aligned} \tag{2.105}$$

Introducing the notations

$$\delta\rho'_{st} = e^{-2I\Omega_R} R_{st}\,, \quad \delta\rho'_{ts} = e^{2I\Omega_R} R_{ts}\,, \quad \delta\rho'_{ss} = R_{ss}\,, \tag{2.106}$$

we obtain

$$\begin{aligned} \frac{d}{dt}R_{st} &= \Gamma_{tstt}R_{st} + \mathscr{O}(1/\Omega_R)\,, \\ \frac{d}{dt}R_{ss} &= (\Gamma_{ssss} - \Gamma_{sstt})R_{ss} + \mathscr{O}(1/\Omega_R)\,, \\ \frac{d}{dt}R_{ts} &= \Gamma_{tsts}R_{st} + \mathscr{O}(1/\Omega_R)\,, \end{aligned} \tag{2.107}$$

where $\mathscr{O}(1/\Omega_R)$ denotes rapidly oscillating terms. In the view of the assumed large value of Ω_R, we drop the oscillating contributions so that, in terms of the original variable, we have

$$\begin{aligned} \frac{d}{dt}R_{st} &= (\Gamma_{tstt} - 2I\Omega_R)R_{st}\,, \\ \frac{d}{dt}R_{ss} &= (\Gamma_{ssss} - \Gamma_{sstt})R_{ss}\,, \\ \frac{d}{dt}R_{ts} &= (\Gamma_{tsts} + 2I\Omega_R)R_{st}\,. \end{aligned} \tag{2.108}$$

Hence, by neglecting the rapidly oscillating components, the new matrix L_0 can be obtained from the original matrix L after ignoring the off-diagonal elements

$$L_0 = \begin{pmatrix} \Gamma_{stst} - 2I\Omega_R & 0 & 0 \\ 0 & \Gamma_{ssss} - \Gamma_{sstt} & 0 \\ 0 & 0 & \Gamma_{tsts} + 2I\Omega_R \end{pmatrix}. \tag{2.109}$$

In terms of the original vector Ψ [see Eq. (2.103)]

$$\frac{d}{dt}\Psi(t) = L_0\Psi(t) + I_\infty\,, \tag{2.110}$$

where $I_\infty = -L_0\Psi(\infty)$, with the components

$$I_{\infty 1} = I_{\infty 3} = 0\,, \quad I_{\infty 2} = \frac{\Gamma_{sstt}}{\Gamma_{sstt} - \Gamma_{ssss}}\,, \tag{2.111}$$

we get $I_\infty \equiv I_{\infty 2} = \Gamma_{sstt}$.

One can express the $\Gamma_{\mu\nu\sigma\tau}$ in terms of the $\Lambda_{\mu\nu\sigma\tau}$ as

$$\begin{aligned} \Gamma_{stst} &= \tfrac{1}{4}(\Lambda_{1111} - \Lambda_{1112} + \Lambda_{1121} - \Lambda_{1122} - \Lambda_{1211} + \Lambda_{1212} - \Lambda_{1221} + \Lambda_{1222} + \Lambda_{2111} \\ &- \Lambda_{2112} + \Lambda_{2121} - \Lambda_{2122} - \Lambda_{2211} + \Lambda_{2212} - \Lambda_{2221} + \Lambda_{2222})\,, \\ \Gamma_{ssss} &= \tfrac{1}{4}(\Lambda_{1111} + \Lambda_{1112} + \Lambda_{1121} + \Lambda_{1122} + \Lambda_{1211} + \Lambda_{1212} + \Lambda_{1221} + \Lambda_{1222} + \Lambda_{2111} \\ &+ \Lambda_{2112} + \Lambda_{2121} + \Lambda_{2122} + \Lambda_{2211} + \Lambda_{2212} + \Lambda_{2221} + \Lambda_{2222})\,, \end{aligned} \tag{2.112}$$

where

$$\begin{aligned} \Lambda_{1211} &= 0\,, \quad \Lambda_{1212} = -\mu_{12}\,, \quad \Lambda_{1221} = 0\,, \quad \Lambda_{1222} = 0\,, \\ \Lambda_{2111} &= 0\,, \quad \Lambda_{2112} = -\mu_{12}\,, \quad \Lambda_{2121} = 0\,, \quad \Lambda_{2122} = 0\,, \\ \Lambda_{1111} &= -\Gamma_{21}\,, \quad \Lambda_{1112} = 0\,, \quad \Lambda_{1121} = 0\,, \quad \Lambda_{1122} = \Gamma_{12}\,, \\ \Lambda_{2211} &= \Gamma_{21}\,, \quad \Lambda_{2212} = 0\,, \quad \Lambda_{2221} = 0\,, \quad \Lambda_{2222} = -\Gamma_{12}\,. \end{aligned} \tag{2.113}$$

It is easy to see that

$$\begin{aligned}\Gamma_{ststst} &= \tfrac{1}{4}(-2\Gamma_{21}+\gamma_x)+\Gamma_{21}\Delta_R/8\,, \quad \Gamma_{ssss} = -\tfrac{1}{4}(\Gamma_{21}+\gamma_x)+\Gamma_{21}\Delta_R/4 \\ \Gamma_{sstt} &= \tfrac{1}{4}(\Gamma_{21}+\gamma_x)+\Gamma_{21}\Delta_R/4\,, \quad \Gamma_{tsts} = -\tfrac{1}{2}(\Gamma_{21}+\gamma_x/2)-\tfrac{1}{4}(\Gamma_{21}/2+\gamma_x/2)\Delta_R/4\,,\end{aligned} \tag{2.114}$$

where γ_x is the laser's decoherence rate. It was added in the theory to the corresponding polarization decay rate.

The solution of Eq. (2.111) in Laplace space is

$$\hat{\Psi}(z) = M^0(z)\Psi(t_0) + \frac{1}{z}M^0(z)I_\infty\,, \tag{2.115}$$

where the matrix M^0 is given as

$$M^0(z) = (z - L_0)^{-1}\,. \tag{2.116}$$

The polarization operator is defined as

$$P^{(+)} = \gamma_{12}|1\rangle\langle 2|\,, \quad P^{(-)} = \gamma_{12}|2\rangle\langle 1|\,. \tag{2.117}$$

Its single-time average is

$$\langle P^{(-)}(t_1)\rangle = \gamma_{12}Tr[\rho'(0)|2\rangle\langle 1|]e^{i\omega t_1}\,. \tag{2.118}$$

In terms of the dressed states we have

$$|2\rangle\langle 1|s\rangle = \tfrac{1}{2}|s\rangle + \left(-\tfrac{1}{2}+\Delta_R/4\right)|t\rangle\,, \quad |2\rangle\langle 1|t\rangle = \left(\tfrac{1}{2}+\Delta_R/4\right)|s\rangle - \tfrac{1}{2}|t\rangle\,, \tag{2.119}$$

so that, in Laplace space, it follows that

$$\langle\hat{P}^{(-)}(z)\rangle = \tfrac{1}{2}[2\hat{\Psi}_2(z') - (1-\Delta_R/2)\,\hat{\Psi}_1(z') + (1+\Delta_R/2)\,\hat{\Psi}_3(z')] - \frac{1}{2z'}\,, \tag{2.120}$$

where $z' = z - i\omega$. It is easy to express then the matrix M^0:

$$M^0 = \begin{pmatrix} \frac{1}{2i\Omega_R+z-\Gamma_{ststst}} & 0 & 0 \\ 0 & \frac{1}{z-\Gamma_{ssss}+\Gamma_{sstt}} & 0 \\ 0 & 0 & \frac{1}{-2i\Omega_R+z-\Gamma_{tsts}}\,. \end{pmatrix} \tag{2.121}$$

Using Eq. (2.115), one can write

$$\begin{aligned}\hat{\Psi}_1(z) &= M^0_{11}(z)\Psi_1(t_0)\,, \quad \hat{\Psi}_2(z) = M^0_{22}(z)\Psi_2(t_0) + \frac{1}{z}M^0_{22}(z)I_{\infty 2}\,, \\ \hat{\Psi}_3(z) &= M^0_{33}(z)\Psi_3(t_0)\,,\end{aligned} \tag{2.122}$$

and then

$$\begin{aligned}\langle\hat{P}^{(-)}(z)\rangle &= \tfrac{1}{2}[2M^0_{22}(z')\Psi_2(t_0) - (1-\Delta_R/2)M^0_{11}(z')\Psi_1(t_0) \\ &+ (1+\Delta_R/2)M^0_{33}(z')\Psi_3(t_0)] + \frac{1}{2z'}[M^0_{22}(z')I_{\infty 2} - 1]\,.\end{aligned} \tag{2.123}$$

The regression theorem gives

$$\begin{aligned}\Psi_1(t_0) &\rightarrow \gamma_{12}Tr[\rho'(t_0)|\overline{t\rangle\langle s}|1\rangle\langle 2|] = \gamma_{12}Tr[\rho'(t_0)|t\rangle\langle s|\overline{1\rangle\langle 2}|] \\ &= \gamma_{12}\exp(-i\omega t_0)\tfrac{1}{2}\left(\rho'_{st} - (1-\Delta_R/2)\rho'_{tt}\right)\,, \\ \Psi_2(t_0) &\rightarrow \gamma_{12}\exp(-i\omega t_0)\tfrac{1}{2}\left(\rho'_{ss} - (1-\Delta_R/2)\rho'_{ts}\right)\,, \\ \Psi_3(t_0) &\rightarrow \gamma_{12}\exp(-i\omega t_0)\tfrac{1}{2}\left((1+\Delta_R/2)\rho'_{ss} - \rho'_{ts}\right)\,,\end{aligned} \tag{2.124}$$

where the over-bars indicate that the operators are in the interaction picture. In the stationary limit, the off-diagonal elements of $\rho_{\mu\nu}$ vanish and the only nonzero element is $\rho'_{ss} = \Psi_\infty$, as given by Eq. (2.102). In this way, Eq. (2.124) becomes

$$\begin{aligned} \Psi_1(t_0) &\rightarrow -\tfrac{1}{2}\gamma_{12}(1-\Delta_R/2)(1-\Psi_2(\infty))e^{-i\omega t_0}\,, \quad \Psi_2(t_0) \rightarrow \tfrac{1}{2}\gamma_{12}\Psi_2(\infty)e^{-i\omega t_0}\,, \\ \Psi_3(t_0) &\rightarrow \tfrac{1}{2}\gamma_{12}(1+\Delta_R/2)\Psi_2(\infty)e^{-i\omega t_0}\,. \end{aligned} \tag{2.125}$$

For the inhomogeneous part of the equation, we get

$$\begin{aligned} \langle 1\rangle_{t_0} &\rightarrow \langle|1\rangle\langle 2|\rangle_{t_0} = Tr[\rho'(t_0)\overline{1\rangle\langle 2}] \\ &= \tfrac{1}{2}[2\rho_{ss} + (1+\Delta_R/2)\rho_{st} - (1-\Delta_R/2)\rho_{ts} - 1]e^{-i\omega t_0}\,, \end{aligned} \tag{2.126}$$

therefore, we arrive at the result:

$$\begin{aligned} \langle\hat{P}^{(-)}(z)P^{(+)}(\infty)\rangle &= \tfrac{\gamma_{12}}{4}[2M^0_{22}\Psi_2(\infty) + (1-\Delta_R/2)M^0_{11}(1-\Delta_R/2)(1-\Psi_2(\infty)) \\ &+ (1+\Delta_R/2)M^0_{33}(1+\Delta_R/2)\Psi_2(\infty)] - \tfrac{\gamma_{12}}{4z'}(2M^0_{22}I_{\infty 2} - 1)(1-2\Psi_2(\infty))\,. \end{aligned} \tag{2.127}$$

We obtain the final results in the first order of Δ_R as

$$\begin{aligned} \langle\hat{P}^{(-)}(z)P^{(+)}(\infty)\rangle &= \frac{\gamma_{12}}{2}\left[\frac{1}{2z+\Gamma_{21}+\gamma_x} + \frac{1}{4z+2\Gamma_{21}+\gamma_x-8I\Omega_R}\right. \\ &\left. + \frac{1}{4z+2\Gamma_{21}+\gamma_x+8I\Omega_R}\right] + \frac{\gamma_{12}}{4}\left[\frac{2\Gamma_{21}}{(\Gamma_{21}+\gamma_x)(2z+\Gamma_{21}+\gamma_x)} - \frac{\Gamma_{21}+2\gamma_x}{(4z+2\Gamma_{21}+\gamma_x-8I\Omega_R)^2}\right. \\ &+ \frac{2(2\Gamma_{21}+\gamma_x)}{(\Gamma_{21}+\gamma_x)(4z+2\Gamma_{21}+\gamma_x-8I\Omega_R)} + \frac{\Gamma_{21}+2\gamma_x}{(4z+2\Gamma_{21}+\gamma_x+8I\Omega_R)^2} \\ &\left. - \frac{2(2\Gamma_{21}+\gamma_x)}{(\Gamma_{21}+\gamma_x)(4z+2\Gamma_{21}+\gamma_x+8I\Omega_R)}\right]\Delta_R + \mathscr{O}(\Delta_R)\,. \end{aligned} \tag{2.128}$$

In the case of a resonant interaction ($\Delta_R = 0$), and an ideal laser without decoherence ($\gamma_x = 0$), we get the well-known formula

$$\langle\hat{P}^{(-)}(z)P^{(+)}(\infty)\rangle = \frac{\gamma_{12}}{2}\left[\frac{1}{2z+\Gamma_{21}} + \frac{1}{4z+2\Gamma_{21}-8I\Omega_R} + \frac{1}{4z+2\Gamma_{21}+8I\Omega_R}\right]\,. \tag{2.129}$$

The emission spectrum will be given by the real part of this expression with the corresponding substitution of the complex energy variable:

$$S(\omega_0) = \Re\langle\hat{P}^{(-)}(z)P^{(+)}(\infty)\rangle|_{z=i(\omega_0-\omega)}\,. \tag{2.130}$$

2.2.6 Appearance of sidebands in the strong field limit

As depicted in Fig 2.3, a field of spectral width D and central frequency ν is incident on an atom with spectral width Γ and central frequency ω. The field induces a dipole or multipole moment in the atom which governs the emitted or scattered light.

When the Rabi frequency associated with the driving field, Ω_R, becomes comparable to or larger than the spectral width of the atom Γ, sidebands start emerging in the spectrum of fluorescent light, leading to a three-peak spectrum. The emergence of the sidebands at frequencies $\nu + \Omega_R$ and $\nu - \Omega_R$ is due to the modulation of the dipole moment by the Rabi oscillations.

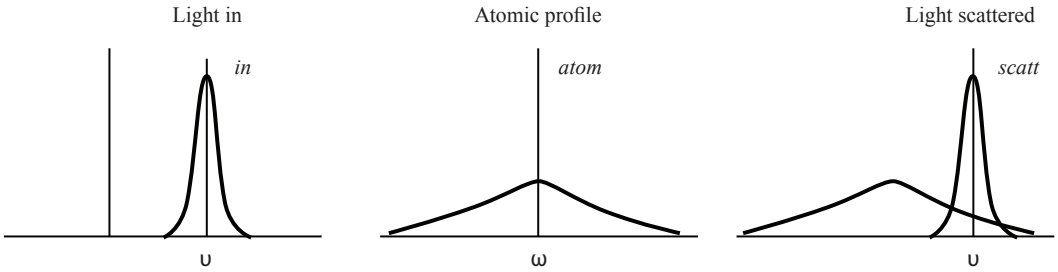

Figure 2.3: The incident light has a spectrum centered at a frequency ν and bandwidth D. The scattered light has a bandwidth D, it is centered at ν for $\Gamma \gg D$.

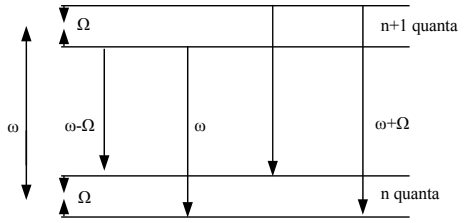

Figure 2.4: Splitting of the atomic states by the dynamic Stark effect. See text for notations and further explanations.

A physical understanding of this interesting behavior can be achieved by considering a dressed- atom picture of the atom-field interaction. The interaction Hamiltonian of a quantized field mode interacting resonantly with a two-level atom, in the rotating-wave approximation, is (see Eq. (2.46))

$$\mathscr{H} = \mathscr{H}_0 + \mathscr{H}_1 = \frac{\hbar\omega}{2}\sigma_z + \hbar\nu a^\dagger a + \hbar g(\sigma_+ a + a^\dagger \sigma_-),. \tag{2.131}$$

We will consider the case in which $\omega = \nu$ and we are therefore concerned only with the interaction picture Hamiltonian

$$\mathscr{H}_1' = \hbar g(\sigma_+ a + a^\dagger \sigma_-)\,. \tag{2.132}$$

As can be verified by direct substitution, the eigenstates of the Hamiltonian (2.132) are

$$|\pm, n\rangle = \frac{1}{\sqrt{2}}(|a, n\rangle \pm |b, n+1\rangle)\,, \tag{2.133}$$

with eigenvalues $+\hbar\Omega_n/2$ and $-\hbar\Omega_n/2$, respectively, where the "generalized" Rabi frequency is defined by $\Omega_n = 2g\sqrt{n+1}$. Thus, the previously degenerate state $|a, n\rangle$ and $|b, n+1\rangle$ are split into a doublet of dressed states separated by Ω_n as shown in Fig. 2.4. This is called *dynamic Stark splitting*. The dynamic Stark split doublets have almost equal spacing for $n \gg 1$. As indicated in the Fig. 2.4, the single-photon spontaneous decay spectrum consist of a triplet of lines by the Rabi frequency Ω_n, with the central component being made of two equal contributions.

2.3 Calculation of transition matrix elements

The expression for the fluorescence spectrum is now known. What remains is to calculate the corresponding non-relativistic and relativistic matrix elements, i.e. the matrix elements of the radiation field with the Schrödinger or Dirac wave functions which determine the Rabi frequencies and the radiative decay widths. In this section we derive analytical formulas for these quantities.

2.3.1 Electric dipole interaction matrix elements with Schrödinger wave functions

The interaction of a radiation field with a single-electron atom in dipole approximation has the matrix element

$$\boldsymbol{\gamma}_{ab} = e\langle\Phi_a|\hat{\epsilon}\cdot\mathbf{r}|\Phi_b\rangle\,, \tag{2.134}$$

where Ψ_a and Ψ_b are non-relativistic wave functions, solutions of the Schrödinger equation in a Coulomb potential, e is the elementary charge, and $\hat{\epsilon}$ is a unit vector defining the polarization of the electric field component. The subscript a stands collectively for the principal quantum number n_a as well as the angular momentum quantum number l_a and the magnetic quantum number M_a: $a \equiv (n_a, l_a, M_a)$, and the index b plays a similar role. The electric-dipole matrix elements depend on the electric field polarization, thus we need to discuss the *linear*, *left circular* and *right circular* cases.

1° *Linear polarization*

First we consider linear polarization along the z axis, and we calculate this matrix elements in spherical coordinates, $z = r\cos\phi$. In this case the transition matrix element has the form

$$\gamma^z_{ab} = e\langle\Phi_a|\hat{\epsilon}_z\cdot\mathbf{r}|\Phi_b\rangle = e\int d\mathbf{r}\Phi^\dagger_a(\mathbf{r})r\cos\theta\Phi_b(\mathbf{r}) = eRK^z\,. \tag{2.135}$$

1° *Circular polarization*

The definition of right- and left-handed polarization is $\hat{\epsilon}_\pm = \frac{1}{\sqrt{2}}(\hat{\epsilon}_x \pm i\hat{\epsilon}_y)$. In spherical coordinates, i.e. $x = r\sin\theta\cos\phi$ and $y = r\sin\theta\sin\phi$, the transition matrix elements are

$$\begin{aligned}
\gamma^+_{ab} &= e\langle\Phi_a|\hat{\epsilon}_+\cdot\mathbf{r}|\Phi_b\rangle = \tfrac{e}{\sqrt{2}}\int d\mathbf{r}\Phi^\dagger_a(\mathbf{r})\mathbf{r}\cdot(\hat{\epsilon}_x + i\hat{\epsilon}_y)\Phi_b(\mathbf{r}) = \tfrac{e}{\sqrt{2}}R[K^x + iK^y]\,, \qquad (2.136)\\
\gamma^-_{ab} &= e\langle\Phi_a|\hat{\epsilon}_-\cdot\mathbf{r}|\Phi_b\rangle = \tfrac{e}{\sqrt{2}}\int d\mathbf{r}\Phi^\dagger_a(\mathbf{r})\mathbf{r}\cdot(\hat{\epsilon}_x - i\hat{\epsilon}_y)\Phi_b(\mathbf{r}) = \tfrac{e}{\sqrt{2}}\tfrac{e}{\sqrt{2}}R[K^x - iK^y]\,.
\end{aligned}$$

The integral expression of the radial matrix element R is

$$R = \int dr r^3 R_{n_a l_a}(r)R_{n_b l_b}(r)\,. \tag{2.137}$$

For the Coulomb potential of a point-like nucleus with charge $Z|e|$, the bound radial function $R_a(r)$ can be given in an analytical form by means of the generalized Laguerre polynomials:

$$R_a(r) = -\frac{2Z^{3/2}}{n_a^2 a_0^{3/2}}\sqrt{\frac{(n_a - l_a - 1)!}{(n_a + l_a)!}}\left(\frac{2rZ}{a_0 n_a}\right)^{l_a} e^{-rZ/a_0 n_a} L^{2l_a+1}_{n_a - l_a - 1}\left(\frac{2rZ}{a_0 n_a}\right)\,. \tag{2.138}$$

The Bohr radius a_0 is defined $a_0 = \frac{\hbar}{mc\alpha}$, with α being the fine structure constant. The angular matrix elements have the integral representation

$$\begin{aligned}
K^x &= \sqrt{\frac{2\pi}{3}}\int do_r Y^\dagger_{l_a M_a}(\hat{r})(Y_{1-1} - Y_{11})Y_{l_b M_b}(\hat{r})\,, \quad K^z = \sqrt{\frac{2\pi}{3}}\int do_r Y^\dagger_{l_a M_a}(\hat{r})Y_{10}Y_{l_b M_b}(\hat{r})\,,\\
K^y &= \sqrt{\frac{2\pi}{3}}\int do_r Y^\dagger_{l_a M_a}(\hat{r})(Y_{1-1} + Y_{11})Y_{l_b M_b}(\hat{r})\,, \qquad (2.139)
\end{aligned}$$

which can be reduced to the result

$$\begin{aligned}
K_1^x &= \frac{(-1)^{M_a}}{\sqrt{2}}\sqrt{(2l_a+1)(2l_b+1)}\begin{pmatrix} l_a & 1 & l_b \\ 0 & 0 & 0 \end{pmatrix}\left[\begin{pmatrix} l_a & 1 & l_b \\ -M_a & -1 & -M_b \end{pmatrix} - \begin{pmatrix} l_a & 1 & l_b \\ -M_a & 1 & M_b \end{pmatrix}\right], \\
K_1^y &= \frac{(-1)^{M_a}}{\sqrt{2}}\sqrt{(2l_a+1)(2l_b+1)}\begin{pmatrix} l_a & 1 & l_b \\ 0 & 0 & 0 \end{pmatrix}\left[\begin{pmatrix} l_a & 1 & l_b \\ -M_a & -1 & -M_b \end{pmatrix} + \begin{pmatrix} l_a & 1 & l_b \\ -M_a & 1 & M_b \end{pmatrix}\right], \\
K_1^z &= (-1)^{M_a}\sqrt{(2l_a+1)(2l_b+1)}\begin{pmatrix} l_a & 1 & l_b \\ 0 & 0 & 0 \end{pmatrix}\begin{pmatrix} l_a & 1 & l_b \\ -M_a & 0 & M_b \end{pmatrix}. \qquad (2.140)
\end{aligned}$$

The final analytical result of radial integration can be expressed in terms of generalized hypergeometric functions as

$$\begin{aligned}
R &= \frac{4Z^3}{n_a^2 n_b^2 a_0^3}\sqrt{\frac{(n_a+l_a)!}{(n_a-l_a-1)!}}\sqrt{\frac{(n_b+l_b)!}{(n_b-l_b-1)!}}\left(\frac{2Z}{a_0 n_a}\right)^{l_a}\left(\frac{2Z}{a_0 n_b}\right)^{l_b}\frac{1}{(2l_a+1)}\frac{1}{(2l_b+1)} \\
&\times \sum_{p=0}^{n_a-l_a-1}\frac{(-n_a+l_a+1)_p}{(2l_a+2)_p}\frac{1}{p!}\left(\frac{2Z}{a_0 n_0}\right)^p (3+l_a+l_b+p)!\left(\frac{a_0 n_a n_b}{Z(n_a+n_b)}\right)^{4+l_a+l_b+p} \\
&\times {}_2F_1\left(-n_b+l_b+1, 4+l_a+l_b+p, 2l_b+2; \frac{a_0 n_a n_b}{Z(n_a+n_b)}\right). \qquad (2.141)
\end{aligned}$$

2.3.2 Relativistic dipole interaction matrix elements in the length gauge

We will work first in the so-called *length gauge*, where the transition matrix elements $\boldsymbol{\gamma}_{ab}$ are defined, similarly to the non-relativistic case, as

$$\boldsymbol{\gamma}_{ab} = e\langle\Phi_a|\hat{\epsilon}\cdot\mathbf{r}|\Phi_b\rangle\,, \qquad (2.142)$$

where Ψ_a and Ψ_b are relativistic wave functions, solutions of the Dirac equation in a Coulomb potential, and e is the elementary charge. Because the laser field has a certain polarization, we should again consider all three possibilities.

1° *Linear polarization*

Let us consider the polarization along the z axis, and calculate the matrix elements in spherical coordinates, $z = r\cos\phi$. In this case the transition matrix element has the form

$$\gamma_{ab}^z = e\langle\Phi_a|\hat{\epsilon}_z\cdot\mathbf{r}|\Phi_b\rangle = e\int d\mathbf{r}\Phi_a^\dagger(\mathbf{r})r\cos\theta\Phi_b(\mathbf{r}) = e[R_1K_1^z + R_2K_2^z]\,. \qquad (2.143)$$

2° *Circular polarization*

We consider the right ($\hat{\epsilon}_+$) and left ($\hat{\epsilon}_-$) circular polarization, defined with the polarization unit vectors $\hat{\epsilon}_\pm = \frac{1}{\sqrt{2}}(\hat{\epsilon}_x \pm i\hat{\epsilon}_y)$. In spherical coordinates, i.e. $x = r\sin\theta\cos\phi$ and $y = r\sin\theta\sin\phi$, the transition matrix elements are

$$\begin{aligned}
\gamma_{ab}^+ &= e\langle\Phi_a|\hat{\epsilon}_+\cdot\mathbf{r}|\Phi_b\rangle = \tfrac{e}{\sqrt{2}}\int d\mathbf{r}\Phi_a^\dagger(\mathbf{r})\mathbf{r}\cdot(\hat{\epsilon}_x + i\hat{\epsilon}_y)\Phi_b(\mathbf{r}) \\
&= \tfrac{e}{\sqrt{2}}[R_1K_1^x + R_2K_2^x + iR_1K_1^y + iR_2K_2^y]\,, \\
\gamma_{ab}^- &= e\langle\Phi_a|\hat{\epsilon}_-\cdot\mathbf{r}|\Phi_b\rangle = \tfrac{e}{\sqrt{2}}\int d\mathbf{r}\Phi_a^\dagger(\mathbf{r})\mathbf{r}\cdot(\hat{\epsilon}_x - i\hat{\epsilon}_y)\Phi_b(\mathbf{r}) \\
&= \tfrac{e}{\sqrt{2}}[R_1K_1^x + R_2K_2^x - iR_1K_1^y - iR_2K_2^y]\,. \qquad (2.144)
\end{aligned}$$

The radial matrix elements are denoted as

$$R_1 = \int dr r^3 G_{n_a\kappa_a}(r) G_{n_b\kappa_b}(r)\,, \quad R_2 = \int dr r^3 F_{n_a\kappa_a}(r) F_{n_b\kappa_b}(r)\,, \tag{2.145}$$

and

$$\begin{aligned}
K_1^x &= \int do_r \Omega^\dagger_{\kappa_a M_a}(\hat{r}) \sin\theta\cos\phi \Omega_{\kappa_b M_b}(\hat{r})\,, & K_2^x &= \int do_r \Omega^\dagger_{-\kappa_a M_a}(\hat{r}) \sin\theta\cos\phi \Omega_{-\kappa_b M_b}(\hat{r})\,,\\
K_1^y &= \int do_r \Omega^\dagger_{\kappa_a M_a}(\hat{r}) \sin\theta\sin\phi \Omega_{\kappa_b M_b}(\hat{r})\,, & K_2^y &= \int do_r \Omega^\dagger_{-\kappa_a M_a}(\hat{r}) \sin\theta\sin\phi \Omega_{-\kappa_b M_b}(\hat{r})\,,\\
K_1^z &= \int do_r \Omega^\dagger_{\kappa_a M_a}(\hat{r}) \cos\theta \Omega_{\kappa_b M_b}(\hat{r})\,, & K_2^z &= \int do_r \Omega^\dagger_{-\kappa_a M_a}(\hat{r}) \cos\theta \Omega_{-\kappa_b M_b}(\hat{r})\,.
\end{aligned} \tag{2.146}$$

To bring the angular part to a simpler form we use the formula [BS88]

$$\begin{aligned}
&\int do_r \Omega^\dagger_{\kappa_a M_a}(\hat{r}) Y_{lm}(\hat{r}) \Omega_{\kappa_b M_b}(\hat{r}) = \frac{(-1)^{M_a-1/2}}{\sqrt{4\pi}} \sqrt{(2j_a+1)(2j_b+1)(2l+1)(2l_a+1)(2l_b+1)}\\
&\begin{pmatrix} l_a & l_b & l \\ 0 & 0 & 0 \end{pmatrix} \begin{pmatrix} j_a & j_b & l \\ -M_a & M_b & m \end{pmatrix} \begin{Bmatrix} j_a & j_b & l \\ l_b & l_a & 1/2 \end{Bmatrix}.
\end{aligned} \tag{2.147}$$

Applying Euler's formula, it is easy to see that

$$\sin\theta\sin\phi = i\sqrt{\frac{2\pi}{3}}\left(Y_{1-1} + Y_{11}\right)\,,\ \sin\theta\cos\phi = \sqrt{\frac{2\pi}{3}}\left(Y_{1-1} - Y_{11}\right)\,,\ \cos\theta = 2\sqrt{\frac{\pi}{3}} Y_{10}\,, \tag{2.148}$$

and the final result for the angular parts are

$$\begin{aligned}
K_1^x &= \frac{(-1)^{M_a-1/2}}{\sqrt{2}} \sqrt{(2j_a+1)(2j_b+1)(2l_a+1)(2l_b+1)} \begin{pmatrix} l_a & l_b & 1 \\ 0 & 0 & 0 \end{pmatrix} \\
&\times \left[\begin{pmatrix} j_a & j_b & 1 \\ -M_a & M_b & -1 \end{pmatrix} - \begin{pmatrix} j_a & j_b & 1 \\ -M_a & M_b & 1 \end{pmatrix} \right] \begin{Bmatrix} j_a & j_b & 1 \\ l_b & l_a & 1/2 \end{Bmatrix},
\end{aligned} \tag{2.149}$$

$$\begin{aligned}
K_2^x &= \frac{(-1)^{M_a-1/2}}{\sqrt{2}} \sqrt{(2j_a+1)(2j_b+1)(2l'_a+1)(2l'_b+1)} \begin{pmatrix} l'_a & l'_b & 1 \\ 0 & 0 & 0 \end{pmatrix} \\
&\times \left[\begin{pmatrix} j_a & j_b & 1 \\ -M_a & M_b & -1 \end{pmatrix} - \begin{pmatrix} j_a & j_b & 1 \\ -M_a & M_b & 1 \end{pmatrix} \right] \begin{Bmatrix} j_a & j_b & 1 \\ l'_b & l'_a & 1/2 \end{Bmatrix},
\end{aligned} \tag{2.150}$$

$$\begin{aligned}
K_1^y &= i\frac{(-1)^{M_a-1/2}}{\sqrt{2}} \sqrt{(2j_a+1)(2j_b+1)(2l_a+1)(2l_b+1)} \begin{pmatrix} l_a & l_b & 1 \\ 0 & 0 & 0 \end{pmatrix} \\
&\times \left[\begin{pmatrix} j_a & j_b & 1 \\ -M_a & M_b & -1 \end{pmatrix} + \begin{pmatrix} j_a & j_b & 1 \\ -M_a & M_b & 1 \end{pmatrix} \right] \begin{Bmatrix} j_a & j_b & 1 \\ l_b & l_a & 1/2 \end{Bmatrix},
\end{aligned} \tag{2.151}$$

$$\begin{aligned}
K_2^y &= i\frac{(-1)^{M_a-1/2}}{\sqrt{2}} \sqrt{(2j_a+1)(2j_b+1)(2l'_a+1)(2l'_b+1)} \begin{pmatrix} l'_a & l'_b & 1 \\ 0 & 0 & 0 \end{pmatrix} \\
&\times \left[\begin{pmatrix} j_a & j_b & 1 \\ -M_a & M_b & -1 \end{pmatrix} + \begin{pmatrix} j_a & j_b & 1 \\ -M_a & M_b & 1 \end{pmatrix} \right] \begin{Bmatrix} j_a & j_b & 1 \\ l'_b & l'_a & 1/2 \end{Bmatrix},
\end{aligned} \tag{2.152}$$

$$K_1^z = (-1)^{M_a-1/2}\sqrt{(2j_a+1)(2j_b+1)(2l_a+1)(2l_b+1)}\begin{pmatrix} l_a & l_b & 1 \\ 0 & 0 & 0 \end{pmatrix} \times \begin{pmatrix} j_a & j_b & 1 \\ -M_a & M_b & 0 \end{pmatrix}\begin{Bmatrix} j_a & j_b & 1 \\ l_b & l_a & 1/2 \end{Bmatrix}, \tag{2.153}$$

$$K_2^z = (-1)^{M_a-1/2}\sqrt{(2j_a+1)(2j_b+1)(2l'_a+1)(2l'_b+1)}\begin{pmatrix} l'_a & l'_b & 1 \\ 0 & 0 & 0 \end{pmatrix} \times \begin{pmatrix} j_a & j_b & 1 \\ -M_a & M_b & 0 \end{pmatrix}\begin{Bmatrix} j_a & j_b & 1 \\ l'_b & l'_a & 1/2 \end{Bmatrix}. \tag{2.154}$$

The radial integrals can be calculated to yield

$$R_1 = \left(1+\frac{E_a}{mc^2}\right)^{1/2}\left(1+\frac{E_b}{mc^2}\right)^{1/2} U_a U_b [R_1^1 - R_1^2 - R_1^3 + R_1^4], \tag{2.155}$$
$$R_2 = \left(1-\frac{E_a}{mc^2}\right)^{1/2}\left(1-\frac{E_b}{mc^2}\right)^{1/2} U_a U_b [R_1^1 + R_1^2 + R_1^3 + R_1^4],$$

where we introduced the following shorthand notations:

$$R_1^1 = n_a^r n_b^r (2\lambda_a)^{\gamma_a-1}(2\lambda_b)^{\gamma_b-1}\sum_{m=0}^{n_a^r-1}\frac{(-n_a^r+1)_m}{(2\gamma_a+1)_m}\frac{(2\lambda_a)^m}{m!}\frac{\Gamma(m+\gamma_a+\gamma_b+2)}{(\lambda_a+\lambda_b)^{m+\gamma_a+\gamma_b+2}} \times {}_2F_1\left(m+\gamma_a+\gamma_b+2, -n_b^r+1, 2\gamma_b+1; \frac{2\lambda_b}{\lambda_a+\lambda_b}\right), \tag{2.156}$$

$$R_1^2 = n_a^r (N_b-\kappa_b)(2\lambda_a)^{\gamma_a-1}(2\lambda_b)^{\gamma_b-1}\sum_{m=0}^{n_a^r-1}\frac{(-n_a^r+1)_m}{(2\gamma_a+1)_m}\frac{(2\lambda_a)^m}{m!}\frac{\Gamma(m+\gamma_a+\gamma_b+2)}{(\lambda_a+\lambda_b)^{m+\gamma_a+\gamma_b+2}} \times {}_2F_1\left(m+\gamma_a+\gamma_b+2, -n_b^r, 2\gamma_b+1; \frac{2\lambda_b}{\lambda_a+\lambda_b}\right),$$

$$R_1^3 = (N_a-\kappa_a) n_b^r (2\lambda_a)^{\gamma_a-1}(2\lambda_b)^{\gamma_b-1}\sum_{m=0}^{n_a^r}\frac{(-n_a^r)_m}{(2\gamma_a+1)_m}\frac{(2\lambda_a)^m}{m!}\frac{\Gamma(m+\gamma_a+\gamma_b+2)}{(\lambda_a+\lambda_b)^{m+\gamma_a+\gamma_b+2}} \times {}_2F_1\left(m+\gamma_a+\gamma_b+2, -n_b^r+1, 2\gamma_b+1; \frac{2\lambda_b}{\lambda_a+\lambda_b}\right),$$

$$R_1^4 = (N_a-\kappa_a)(N_b-\kappa_b)(2\lambda_a)^{\gamma_a-1}(2\lambda_b)^{\gamma_b-1}\sum_{m=0}^{n_a^r}\frac{(-n_a^r)_m}{(2\gamma_a+1)_m}\frac{(2\lambda_a)^m}{m!}\frac{\Gamma(m+\gamma_a+\gamma_b+2)}{(\lambda_a+\lambda_b)^{m+\gamma_a+\gamma_b+2}} \times {}_2F_1\left(m+\gamma_a+\gamma_b+2, -n_b^r, 2\gamma_b+1; \frac{2\lambda_b}{\lambda_a+\lambda_b}\right).$$

Again, for Coulomb potentials, we used the representation of bound radial functions $G_a(r)$ and $F_a(r)$ in terms of confluent hypergeometric functions with negative-integral first argument (see, e.g. Ref. [BS88]):

$$G_a(r) = \left(1+\frac{E_a}{mc^2}\right)^{1/2} U_a (A_a - B_a), \tag{2.157}$$
$$F_a(r) = -\left(1-\frac{E_a}{mc^2}\right)^{1/2} U_a (A_a + B_a),$$

where the eigenenergies are given by the Sommerfeld formula

$$E_a = mc^2 \left(1 + \frac{(Z\alpha)^2}{\left(n_a - j_a - 1/2 + \sqrt{(j_a+1/2)^2 - (Z\alpha)^2} \right)^2} \right)^{-1/2} . \tag{2.158}$$

In the above equations, furthermore, the following functions are used:

$$\begin{aligned} U_a &= \frac{(2\lambda_a)^{3/2}}{\Gamma(2\gamma_a+1)} \left(\frac{\Gamma(2\gamma_a + n_a^r + 1)}{4N_a(N_a-\kappa_a) n_a^r!} \right)^{1/2} , \\ A_a(r) &= n_{a1}^r F_1(-n_a^r + 1, 2\gamma_a + 1; 2\lambda_a r) e^{-\lambda_a r} (2\lambda_a r)^{\gamma_a - 1} , \\ B_a(r) &= (N_a - \kappa_a)_1 F_1(-n_a^r, 2\gamma_a + 1; 2\lambda_a r) e^{-\lambda_a r} (2\lambda_a r)^{\gamma_a - 1} . \end{aligned} \tag{2.159}$$

Here, ${}_1F_1$ is the confluent hyper-geometric function defined by its expansion [AS72] with coefficients involving Gamma functions:

$$\begin{aligned} {}_1F_1(-n, b; z) &= \sum_{m=0}^{n} \frac{(-n)_m}{(b)_m} \frac{z^m}{m!} , \\ (a)_m &= \frac{\Gamma(a+m)}{\Gamma(a)}, \quad (a)_0 \equiv 1 , \end{aligned} \tag{2.160}$$

and its parameters are

$$\begin{aligned} \lambda_a &= \frac{\sqrt{m^2c^4 - E_a^2}}{\hbar c}, \quad N_a = \frac{(n_a^r + \gamma_a) mc^2}{E_a} , \\ \gamma_a &= \sqrt{\kappa_a^2 - (Z\alpha)^2}, \quad n_a^r = n_a - |\kappa_a| , \\ \kappa_a &= \begin{cases} -(l_a+1) & \text{if } j_a = l_a + \frac{1}{2}, \\ l_a & \text{if } j_a = l_a - \frac{1}{2}. \end{cases} \end{aligned} \tag{2.161}$$

As the first argument of the confluent hypergeometric function is an integer, it can be written as a polynomial [AS72], simplifying the numerical evaluation of the wave function. The spin-angular part of the Dirac wave function is defined by the spherical spinors

$$\Omega_{\kappa_a M_a}(\hat{r}) = \sum_{m_a=-l_a}^{l_a} \sum_{\mu_a = \pm 1/2} C\left(l_a \frac{1}{2} j_a; m_a \mu_a M_a \right) Y_{l_a m_a}(\theta, \phi) \chi_{\mu_a} . \tag{2.162}$$

Here, χ_{μ_a} denotes the usual two-component Pauli spinors:

$$\chi_{1/2} = \begin{pmatrix} 1 \\ 0 \end{pmatrix}, \quad \chi_{-1/2} = \begin{pmatrix} 0 \\ 1 \end{pmatrix} . \tag{2.163}$$

2.3.3 Relativistic dipole interaction matrix elements in the transverse gauge

The transverse gauge (also called Coulomb gauge) can be regarded as the relativistic generalization of the familiar velocity form. In the following we formulate the atom-field interaction in this gauge. As in the case of the form $\mathbf{r} \cdot \mathbf{E}$, in the case of the $\boldsymbol{\alpha} \cdot \mathbf{A}$ interaction, the transition matrix element can be defined as

$$\boldsymbol{\gamma}_{ab} = \frac{ec}{\omega} \langle \Phi_a | \hat{\epsilon} \cdot \boldsymbol{\alpha} | \Phi_b \rangle . \tag{2.164}$$

One should consider also the two cases of *linear* and *circular* polarization for the laser field.

1° *Linear polarization*

For the polarization along the z axis, the matrix elements have the form

$$\boldsymbol{\gamma}^z_{ab} = \frac{ec}{\omega}\langle\Phi_a|\boldsymbol{\alpha}_z|\Phi_b\rangle = \frac{ec}{\omega}\int d\mathbf{r}\Phi^\dagger_a(\mathbf{r})\boldsymbol{\alpha}_z\Phi_b(\mathbf{r}) = -i\frac{ec}{\omega}[R_1K^z_1 - R_2K^z_2]\,. \tag{2.165}$$

2° *Circular polarization*

For the right- and left-circular polarization, the matrix elements are

$$\begin{aligned}
\boldsymbol{\gamma}^+_{ab} &= \frac{ec}{\omega}\langle\Phi_a|\boldsymbol{\alpha}\cdot\hat{\epsilon}_+|\Phi_b\rangle = \frac{1}{\sqrt{2}}\frac{ec}{\omega}\int d\mathbf{r}\Phi^\dagger_a(\mathbf{r})\boldsymbol{\alpha}\cdot(\hat{\epsilon}_x + i\hat{\epsilon}_y)\Phi_b(\mathbf{r}) \\
&= -\frac{i}{\sqrt{2}}\frac{ec}{\omega}\{R_1[K^x_1 + iK^y_1] - R_2[K^x_2 + iK^y_2]\}\,, \\
\boldsymbol{\gamma}^-_{ab} &= \frac{ec}{\omega}\langle\Phi_a|\boldsymbol{\alpha}\cdot\hat{\epsilon}_-|\Phi_b\rangle = \frac{1}{\sqrt{2}}\frac{ec}{\omega}\int d\mathbf{r}\Phi^\dagger_a(\mathbf{r})\boldsymbol{\alpha}\cdot(\hat{\epsilon}_x - i\hat{\epsilon}_y)\Phi_b(\mathbf{r}) \\
&= -\frac{i}{\sqrt{2}}\frac{ec}{\omega}\{R_1[K^x_1 - iK^y_1] - R_2[K^x_2 - iK^y_2]\}\,,
\end{aligned} \tag{2.166}$$

with the radial parts

$$R_1 \equiv \int drr^2 G_{n_b\kappa_b}(r)F_{n_a\kappa_a}(r), \quad R_2 \equiv \int drr^2 F_{n_b\kappa_b}(r)G_{n_a\kappa_a}(r), \tag{2.167}$$

and angular parts

$$\begin{aligned}
K^x_1 &= \int do_r\Omega^\dagger_{-\kappa_aM_a}(\hat{r})\sigma_x\Omega_{\kappa_bM_b}(\hat{r}), \quad K^x_2 = \int do_r\Omega^\dagger_{\kappa_aM_a}(\hat{r})\sigma_x\Omega_{-\kappa_bM_b}(\hat{r})\,, \\
K^y_1 &= \int do_r\Omega^\dagger_{-\kappa_aM_a}(\hat{r})\sigma_y\Omega_{\kappa_bM_b}(\hat{r}), \quad K^y_2 = \int do_r\Omega^\dagger_{\kappa_aM_a}(\hat{r})\sigma_y\Omega_{-\kappa_bM_b}(\hat{r})\,, \\
K^z_1 &= \int do_r\Omega^\dagger_{-\kappa_aM_a}(\hat{r})\sigma_z\Omega_{\kappa_bM_b}(\hat{r}), \quad K^z_2 = \int do_r\Omega^\dagger_{\kappa_aM_a}(\hat{r})\sigma_z\Omega_{-\kappa_bM_b}(\hat{r})\,.
\end{aligned} \tag{2.168}$$

After some lengthy but straightforward calculation, we get the final results for the angular parts:

$$\begin{aligned}
K^x_1 &= (-1)^{j_a+j_b-M_b+3/2}\sqrt{(2j_a+1)(2j_b+1)(2l'_a+1)(2l_b+1)}\begin{pmatrix} l'_a & l_b & 0 \\ 0 & 0 & 0\end{pmatrix}(a^1_1 - a^1_2)\,, \\
K^x_2 &= (-1)^{j_a+j_b-M_b+3/2}\sqrt{(2j_a+1)(2j_b+1)(2l_a+1)(2l'_b+1)}\begin{pmatrix} l_a & l'_b & 0 \\ 0 & 0 & 0\end{pmatrix}(a^2_1 - a^2_2)\,, \\
K^y_1 &= -i(-1)^{j_a+j_b-M_b+3/2}\sqrt{(2j_a+1)(2j_b+1)(2l'_a+1)(2l_b+1)}\begin{pmatrix} l'_a & l_b & 0 \\ 0 & 0 & 0\end{pmatrix}(a^1_1 + a^1_2)\,, \\
K^y_2 &= -i(-1)^{j_a+j_b-M_b+3/2}\sqrt{(2j_a+1)(2j_b+1)(2l_a+1)(2l'_b+1)}\begin{pmatrix} l_a & l'_b & 0 \\ 0 & 0 & 0\end{pmatrix}(a^2_1 + a^2_2)\,, \\
K^z_1 &= (-1)^{j_a+j_b-M_b+3/2}\sqrt{(2j_a+1)(2j_b+1)(2l'_a+1)(2l_b+1)}\begin{pmatrix} l'_a & l_b & 0 \\ 0 & 0 & 0\end{pmatrix}(b^1_1 + b^1_2)\,, \\
K^z_2 &= (-1)^{j_a+j_b-M_b+3/2}\sqrt{(2j_a+1)(2j_b+1)(2l_a+1)(2l'_b+1)} \\
&\times \begin{pmatrix} l_a & l'_b & 0 \\ 0 & 0 & 0\end{pmatrix}(b^2_1 + b^2_2)\,,
\end{aligned} \tag{2.169}$$

where the following notations were used:

$$
\begin{aligned}
a_1^1 &= \begin{pmatrix} l'_a & j_a & 1/2 \\ M_a - 1/2 & -M_a & 1/2 \end{pmatrix} \begin{pmatrix} l_b & j_b & 1/2 \\ M_b + 1/2 & -M_b & -1/2 \end{pmatrix} \begin{pmatrix} l'_a & l_b & 0 \\ -M_a + 1/2 & M_b + 1/2 & 0 \end{pmatrix}, \\
a_2^1 &= \begin{pmatrix} l'_a & j_a & 1/2 \\ M_a + 1/2 & -M_a & -1/2 \end{pmatrix} \begin{pmatrix} l_b & j_b & 1/2 \\ M_b - 1/2 & -M_b & 1/2 \end{pmatrix} \begin{pmatrix} l'_a & l_b & 0 \\ -M_a - 1/2 & M_b - 1/2 & 0 \end{pmatrix}, \\
b_1^1 &= \begin{pmatrix} l'_a & j_a & 1/2 \\ M_a - 1/2 & -M_a & 1/2 \end{pmatrix} \begin{pmatrix} l_b & j_b & 1/2 \\ M_b - 1/2 & -M_b & 1/2 \end{pmatrix} \begin{pmatrix} l'_a & l_b & 0 \\ -M_a + 1/2 & M_b - 1/2 & 0 \end{pmatrix}, \\
b_2^1 &= \begin{pmatrix} l'_a & j_a & 1/2 \\ M_a + 1/2 & -M_a & -1/2 \end{pmatrix} \begin{pmatrix} l_b & j_b & 1/2 \\ M_b + 1/2 & -M_b & -1/2 \end{pmatrix} \begin{pmatrix} l'_a & l_b & 0 \\ -M_a - 1/2 & M_b + 1/2 & 0 \end{pmatrix}, \\
a_1^2 &= \begin{pmatrix} l_a & j_a & 1/2 \\ M_a - 1/2 & -M_a & 1/2 \end{pmatrix} \begin{pmatrix} l'_b & j_b & 1/2 \\ M_b + 1/2 & -M_b & -1/2 \end{pmatrix} \begin{pmatrix} l_a & l'_b & 0 \\ -M_a + 1/2 & M_b + 1/2 & 0 \end{pmatrix}, \\
a_2^2 &= \begin{pmatrix} l_a & j_a & 1/2 \\ M_a + 1/2 & -M_a & -1/2 \end{pmatrix} \begin{pmatrix} l'_b & j_b & 1/2 \\ M_b - 1/2 & -M_b & 1/2 \end{pmatrix} \begin{pmatrix} l_a & l'_b & 0 \\ -M_a - 1/2 & M_b - 1/2 & 0 \end{pmatrix}, \\
b_1^2 &= \begin{pmatrix} l_a & j_a & 1/2 \\ M_a - 1/2 & -M_a & 1/2 \end{pmatrix} \begin{pmatrix} l'_b & j_b & 1/2 \\ M_b - 1/2 & -M_b & 1/2 \end{pmatrix} \begin{pmatrix} l_a & l'_b & 0 \\ -M_a + 1/2 & M_b - 1/2 & 0 \end{pmatrix}, \\
b_2^2 &= \begin{pmatrix} l_a & j_a & 1/2 \\ M_a + 1/2 & -M_a & -1/2 \end{pmatrix} \begin{pmatrix} l'_b & j_b & 1/2 \\ M_b + 1/2 & -M_b & -1/2 \end{pmatrix} \\
&\quad \times \begin{pmatrix} l_a & l'_b & 0 \\ -M_a - 1/2 & M_b + 1/2 & 0 \end{pmatrix}.
\end{aligned} \tag{2.170}
$$

For the radial part we find the final expressions

$$
\begin{aligned}
R_1 &= -\left(1 - \frac{E_a}{mc^2}\right)^{1/2} \left(1 + \frac{E_b}{mc^2}\right)^{1/2} U_a U_b [R_1^1 + R_1^2 - R_1^3 - R_1^4], \\
R_2 &= -\left(1 + \frac{E_a}{mc^2}\right)^{1/2} \left(1 - \frac{E_b}{mc^2}\right)^{1/2} U_a U_b [R_1^1 - R_1^2 + R_1^3 - R_1^4],
\end{aligned} \tag{2.171}
$$

where the following polynomials need to be inserted:

$$
\begin{aligned}
R_1^1 &= n_a^r n_b^r (2\lambda_a)^{\gamma_a - 1} (2\lambda_b)^{\gamma_b - 1} \sum_{m=0}^{n_b^r - 1} \frac{(-n_b^r + 1)_m}{(2\gamma_b + 1)_m} \frac{(2\lambda_b)^m}{m!} \frac{\Gamma(m + \gamma_a + \gamma_b + 1)}{(\lambda_a + \lambda_b)^{m + \gamma_a + \gamma_b + 1}} \\
&\quad \times \; {}_2F_1\left(m + \gamma_a + \gamma_b + 1, -n_a^r + 1, 2\gamma_a + 1; \frac{2\lambda_a}{\lambda_a + \lambda_b}\right),
\end{aligned} \tag{2.172}
$$

$$
\begin{aligned}
R_1^2 &= (N_a - \kappa_a) n_b^r (2\lambda_a)^{\gamma_a - 1} (2\lambda_b)^{\gamma_b - 1} \sum_{m=0}^{n_b^r - 1} \frac{(-n_b^r + 1)_m}{(2\gamma_b + 1)_m} \frac{(2\lambda_b)^m}{m!} \frac{\Gamma(m + \gamma_a + \gamma_b + 1)}{(\lambda_a + \lambda_b)^{m + \gamma_a + \gamma_b + 1}} \\
&\quad \times \; {}_2F_1\left(m + \gamma_a + \gamma_b + 1, -n_a^r, 2\gamma_a + 1; \frac{2\lambda_a}{\lambda_a + \lambda_b}\right),
\end{aligned} \tag{2.173}
$$

$$
\begin{aligned}
R_1^3 &= n_a^r (N_b - \kappa_b) (2\lambda_a)^{\gamma_a - 1} (2\lambda_b)^{\gamma_b - 1} \sum_{m=0}^{n_b^r} \frac{(-n_b^r)_m}{(2\gamma_b + 1)_m} \frac{(2\lambda_b)^m}{m!} \frac{\Gamma(m + \gamma_a + \gamma_b + 1)}{(\lambda_a + \lambda_b)^{m + \gamma_a + \gamma_b + 1}} \\
&\quad \times \; {}_2F_1\left(m + \gamma_a + \gamma_b + 1, -n_a^r + 1, 2\gamma_a + 1; \frac{2\lambda_a}{\lambda_a + \lambda_b}\right),
\end{aligned} \tag{2.174}
$$

$$R_1^4 = (N_a-\kappa_a)(N_b-\kappa_b)(2\lambda_a)^{\gamma_a-1}(2\lambda_b)^{\gamma_b-1}\sum_{m=0}^{n_b^r}\frac{(-n_b^r)_m}{(2\gamma_b+1)_m}\frac{(2\lambda_b)^m}{m!}\frac{\Gamma(m+\gamma_a+\gamma_b+1)}{(\lambda_a+\lambda_b)^{m+\gamma_a+\gamma_b+1}}$$
$$\times \ {}_2F_1\left(m+\gamma_a+\gamma_b+1,-n_a^r,2\gamma_a+1;\frac{2\lambda_a}{\lambda_a+\lambda_b}\right). \quad (2.175)$$

Now, we have all analytical expressions needed to calculate the transition matrix elements.

2.3.4 Magnetic dipole interaction in the transverse gauge

We follow the procedure applied in the previous two subsections. Here we are going beyond the electric dipole approximation, which allows us to describe magnetic transitions and electric transitions of higher multipolarity. We expand the exponential $e^{\pm i\mathbf{kr}}$ in a sum of the electric and magnetic dipole terms (the first two terms)

$$\langle\Phi_a|\boldsymbol{\alpha}\cdot\mathbf{A}|\Phi_b\rangle \simeq \langle\Phi_a|\boldsymbol{\alpha}\cdot\hat{\epsilon}_{\mathbf{k}}\mathcal{A}_{\mathbf{k}}\left(a_{\mathbf{k}}+i\mathbf{k}\cdot\mathbf{r}a_{\mathbf{k}}+a_{\mathbf{k}}^\dagger-i\mathbf{k}\cdot\mathbf{r}a_{\mathbf{k}}^\dagger\right)|\Phi_b\rangle \quad (2.176)$$
$$= \langle\Phi_a|\boldsymbol{\alpha}\cdot\hat{\epsilon}_{\mathbf{k}}\mathcal{A}_{\mathbf{k}}\left(a_{\mathbf{k}}+a_{\mathbf{k}}^\dagger\right)|\Phi_b\rangle + \langle\Phi_a|\boldsymbol{\alpha}\cdot\hat{\epsilon}_{\mathbf{k}}\mathcal{A}_{\mathbf{k}}i\mathbf{k}\cdot\mathbf{r}\left(a_{\mathbf{k}}-a_{\mathbf{k}}^\dagger\right)|\Phi_b\rangle.$$

We recognize the first term as the term for the $E1$ transition, for which

$$\boldsymbol{\gamma}_{ab}^{E1} = \frac{ec}{\omega}\langle\Phi_a|\hat{\epsilon}_\lambda\cdot\boldsymbol{\alpha}|\Phi_b\rangle\,. \quad (2.177)$$

The second term corresponds to a magnetic transition, and the corresponding $\boldsymbol{\gamma}_{ab}$ matrix is defined as

$$\boldsymbol{\gamma}_{ab}^{M1} = \frac{ec}{\omega}\langle\Phi_a|\hat{\epsilon}_\lambda\cdot\boldsymbol{\alpha}i\mathbf{k}\cdot\mathbf{r}|\Phi_b\rangle\,. \quad (2.178)$$

As in the previous calculations, we need to analyze the problem considering the laser polarization.

1° *Linear polarization*

First we take the polarization along the z direction:

$$\boldsymbol{\gamma}_{ab}^z = -e\langle\Phi_a|\hat{\epsilon}_z\cdot\boldsymbol{\alpha}r\cos\theta|\Phi_b\rangle = -e\int d\mathbf{r}\Phi_a^\dagger(\mathbf{r})\boldsymbol{\alpha}_z r\cos\theta\Phi_b(\mathbf{r}) = ie[R_1K_1^z - R_2K_2^z]\,. \quad (2.179)$$

2° *Circular polarization*

In this case, the matrix elements are

$$\boldsymbol{\gamma}_{ab}^+ = -e\langle\Phi_a|\hat{\epsilon}_+\cdot\boldsymbol{\alpha}r\cos\theta|\Phi_b\rangle = -\frac{e}{\sqrt{2}}\int d\mathbf{r}\Phi_a^\dagger(\mathbf{r})\boldsymbol{\alpha}\cdot(\hat{\epsilon}_x+i\hat{\epsilon}_y)r\cos\theta\Phi_b(\mathbf{r}) \quad (2.180)$$
$$= -i\frac{e}{\sqrt{2}}\{R_1[-iK_1^x+K_1^y]+R_2[iK_2^x+K_2^y]\}\,,$$
$$\boldsymbol{\gamma}_{ab}^- = -e\langle\Phi_a|\hat{\epsilon}_-\cdot\boldsymbol{\alpha}r\cos\theta|\Phi_b\rangle = -\frac{e}{\sqrt{2}}\int d\mathbf{r}\Phi_a^\dagger(\mathbf{r})\boldsymbol{\alpha}\cdot(\hat{\epsilon}_x-i\hat{\epsilon}_y)r\cos\theta\Phi_b(\mathbf{r})$$
$$= -i\frac{e}{\sqrt{2}}\{R_1[-iK_1^x-K_1^y]+R_2[iK_2^x-K_2^y]\}\,,$$

with the radial integrals

$$R_1 = \int drr^3G_{n_b\kappa_b}(r)F_{n_a\kappa_a}(r), \quad R_2 = \int drr^3F_{n_b\kappa_b}(r)G_{n_a\kappa_a}(r)\,, \quad (2.181)$$

and angular parts

$$
\begin{aligned}
K_1^x &= \int do_r \Omega^\dagger_{-\kappa_a M_a}(\hat{r})\sigma_x \cos\theta \Omega_{\kappa_b M_b}(\hat{r})\,, \quad K_2^x = \int do_r \Omega^\dagger_{\kappa_a M_a}(\hat{r})\sigma_x \cos\theta \Omega_{-\kappa_b M_b}(\hat{r})\,,\\
K_1^y &= \int do_r \Omega^\dagger_{-\kappa_a M_a}(\hat{r})\sigma_y \cos\theta \Omega_{\kappa_b M_b}(\hat{r})\,, \quad K_2^y = \int do_r \Omega^\dagger_{\kappa_a M_a}(\hat{r})\sigma_y \cos\theta \Omega_{-\kappa_b M_b}(\hat{r})\,,\\
K_1^z &= \int do_r \Omega^\dagger_{-\kappa_a M_a}(\hat{r})\sigma_z \cos\theta \Omega_{\kappa_b M_b}(\hat{r})\,,\\
K_2^z &= \int do_r \Omega^\dagger_{\kappa_a M_a}(\hat{r})\sigma_z \cos\theta \Omega_{-\kappa_b M_b}(\hat{r})\,.
\end{aligned}
\tag{2.182}
$$

The integrations can again be performed using group theoretic methods, and yield

$$
\begin{aligned}
K_1^x &= (-1)^{j_a+j_b-M_b+3/2}\sqrt{(2j_a+1)(2j_b+1)(2l'_a+1)(2l_b+1)}\begin{pmatrix} l'_a & l_b & 1\\ 0 & 0 & 0\end{pmatrix}(a_1^1 - a_2^1)\,,\\
K_2^x &= (-1)^{j_a+j_b-M_b+3/2}\sqrt{(2j_a+1)(2j_b+1)(2l_a+1)(2l'_b+1)}\begin{pmatrix} l_a & l'_b & 1\\ 0 & 0 & 0\end{pmatrix}(a_1^2 - a_2^2)\,,\\
K_1^y &= -i(-1)^{j_a+j_b-M_b+3/2}\sqrt{(2j_a+1)(2j_b+1)(2l'_a+1)(2l_b+1)}\begin{pmatrix} l'_a & l_b & 1\\ 0 & 0 & 0\end{pmatrix}(a_1^1 + a_2^1)\,,\\
K_2^y &= -i(-1)^{j_a+j_b-M_b+3/2}\sqrt{(2j_a+1)(2j_b+1)(2l_a+1)(2l'_b+1)}\begin{pmatrix} l_a & l'_b & 1\\ 0 & 0 & 0\end{pmatrix}(a_1^2 + a_2^2)\,,\\
K_1^z &= (-1)^{j_a+j_b-M_b+3/2}\sqrt{(2j_a+1)(2j_b+1)(2l'_a+1)(2l_b+1)}\begin{pmatrix} l'_a & l_b & 1\\ 0 & 0 & 0\end{pmatrix}(b_1^1 + b_2^1)\,,\\
K_2^z &= (-1)^{j_a+j_b-M_b+3/2}\sqrt{(2j_a+1)(2j_b+1)(2l_a+1)(2l'_b+1)}\\
&\times \begin{pmatrix} l_a & l'_b & 1\\ 0 & 0 & 0\end{pmatrix}(b_1^2 + b_2^2)\,,
\end{aligned}
\tag{2.183}
$$

with the expressions

$$
\begin{aligned}
a_1^1 &= \begin{pmatrix} l'_a & j_a & 1/2\\ M_a - 1/2 & -M_a & 1/2\end{pmatrix}\begin{pmatrix} l_b & j_b & 1/2\\ M_b + 1/2 & -M_b & -1/2\end{pmatrix}\begin{pmatrix} l'_a & l_b & 1\\ -M_a + 1/2 & M_b + 1/2 & 0\end{pmatrix},\\
a_2^1 &= \begin{pmatrix} l'_a & j_a & 1/2\\ M_a + 1/2 & -M_a & -1/2\end{pmatrix}\begin{pmatrix} l_b & j_b & 1/2\\ M_b - 1/2 & -M_b & 1/2\end{pmatrix}\begin{pmatrix} l'_a & l_b & 1\\ -M_a - 1/2 & M_b - 1/2 & 0\end{pmatrix},\\
b_1^1 &= \begin{pmatrix} l'_a & j_a & 1/2\\ M_a - 1/2 & -M_a & 1/2\end{pmatrix}\begin{pmatrix} l_b & j_b & 1/2\\ M_b - 1/2 & -M_b & 1/2\end{pmatrix}\begin{pmatrix} l'_a & l_b & 1\\ -M_a + 1/2 & M_b - 1/2 & 0\end{pmatrix},\\
b_2^1 &= \begin{pmatrix} l'_a & j_a & 1/2\\ M_a + 1/2 & -M_a & -1/2\end{pmatrix}\begin{pmatrix} l_b & j_b & 1/2\\ M_b + 1/2 & -M_b & -1/2\end{pmatrix}\begin{pmatrix} l'_a & l_b & 1\\ -M_a - 1/2 & M_b + 1/2 & 0\end{pmatrix},\\
a_1^2 &= \begin{pmatrix} l_a & j_a & 1/2\\ M_a - 1/2 & -M_a & 1/2\end{pmatrix}\begin{pmatrix} l'_b & j_b & 1/2\\ M_b + 1/2 & -M_b & -1/2\end{pmatrix}\begin{pmatrix} l_a & l'_b & 1\\ -M_a + 1/2 & M_b + 1/2 & 0\end{pmatrix},\\
a_2^2 &= \begin{pmatrix} l_a & j_a & 1/2\\ M_a + 1/2 & -M_a & -1/2\end{pmatrix}\begin{pmatrix} l'_b & j_b & 1/2\\ M_b - 1/2 & -M_b & 1/2\end{pmatrix}\begin{pmatrix} l_a & l'_b & 1\\ -M_a - 1/2 & M_b - 1/2 & 0\end{pmatrix},\\
b_1^2 &= \begin{pmatrix} l_a & j_a & 1/2\\ M_a - 1/2 & -M_a & 1/2\end{pmatrix}\begin{pmatrix} l'_b & j_b & 1/2\\ M_b - 1/2 & -M_b & 1/2\end{pmatrix}\begin{pmatrix} l_a & l'_b & 1\\ -M_a + 1/2 & M_b - 1/2 & 0\end{pmatrix},\\
b_2^2 &= \begin{pmatrix} l_a & j_a & 1/2\\ M_a + 1/2 & -M_a & -1/2\end{pmatrix}\begin{pmatrix} l'_b & j_b & 1/2\\ M_b + 1/2 & -M_b & -1/2\end{pmatrix}\\
&\times \begin{pmatrix} l_a & l'_b & 1\\ -M_a - 1/2 & M_b + 1/2 & 0\end{pmatrix}.
\end{aligned}
\tag{2.184}
$$

The analytical results for radial integrals can be written in the rather concise form as

$$R_1 = -\left(1-\frac{E_a}{mc^2}\right)^{1/2}\left(1+\frac{E_b}{mc^2}\right)^{1/2} U_a U_b[R_1^1 - R_1^2 + R_1^3 - R_1^4]\,, \tag{2.185}$$
$$R_2 = -\left(1+\frac{E_a}{mc^2}\right)^{1/2}\left(1-\frac{E_b}{mc^2}\right)^{1/2} U_a U_b[R_1^1 + R_1^2 - R_1^3 - R_1^4]\,,$$

where the quantities R_1^i, $i \in \{1,2,3,4\}$, have been given previously in the Eqs. (2.156).

2.3.5 Multipole interaction matrix elements in the transverse gauge

We start using the expansion

$$e^{i\mathbf{kr}} = 4\pi \sum_{lm} i^l j_l(kr) Y^*_{lm}(\hat{k}) Y_{lm}(\hat{r})\,. \tag{2.186}$$

Taking the photons direction along the z-axis, we get

$$\begin{aligned} Y^*_{lm}(\theta = 0\,, \phi = 0) &= Y^*_{l0}(0,0) = \sqrt{\frac{2l+1}{4\pi}} \\ Y^*_{lm,m\neq 0}(0,0) &= 0\,, \end{aligned} \tag{2.187}$$

and with this geometry the expansion of the exponential function simplifies to

$$e^{i\mathbf{kr}} = 4\pi \sum_{l} i^l \sqrt{2l+1}\, j_l(kr) Y_{l0}(\hat{r})\,. \tag{2.188}$$

The matrix element $\boldsymbol{\gamma}_{ab} = \frac{ec}{\omega}\langle \Phi_a | \hat{\epsilon}_\lambda \cdot \boldsymbol{\alpha} e^{i\mathbf{kr}} | \Phi_b \rangle$ can then be written in the form

$$\boldsymbol{\gamma}_{ab} = i\sqrt{4\pi}\frac{ec}{\omega} \sum_l i^l \sqrt{2l+1} \langle \Phi_a | \hat{\epsilon}_\lambda \cdot \boldsymbol{\alpha} j_l(kr) Y_{l0}(\hat{r}) | \Phi_b \rangle\,. \tag{2.189}$$

1° *Linear polarization*

For the polarization in the z direction, the matrix element takes the form

$$\begin{aligned} \boldsymbol{\gamma}^z_{ab} &= \sqrt{4\pi}\frac{ec}{\omega} \sum_l i^{l+1} \sqrt{2l+1} \langle \Phi_a | \hat{\epsilon}_z \cdot \boldsymbol{\alpha} j_l(kr) Y_{l0}(\hat{r}) | \Phi_b \rangle \\ &= i\sqrt{4\pi}\frac{ec}{\omega} \sum_l i^{l+1} \sqrt{2l+1} \int d\mathbf{r} \Phi^\dagger_a(\mathbf{r}) \alpha_z j_l(kr) Y_{l0}(\hat{r}) \Phi_b(\mathbf{r}) \\ &= -\sqrt{4\pi}\frac{ec}{\omega} \sum_l i^l \sqrt{2l+1} [-R_1 K_1^z + R_2 K_2^z]\,. \end{aligned} \tag{2.190}$$

1° *Circular polarization*

For the case of right- and left-circular polarization, we can express the matrix elements as

$$\begin{aligned}
\gamma^{+}_{ab} &= \sqrt{4\pi}\frac{ec}{\omega}\sum_l i^{l+1}\sqrt{2l+1}\langle\Phi_a|\hat{\epsilon}_+\cdot\boldsymbol{\alpha}j_l(kr)Y_{l0}(\hat{r})|\Phi_b\rangle \qquad (2.191)\\
&= i\sqrt{2\pi}\frac{ec}{\omega}\sum_l i^{l+1}\sqrt{2l+1}\int d\mathbf{r}\Phi^{\dagger}_a(\mathbf{r})(\hat{\epsilon}_x+i\hat{\epsilon}_y)\boldsymbol{\alpha}j_l(kr)Y_{l0}(\hat{r})\Phi_b(\mathbf{r})\\
&= -\sqrt{2\pi}\frac{ec}{\omega}\sum_l i^{l}\sqrt{2l+1}\{-R_1[K^x_1+iK^y_1]+R_2[K^x_2+iK^y_2]\}\,,\\
\gamma^{-}_{ab} &= \sqrt{4\pi}\frac{ec}{\omega}\sum_l i^{l+1}\sqrt{2l+1}\langle\Phi_a|\hat{\epsilon}_-\cdot\boldsymbol{\alpha}j_l(kr)Y_{l0}(\hat{r})|\Phi_b\rangle\\
&= i\sqrt{2\pi}\frac{ec}{\omega}\sum_l i^{l+1}\sqrt{2l+1}\int d\mathbf{r}\Phi^{\dagger}_a(\mathbf{r})(\hat{\epsilon}_x-i\hat{\epsilon}_y)\boldsymbol{\alpha}j_l(kr)Y_{l0}(\hat{r})\Phi_b(\mathbf{r})\\
&= -\sqrt{2\pi}\frac{ec}{\omega}\sum_l i^{l}\sqrt{2l+1}\{-R_1[K^x_1-iK^y_1]+R_2[K^x_2-iK^y_2]\}\,,
\end{aligned}$$

with the radial integrals

$$R_1=\int drr^2F_{n_a\kappa_a}(r)j_l(kr)G_{n_b\kappa_b}(r)\,,\quad R_2=\int drr^2G_{n_a\kappa_a}(r)j_l(kr)F_{n_b\kappa_b}(r)\,, \qquad (2.192)$$

and the angular parts

$$\begin{aligned}
K^x_1 &= \int do_r\Omega^{\dagger}_{-\kappa_aM_a}(\hat{r})\sigma_xY_{l0}\Omega_{\kappa_bM_b}(\hat{r}),\quad K^x_2=\int do_r\Omega^{\dagger}_{\kappa_aM_a}(\hat{r})\sigma_xY_{l0}\Omega_{-\kappa_bM_b}(\hat{r})\,, \qquad (2.193)\\
K^y_1 &= \int do_r\Omega^{\dagger}_{-\kappa_aM_a}(\hat{r})\sigma_yY_{l0}\Omega_{\kappa_bM_b}(\hat{r}),\quad K^y_2=\int do_r\Omega^{\dagger}_{\kappa_aM_a}(\hat{r})\sigma_yY_{l0}\Omega_{-\kappa_bM_b}(\hat{r})\,,\\
K^z_1 &= \int do_r\Omega^{\dagger}_{-\kappa_aM_a}(\hat{r})\sigma_zY_{l0}\Omega_{\kappa_bM_b}(\hat{r}),\quad K^z_2=\int do_r\Omega^{\dagger}_{\kappa_aM_a}(\hat{r})\sigma_zY_{l0}\Omega_{-\kappa_bM_b}(\hat{r})\,.
\end{aligned}$$

The results of the integration are

$$\begin{aligned}
K^x_1 &= \frac{(-1)^{j_a+j_b-M_b+3/2}}{\sqrt{4\pi}}\sqrt{(2j_a+1)(2j_b+1)(2l+1)(2l'_a+1)(2l_b+1)}\\
&\times \begin{pmatrix} l'_a & l_b & l\\ 0 & 0 & 0\end{pmatrix}(a^1_1-a^1_2)\,, \qquad (2.194)
\end{aligned}$$

$$K^x_2=\frac{(-1)^{j_a+j_b-M_b+3/2}}{\sqrt{4\pi}}\sqrt{(2j_a+1)(2j_b+1)(2l+1)(2l_a+1)(2l'_b+1)}\begin{pmatrix} l_a & l'_b & l\\ 0 & 0 & 0\end{pmatrix}(a^2_1-a^2_2)\,,$$

$$K^y_1=-i\frac{(-1)^{j_a+j_b-M_b+3/2}}{\sqrt{4\pi}}\sqrt{(2j_a+1)(2j_b+1)(2l+1)(2l'_a+1)(2l_b+1)}\begin{pmatrix} l'_a & l_b & l\\ 0 & 0 & 0\end{pmatrix}(a^1_1+a^1_2)\,,$$

$$K^y_2=-i\frac{(-1)^{j_a+j_b-M_b+3/2}}{\sqrt{4\pi}}\sqrt{(2j_a+1)(2j_b+1)(2l+1)(2l_a+1)(2l'_b+1)}\begin{pmatrix} l_a & l'_b & l\\ 0 & 0 & 0\end{pmatrix}(a^2_1+a^2_2)\,,$$

$$K^z_1=\frac{(-1)^{j_a+j_b-M_b+3/2}}{\sqrt{4\pi}}\sqrt{(2j_a+1)(2j_b+1)(2l+1)(2l'_a+1)(2l_b+1)}\begin{pmatrix} l'_a & l_b & l\\ 0 & 0 & 0\end{pmatrix}(b^1_1+b^1_2)\,,$$

$$K_2^z = \frac{(-1)^{j_a+j_b-M_b+3/2}}{\sqrt{4\pi}}\sqrt{(2j_a+1)(2j_b+1)(2l+1)(2l_a+1)(2l'_b+1)}\begin{pmatrix} l_a & l'_b & l \\ 0 & 0 & 0 \end{pmatrix}(b_1^2+b_2^2)\,,$$

with the angular coefficients defined as

$$\begin{aligned}
a_1^1 &= \begin{pmatrix} l'_a & j_a & 1/2 \\ M_a-1/2 & -M_a & 1/2 \end{pmatrix}\begin{pmatrix} l_b & j_b & 1/2 \\ M_b+1/2 & -M_b & -1/2 \end{pmatrix} \\
&\times \begin{pmatrix} l'_a & l_b & l \\ -M_a+1/2 & M_b+1/2 & 0 \end{pmatrix}, \qquad (2.195)\\
a_2^1 &= \begin{pmatrix} l'_a & j_a & 1/2 \\ M_a+1/2 & -M_a & -1/2 \end{pmatrix}\begin{pmatrix} l_b & j_b & 1/2 \\ M_b-1/2 & -M_b & 1/2 \end{pmatrix}\begin{pmatrix} l'_a & l_b & l \\ -M_a-1/2 & M_b-1/2 & 0 \end{pmatrix}, \\
b_1^1 &= \begin{pmatrix} l'_a & j_a & 1/2 \\ M_a-1/2 & -M_a & 1/2 \end{pmatrix}\begin{pmatrix} l_b & j_b & 1/2 \\ M_b-1/2 & -M_b & 1/2 \end{pmatrix}\begin{pmatrix} l'_a & l_b & l \\ -M_a+1/2 & M_b-1/2 & 0 \end{pmatrix}, \\
b_2^1 &= \begin{pmatrix} l'_a & j_a & 1/2 \\ M_a+1/2 & -M_a & -1/2 \end{pmatrix}\begin{pmatrix} l_b & j_b & 1/2 \\ M_b+1/2 & -M_b & -1/2 \end{pmatrix}\begin{pmatrix} l'_a & l_b & l \\ -M_a-1/2 & M_b+1/2 & 0 \end{pmatrix}, \\
a_1^2 &= \begin{pmatrix} l_a & j_a & 1/2 \\ M_a-1/2 & -M_a & 1/2 \end{pmatrix}\begin{pmatrix} l'_b & j_b & 1/2 \\ M_b+1/2 & -M_b & -1/2 \end{pmatrix}\begin{pmatrix} l_a & l'_b & l \\ -M_a+1/2 & M_b+1/2 & 0 \end{pmatrix}, \\
a_2^2 &= \begin{pmatrix} l_a & j_a & 1/2 \\ M_a+1/2 & -M_a & -1/2 \end{pmatrix}\begin{pmatrix} l'_b & j_b & 1/2 \\ M_b-1/2 & -M_b & 1/2 \end{pmatrix}\begin{pmatrix} l_a & l'_b & l \\ -M_a-1/2 & M_b-1/2 & 0 \end{pmatrix}, \\
b_1^2 &= \begin{pmatrix} l_a & j_a & 1/2 \\ M_a-1/2 & -M_a & 1/2 \end{pmatrix}\begin{pmatrix} l'_b & j_b & 1/2 \\ M_b-1/2 & -M_b & 1/2 \end{pmatrix}\begin{pmatrix} l_a & l'_b & l \\ -M_a+1/2 & M_b-1/2 & 0 \end{pmatrix}, \\
b_2^2 &= \begin{pmatrix} l_a & j_a & 1/2 \\ M_a+1/2 & -M_a & -1/2 \end{pmatrix}\begin{pmatrix} l'_b & j_b & 1/2 \\ M_b+1/2 & -M_b & -1/2 \end{pmatrix}\begin{pmatrix} l_a & l'_b & l \\ -M_a-1/2 & M_b+1/2 & 0 \end{pmatrix}.
\end{aligned}$$

For the radial parts, the results are

$$\begin{aligned}
R_1 &= -\sqrt{\pi}\left(1-\frac{E_a}{mc^2}\right)^{1/2}\left(1+\frac{E_b}{mc^2}\right)^{1/2}U_aU_b\sum_{\alpha=0}^{\infty}\frac{(-1)^\alpha\omega^{2\alpha+l}}{2^{2\alpha+l+1}\alpha!\Gamma(\alpha+l+3/2)} \qquad (2.196)\\
&\times[R_1^1-R_1^2+R_1^3-R_1^4]\,,\\
R_2 &= -\sqrt{\pi}\left(1+\frac{E_a}{mc^2}\right)^{1/2}\left(1-\frac{E_b}{mc^2}\right)^{1/2}U_aU_b\sum_{\alpha=0}^{\infty}\frac{(-1)^\alpha\omega^{2\alpha+l}}{2^{2\alpha+l+1}\alpha!\Gamma(\alpha+l+3/2)}\\
&\times[R_1^1+R_1^2-R_1^3-R_1^4]\,,
\end{aligned}$$

with the quantities

$$
\begin{aligned}
R_1^1 &= n_a^r n_b^r (2\lambda_a)^{\gamma_a-1}(2\lambda_b)^{\gamma_b-1}\sum_{m=0}^{n_a^r-1}\frac{(-n_a^r+1)_m}{(2\gamma_a+1)_m}\frac{(2\lambda_a)^m}{m!}\frac{\Gamma(m+\gamma_a+\gamma_b+1+2\alpha+l)}{(\lambda_a+\lambda_b)^{m+\gamma_a+\gamma_b+1+2\alpha+l}} \\
&\quad {}_2F_1\left(m+\gamma_a+\gamma_b+1+2\alpha+l,-n_b^r+1,2\gamma_b+1;\frac{2\lambda_b}{\lambda_a+\lambda_b}\right), \\
R_1^2 &= n_a^r (N_b-\kappa_b)(2\lambda_a)^{\gamma_a-1}(2\lambda_b)^{\gamma_b-1}\sum_{m=0}^{n_a^r-1}\frac{(-n_a^r+1)_m}{(2\gamma_a+1)_m}\frac{(2\lambda_a)^m}{m!}\frac{\Gamma(m+\gamma_a+\gamma_b+1+2\alpha+l)}{(\lambda_a+\lambda_b)^{m+\gamma_a+\gamma_b+1+2\alpha+l}} \\
&\quad {}_2F_1\left(m+\gamma_a+\gamma_b+1+2\alpha+l,-n_b^r,2\gamma_b+1;\frac{2\lambda_b}{\lambda_a+\lambda_b}\right), \\
R_1^3 &= (N_a-\kappa_a) n_b^r (2\lambda_a)^{\gamma_a-1}(2\lambda_b)^{\gamma_b-1}\sum_{m=0}^{n_a^r}\frac{(-n_a^r+1)_m}{(2\gamma_a+1)_m}\frac{(2\lambda_a)^m}{m!}\frac{\Gamma(m+\gamma_a+\gamma_b+1+2\alpha+l)}{(\lambda_a+\lambda_b)^{m+\gamma_a+\gamma_b+1+2\alpha+l}} \\
&\quad {}_2F_1\left(m+\gamma_a+\gamma_b+1+2\alpha+l,-n_b^r+1,2\gamma_b+1;\frac{2\lambda_b}{\lambda_a+\lambda_b}\right), \\
R_1^4 &= (N_a-\kappa_a)(N_b-\kappa_b)(2\lambda_a)^{\gamma_a-1}(2\lambda_b)^{\gamma_b-1}\sum_{m=0}^{n_a^r}\frac{(-n_a^r+1)_m}{(2\gamma_a+1)_m}\frac{(2\lambda_a)^m}{m!}\frac{\Gamma(m+\gamma_a+\gamma_b+1+2\alpha+l)}{(\lambda_a+\lambda_b)^{m+\gamma_a+\gamma_b+1+2\alpha+l}} \\
&\quad {}_2F_1\left(m+\gamma_a+\gamma_b+1+2\alpha+l,-n_b^r,2\gamma_b+1;\frac{2\lambda_b}{\lambda_a+\lambda_b}\right).
\end{aligned}
\tag{2.197}
$$

For the matrix elements in the case of driving between hyperfine-split atomic levels, which will be necessary later, we are using the formula [LL91]

$$
\begin{aligned}
\langle n_1' j_1' J' || f_k^{(1)} || n_1 j_1 J\rangle &= (-1)^{j_{1,max}+j_2+J_{min}+k}\sqrt{(2J+1)(2J'+1)} \\
&\quad \times \left\{ \begin{array}{ccc} j_1' & J' & j_2 \\ J & j_1 & k \end{array} \right\} \langle n_1' j_1' || f_k^{(1)} || n_1 j_1\rangle ,
\end{aligned}
\tag{2.198}
$$

where $f_{1,max} = \max\{j_1, j_1'\}$, and $(n_1' n_2' j_1' j_2' J) \equiv (n_1' j_1' J)$, i.e. the n_2', j_2' are omitted. It is then easy to find the transition matrix element

$$
\begin{aligned}
&\gamma_{ab}(n_b j_b I F_b \to n_a j_a I F_a) = (-1)^{j_{max}+I+F_{min}+J}\sqrt{(2F_a+1)(2F_b+1)} \\
&\times \left(\begin{array}{ccc} F_a & J & F_b \\ -M_{F_a} & M_{F_a}-M_{F_b} & M_{F_b} \end{array} \right) \Big/ \left(\begin{array}{ccc} j_a & J & j_b \\ -M_a & M_a-M_b & M_b \end{array} \right) \left\{ \begin{array}{ccc} j_a & F_a & I \\ F_a & j_b & J \end{array} \right\} \\
&\times \gamma_{ab}(n_b j_b \to n_a j_a) ,
\end{aligned}
\tag{2.199}
$$

where $\mathbf{F}_a = \mathbf{j}_a + \mathbf{I}$, with $\mathbf{I}$ being the nuclear angular momentum.

2.4 Calculation of relativistic decay widths

In this section we derive formulas for the width of radiative decay involving relativistic electrons. Let us consider the effect of adding the interaction Hamiltonian $\mathscr{H}_I$ to the sum of the electronic Hamiltonian – in general, a many-electronic atomic Hamiltonian – $\mathscr{H}_0 + \mathscr{V}_I$ and the electromagnetic Hamiltonian $\mathscr{H}_{EM}$,

$$
\mathscr{H} = \mathscr{H}_0 + \mathscr{V}_I + \mathscr{H}_{EM} . \tag{2.200}
$$

We let Ψ_k represent an eigenfunction of $\mathscr{H}_0 + \mathscr{V}_I$ with the eigenvalue E_k,

$$(\mathscr{H}_0 + \mathscr{V}_I)\Psi_k = E_k\Psi_k\,, \tag{2.201}$$

and let $|n_k\rangle$ be an n_k-photon eigenstate of $\mathscr{H}_{EM}$ with the eigenvalue $n_k\hbar\omega$,

$$\mathscr{H}_{EM}|n_k\rangle = n_k\hbar\omega|n_k\rangle\,. \tag{2.202}$$

An eigenstate of $\mathscr{H}$ corresponding to a many-electron atom in the state Ψ_k and n_k photons is the product state

$$\Phi_k \equiv \Psi_k|n_k\rangle\,. \tag{2.203}$$

This is an eigenstate of $\mathscr{H}$ with the eigenvalue $E_k + n_k\hbar\omega$. We are interested in radiative transitions between such stationary states induced by the interaction $\mathscr{H}_I$. In the *interaction representation*, the Schrödinger equation for a state $\Phi(t)$ is written as

$$i\hbar\frac{\partial\Phi(t)}{\partial t} = \hat{\mathscr{H}_I}(t)\Phi(t)\,, \tag{2.204}$$

where $\hat{\mathscr{H}_I}(t)$ is the time-dependent interaction Hamiltonian

$$\hat{\mathscr{H}_I}(t) = e^{i\mathscr{H}t/\hbar}\mathscr{H}_I e^{-i\mathscr{H}t/\hbar}\,. \tag{2.205}$$

Let us introduce the unitary operator $U(t,t_0)$ describing the evolution of stationary states Φ_k prepared at $t = t_0$,

$$\Phi_k(t) = U(t,t_0)\Phi_k\,. \tag{2.206}$$

It follows from Eq. (2.204) that $U(t,t_0)$ satisfies

$$\begin{aligned} i\hbar\frac{\partial U(t,t_0)}{\partial t} &= \hat{\mathscr{H}_I}U(t,t_0)\,, \\ U(t_0,t_0) &= I\,, \end{aligned} \tag{2.207}$$

where I is the identity operator. These equations can be rewritten as an equivalent integral equation

$$U(t,t_0) = I - \frac{i}{\hbar}\int_{t_0}^{t} dt_1\hat{\mathscr{H}_I}(t_1)U(t_1,t_0)\,. \tag{2.208}$$

The iterative solution of Eq. (2.208) is

$$\begin{aligned} U(t,t_0) &= I - \frac{i}{\hbar}\int_{t_0}^{t} dt_1\hat{\mathscr{H}_I}(t_1) + \frac{(-i)^2}{\hbar^2}\int_{t_0}^{t} dt_1\hat{\mathscr{H}_I}(t_1)\int_{t_0}^{t_1} dt_2\hat{\mathscr{H}_I}(t_2)U(t_2,t_0) \\ &= \sum_{n=0}^{\infty}\frac{(-i)^n}{\hbar^n}\int_{t_0}^{t} dt_1\hat{\mathscr{H}_I}(t_1)\int_{t_0}^{t_1} dt_2\hat{\mathscr{H}_I}(t_2)\cdots\int_{t_0}^{t_{n-1}} dt_n\hat{\mathscr{H}_I}(t_n). \end{aligned} \tag{2.209}$$

The S operator is the unitary operator that transforms states prepared at times in the remote past ($t = -\infty$), when the interaction $\mathscr{H}_I(t)$ is assumed to vanish, into states in the remote future ($t = \infty$), when $\mathscr{H}_I(t)$ is also assumed to vanish. Thus

$$S = U(\infty,-\infty). \tag{2.210}$$

Expanding S in power of $\mathscr{H}_I(t)$, we have

$$S = I + \sum_{n=1}^{\infty} S^{(n)} \,, \tag{2.211}$$

where

$$S^{(n)} = \frac{(-i)^n}{\hbar^n} \int_{-\infty}^{\infty} dt_1 \hat{\mathscr{H}}_I(t_1) \int_{-\infty}^{t_1} dt_2 \hat{\mathscr{H}}_I(t_2) \cdots \int_{-\infty}^{t_{n-1}} dt_n \hat{\mathscr{H}}_I(t_n) \,. \tag{2.212}$$

To first order in $\mathscr{H}_I(t)$ we have

$$S \approx I - \frac{i}{\hbar} \int_{-\infty}^{\infty} dt \hat{\mathscr{H}}_I(t) \,. \tag{2.213}$$

The first-order transition amplitude for a state Φ_i prepared in the remote past to evolve into a state Φ_f in the remote future is

$$S_{fi}^{(1)} = \langle \Phi_f | S^{(1)} | \Phi_i \rangle = -\frac{i}{\hbar} \int_{-\infty}^{\infty} dt \langle \Phi_f^\dagger | e^{i\mathscr{H}t/\hbar} \mathscr{H}_I e^{-i\mathscr{H}t/\hbar} | \Phi_i \rangle \,. \tag{2.214}$$

Let us consider an atomic system in an initial state Ψ_i, interacting with n_i photons. The initial state is 5

$$\Phi_i = \Psi_i | n_i \rangle \,. \tag{2.215}$$

The operator c_i in $\mathscr{H}_I(t)$ will cause transitions to states with $n_i - 1$ photons, while the operator $c_i^\dagger$ will lead to states with $n_i + 1$ photons. Thus, we must consider two possibilities: (i) photon absorption, leading to a final state

$$\Phi_f = \Psi_f | n_i - 1 \rangle \,, \tag{2.216}$$

and (ii) photon emission, leading to a final state

$$\Phi_f = \Psi_f | n_i + 1 \rangle \,. \tag{2.217}$$

For the case of photon absorption, using the fact that

$$\langle n_i - 1 | c_i | n_i \rangle = \sqrt{n_i} \,, \tag{2.218}$$

we may write

$$\begin{aligned} S_{fi}^{(1)} &= -\frac{i}{\hbar} \sqrt{n_i} \int_{-\infty}^{\infty} dt e^{i(E_f - E_i - \hbar\omega)t/\hbar} \langle \Psi_f | \mathscr{H}_I | \Psi_i \rangle \\ &= -2\pi i \delta(E_f - E_i - \hbar\omega) \sqrt{n_i} \langle \Psi_f | \mathscr{H}_I | \Psi_i \rangle \,. \end{aligned} \tag{2.219}$$

Similarly, for the case of photon emission, we find

$$\begin{aligned} S_{fi}^{(1)} &= -\frac{i}{\hbar} \sqrt{n_i + 1} \int_{-\infty}^{\infty} dt e^{i(E_f - E_i - \hbar\omega)t/\hbar} \langle \Psi_f | \mathscr{H}_I^\dagger | \Psi_i \rangle \\ &= -2\pi i \delta(E_f - E_i + \hbar\omega) \sqrt{n_i + 1} \langle \Psi_f | \mathscr{H}_I^\dagger | \Psi_i \rangle \,. \end{aligned} \tag{2.220}$$

We introduce the *transition amplitude*

$$T_{fi} = \begin{cases} \langle \Psi_f | \mathscr{H}_I | \Psi_i \rangle, & \text{for absorption of radiation,} \\ \langle \Psi_f | \mathscr{H}_I^\dagger | \Psi_i \rangle, & \text{for emission of radiation.} \end{cases} \tag{2.221}$$

We treat the two cases simultaneously using

$$S_{fi} = -2\pi\delta(E_f - E_i \mp \hbar\omega)T_{fi}\begin{pmatrix}\sqrt{n_i}\\ \sqrt{n_i+1}\end{pmatrix}, \tag{2.222}$$

where the upper contribution refers to absorption and the lower refers to emission. The probability of a transition from state Ψ_i to state Ψ_f is just the square of $S_{fi}^{(1)}$. In evaluating the square, we replace one factor of $2\pi\delta(E_f - E_i \pm \hbar\omega)$ by $T/\hbar$, where T is the total interaction time. Thus, we find that the transition probability per unit time W_{fi} is given by

$$W_{fi} = \frac{2\pi}{\hbar}\delta(E_f - E_i \mp \hbar\omega)|T_{fi}|^2\begin{pmatrix}n_i\\ n_i+1\end{pmatrix}. \tag{2.223}$$

In an interval of wave numbers d^3k, there are

$$d^3n_i = \frac{V}{(2\pi)^3}d^3k = \frac{V}{(2\pi c)^3}\omega^2 d\omega d\Omega_k \tag{2.224}$$

photon states of given polarization. The corresponding number of transitions per unit time d^3w_{fi} is thus given by

$$d^3w_{fi} = W_{fi}d^3n_i = \frac{V}{(2\pi)^2c^3\hbar}\delta(E_f - E_i \mp \hbar\omega)\omega^2 d\omega d\Omega_k|T_{fi}|^2\begin{pmatrix}n_i\\ n_i+1\end{pmatrix}. \tag{2.225}$$

Integrating over ω, we obtain

$$d^3w_{fi} = \frac{V}{(2\pi\hbar)^2c^3}\omega^2 d\Omega_k|T_{fi}|^2\begin{pmatrix}n_i\\ n_i+1\end{pmatrix}, \tag{2.226}$$

where n_i is now the number of photons with energy $\hbar\omega = E_f - E_i$ for absorption and $E_i - E_f$ for emission. Factoring $-ec\sqrt{\hbar/2\epsilon_0\omega V}$ from the interaction Hamiltonian, we obtain

$$d^2w_{fi} = \frac{\alpha}{2\pi}\omega d\Omega_k|T_{fi}|^2\begin{pmatrix}n_i\\ n_i+1\end{pmatrix}, \tag{2.227}$$

where the single-particle interaction Hamiltonian is now replaced by

$$h_I(\mathbf{r},\omega) \to \boldsymbol{\alpha}\cdot\hat{\epsilon}_\lambda e^{i\boldsymbol{k}\cdot\boldsymbol{r}}. \tag{2.228}$$

Let us assume that we have a collection of atoms in equilibrium with a radiation field. Further, let us assume that the photons of frequency ω in the radiation field are distributed isotropically and that the number of photons in each of the two polarization states is equal. In this case, the photon number n can be related to the spectral density function $\rho(\omega)$ which is defined as the photon energy per unit volume in the frequency interval $d\omega$. One finds from Eq. (2.224) that

$$\rho(\omega) = 2n\hbar\omega\frac{4\pi\omega^2}{(2\pi c)^3} = \frac{\hbar\omega^3}{\pi^2c^3}n. \tag{2.229}$$

The Hamiltonian governing the electromagnetic field is

$$\begin{aligned}\mathscr{H}_{EM} &= \frac{\epsilon_0}{2}\int d^3r\boldsymbol{E}(\boldsymbol{r},t)\cdot\boldsymbol{E}(\boldsymbol{r},t) + \frac{1}{2\mu_0}\int d^3r\boldsymbol{B}(\boldsymbol{r},t)\cdot\boldsymbol{B}(\boldsymbol{r},t) \\ &= \frac{1}{4}\sum_i\hbar\omega\left(\hat{\epsilon}_\lambda^*\cdot\hat{\epsilon}_\lambda + [\hat{k}\times\hat{\epsilon}_\lambda]\cdot[\hat{k}\times\hat{\epsilon}_\lambda^*]\right)\left(c_ic_i^\dagger + c_i^\dagger c_i\right) \\ &= \sum_i\hbar\omega\left(\mathscr{N}_i + \frac{1}{2}\right),\end{aligned} \tag{2.230}$$

where $\mathscr{N}_i = c_i^\dagger c_i$ is the photon number operator.

For isotropic, unpolarized radiation, we can integrate Eq. (2.230) over angles Ω_k and sum over polarizations $\hat{\epsilon}_\lambda$, treating n as a multiplicative factor. The resulting absorption probability per second, $w_{b\to a}$, leading from an initial (lower energy) state a to final (higher energy) state b in presence of n photons of energy $\hbar\omega$ is given in terms of the spectral density function $\rho(\omega)$ as

$$w_{a\to b}^{ab} = \frac{\pi^2 c^3}{\hbar\omega^3}\rho(\omega)\frac{\alpha}{2\pi}\omega\sum_\lambda \int d\Omega_k |T_{ba}|^2 \,. \tag{2.231}$$

Similarly, the emission probability per second leading from state b to state a in presence of n photons of energy $\hbar\omega$ is given in terms of $\rho(\omega)$ by

$$w_{b\to a}^{em} = \left(1 + \frac{\pi^2 c^3}{\hbar\omega^3}\rho(\omega)\right)\frac{\alpha}{2\pi}\omega\sum_\lambda \int d\Omega_k |T_{ba}|^2 \,. \tag{2.232}$$

The emission probability consists of two parts, a *spontaneous emission* contribution, $w_{b\to a}^{sp}$, that is independent of $\rho(\omega)$, and an *induced* or *stimulated* emission contribution, $w_{b\to a}^{ie}$ that is proportional to $\rho(\omega)$.

The transition amplitude for a one-electron atom is

$$T_{ba} = \int d^3 r \Psi_b^\dagger \boldsymbol{\alpha}\cdot\boldsymbol{A}(\boldsymbol{r},\omega)\Psi_a \,, \tag{2.233}$$

where $\boldsymbol{A}(\boldsymbol{r},\omega)$ is the transverse-gauge vector potential

$$\boldsymbol{A}(\boldsymbol{r},\omega) = \hat{\epsilon} e^{i\mathbf{k}\cdot\mathbf{r}} \,. \tag{2.234}$$

The multipole expansion of the vector potential leads to a corresponding multipole expansion of the transition operator

$$T_{ba} = 4\pi\sum_{JM\lambda} i^{J-\lambda}\left[\mathbf{Y}_{JM}^{(\lambda)}(\hat{k})\cdot\hat{\epsilon}\right]\left[T_{JM}^{(\lambda)}\right]_{ba} \,, \tag{2.235}$$

where

$$\left[T_{JM}^{(\lambda)}\right]_{ba} = \int d^3 r \Psi_b^\dagger \boldsymbol{\alpha}\cdot\boldsymbol{a}_{JM}^{(\lambda)}(\mathbf{r})\Psi_a \,. \tag{2.236}$$

To obtain the transition probability, we must square the amplitude, sum over polarization states, and integrate over photon directions. On squaring the amplitude, we encounter terms of the form

$$\left[\mathbf{Y}_{JM}^{(\lambda)}(\hat{k})\cdot\hat{\epsilon}_\nu\right]\left[\hat{\epsilon}_\nu\cdot\mathbf{Y}_{J'M'}^{(\lambda')}(\hat{k})\right] \,, \tag{2.237}$$

to be summed over polarization directions $\hat{\epsilon}_\nu$. Using the fact that the vector spherical harmonics with $\lambda = 0, 1$ are orthogonal to $\hat{k}$, the polarization sum becomes

$$\sum_\nu \left[\mathbf{Y}_{JM}^{(\lambda)}(\hat{k})\cdot\hat{\epsilon}_\nu\right]\left[\hat{\epsilon}_\nu\cdot\mathbf{Y}_{J'M'}^{(\lambda')}(\hat{k})\right] = \left[\mathbf{Y}_{JM}^{(\lambda)}(\hat{k})\cdot\mathbf{Y}_{J'M'}^{(\lambda')}(\hat{k})\right] \,. \tag{2.238}$$

This expression is easily integrated over photon directions leading to

$$\int d\Omega_k \left[\mathbf{Y}_{JM}^{(\lambda)}(\hat{k})\cdot\mathbf{Y}_{J'M'}^{(\lambda')}(\hat{k})\right] = \delta_{JJ'}\delta_{MM'}\delta_{\lambda\lambda'} \,. \tag{2.239}$$

We therefore obtain for the transition rate

$$w_{ba} = \frac{\alpha}{2\pi}\omega \sum_{\nu} \int d\Omega_k |T_{ba}|^2 = 8\pi\alpha\omega \sum_{JM\lambda} \left| \left[T^{(\lambda)}_{JM} \right]_{ba} \right|^2 . \tag{2.240}$$

We see that the rate is an incoherent sum of all possible multipoles. Angular momentum selection rules, of course, limit the type and number of contributing multipoles.

A gauge transformation leaves single-particle amplitudes invariant, provided the energy difference between the initial and final states equals the energy carried off by the photon. The transformed multipole potential can be written as

$$\begin{aligned} \mathbf{a}^{(\lambda)}_{JM}(\mathbf{r}) &\rightarrow \mathbf{a}^{(\lambda)}_{JM}(\mathbf{r}) + \nabla\chi_{JM}(\mathbf{r}), \\ \Phi_{JM}(\mathbf{r}) &\rightarrow i\omega\chi_{JM}(\mathbf{r}) , \end{aligned} \tag{2.241}$$

where the gauge function $\chi_{JM}(\mathbf{r})$ is a solution to the Helmholtz equation. We choose the gauge function to be

$$\chi_{JM}(\mathbf{r}) = -\frac{1}{k}\sqrt{\frac{J+1}{J}} j_J(kr) Y_{JM}(\hat{r}) , \tag{2.242}$$

to cancel the lowest-order (in powers of kr) contribution to the interaction. The resulting transformation has no effect on the magnetic multipoles, but transforms electric multipole potentials to the form

$$\begin{aligned} \mathbf{a}^{(1)}_{JM}(\mathbf{r}) &= -j_{J+1}(kr) \left[\mathbf{Y}^{(1)}_{JM}(\hat{r}) - \sqrt{\frac{J+1}{J}} \mathbf{Y}^{(-1)}_{JM}(\hat{r}) \right] , \\ \Phi^{(1)}_{JM}(kr) &= -ic\sqrt{\frac{J+1}{J}} j_J(kr) Y_{JM}(\hat{r}) . \end{aligned} \tag{2.243}$$

The resulting potentials reduce to the *length-form* multipole potentials in the non-relativistic limit.

In either gauge, the multipole-interaction can be written in terms of a dimensionless multipole-transition operator $t^{(\lambda)}_{JM}(\mathbf{r})$ defined by

$$\left[\boldsymbol{\alpha} \cdot \boldsymbol{a}^{(\lambda)}_{JM}(\mathbf{r}) - \frac{1}{c}\Phi_{JM}(\mathbf{r}) \right] = i\sqrt{\frac{(2J+1)(J+1)}{4\pi J}} t^{(\lambda)}_{JM}(\mathbf{r}) . \tag{2.244}$$

The one-electron reduced matrix elements $\langle i||t^{(\lambda)}_J||j\rangle$ are given in the *transverse gauge*:

$$\begin{aligned} \langle\kappa_i||t^{(0)}_J||\kappa_j\rangle &= \langle -\kappa_i||C_J||\kappa_j\rangle \int_0^\infty dr \frac{\kappa_i+\kappa_j}{J+1} j_J(kr) \left[G_i(r)F_j(r) + F_i(r)G_j(r) \right] , \\ \langle\kappa_i||t^{(1)}_J||\kappa_j\rangle &= \langle\kappa_i||C_J||\kappa_j\rangle \int_0^\infty dr \left\{ -\frac{\kappa_i-\kappa_j}{J+1} \left[j'_J(kr) + \frac{j_J(kr)}{kr} \right] \times \right. \\ &\qquad \left. \left[F_i(r)G_j(r) + G_i(r)F_j(r) \right] + J\frac{j_J(kr)}{kr} \left[F_i(r)G_j(r) - G_i(r)F_j(r) \right] \right\} , \end{aligned} \tag{2.245}$$

and in the *Babushkin gauge*:

$$\begin{aligned} \langle\kappa_i||t^{(1)}_J||\kappa_j\rangle = \langle\kappa_i||C_J||\kappa_j\rangle \int_0^\infty dr \Bigg\{ & j_J(kr) \left[F_i(r)F_j(r) + G_i(r)G_j(r) \right] + \\ & + j_{J+1}(kr) \left[\frac{\kappa_i-\kappa_j}{J+1} \left[F_i(r)G_j(r) + G_i(r)F_j(r) \right] + \left[F_i(r)G_j(r) - G_i(r)F_j(r) \right] \right] \Bigg\} . \end{aligned} \tag{2.246}$$

The functions $F_i(r)$ and $G_i(r)$ in the above equations are the large and small components, respectively, of the radial Dirac wave functions for the orbital with quantum numbers (n_i, κ_i).

Using the Wigner-Eckart theorem

$$\langle \Phi_b | t^{(\lambda)}_{JM} | \Phi_a \rangle = (-1)^{(j_b - m_b)} \begin{pmatrix} j_b & J & j_a \\ -M_b & M & M_a \end{pmatrix} \langle \Phi_b || t^{(\lambda)}_J || \Phi_a \rangle \tag{2.247}$$

we can find the final expression of the *decay rate*, i.e. the transition probability per unit time:

$$\Gamma_{ba} = 2\alpha\omega \frac{(2J+1)(J+1)}{J} \sum_{J\lambda} |\langle \Phi_b || t^{(\lambda)}_J || \Phi_a \rangle|^2 \sum_{M m_b} \begin{pmatrix} j_b & J & j_a \\ -M_b & M & M_a \end{pmatrix}^2 . \tag{2.248}$$

In a two-level approximation, we know all quantum numbers of the initial state, therefore, no averaging over unresolved quantum numbers has to be performed as in the usual case.

We can express, using the formula (2.198), the decay rate between hyperfine components (F_a, M_{F_a}), (F_b, M_{F_b}) as

$$\begin{aligned} \Gamma_{ab}(n_a j_a I F_a \to n_b j_b I F_b) = (2F_a+1)(2F_b+1) \begin{pmatrix} F_b & J & F_a \\ -M_{F_b} & M_{F_b} - M_{F_a} & M_{F_a} \end{pmatrix}^2 \\ / \begin{pmatrix} j_b & J & j_a \\ -M_b & M_b - M_a & M_a \end{pmatrix}^2 \begin{Bmatrix} j_b & F_b & I \\ F_a & j_a & J \end{Bmatrix}^2 \Gamma_{ab}(n_a j_a \to n_b j_b) , \end{aligned} \tag{2.249}$$

2.5 Nuclear proton distributions explored by relativistic resonance fluorescence

A promising application of relativistic resonance fluorescence employing x-ray lasers is the determination of isotope shifts in highly charged ions. In these species, the large mutual overlap of the nuclear matter with inner-shell electrons ensures a large sensitivity of ionic transition energies to the protonic charge distribution. First we summarize the phenomenology of isotope shifts, then, as an application of the relativistic theory of resonance fluorescence in two-level systems presented in the previous sections we discuss our results on isotope shift measurements via x-ray lasers.

2.5.1 Isotope shifts and nuclear charge distribution parameters

Isotope shifts are slight variations of the electron energies without their splitting like in the case of hyperfine structure effects. The isotope shifts are caused by two effects, which lead to the mass shift (MS) and the field or volume shift (FS).

The first effect appears due to the fact that the nuclear mass is finite. In the lowest order, it is taken into account by replacing the electron mass (m_e) with the reduced mass

$$\mu = \frac{m_e M_{nuc}}{m_e + M_{nuc}} , \tag{2.250}$$

so the energy of an atomic state will become

$$E = \frac{\mu}{m_e} E_\infty . \tag{2.251}$$

E_∞ is the energy value corresponding to infinite nuclear mass ($M_{nuc} = \infty$). This replacement is only valid for the non-relativistic case, when the center of the mass can be defined geometrically. In the case of relativistic electrons, precise nuclear recoil corrections are more elaborate to calculate. For atoms with more than one electron, further corrections, the so-called specific mass shifts arise due to the correlated motion of the electrons. These relativistic and many-body effects can be taken into account by, e.g., perturbative means by the use of the relativistic recoil operator for a general atomic system of electrons with indices i, j (see Refs. [SA95, Pal87], in relativistic units, $\hbar = c = \epsilon_0 = 1$):

$$R_{ij} = \frac{\boldsymbol{p}_i \cdot \boldsymbol{p}_j}{2M} - \frac{Z\alpha}{2Mr_i}\left(\boldsymbol{\alpha}_i + \frac{(\boldsymbol{\alpha}_i \cdot \boldsymbol{r}_i)\boldsymbol{r}_i}{r_i^2}\right) \cdot \boldsymbol{p}_j \,. \tag{2.252}$$

Here, $\boldsymbol{r}_i$ and $\boldsymbol{p}_i$ are the position vector and the momentum operator of the ith electron, respectively, and $\boldsymbol{\alpha}_i$ is the vector of Dirac matrices acting on its bispinor wave function. The isotope-dependent nuclear mass is denoted by M and α is the fine-structure constant. There is no summation convention on i and j. The normal mass shift correction to a given atomic state is obtained as the expectation value $\langle \sum_i R_{ii} \rangle$, whereas the specific mass shift term is given by $\langle \sum_{i \neq j} R_{ij} \rangle$. The first term in Eq. (2.252) corresponds to the mass shift operator also known in the non-relativistic theory.

The second effect is caused by the fact that the nuclear charge is distributed within a finite volume and by the distinct isotope-dependent nuclear properties, like different distributions of protons in the nuclear volume. The electrostatic potential induced by the protonic distribution influences the motion of the electrons at short distances on the order of the nuclear radius, i.e. a few femtometers.

In order to have a good approximation of the nuclear volume effect, one may use a spherical nuclear charge distribution. However, not all the nuclei have a spherical shape. The deviation from a spherical charge distribution in a nucleus determines the electric quadrupole and higher order moments. The electric multipole moments of higher order than monopole electric moments contribute to the splitting of the energy levels in an atom, the so-called hyperfine structure effects.

Starting with electron scattering experiments on the nuclei, the most studied nuclear charge density function is the Fermi distribution. Most published data on nuclear parameters employ this type of distribution, which is given by the expression

$$\rho_{nuc}(\mathbf{r}) = \frac{\rho_0}{1 + e^{(r-c)/a}} \,, \tag{2.253}$$

where c is the half-density radius. For the case of a spherical distribution, the Fermi charge distribution depends on two parameters. In this case, c is a constant and it is defined as the radius at witch the density reaches the half of its maximum value. We may express the distance in the surface layer over whitch the density decreases from 90% to 10% of its maximum by

$$t = 4a \ln 3. \tag{2.254}$$

Here, t represents the surface thickness of the distribution. The normalization condition is

$$\int_0^\infty \rho_{nuc}(r) 4\pi r^2 dr = Ze \,. \tag{2.255}$$

For $c \gg a$, the density is essentially ρ_0. When the difference $r - c$ becomes larger than a, it starts to fall into negligible values with the distance, determined by a and independent of c. The Fermi distribution is illustrated in Fig. 2.5.

For deformed nuclei, one may use a four-parameter Fermi charge distribution. The angular dependence of c can be written as [ZST$^+$84]

$$c = R_0[1 + \beta_2 Y_{20}(\theta, \phi) + \beta_4 Y_{40}(\theta, \phi)] \,, \tag{2.256}$$

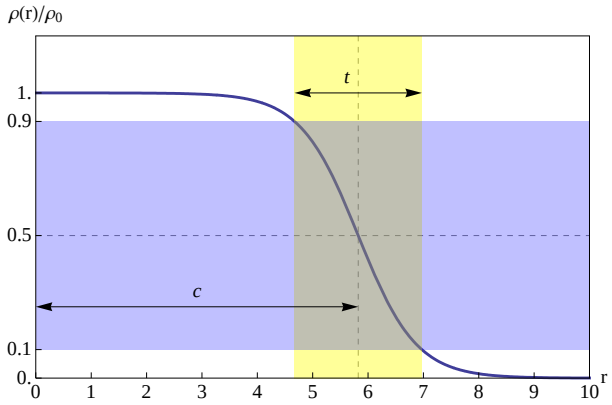

Figure 2.5: The two-parameter Fermi charge distribution normalized by the constant ρ_0 (see text). The half-density radius c and the surface thickness t are indicated.

where R_0 is the monopole radius and the parameters β_2 and β_4 are the quadrupole and hexadecapole deformation parameters, respectively. The root mean square (RMS) radius is defined by

$$r_{RMS} = \sqrt{\frac{1}{Ze}\int_0^\infty r^2 \rho_{nuc}(r) 4\pi r^2 dr}\,. \tag{2.257}$$

In general, the energy shift depends on other radial moments

$$\langle r^n \rangle = \frac{1}{Ze}\int_0^\infty \rho_{nuc}(r) 4\pi r^{n+2} dr\,. \tag{2.258}$$

For light nuclei, the energy shift depends essentially on the mean square radius $\langle r^2 \rangle = r^2_{RMS}$.

The relation between the density distribution and the corresponding nuclear potential is given by Poisson's equation

$$\nabla^2 V_{nuc}(r) = -4\pi\rho_{nuc}(r)\,. \tag{2.259}$$

For a spherically symmetrical distribution with the boundary condition $V_{nuc} \to 0$ for $r \to \infty$, the potential is given by the identity:

$$-rV_{nuc}(r) = 4\pi\left(\int_0^r \rho_{nuc}(s)s^2 ds + r\int_r^\infty \rho_{nuc}(s) s ds\right)\,. \tag{2.260}$$

We consider three different types of nuclear charge distribution

1. For point-like nucleus we will have the Coulomb potential given by

$$-rV_{nuc}(r) = Z\,. \tag{2.261}$$

2. The homogeneous distribution is described by

$$\rho_{nuc}(r) = \begin{cases} \rho_0\,, & \text{for} \quad r \le r_{nuc} \\ 0\,, & \text{otherwise} \end{cases}\,, \tag{2.262}$$

where r_{nuc} is the nuclear radius. On can calculate the nuclear radius using the formula

$$r_{nuc} = (1.0793A^{1/3} + 0.73587)\text{fm}\,. \tag{2.263}$$

3. In the case of the Fermi charge distribution for a spherical symmetric nucleus we can consider

$$r_{RMS} = (0.836A^{1/3} + 0.570)\text{fm}\,, \tag{2.264}$$

and the thickness parameter

$$t = 2.30\text{fm}\,, \tag{2.265}$$

unless some other value is provided.

There are four electromagnetic methods sensitive to the different properties of the nuclear ground-state charge distributions: elastic electron scattering, optical spectroscopy, K x-ray spectroscopy and muonic atom spectroscopy. Some nuclear parameters can be obtained with high precision from a combined analysis using data from different types of experiments.

1. Elastic electron scattering

Since in our present discussion the only interaction of importance between the electrons and nucleons is the electromagnetic one, the electron is an ideal probe particle. If the electrons have sufficient energy not to be affected by the atomic electrons in the target and to penetrate the nucleus, they will have their motion influenced by the nuclear charge distribution. The measured quantity in elastic electron scattering is the differential cross section. The deviation from the cross section of a point charge distribution is given by the form factor $F(q)$ through the formula [FBH$^+$95]

$$\left.\frac{d\sigma}{d\Omega}\right|_{exp} = \left.\frac{d\sigma}{d\Omega}\right|_{Mott} |F(q)|^2\,, \tag{2.266}$$

where q is the momentum transfer in the collision and it has the magnitude

$$q = \frac{2E}{\hbar c}\sin\frac{\theta}{2}\,, \tag{2.267}$$

where $E \gg m_e c^2$. The Mott cross section for a point-like nucleus is given by

$$\left.\frac{d\sigma}{d\Omega}\right|_{Mott} = \frac{Z^2e^4}{4E^4}\frac{\cos^2\frac{\theta}{2}}{\sin^4\frac{\theta}{2}}\,, \tag{2.268}$$

for the scattering of an electron of energy E through an angle θ. The form factor is related to the nuclear charge distribution through a Bessel-Fourier transform

$$F(q) = 4\pi\int_0^\infty \rho_{nuc}(r) j_0(qr) r^2 dr\,, \quad 0 < q < \infty\,, \tag{2.269}$$

where $j_0(qr) = \frac{\sin(qr)}{qr}$ denotes the spherical Bessel function of order zero. With the Fourier transform of the previous relation one can obtain the nuclear charge distribution density

$$\rho_{nuc}(r) = \frac{1}{2\pi^2}\int_0^\infty F(q) j_0(qr) q^2 dq\,. \tag{2.270}$$

The electron scattering offers the only possibility of determining the radial dependence of the charge distribution $\rho_{nuc}(r)$, the other methods only deliver integral quantities of $\rho_{nuc}(r)$. One of the principal results of the electron scattering experiment was the conclusion that the nucleus does not have sharp edges and that the most likely distribution is of Fermi type.

However, the accuracy of this experiment is limited by the systematic errors (more than 1%), by the q range accessible to experiment, and by the dispersion correction that takes into account virtual excitations

of the nucleus during the scattering process, which might modify the charge distributions. Usually, the RMS radius determined using the electron scattering technique has an approximate error of 0.2%.

2. Optical spectroscopy

As in the case of all the other spectroscopic methods, from the analysis of the optical transitions only information about the nuclear charge parameters can be obtained. This type of spectroscopy and the K x-ray method are sensitive to the isotopic variation of the mean-square radii $\delta\langle r^2\rangle$, with small contributions from higher radial moments like $\delta\langle r^4\rangle$ and $\delta\langle r^6\rangle$.

The isotope shift of optical transitions as a small energy shift of the gravity centers of the spectral components for different isotopes. The shift observed between two isotopes in an atomic spectral line is the sum of the field effect and the mass effect. Considering the mass number for two isotopes A and A' in a spectral line i of frequency ν the shift will be

$$\delta\nu_i^{AA'} = \delta\nu_{i,MS}^{AA'} + \delta\nu_{i,FS}^{AA'} \,. \tag{2.271}$$

The FS reflects the isotopic variation of the root mean square radius. For a transition i we have

$$\delta\nu_{i,FS}^{AA'} = F_i \lambda^{AA'} \,, \tag{2.272}$$

where

$$\lambda^{AA'} = \delta\langle r^2\rangle^{AA'} + \frac{C_2}{C_1}\delta\langle r^4\rangle^{AA'} + \frac{C_3}{C_1}\delta\langle r^6\rangle^{AA'} + \dots \,, \tag{2.273}$$

The coefficients C_1, C_2, C_3,... are tabulated in the literature and $\delta\langle r^2\rangle^{AA'} = \langle r^2\rangle^A - \langle r^2\rangle^{A'}$. F_i represents the electronic factor and is proportional to the change of the electronic charge density in the nucleus, in the studied transition i. In order to determine $\lambda^{AA'}$ from the FS, the electronic factor has to be known. There are several possibilities to calculate it: semi-empirical, using Goudsmit-Fermi Segre method, theoretical with a multiconfiguration Dirac-Fock method or experimental with the King plot. References concerning these methods can be found in [FBH$^+$95].

3. K x-ray spectroscopy

For K x-ray spectroscopy, similar parameters as the ones for the optical spectroscopy are determined. The expressions (2.271) and (2.273) describing the shifts are the same for the x-ray experiments, and for the nuclear parameter $\lambda^{AA'}$ the same determination methods can be used. The transition implied in this experiment are to the K level, while the optical transitions are in the upper levels, therefore the calculations are more precise in the case of the x-ray transitions. Due to the equipment constrains, the experimental errors can range from a few 50%, while in optical-laser measurements they are smaller by at least one order of magnitude.

4. Muonic atom spectroscopy

The μ meson or the muon is a particle having the same properties as the electron, except for its larger mass: $m_\mu = 207 m_e$ ($m_e c^2 = 0.511004\text{MeV}$; $m_\mu c^2 = 105.655\text{MeV}$). Since the muon has also spin $\frac{1}{2}$ and negative charge, it can be bound by a nucleus to form a muonic atom and it obeys the Dirac equation. Some effects negligible for normal atoms are important for muonic atoms. These effects are related to the large mass and to the fact that the Bohr radius of the muon is approximately 207 times smaller than the one for the electron. This makes all the nuclear size effects relatively larger.

The transitions between internal muonic shells are followed by γ-emissions, which will be detected. The binding energies and the measured γ energies depend on the nuclear charge distribution. This provides a tool for the determination of nuclear parameters by the comparison of the experimental and theoretical

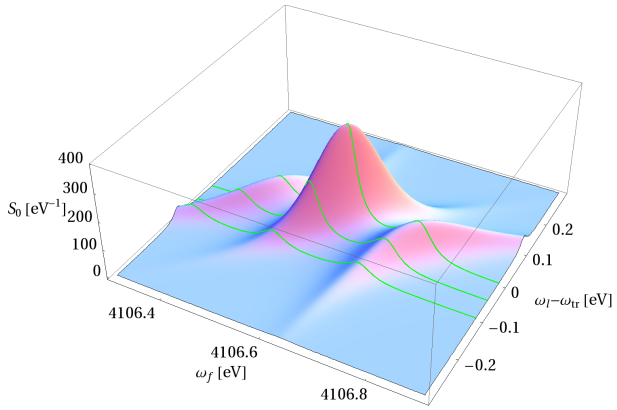

Figure 2.6: Spectrum of fluorescence photons for the $2s$–$2p_{3/2}$ circular (m=3/2–1/2) transition in Li-like U as a function of the fluorescence photon frequency ω_f and the detuning of the laser frequency ω_l from the ionic transition with $\omega_{tr} = 4106.6$ eV. The laser intensity is 10^{12} W/cm^2. The dashed curve shows the frequency-integrated detected signal as a function of the detuning.

spectra [FBH$^+$95]. The energy measurements provide only integral quantities of the nuclear charge distribution, so they do not give detailed information about the shape of the radial dependence.

In the heavy nuclei, the μ-mesic x-ray studies give values of parameters, which differ from those obtained from electron scattering, making the knowledge about the charge distribution more precise, while for light nuclei they give an independent measure of the RMS radius. The measurement error is determined mainly by statistics and to a minor part by the subtraction of the background of the spectrum. The main errors come from the uncertainty of the calculated nuclear polarization correction. An additional independent method such as measuring IS by employing x-ray free electron lasers will be by no doubt of great use in extending our knowledge on nuclear electromagnetic properties.

2.5.2 Isotope shifts investigated by means of relativistic resonance fluorescence

In Fig. 2.6 we plot the power spectrum of resonance fluorescence for the case of the $2s \rightarrow 2p_{3/2}$ E1 transition in Li-like uranium (Z=92) ions. The dynamic (AC) Stark shift leads to a splitting of the central peak. At an intensity of 10^{12} W/cm^2, the Rabi frequency of 150 meV is only slightly larger than the natural line width of $\Gamma = 45$ meV. As the figure shows, this leads to a rapid decrease of the fluorescence signal as function of the laser detuning from the transition frequency of the ion, especially when the central peak is considered. This enables the determination of ionic resonance energies with a resolution on the order of the natural line width of the transition. At higher intensities, however, the Rabi frequency which dominates the width of the detected signal peak (see dashed curve on Fig. 2.6) increases, thus corrupting the energy resolution.

In order to deduce nuclear proton distribution parameters via resonance fluorescence spectra, the isotope shifts for a pair of isotopes shall preferably be larger or at least comparable to the width of the fluorescence peaks.

The structure of the relativistic spectra is different from the non-relativistic one due to the spin-orbit interaction and the velocity-dependent electron mass only accounted for in the relativistic theory: the Rabi frequencies depend on the relativistic magnetic sublevels of the upper and lower states, leading to a complex splitting of the usual three-peak Mollow structure.

Current x-ray laser systems such as the LCLS possess a photon beam bandwidth of 200 meV, which is

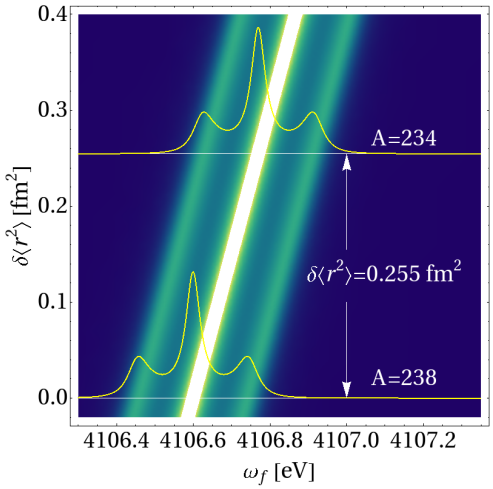

Figure 2.7: Shift of the relativistic resonance fluorescence spectrum as a function of the mean square proton radius variation $\delta\langle r^2\rangle$ for the case of the $2s$–$2p_{3/2}$ transition in Li-like uranium. The spectrum at the bottom corresponds to the reference isotope A=238 and is plotted against the fluorescence photon frequency ω_f around the transition frequency ω_{tr} of 4106.6 eV. The laser intensity is 10^{12} W/cm^2 and the laser detuning is assumed to be 0 for any isotope. See text for more details.

expected to yield an accuracy on the 1 meV level for the IS of the transition mentioned above, thus potentially outperforming the ∼50 meV precision of emission spectroscopy techniques [EBC96] by more than an order of magnitude. Since the only theoretical limitation in our scheme is the rather small natural line width, anticipated improvements of the bandwidth of short-wavelength lasers in the immediate future will allow to push these boundaries even further. Besides the radius, further properties of the nuclear charge distribution such as higher moments, deformation parameters [Coo06] and nuclear polarization contributions may even be accessible. In the optical range, the superior frequency resolution and intensity of existing lasers may be exploited by addressing, e.g., hyperfine transitions in few-electron highly charged ions.

In order to infer nuclear proton radii from experimental IS values, the dependence of the complete fluorescence spectrum on the variation $\delta\langle r^2\rangle$ of the mean square charge radius (averaged over the nuclear volume) is needed. Given the relative simplicity of such few-electron atomic states, this dependence can be calculated to higher precision than in the case of light elements [SNE$^+$06]. Such a spectrum is shown in Fig. 2.7 for the case of uranium, delivering directly the radius with respect to that of the ^{238}U isotope.

Laser systems with photon energies of up to a few keV (in the range of Li-like transitions) are presently available [ABB$^+$06, ECB$^+$07], allowing to excite elements as heavy as U. Future laser facilities are expected to increase the frequency limit to the order of tens of keVs, permitting to directly address the most relativistic very heavy H-like systems. E.g. for the case of Fig. 2.7, experimental photon emission rates are estimated to be on the order of 10^7 $1/s$ per ion at a laser intensity of 10^{12} W/cm^2, providing sufficient count statistics for a high-precision determination of the IS value. Table 2.1 lists values for further elements and charge states.

Table 2.1: Parameters for H-like ($1s$–$2p_{1/2}$) and Li-like ($2s$–$2p_{3/2}$) ions. Transition energies, line widths Γ, laser intensities I, and isotope shifts $\Delta\omega_{IS}$, are given. $x(y)$ stands for $x \times 10^y$.

Z	charge state	ω_{tr} [eV]	Γ [eV]	I [W/cm^2]	$\Delta\omega_{IS}$ [eV]
54	H	3.0904(4)	3.03(0)	1(15)	2.96(-2)
	Li	3.6406(2)	1.07(-4)	1(7)	3.44(-3)
60	H	3.8521(4)	5.47(0)	1(16)	3.00(-1)
	Li	5.7763(2)	3.38(-4)	1(8)	3.65(-2)
92	H	9.8065(4)	1.81(1)	1(17)	1.07(0)
	Li	4.1066(3)	4.48(-2)	1(12)	1.70(-1)

2.6 The spectrum of resonance fluorescence in three-level approximation

Resonance fluorescence in a two-level system discussed sofar constitutes the simplest model of bound atomic dynamics. A whole range of new phenomena becomes possible if one extends this picture with a third level and an additional coherent driving. In particular, the quantum manipulation of the system dynamics becomes possible when using a second laser field. In the following we develop a consistent relativistic theory of resonance fluorescence in an atomic three-level system.

2.6.1 Description of the model and equations of motion

The state function of a three-level atom can be written in the form

$$|\Psi(t)\rangle = C_a(t)|a\rangle + C_b(t)|b\rangle + C_c(t)|c\rangle\,. \tag{2.274}$$

It is easy to see following the calculations of two-levels atoms that the Hamiltonian of the three-level system interacting with two classical fields is given by

$$\mathscr{H} = \sum_{i=1}^{3} \varepsilon_i |i\rangle\langle i| + \Omega_R^{13}(e^{-i\omega_1 t}|3\rangle\langle 1| + e^{i\omega_1 t}|1\rangle\langle 3|) + \Omega_R^{12}(e^{-i\omega_2 t}|2\rangle\langle 1| + e^{i\omega_2 t}|1\rangle\langle 2|)\,, \tag{2.275}$$

where ε_i ($i \in \{1,2,3\}$) are the energies of the three stationary states of the atom, Ω_R^{12} and Ω_R^{13} are the Rabi frequencies of the driving field and $|j\rangle\langle i|$ are fermion operators that describe the creation of an electron in level i and annihilation in level j. ω_1 and ω_2 are the field frequencies between the levels $1 \to 3$ respectively $1 \to 2$. The reversible part of the master equation in the interaction picture has the form

$$\dot{\rho}' = -\frac{i}{\hbar}[\mathscr{H}_1', \rho']\,, \tag{2.276}$$

where

$$\mathscr{H}_1' = \hbar\Omega_R^{13}(|3\rangle\langle 1|e^{i\Delta_1 t} + |1\rangle\langle 3|e^{-i\Delta_1 t}) + \hbar\Omega_R^{12}(|2\rangle\langle 1|e^{i\Delta_2 t} + |1\rangle\langle 2|e^{-i\Delta_2 t})\,, \tag{2.277}$$

and

$$\Delta_1 = \omega_{31} - \omega_1\,, \quad \Delta_2 = \omega_{21} - \omega_2\,. \tag{2.278}$$

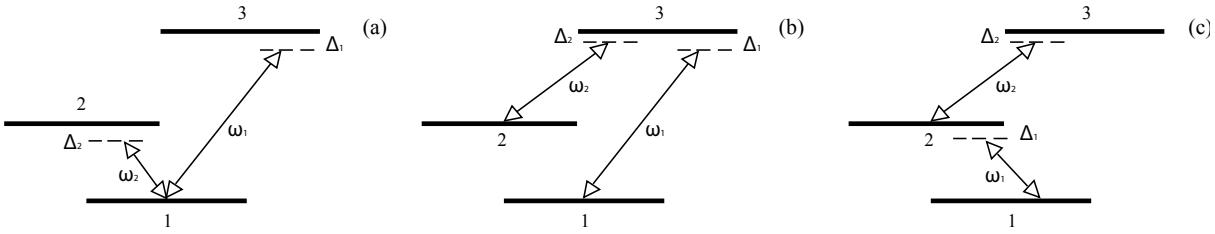

Figure 2.8: Level scheme of an (a) V-system, (b) Λ-system, and (c) Ξ-system. Here, ω_1 and ω_2 are laser frequencies, and Δ_1 and Δ_2 are the corresponding detunings from the atomic transition frequencies.

The prime denotes quantities in the interaction representation and ω_{31} and ω_{21} are atomic transition frequencies. The matrix elements of ρ' according to Eq. (2.276) satisfy coupled linear equations of motion containing explicit time-dependent factors of the complex exponential type. These can be removed with the transformation

$$R_{ii} = \rho'_{ii}\,(i = 1, 2, 3), \quad R_{12} = \rho'_{12}e^{i\Delta_2 t}, \quad R_{13} = \rho'_{13}e^{i\Delta_1 t}, \quad R_{23} = \rho'_{23}e^{i(\Delta_2 - \Delta_2)t}\,, \tag{2.279}$$

whose effect is to produce autonomous equations for the matrix elements R_{ij}.

The full master equation reads

$$\dot{\rho}' = -\frac{i}{\hbar}[\mathscr{H}'_1, \rho'] + \Lambda\rho'\,, \tag{2.280}$$

where the irreversible part of Eq. (2.280) is given by Eq. (2.14). Written in terms of the variable R_{ij}, Eq. (2.280) takes the explicit form

$$\begin{aligned}
\frac{dR_{12}}{d\tau} &= i\tilde{\Delta}_2 R_{12} - i\beta_1 R_{32} - i\beta_2(R_{22} - R_{11}) - \tilde{\gamma}_{12}R_{12}\,, \\
\frac{dR_{13}}{d\tau} &= i\tilde{\Delta}_1 R_{13} - i\beta_1(R_{33} - R_{11}) - i\beta_2 R_{23} - \tilde{\gamma}_{13}R_{13}\,, \\
\frac{dR_{22}}{d\tau} &= -i\beta_2(R_{12} - R_{21}) + \tilde{\Gamma}_{12}R_{11} + \tilde{\Gamma}_{32}R_{33} - (\tilde{\Gamma}_{21} + \tilde{\Gamma}_{23})R_{22}\,, \\
\frac{dR_{23}}{d\tau} &= i(\tilde{\Delta}_1 - \tilde{\Delta}_2)R_{23} + i\beta_1 R_{21} - i\beta_2 R_{13} - \tilde{\gamma}_{23}R_{23}\,, \\
\frac{dR_{33}}{d\tau} &= -i\beta_1(R_{13} - R_{31}) + \tilde{\Gamma}_{13}R_{11} + \tilde{\Gamma}_{23}R_{22} - (1 + \tilde{\Gamma}_{32})R_{33}\,,
\end{aligned} \tag{2.281}$$

where $R_{11} = 1 - R_{22} - R_{33}$, $\quad R_{21} = R^*_{12}$, $\quad R_{31} = R^*_{13}$ $\quad R_{32} = R^*_{23}$. In arriving at Eqs. (2.281) we have introduced the dimensionless time $\tau = \Gamma_{31}t$ and the scaled Rabi frequencies $\beta_1 = \Omega_R^{13}/\Gamma_{31}$ and $\beta_2 = \Omega_R^{12}/\Gamma_{31}$. The remaining rate constants are scaled to Γ_{31} and are labeled with a tilde.

It is convenient to represent the set of eight linearly independent equation for the matrix elements R_{ij} in the compact form

$$\frac{d}{d\tau}\Psi = L\Psi + I\,, \tag{2.282}$$

where the eight components of the vector Ψ are defined by

$$\begin{aligned}
\Psi_1 &= R_{12}\,, \quad \Psi_2 = R_{13}\,, \quad \Psi_3 = R_{21}\,, \quad \Psi_4 = R_{22}\,, \\
\Psi_5 &= R_{23}\,, \quad \Psi_6 = R_{31}\,, \quad \Psi_7 = R_{32}\,, \quad \Psi_8 = R_{33}\,,
\end{aligned} \tag{2.283}$$

and L is an 8×8 matrix:

$$L = \begin{pmatrix}
-(\tilde{\gamma}_{12}-i\tilde{\Delta}_2) & 0 & 0 & -2i\beta_2 & 0 & 0 & -i\beta_2 & \\
0 & -(\tilde{\gamma}_{13}-i\tilde{\Delta}_1) & 0 & -i\beta_1 & -i\beta_2 & 0 & -2i\beta_1 & \\
0 & 0 & -(\tilde{\gamma}_{12}+i\tilde{\Delta}_2) & 2i\beta_2 & i\beta_1 & 0 & i\beta_2 & \\
-i\beta_2 & 0 & i\beta_2 & -(\tilde{\Gamma}_{12}+\tilde{\Gamma}_{21}+\tilde{\Gamma}_{23}) & 0 & 0 & -(\tilde{\Gamma}_{12}-\tilde{\Gamma}_{32}) & \\
0 & -i\beta_2 & i\beta_1 & 0 & -[\tilde{\gamma}_{23}-i(\tilde{\Delta}_1-\tilde{\Delta}_2)] & 0 & 0 & \\
0 & 0 & 0 & i\beta_1 & 0 & -(\tilde{\gamma}_{13}+i\tilde{\Delta}_1) & 0 & \\
-i\beta_1 & 0 & 0 & 0 & 0 & i\beta_2 & 2i\beta_1 & \\
0 & -i\beta_1 & 0 & (\tilde{\Gamma}_{23}-\tilde{\Gamma}_{13}) & 0 & i\beta_1 & -(1+\tilde{\Gamma}_{12}+\tilde{\Gamma}_{13}) &
\end{pmatrix}. \tag{2.284}$$

The vector I is an inhomogeneous term with the components

$$\begin{aligned} I_1 &= i\beta_2\,, \quad I_2 = i\beta_1\,, \quad I_3 = -i\beta_2\,, \quad I_4 = \tilde{\Gamma}_{12}\,, \\ I_5 &= 0\,, \quad I_6 = -i\beta_1\,, \quad I_7 = 0\,, \quad I_8 = \tilde{\Gamma}_{13}\,. \end{aligned} \tag{2.285}$$

2.6.2 The calculation of the spectrum

Like in the case of the two-level atom, in the calculation of the spectra we only need to limit our considerations to the atomic correlation function

$$\Gamma(\tau_1, \tau_0) = \langle P^{(-)}(\tau_1) P^{(+)}(\tau_0) \rangle\,. \tag{2.286}$$

The total polarization operator of the three-level atom is given by

$$P(\tau) = \gamma_{12}(|1\rangle\langle 2| + |2\rangle\langle 1|) + \gamma_{13}(|1\rangle\langle 3| + |3\rangle\langle 1|)\,, \tag{2.287}$$

where γ_{ij} are the moduli of the induced transition matrix elements and we have assumed $\gamma_{23} = 0$, i.e. the 2–3 transition is not driven with a third laser field. The positive and the negative parts of the polarization operator are given by

$$\langle P^{(+)}(t) \rangle = \gamma_{12}|1\rangle\langle 2| + \gamma_{13}|1\rangle\langle 3|\,, \quad P^{(-)}(t) = [P^{(+)}(t)]^\dagger\,. \tag{2.288}$$

The starting point is the one-time average

$$P^{(-)}(\tau_1) = Tr[\rho(\tau_1)(\gamma_{12}(|2\rangle\langle 1| + \gamma_{13}|3\rangle\langle 1|)]\,, \tag{2.289}$$

which can be written in terms of $\Psi_i(\tau_1)$ as follows:

$$\langle P^{(-)}(\tau_1) \rangle = \gamma_{12} e^{i\omega_2\tau_1} \Psi_1(\tau_1) + \gamma_{13} e^{i\omega_1\tau_1} \Psi_2(\tau_1)\,. \tag{2.290}$$

At this point the essential step is to express each of the matrix elements $\Psi_i(\tau_1)$ that appear in Eq. (2.290) in terms of their *initial* values $\tau = \tau_0$. While this could be done beginning with the formal integration of Eq. (2.282), here we operate in the space of the Laplace transform. Thus, Eq. (2.290) yields

$$\langle \hat{P}^{(-)}(z) \rangle = \gamma_{12} \hat{\Psi}_1(z_2) + \gamma_{13} \hat{\Psi}_2(z_1)\,, \tag{2.291}$$

where $z_1 = z - i\omega_1$ and $z_2 = z - i\omega_2$.

Using Eq. (2.25), Eq. (2.291) can be cast into the required form

$$\langle \hat{P}^{(-)}(z) \rangle = \sum_j [\gamma_{12} M_{1j}(z_2) + \gamma_{13} M_{2j}(z_1)] \Psi_j(\tau_0) + \sum_j \left[\frac{\gamma_{12}}{z_2} M_{1j}(z_2) + \frac{\gamma_{13}}{z_1} M_{2j}(z_1) \right] I_j\,. \tag{2.292}$$

In the following, we need to express $\Psi_j(\tau_0)$ and I_j in the form of expectation values of system operators at $\tau = \tau_0$. Applying the regression theorem yields

$$\begin{aligned} \langle \hat{P}^{(-)}(z) P^{(+)}(\tau_0) \rangle_{\tau_0} &= \gamma_{12}[\gamma_{12} M_{11}(z_2) + \gamma_{13} M_{21}(z_1)] \Psi_4(\tau_0) e^{-i\omega_2\tau_0} \\ &+ \gamma_{13}[\gamma_{12} M_{11}(z_2) + \gamma_{13} M_{21}(z_1)] \Psi_7(\tau_0) e^{-i\omega_1\tau_0} \\ &+ \gamma_{12}[\gamma_{12} M_{12}(z_2) + \gamma_{13} M_{22}(z_1)] \Psi_5(\tau_0) e^{-i\omega_2\tau_0} \\ &+ \gamma_{13}[\gamma_{12} M_{12}(z_2) + \gamma_{13} M_{22}(z_1)] \Psi_8(\tau_0) e^{-i\omega_1\tau_0} \\ &+ \sum_j [\frac{\gamma_{12}}{z_2} M_{1j}(z_2) + \frac{\gamma_{13}}{z_1} M_{2j}(z_1)] I_j [\gamma_{12} \Psi_3(\tau_0) e^{-i\omega_2\tau_0} + \gamma_{13} \Psi_6(\tau_0) e^{-i\omega_1\tau_0}]\,. \end{aligned} \tag{2.293}$$

Since we consider the laser fields with perpendicular polarization, we are not keeping the terms with $\gamma_{12}\gamma_{13}$. In the limiting case $\tau_0 \to \infty$ one has then

$$\langle \hat{P}^{(-)}(z)P^{(+)}(\infty)\rangle_{\tau_0} = \gamma_{12}^2 \left[M_{11}(z_2)\Psi_4(\infty) + M_{12}(z_2)\Psi_5(\infty) + \frac{1}{z_2}\sum_j M_{1j}(z_2)\Psi_3(\infty)I_j \right]$$

$$+\gamma_{13}^2 \left[M_{21}(z_1)\Psi_7(\infty) + M_{22}(z_1)\Psi_8(\infty) + \frac{1}{z_1}\sum_j M_{2j}(z_1)\Psi_6(\infty)I_j \right] . \tag{2.294}$$

Eq. (2.294) shows that the spectrum of resonance fluorescence is composed of two separate structures with center frequencies located at ω_2 and ω_1, respectively, and magnitudes proportional to the transition matrix elements of the two atomic transitions. The incoherent part can be calculated according to the prescription

$$\hat{\Gamma}_V^{\rm incoh}(z) = \hat{\Gamma}(z) - \frac{1}{z_1}\lim_{z_1\to 0} z_1\hat{\Gamma}(z) - \frac{1}{z_2}\lim_{z_2\to 0} z_2\hat{\Gamma}(z) . \tag{2.295}$$

Finally, the required emission spectrum is given by

$$S(\omega) = \Re\hat{\Gamma}_V^{\rm incoh}(z)|_{z=i\omega} , \tag{2.296}$$

where

$$\begin{aligned} \hat{\Gamma}_V^{\rm incoh}(z) &= \gamma_{12}^2[M_{11}(z_2)\Psi_4(\infty) + M_{12}(z_2)\Psi_5(\infty) + \sum_j N_{1j}(z_2)\Psi_3(\infty)I_j] \\ &+ \gamma_{13}^2[M_{21}(z_1)\Psi_7(\infty) + M_{22}(z_1)\Psi_8(\infty) + \sum_j N_{2j}(z_1)\Psi_6(\infty)I_j] , \end{aligned} \tag{2.297}$$

and the matrix N is defined as

$$N_{ij}(z) = (L^{-1}(z-L)^{-1})_{ij} . \tag{2.298}$$

The result of the calculation in the case of the $3 \to 1$ transition in a Λ system (see Fig. 2.8 b)) is

$$\hat{\Gamma}_{\Lambda 1}^{\rm incoh}(z) = \gamma_{13}^2[M_{21}(z_1)\Psi_7(\infty) + M_{22}(z_1)\Psi_8(\infty) + \sum_j N_{2j}(z_1)\Psi_6(\infty)I_j] . \tag{2.299}$$

The same procedure can be applied to the three polarization operators, with the results (for the $3 \to 2$ emission):

$$\begin{aligned} \hat{\Gamma}_{\Lambda 2}^{\rm incoh}(z) &= \gamma_{23}^2[M_{53}(z_2)\Psi_6(\infty) + M_{56}(z_2)\Psi_7(\infty) + M_{55}(z_2)\Psi_8(\infty) \\ &+ \sum_j N_{5j}(z_2)\Psi_7(\infty)I_j] , \end{aligned} \tag{2.300}$$

where $z_1 = z - i\tilde{\omega}_1$, and $z_2 = z - i\tilde{\omega}_2$.

In the case of the Ξ (or ladder-type) system (see Fig. 2.8 c)), the $2 \to 1$ power spectrum is

$$\hat{\Gamma}_{\Xi 1}^{\rm incoh}(z) = \gamma_{12}^2[M_{11}(z_1)\Psi_4(\infty) + M_{12}(z_1)\Psi_5(\infty) + \sum_j N_{1j}(z_1)\Psi_3(\infty)I_j] , \tag{2.301}$$

and the $3 \to 2$ emission spectrum is given as

$$\begin{aligned} \hat{\Gamma}_{\Xi 2}^{\rm incoh}(z) &= \gamma_{23}^2[M_{53}(z_2)\Psi_6(\infty) + M_{54}(z_2)\Psi_7(\infty) + M_{55}(z_2)\Psi_8(\infty) \\ &+ \sum_j N_{5j}(z_2)\Psi_7(\infty)I_j] . \end{aligned} \tag{2.302}$$

2.6.3 Analytic calculation of the spectra in the strong field approximation

In what follows we only consider the case of a resonant interaction of a laser with the $1 \rightarrow 2$ transition, i.e. the detuning is $\tilde{\Delta}_1 = 0$ (see Fig.2.8(a)) and we study the emission spectrum of the $3 \rightarrow 1$ transition. We employ the interaction Hamiltonian of Eq. (2.277) assuming $\tilde{\Delta}_1 = 0$. We consider the dressed atomic states

$$
\begin{aligned}
|r\rangle &= \left[\frac{\lambda_1^2}{\Omega_2^2} + 1 + \left(\frac{\lambda_1^2}{\Omega_1\Omega_2} - \frac{\Omega_2}{\Omega_1}\right)^2\right]^{-1/2} \left[\frac{\lambda_1}{\Omega_2}|1\rangle + |2\rangle + \left(\frac{\lambda_1^2}{\Omega_1\Omega_2} - \frac{\Omega_2}{\Omega_1}\right)|3\rangle\right], \quad (2.303)\\
|s\rangle &= \left[\frac{\lambda_2^2}{\Omega_2^2} + 1 + \left(\frac{\lambda_2^2}{\Omega_1\Omega_2} - \frac{\Omega_2}{\Omega_1}\right)^2\right]^{-1/2} \left[\frac{\lambda_2}{\Omega_2}|1\rangle + |2\rangle + \left(\frac{\lambda_2^2}{\Omega_1\Omega_2} - \frac{\Omega_2}{\Omega_1}\right)|3\rangle\right],\\
|t\rangle &= \left[\frac{\lambda_3^2}{\Omega_2^2} + 1 + \left(\frac{\lambda_3^2}{\Omega_1\Omega_2} - \frac{\Omega_2}{\Omega_1}\right)^2\right]^{-1/2} \left[\frac{\lambda_3}{\Omega_2}|1\rangle + |2\rangle + \left(\frac{\lambda_3^2}{\Omega_1\Omega_2} - \frac{\Omega_2}{\Omega_1}\right)|3\rangle\right],
\end{aligned}
$$

with the λ_i defined as

$$
\begin{aligned}
\lambda_1 &= \frac{\hbar\Omega_2^2\Delta_1}{\Omega_1^2+\Omega_2^2} + \mathscr{O}(\Delta_1)^2, \quad (2.304)\\
\lambda_2 &= \hbar\sqrt{\Omega_1^2+\Omega_2^2} + \frac{\hbar\Omega_1^2\Delta_1}{2(\Omega_1^2+\Omega_2^2)} + \mathscr{O}(\Delta_1)^2,\\
\lambda_3 &= -\hbar\sqrt{\Omega_1^2+\Omega_2^2} + \frac{\hbar\Omega_1^2\Delta_1}{2(\Omega_1^2+\Omega_2^2)} + \mathscr{O}(\Delta_1)^2.
\end{aligned}
$$

In the first order of Δ_1, the dressed atomic states become

$$
\begin{aligned}
|r\rangle &= \frac{\Delta_1}{\Omega_2}\sin\theta^2\cos\theta|1\rangle + \cos\theta|2\rangle - \sin\theta|3\rangle, \quad (2.305)\\
|s\rangle &= \left(\frac{1}{\sqrt{2}} - \frac{1}{\sqrt{32}}\frac{\Delta_1}{\Omega_2}\sin\theta\cos\theta^2\right)|1\rangle + \left(\frac{\sin\theta}{\sqrt{2}} - \frac{3}{\sqrt{32}}\frac{\Delta_1}{\Omega_2}\sin\theta\cos\theta^2\right)|2\rangle\\
&+ \left(\frac{\cos\theta}{\sqrt{2}} + \frac{1}{\sqrt{32}}\frac{\Delta_1}{\Omega_2}\sin\theta\cos\theta(1+3\sin\theta^2)\right)|3\rangle,\\
|t\rangle &= \left(-\frac{1}{\sqrt{2}} - \frac{1}{\sqrt{32}}\frac{\Delta_1}{\Omega_2}\sin\theta\cos\theta^2\right)|1\rangle + \left(\frac{\sin\theta}{\sqrt{2}} + \frac{3}{\sqrt{32}}\frac{\Delta_1}{\Omega_2}\sin\theta\cos\theta^2\right)|2\rangle\\
&+ \left(\frac{\cos\theta}{\sqrt{2}} - \frac{1}{\sqrt{32}}\frac{\Delta_1}{\Omega_2}\sin\theta\cos\theta(1+3\sin\theta^2)\right)|3\rangle,
\end{aligned}
$$

with the angle θ abstractly defined by $\tan\theta = \Omega_2/\Omega_1$. These states are eigenstates of $\mathscr{H}_1'$, i.e.,

$$
\begin{aligned}
\mathscr{H}_1'|r\rangle &= \sin\theta^2\Delta_1|r\rangle, \quad (2.306)\\
\mathscr{H}_1'|s\rangle &= \hbar(\Omega_R + \cos\theta^2\Delta_1)|s\rangle,\\
\mathscr{H}_1'|t\rangle &= \hbar(-\Omega_R + \cos\theta^2\Delta_1|t\rangle,
\end{aligned}
$$

and $\Omega_R = (\Omega_1+\Omega_2)^{1/2}$ represents the effective applied Rabi frequency. In fact we show that, while Ω_R must be large for this approximation to hold, no restrictions are posed on the individual magnitudes of the two Rabi frequencies Ω_1 and Ω_2.

We consider again the master equation of the density operator in the interaction picture:

$$
\dot{\rho}' = -\frac{i}{\hbar}[\mathscr{H}_1', \rho'] + \Lambda\rho'. \quad (2.307)
$$

The reversible part of Eq. (2.307) takes a very simple form owing to the fact that the states are exact eigenstates of $\mathscr{H}_1'$. Thus we have

$$\left(\frac{d}{dt}\right)_{rev}\begin{pmatrix}\rho'_{st}\\ \rho'_{sr}\\ \rho'_{rt}\\ \rho'_{ss}\\ \rho'_{tt}\end{pmatrix}=\begin{pmatrix}-2i\Omega_R\rho'_{st}\\ -i(\Omega_R+\cos 2\theta\Delta_1)\rho'_{sr}\\ -i(\Omega_R-\cos 2\theta\Delta_1)\rho'_{rt}\\ 0\\ 0\end{pmatrix}. \tag{2.308}$$

Again, we have the trace condition

$$\rho'_{rr}=1-\rho'_{ss}-\rho'_{tt}\,, \tag{2.309}$$

and the Hermitian symmetry

$$\rho'_{rs}=(\rho'_{sr})^*\,,\quad \rho'_{tr}=(\rho'_{rt})^*\,,\quad \rho'_{ts}=(\rho'_{st})^*\,. \tag{2.310}$$

It is interesting to observe that of the eight independent components $\rho'_{\mu\nu}$ of the density operator (we use Greek indices to denote the matrix elements in the dresses state representation, and Latin indices for the standard energy representation), two are associated with the frequency $+i\Omega_R$, and two with $-i\Omega_R$, two with zero frequency, and one each with $\pm 2i\Omega_R$ (when $\Delta_1=0$). These grouping reflect the various contributions of the density operator to the five spectral components.

In this representations the irreversible part of the master equation becomes rather complex. In fact, the original irreversible part of the master equation is

$$\left(\frac{d}{dt}\right)_{irrev}\rho'_{ij}=\sum_{pq}\Lambda_{ijpq}\rho'_{pq}\,, \tag{2.311}$$

where Λ_{ijpq} are the various decay rates that appear explicitly in Eq. (2.14). From the transformation equation between the two pictures $\rho'_{\mu\nu}=\sum_{ij}\langle\mu|i\rangle\rho'_{ij}\langle j|\nu\rangle$, it is easy to obtain

$$\left(\frac{d}{dt}\right)_{irrev}\rho'_{\mu\nu}=\sum_{\sigma\tau}\left(\sum_{ijpq}\langle\mu|i\rangle\langle j|\nu\rangle\langle p|\sigma\rangle\langle\tau|q\rangle\Lambda_{ijpq}\right)\rho'_{\sigma\tau}\equiv\sum_{\sigma\tau}\Gamma_{\mu\nu\sigma\tau}\rho'_{\sigma\tau}\,, \tag{2.312}$$

where the transformation matrix elements $\langle\mu|i\rangle$ can be taken with comparision with Eq. (2.305).

We now focus on the derivation of an expression for the fluorescence spectrum in the limit in which Ω_R is much larger than all the decay rates. Following a procedure that accounts for the approach to steady state and for the response of the system around the steady state with an accuracy of order $1/\Omega_R$, we introduce the usual vector Ψ with the components

$$\begin{aligned}\Psi_1 &= \rho'_{st}\,,\quad \Psi_2=\rho'_{sr}\,,\quad \Psi_3=\rho'_{rt}\,,\quad \Psi_4=\rho'_{ss}\,,\\ \Psi_5 &= \rho'_{tt}\,,\quad \Psi_6=\rho'_{rs}\,,\quad \Psi_7=\rho'_{tr}\,,\quad \Psi_8=\rho'_{ts}\,,\end{aligned} \tag{2.313}$$

and $\rho'_{rr}=1-\rho'_{ss}-\rho'_{tt}=1-\Psi_4-\Psi_5$. This vector is a solution of the linear equation

$$\frac{d}{dt}\Psi=L\Psi+I\,, \tag{2.314}$$

and, in steady state, it takes the form

$$\Psi(\infty)=-L^{-1}I\,. \tag{2.315}$$

Normally we would solve Eq. (2.315) by numerical techniques. However, we are interested in an approximate asymptotic solution, we note that in the steady state the off-diagonal elements of ρ' are of the order of $1/\Omega_R$, while the diagonal elements are of the order of unity. In this limit the dominant matrix elements are

$$\begin{aligned}\Psi_4(\infty) &= \frac{\Gamma_{sstt}\Gamma_{ttrr} - \Gamma_{ssrr}\Gamma_{tttt})}{\Gamma_{sstt}(\Gamma_{ttrr} - \Gamma_{ttss}) + \Gamma_{ssrr}(\Gamma_{ttss} - \Gamma_{tttt} + \Gamma_{ssss}(-\Gamma_{ttrr} + \Gamma_{tttt})}\,, \\ \Psi_5(\infty) &= \frac{\Gamma_{ssss}\Gamma_{ttrr} - \Gamma_{ssrr}\Gamma_{ttss})}{\Gamma_{sstt}(\Gamma_{ttrr} - \Gamma_{ttss}) + \Gamma_{ssrr}(\Gamma_{ttss} - \Gamma_{tttt} + \Gamma_{ssss}(-\Gamma_{ttrr} + \Gamma_{tttt})}\,.\end{aligned} \tag{2.316}$$

We now define the deviation from the steady state as

$$\delta\Psi = \Psi(t) - \Psi(\infty)\,, \tag{2.317}$$

which satisfies the equation

$$\frac{d}{dt}\delta\Psi(t) = L\delta\Psi(t)\,. \tag{2.318}$$

In the asymptotic limit of interest, however, we can replace the matrix L in Eq. (2.318) with a block-diagonal approximation L_0 which is accurate up to corrections of order $1/\Omega_R$. This step allows the analytic calculation of the spectrum.

In order to understand the nature of this approximation, let us consider the explicit form of the equations for $\delta\rho'_{\mu\nu}$, for simplicity just when $\Delta_1 = 0$. Similar analysis may be performed for $\Delta_1 \neq 0$. Here we only focus on the first three of the eight independent equations because this will be sufficient for our purposes. We have

$$\begin{aligned}\frac{d}{dt}\delta\rho'_{st} = &- 2i\Omega_R\delta\rho'_{st} + \Gamma_{strs}\delta\rho'_{rs} + \Gamma_{strt}\delta\rho'_{rt} + \Gamma_{stsr}\delta\rho'_{sr} + \Gamma_{stst}\delta\rho'_{st} + \Gamma_{sttr}\delta\rho'_{tr} \\ &+ \Gamma_{stts}\delta\rho'_{ts} + (\Gamma_{stss} - \Gamma_{strr})\delta\rho'_{ss} + (\Gamma_{sttt} - \Gamma_{strr})\delta\rho'_{tt}\,, \\ \frac{d}{dt}\delta\rho'_{sr} = &- i\Omega_R\delta\rho'_{sr} + \Gamma_{srrs}\delta\rho'_{rs} + \Gamma_{srrt}\delta\rho'_{rt} + \Gamma_{srsr}\delta\rho'_{sr} + \Gamma_{srst}\delta\rho'_{st} + \Gamma_{srtr}\delta\rho'_{tr} \\ &+ \Gamma_{srts}\delta\rho'_{ts} + (\Gamma_{srss} - \Gamma_{srrr})\delta\rho'_{ss} + (\Gamma_{srtt} - \Gamma_{srrr})\delta\rho'_{tt}\,, \\ \frac{d}{dt}\delta\rho'_{rt} = &- i\Omega_R\delta\rho'_{rt} + \Gamma_{rtrs}\delta\rho'_{rs} + \Gamma_{rtrt}\delta\rho'_{rt} + \Gamma_{rtsr}\delta\rho'_{sr} + \Gamma_{rtst}\delta\rho'_{st} + \Gamma_{rttr}\delta\rho'_{tr} \\ &+ \Gamma_{rtts}\delta\rho'_{ts} + (\Gamma_{rtss} - \Gamma_{rtrr})\delta\rho'_{ss} + (\Gamma_{rttt} - \Gamma_{rtrr})\delta\rho'_{tt}\,.\end{aligned} \tag{2.319}$$

If we let

$$\begin{aligned}&\delta\rho'_{st} = e^{-2i\Omega_R t}R_{st}\,, \quad \delta\rho'_{sr} = e^{-i\Omega_R t}R_{sr}\,, \quad \delta\rho'_{rt} = e^{-i\Omega_R t}R_{rt}\,, \quad \delta\rho'_{ss} = R_{ss}\,, \\ &\delta\rho'_{tt} = R_{tt}\,, \quad \delta\rho'_{rs} = e^{i\Omega_R t}R_{rs}\,, \quad \delta\rho'_{tr} = e^{i\Omega_R t}R_{tr}\,, \quad \delta\rho'_{ts} = e^{2i\Omega_R t}R_{ts}\,,\end{aligned} \tag{2.320}$$

we obtain

$$\begin{aligned}\frac{dR_{st}}{dt} &= \Gamma_{stst}R_{st} + \mathscr{O}(1/\Omega_R)\,, \\ \frac{dR_{sr}}{dt} &= \Gamma_{srrt}R_{rt} + \Gamma_{srsr}R_{sr} + \mathscr{O}(1/\Omega_R)\,, \\ \frac{dR_{rt}}{dt} &= \Gamma_{rtrt}R_{rt} + \Gamma_{rtsr}R_{sr} + \mathscr{O}(1/\Omega_R)\,,\end{aligned} \tag{2.321}$$

where $\mathscr{O}(1/\Omega_R)$ denotes rapidly oscillating terms.

In view of the assumed large value of Ω_R, it is reasonable to drop the oscillating contributions so that, in terms of the original variable, we have

$$\begin{aligned}
\frac{d}{dt}\delta\rho'_{st} &= (\Gamma_{stst} - 2i\Omega_R)\delta\rho'_{st}\,, \\
\frac{d}{dt}\delta\rho'_{sr} &= (\Gamma_{srsr} - i\Omega_R)\delta\rho'_{sr} + \Gamma_{srrt}\delta\rho'_{rt}\,, \\
\frac{d}{dt}\delta\rho'_{rt} &= \Gamma_{rtsr}\delta\rho'_{sr} + (\Gamma_{rtrt} - i\Omega_R)\delta\rho'_{rt}\,.
\end{aligned} \tag{2.322}$$

Hence, by neglecting the rapidly oscillating components, the new matrix L_0 can be obtained from the original matrix L after ignoring the elements outside the block-diagonal structure composed of five submatrices:

$$L_0 = \begin{pmatrix}
(1\times 1) & & & & \\
& (2\times 2) & & & \\
& & (2\times 2) & & \\
& & & (2\times 2) & \\
& & & & (1\times 1)
\end{pmatrix}. \tag{2.323}$$

The result of this procedure is a fluctuation equation of the form

$$\frac{d}{dt}\delta\Psi(t) = L_0\delta\Psi(t)\,, \tag{2.324}$$

or, in terms of the original vector Ψ,

$$\frac{d}{dt}\Psi(t) = L_0\Psi(t) + I_\infty\,, \tag{2.325}$$

where $I_\infty = -L_0\Psi(\infty)$. The diagonal blocks of L_0, denoted by $(L_0)_i$ are given explicitly by

$$\begin{aligned}
(L_0)_1 &= \Gamma_{stst} - 2i\Omega_R\,, \\
(L_0)_2 &= \begin{pmatrix} \Gamma_{srsr} - i(\Omega_R + \Delta_1\cos 2\theta) & \Gamma_{srrt} \\ \Gamma_{stsr} & \Gamma_{rtrt} - i(\Omega_R - \Delta_1\cos 2\theta) \end{pmatrix}, \\
(L_0)_3 &= \begin{pmatrix} \Gamma_{ssss} - \Gamma_{ssrr} & \Gamma_{sstt} - \Gamma_{ssrr} \\ \Gamma_{ttss} - \Gamma_{ttrr} & \Gamma_{tttt} - \Gamma_{ttrr} \end{pmatrix}, \\
(L_0)_4 &= \begin{pmatrix} \Gamma_{rsrs} + i(\Omega_R + \Delta_1\cos 2\theta) & \Gamma_{rstr} \\ \Gamma_{trrs} & \Gamma_{trtr} + i(\Omega_R - \Delta_1\cos 2\theta) \end{pmatrix}, \\
(L_0)_5 &= \Gamma_{tsts} + 2i\Omega_R\,.
\end{aligned} \tag{2.326}$$

The quantities $\Gamma_{\mu\nu\sigma\tau}$ are calculated in the first order of Δ_1

$$\begin{aligned}
\Gamma_{stst} &= \tfrac{1}{8}(-4\Gamma_{31}\cos\theta^2 - 2\Gamma_{32}\cos\theta^2 - \gamma_1\cos\theta^2 - 2\Gamma_{31}\cos\theta^4 - 2\Gamma_{32}\cos\theta^4 - 4\Gamma_{21}\sin\theta^2 \\
&- 2\Gamma_{21}\cos\theta^2\sin\theta^2 - 2\Gamma_{31}\cos\theta^2\sin\theta^2 - 2\Gamma_{21}\sin\theta^4) + \mathscr{O}(\Delta_1)\,,
\end{aligned} \tag{2.327}$$

$$\begin{aligned}
\Gamma_{tsts} &= \tfrac{1}{8}(-4\Gamma_{31}\cos\theta^2 - 2\Gamma_{32}\cos\theta^2 - \gamma_1\cos\theta^2 - 2\Gamma_{31}\cos\theta^4 - 2\Gamma_{32}\cos\theta^4 - 4\Gamma_{21}\sin\theta^2 \\
&- 2\Gamma_{21}\cos\theta^2\sin\theta^2 - 2\Gamma_{31}\cos\theta^2\sin\theta^2 - 2\Gamma_{21}\sin\theta^4) + \tfrac{1}{16}(-\gamma_1\cos\theta^2\sin\theta - \gamma_1\cos\theta^4\sin\theta \\
&- 3\gamma_1\cos\theta^2\sin\theta^3)\frac{\Delta_1}{\Omega_2} + \mathscr{O}(\Delta_1)^2\,,
\end{aligned}$$

$$
\begin{aligned}
\Gamma_{srsr} &= \tfrac{1}{4}(-\Gamma_{21}\cos\theta^2 - \Gamma_{21}\cos\theta^4 - \Gamma_{31}\cos\theta^4 - \Gamma_{32}\cos\theta^4 - \Gamma_{31}\sin\theta^2 - \Gamma_{32}\sin\theta^2 \\
&- \gamma_1\sin\theta^2 - 2\Gamma_{21}\cos\theta^2\sin\theta^2 - 2\Gamma_{31}\cos\theta^2\sin\theta^2 - 4\Gamma_{32}\cos\theta^2\sin\theta^2 - \Gamma_{21}\sin\theta^4 - \Gamma_{31}\sin\theta^4 \\
&- \Gamma_{32}\sin\theta^4) + \tfrac{1}{8}(-\Gamma_{31}\cos\theta^4\sin\theta - \Gamma_{32}\cos\theta^4\sin\theta + 6\Gamma_{21}\cos\theta^4\sin\theta^2 + 3\Gamma_{32}\cos\theta^4\sin\theta^2 \\
&+ 4\Gamma_{21}\cos\theta^2\sin\theta^3 - 5\Gamma_{31}\cos\theta^2\sin\theta^3 - 2\Gamma_{32}\cos\theta^2\sin\theta^3 + \gamma_1\cos\theta^2\sin\theta^3 - 3\Gamma_{21}\cos\theta^4\sin\theta^3 \\
&- 3\Gamma_{31}\cos\theta^4\sin\theta^3 - 3\Gamma_{32}\cos\theta^4\sin\theta^3 + 3\Gamma_{21}\cos\theta^2\sin\theta^4 + 3\Gamma_{31}\cos\theta^2\sin\theta^4 + 3\Gamma_{32}\cos\theta^2\sin\theta^4 \\
&- 6\Gamma_{31}\cos\theta^2\sin\theta^5 - 9\Gamma_{32}\cos\theta^2\sin\theta^5)\frac{\Delta_1}{\Omega_2} + \mathscr{O}(\Delta_1)^2\,,
\end{aligned}
$$

$$
\begin{aligned}
\Gamma_{trtr} &= \tfrac{1}{4}(-\Gamma_{21}\cos\theta^2 - \Gamma_{21}\cos\theta^4 - \Gamma_{31}\cos\theta^4 - \Gamma_{32}\cos\theta^4 - \Gamma_{31}\sin\theta^2 - \Gamma_{32}\sin\theta^2 \\
&- \gamma_1\sin\theta^2 - 2\Gamma_{21}\cos\theta^2\sin\theta^2 - 2\Gamma_{31}\cos\theta^2\sin\theta^2 - 4\Gamma_{32}\cos\theta^2\sin\theta^2 - \Gamma_{21}\sin\theta^4 - \Gamma_{31}\sin\theta^4 \\
&- \Gamma_{32}\sin\theta^4) - \tfrac{1}{8}(-\Gamma_{31}\cos\theta^4\sin\theta - \Gamma_{32}\cos\theta^4\sin\theta + 6\Gamma_{21}\cos\theta^4\sin\theta^2 + 3\Gamma_{32}\cos\theta^4\sin\theta^2 \\
&+ 4\Gamma_{21}\cos\theta^2\sin\theta^3 - 5\Gamma_{31}\cos\theta^2\sin\theta^3 - 2\Gamma_{32}\cos\theta^2\sin\theta^3 + \gamma_1\cos\theta^2\sin\theta^3 - 3\Gamma_{21}\cos\theta^4\sin\theta^3 \\
&- 3\Gamma_{31}\cos\theta^4\sin\theta^3 - 3\Gamma_{32}\cos\theta^4\sin\theta^3 + 3\Gamma_{21}\cos\theta^2\sin\theta^4 + 3\Gamma_{31}\cos\theta^2\sin\theta^4 + 3\Gamma_{32}\cos\theta^2\sin\theta^4 \\
&- 6\Gamma_{31}\cos\theta^2\sin\theta^5 - 9\Gamma_{32}\cos\theta^2\sin\theta^5)\frac{\Delta_1}{\Omega_2} + \mathscr{O}(\Delta_1)^2\,,
\end{aligned}
$$

$$
\begin{aligned}
\Gamma_{rtrt} &= \tfrac{1}{4}(-\Gamma_{21}\cos\theta^2 - \Gamma_{21}\cos\theta^4 - \Gamma_{31}\cos\theta^4 - \Gamma_{32}\cos\theta^4 - \Gamma_{31}\sin\theta^2 - \Gamma_{32}\sin\theta^2 \\
&- 2\Gamma_{21}\cos\theta^2\sin\theta^2 - 2\Gamma_{31}\cos\theta^2\sin\theta^2 - 4\Gamma_{32}\cos\theta^2\sin\theta^2 - \Gamma_{21}\sin\theta^4 - \Gamma_{31}\sin\theta^4 \\
&- \Gamma_{32}\sin\theta^4) - \tfrac{1}{8}(-\Gamma_{31}\cos\theta^4\sin\theta - \Gamma_{32}\cos\theta^4\sin\theta + 6\Gamma_{21}\cos\theta^4\sin\theta^2 + 3\Gamma_{32}\cos\theta^4\sin\theta^2 \\
&+ 4\Gamma_{21}\cos\theta^2\sin\theta^3 - 5\Gamma_{31}\cos\theta^2\sin\theta^3 - 2\Gamma_{32}\cos\theta^2\sin\theta^3 - 3\Gamma_{21}\cos\theta^4\sin\theta^3 \\
&- 3\Gamma_{31}\cos\theta^4\sin\theta^3 - 3\Gamma_{32}\cos\theta^4\sin\theta^3 + 3\Gamma_{21}\cos\theta^2\sin\theta^4 + 3\Gamma_{31}\cos\theta^2\sin\theta^4 + 3\Gamma_{32}\cos\theta^2\sin\theta^4 \\
&- 6\Gamma_{31}\cos\theta^2\sin\theta^5 - 9\Gamma_{32}\cos\theta^2\sin\theta^5)\frac{\Delta_1}{\Omega_2} + \mathscr{O}(\Delta_1)^2\,,
\end{aligned}
$$

$$
\begin{aligned}
\Gamma_{rsrs} &= \tfrac{1}{4}(-\Gamma_{21}\cos\theta^2 - \Gamma_{21}\cos\theta^4 - \Gamma_{31}\cos\theta^4 - \Gamma_{32}\cos\theta^4 - \Gamma_{31}\sin\theta^2 - \Gamma_{32}\sin\theta^2 \\
&- 2\Gamma_{21}\cos\theta^2\sin\theta^2 - 2\Gamma_{31}\cos\theta^2\sin\theta^2 - 4\Gamma_{32}\cos\theta^2\sin\theta^2 - \Gamma_{21}\sin\theta^4 - \Gamma_{31}\sin\theta^4 \\
&- \Gamma_{32}\sin\theta^4) + \tfrac{1}{8}(-\Gamma_{31}\cos\theta^4\sin\theta - \Gamma_{32}\cos\theta^4\sin\theta + 6\Gamma_{21}\cos\theta^4\sin\theta^2 + 3\Gamma_{32}\cos\theta^4\sin\theta^2 \\
&+ 4\Gamma_{21}\cos\theta^2\sin\theta^3 - 5\Gamma_{31}\cos\theta^2\sin\theta^3 - 2\Gamma_{32}\cos\theta^2\sin\theta^3 - 3\Gamma_{21}\cos\theta^4\sin\theta^3 \\
&- 3\Gamma_{31}\cos\theta^4\sin\theta^3 - 3\Gamma_{32}\cos\theta^4\sin\theta^3 + 3\Gamma_{21}\cos\theta^2\sin\theta^4 + 3\Gamma_{31}\cos\theta^2\sin\theta^4 + 3\Gamma_{32}\cos\theta^2\sin\theta^4 \\
&- 6\Gamma_{31}\cos\theta^2\sin\theta^5 - 9\Gamma_{32}\cos\theta^2\sin\theta^5)\frac{\Delta_1}{\Omega_2} + \mathscr{O}(\Delta_1)^2\,,
\end{aligned}
$$

$$
\begin{aligned}
\Gamma_{srrt} &= -\tfrac{1}{2}\Gamma_{32}\cos\theta^2\sin\theta^2 + \tfrac{1}{8}(3\Gamma_{32}\cos\theta^4\sin\theta^2 + 4\Gamma_{21}\cos\theta^2\sin\theta^3 - 4\Gamma_{31}\cos\theta^2\sin\theta^3 \\
&+ \Gamma_{32}\cos\theta^2\sin\theta^3 + 2\gamma_1\cos\theta^2\sin\theta^2 + 3\Gamma_{32}\cos\theta^2\sin\theta^5)\frac{\Delta_1}{\Omega_1} + \mathscr{O}(\Delta_1)^2\,,
\end{aligned}
$$

$$
\begin{aligned}
\Gamma_{rtsr} &= -\tfrac{1}{2}\Gamma_{32}\cos\theta^2\sin\theta^2 + \tfrac{1}{8}(-3\Gamma_{32}\cos\theta^4\sin\theta^2 - 4\Gamma_{21}\cos\theta^2\sin\theta^3 + 4\Gamma_{31}\cos\theta^2\sin\theta^3 \\
&+ -\Gamma_{32}\cos\theta^2\sin\theta^3 + 2\gamma_1\cos\theta^2\sin\theta^2 - 3\Gamma_{32}\cos\theta^2\sin\theta^5)\frac{\Delta_1}{\Omega_2} + \mathscr{O}(\Delta_1)^2\,,
\end{aligned}
$$

$$
\begin{aligned}
\Gamma_{rstr} &= -\tfrac{1}{2}\Gamma_{32}\cos\theta^2\sin\theta^2 + \tfrac{1}{8}(3\Gamma_{32}\cos\theta^4\sin\theta^2 + 4\Gamma_{21}\cos\theta^2\sin\theta^3 - 4\Gamma_{31}\cos\theta^2\sin\theta^3 \\
&+ \Gamma_{32}\cos\theta^2\sin\theta^3 - 2\gamma_1\cos\theta^2\sin\theta^3 - 3\Gamma_{32}\cos\theta^2\sin\theta^5)\frac{\Delta_1}{\Omega_2} + \mathscr{O}(\Delta_1)^2\,,
\end{aligned}
$$

$$\begin{aligned}\Gamma_{trrs} &= -\tfrac{1}{2}\Gamma_{32}\cos\theta^2\sin\theta^2 + \tfrac{1}{8}(-3\Gamma_{32}\cos\theta^4\sin\theta^2 - 4\Gamma_{21}\cos\theta^2\sin\theta^3 + 4\Gamma_{31}\cos\theta^2\sin\theta^3 \\ &- \Gamma_{32}\cos\theta^2\sin\theta^3 - 2\gamma_1\cos\theta^2\sin\theta^3 - \Gamma_{32}\cos\theta^2\sin\theta^5)\frac{\Delta_1}{\Omega_2} + \mathscr{O}(\Delta_1)^2\,,\end{aligned}$$

$$\begin{aligned}\Gamma_{ssss} - \Gamma_{ssrr} &= \tfrac{1}{8}(-4\Gamma_{21}\cos\theta^2 - 2\Gamma_{32}\cos\theta^2 - \gamma_1\cos\theta^2 - 2\Gamma_{31}\cos\theta^4 - 2\Gamma_{32}\cos\theta^4 - 4\Gamma_{31}\sin\theta^2 \\ &- 2\Gamma_{21}\cos\theta^2\sin\theta^2 - 2\Gamma_{31}\cos\theta^2\sin\theta^2 - 2\Gamma_{21}\sin\theta^4 - 4\Gamma_{32}\sin\theta^4) \\ &+ \tfrac{1}{16}(-2\Gamma_{32}\cos\theta^2\sin\theta - \gamma_1\cos\theta^2\sin\theta + 4\Gamma_{21}\cos\theta^4\sin\theta - 4\Gamma_{31}\cos\theta^4\sin\theta \\ &- 2\Gamma_{32}\cos\theta^4\sin\theta + \gamma_1\cos\theta^4\sin\theta + 12\Gamma_{31}\cos\theta^4\sin\theta^2 + 6\Gamma_{32}\cos\theta^4\sin\theta^2 \\ &+ 4\Gamma_{21}\cos\theta^2\sin\theta^3 - 4\Gamma_{31}\cos\theta^2\sin\theta^3 - 12\Gamma_{32}\cos\theta^2\sin\theta^3 - 7\gamma_1\cos\theta^2\sin\theta^3 \\ &- 12\Gamma_{31}\cos\theta^4\sin\theta^3 - 12\Gamma_{32}\cos\theta^4\sin\theta^3 + 12\Gamma_{21}\cos\theta^2\sin\theta^4 + 12\Gamma_{32}\cos\theta^2\sin\theta^4 \\ &- 12\Gamma_{21}\cos\theta^2\sin\theta^5 + 6\Gamma_{32}\cos\theta^2\sin\theta^5)\frac{\Delta_1}{\Omega_2} + \mathscr{O}(\Delta_1)^2\,,\end{aligned}$$

$$\begin{aligned}\Gamma_{tttt} - \Gamma_{ttrr} &= \tfrac{1}{8}(-4\Gamma_{21}\cos\theta^2 - 2\Gamma_{32}\cos\theta^2 - \gamma_1\cos\theta^2 - 2\Gamma_{31}\cos\theta^4 - 2\Gamma_{32}\cos\theta^4 - 4\Gamma_{31}\sin\theta^2 \\ &- 2\Gamma_{21}\cos\theta^2\sin\theta^2 - 2\Gamma_{31}\cos\theta^2\sin\theta^2 - 2\Gamma_{21}\sin\theta^4 - 4\Gamma_{32}\sin\theta^4) \\ &- \tfrac{1}{16}(-2\Gamma_{32}\cos\theta^2\sin\theta - \gamma_1\cos\theta^2\sin\theta + 4\Gamma_{21}\cos\theta^4\sin\theta - 4\Gamma_{31}\cos\theta^4\sin\theta \\ &- 2\Gamma_{32}\cos\theta^4\sin\theta + \gamma_1\cos\theta^4\sin\theta + 12\Gamma_{31}\cos\theta^4\sin\theta^2 + 6\Gamma_{32}\cos\theta^4\sin\theta^2 \\ &+ 4\Gamma_{21}\cos\theta^2\sin\theta^3 - 4\Gamma_{31}\cos\theta^2\sin\theta^3 - 12\Gamma_{32}\cos\theta^2\sin\theta^3 - 7\gamma_1\cos\theta^2\sin\theta^3 \\ &- 12\Gamma_{31}\cos\theta^4\sin\theta^3 - 12\Gamma_{32}\cos\theta^4\sin\theta^3 + 12\Gamma_{21}\cos\theta^2\sin\theta^4 + 12\Gamma_{32}\cos\theta^2\sin\theta^4 \\ &- 12\Gamma_{21}\cos\theta^2\sin\theta^5 + 6\Gamma_{32}\cos\theta^2\sin\theta^5)\frac{\Delta_1}{\Omega_2} + \mathscr{O}(\Delta_1)^2\,,\end{aligned}$$

$$\begin{aligned}\Gamma_{sstt} - \Gamma_{ssrr} &= \tfrac{1}{8}(-4\Gamma_{21}\cos\theta^2 + 4\Gamma_{31}\cos\theta^2 + \gamma_1\cos\theta^2 + 2\Gamma_{32}\cos\theta^2 - 2\Gamma_{31}\cos\theta^4 - 2\Gamma_{32}\cos\theta^4 \\ &+ 4\Gamma_{21}\sin\theta^2 - 4\Gamma_{31}\sin\theta^2 - 2\Gamma_{21}\cos\theta^2\sin\theta^2 - 2\Gamma_{31}\cos\theta^2\sin\theta^2 - 2\Gamma_{21}\sin\theta^4 \\ &- 4\Gamma_{32}\sin\theta^4) + \tfrac{1}{8}(-\Gamma_{31}\cos\theta^2\sin\theta + 2\Gamma_{21}\cos\theta^4\sin\theta - \Gamma_{31}\cos\theta^4\sin\theta \\ &+ 3\Gamma_{21}\cos\theta^2\sin\theta^2 - 3\Gamma_{21}\cos\theta^4\sin\theta^2 + 3\Gamma_{31}\cos\theta^4\sin\theta^2 + 2\Gamma_{21}\cos\theta^2\sin\theta^3 \\ &- 4\Gamma_{31}\cos\theta^2\sin\theta^3 - 4\Gamma_{32}\cos\theta^2\sin\theta^3 - 2\gamma_1\cos\theta^2\sin\theta^3 + 6\Gamma_{32}\cos\theta^2\sin\theta^4 \\ &- 3\Gamma_{21}\cos\theta^2\sin\theta^5 + 3\Gamma_{31}\cos\theta^2\sin\theta^5)\frac{\Delta_1}{\Omega_2} + \mathscr{O}(\Delta_1)^2\,,\end{aligned}$$

$$\begin{aligned}\Gamma_{ttss} - \Gamma_{ttrr} &= \tfrac{1}{8}(-4\Gamma_{21}\cos\theta^2 + 4\Gamma_{31}\cos\theta^2 + \gamma_1\cos\theta^2 + 2\Gamma_{32}\cos\theta^2 - 2\Gamma_{31}\cos\theta^4 - 2\Gamma_{32}\cos\theta^4 \\ &+ 4\Gamma_{21}\sin\theta^2 - 4\Gamma_{31}\sin\theta^2 - 2\Gamma_{21}\cos\theta^2\sin\theta^2 - 2\Gamma_{31}\cos\theta^2\sin\theta^2 - 2\Gamma_{21}\sin\theta^4 \\ &- 4\Gamma_{32}\sin\theta^4) - \tfrac{1}{8}(-\Gamma_{31}\cos\theta^2\sin\theta + 2\Gamma_{21}\cos\theta^4\sin\theta - \Gamma_{31}\cos\theta^4\sin\theta \\ &+ 3\Gamma_{21}\cos\theta^2\sin\theta^2 - 3\Gamma_{21}\cos\theta^4\sin\theta^2 + 3\Gamma_{31}\cos\theta^4\sin\theta^2 + 2\Gamma_{21}\cos\theta^2\sin\theta^3 \\ &- 4\Gamma_{31}\cos\theta^2\sin\theta^3 - 4\Gamma_{32}\cos\theta^2\sin\theta^3 - 2\gamma_1\cos\theta^2\sin\theta^3 + 6\Gamma_{32}\cos\theta^2\sin\theta^4 \\ &- 3\Gamma_{21}\cos\theta^2\sin\theta^5 + 3\Gamma_{31}\cos\theta^2\sin\theta^5)\frac{\Delta_1}{\Omega_2} + \mathscr{O}(\Delta_1)^2\,,\end{aligned}$$

where γ_1 is the decoherence rate of the laser having the ω_1 frequency.

The only nonzero elements of the vector I_∞ (to order $1/\Omega_R$) are

$$I_{\infty 4} = I_{\infty 5} = \Gamma_{ssrr}\,. \tag{2.328}$$

The solution of Eq. (2.325) in Laplace space is

$$\hat{\Psi}(z) = M^0(z)\Psi(t_0) + \frac{1}{z}M^0(z)I_\infty\,, \tag{2.329}$$

where $M^0(z) = (z - L_0)^{-1}$. For simplicity we consider only the emission process for $3 \to 1$ transition so that

$$P^{(+)} = \gamma_{13}|1\rangle\langle 3|\,, \quad P^{(-)} = \gamma_{13}|3\rangle\langle 1|\,. \tag{2.330}$$

As usual, we need the single-time average

$$\langle P^{(-)}(t_1)\rangle = \gamma_{13}Tr[\rho'(t_1)|3\rangle\langle 1|]\exp(I\omega_{31}t_1)\,. \tag{2.331}$$

In terms of dressed states, we have

$$\begin{aligned}
|3\rangle\langle 1|r\rangle &= \frac{\Delta_1}{\Omega_2}\sin\theta^2\cos\theta\left(-\sin\theta|r\rangle + \frac{1}{\sqrt{2}}\cos\theta|s\rangle + \frac{1}{\sqrt{2}}\cos\theta|t\rangle\right)\,, \qquad (2.332)\\
|3\rangle\langle 1|s\rangle &= \frac{1}{2}\cos\theta(|s\rangle + |t\rangle) - \frac{1}{\sqrt{2}}\sin\theta|r\rangle\\
&+ \frac{1}{\sqrt{32}}\frac{\Delta_1}{\Omega_2}\sin 2\theta(\sqrt{2}\sin 2\theta|r\rangle + 8\sin\theta^2|s\rangle - 4(1+\sin\theta^2)|t\rangle)\,,\\
|3\rangle\langle 1|t\rangle &= -\frac{1}{2}\cos\theta(|s\rangle + |t\rangle) + \frac{1}{\sqrt{2}}\sin\theta|r\rangle\\
&+ \frac{1}{\sqrt{32}}\frac{\Delta_1}{\Omega_2}\sin 2\theta(\sqrt{2}\sin 2\theta|r\rangle + 8\sin\theta^2|s\rangle - 4(1+\sin\theta^2)|t\rangle)\,,
\end{aligned}$$

so that, in Laplace space, it follows that

$$\begin{aligned}
\langle P^{(-)}(z)\rangle &= \frac{1}{2}\cos\theta(\hat{\Psi}_4(z_1) + \hat{\Psi}_1(z_1) - \hat{\Psi}_8(z_1) - \hat{\Psi}_5(z_1)) - \frac{1}{\sqrt{2}}\sin\theta(\hat{\Psi}_2(z_1) - \hat{\Psi}_7(z_1)) \qquad (2.333)\\
&+ \frac{\Delta_1}{\Omega_2}\sin\theta^2\cos\theta\left[\sin\theta(-\frac{1}{z_1} + \hat{\Psi}_4(z_1) + \hat{\Psi}_5(z_1)) + \frac{1}{\sqrt{2}}\cos\theta(\hat{\Psi}_6(z_1) + \hat{\Psi}_3(z_1) + \frac{1}{4}\hat{\Psi}_2(z_1)\right.\\
&+ \left.\frac{1}{4}\hat{\Psi}_7(z_1)) + \cos\theta\sin\theta^2(\hat{\Psi}_4(z_1) + \hat{\Psi}_8(z_1)) - \frac{1}{2}\cos\theta(\hat{\Psi}_1(z_1) + \hat{\Psi}_5(z_1))\right]\,,
\end{aligned}$$

where $z_1 = z - i\omega_{31}$, and the components of Ψ are defined according to Eqs. (2.313). After replacing $\hat{\Psi}_i(z_1)$ by the appropriate expressions in terms of $\Psi_i(t_0)$, we only need to cast the various $\Psi_i(t_0)$ in the form of expectation values and to carry out the standard replacements required by regression theorem. Thus, for example, we have

$$\begin{aligned}
\Psi_1(t_0) \to \gamma_{13}Tr[\rho(t_0)|\overline{t\rangle\langle s}|1\rangle\langle 3|] &= \gamma_{13}Tr[\rho'(t_0)|t\rangle\langle s|\overline{1\rangle\langle 3}|] \qquad (2.334)\\
&= \gamma_{13}\exp(-i\omega_{31}t_0)\langle s|1\rangle\langle 3|\rho'(t_0)|t\rangle\,,
\end{aligned}$$

$$\begin{aligned}
&\Psi_1(t_0) \to \gamma_{13}exp(-i\omega_{31}t_0)\left(\tfrac{1}{2}\cos\theta(\rho'_{st} + \rho'_{tt}) - \frac{1}{\sqrt{2}}\sin\theta\rho'_{rt}\right) \qquad (2.335)\\
&+\gamma_{13}\frac{\Delta_1}{\Omega_2}\exp(-i\omega_{31}t_0)\left(\frac{1}{\sqrt{32}}\sin\theta^3\cos\theta^2\rho'_{rt} + \frac{1}{2}\sin\theta^3\cos\theta\rho'_{st} - \frac{1}{4}\sin\theta\cos\theta(1+\sin\theta^2)\rho'_{tt}\right)\,,
\end{aligned}$$

where the over-bars indicate that the operators are in interaction picture. Similar expressions hold for the remaining components of $\Psi(t_0)$.

$$\Psi_2(t_0) \to \gamma_{13}\exp(-i\omega_{31}t_0)\left(\tfrac{1}{2}\cos\theta(\rho'_{sr}+\rho'_{tr})-\frac{1}{\sqrt{2}}\sin\theta\rho'_{rr}\right) \tag{2.336}$$
$$+\gamma_{13}\frac{\Delta_1}{\Omega_2}\exp(-i\omega_{31}t_0)\left(\frac{1}{\sqrt{32}}\sin\theta^2\cos\theta^2\rho'_{rr}+\frac{1}{2}\sin\theta^3\cos\theta\rho'_{sr}-\frac{1}{4}\sin\theta\cos\theta(1+\sin\theta^2)\rho'_{tr}\right),$$
$$\Psi_3(t_0) \to \gamma_{13}\frac{\Delta_1}{\Omega_2}\exp(-i\omega_{31}t_0)\left(-\sin\theta^3\cos\theta\rho'_{rt}+\frac{1}{\sqrt{2}}\sin\theta^2\cos\theta^2\rho'_{st}+\frac{1}{\sqrt{2}}\sin\theta^2\cos\theta^2\rho'_{tt}\right),$$
$$\Psi_4(t_0) \to \gamma_{13}\exp(-i\omega_{31}t_0)\left(\tfrac{1}{2}\cos\theta(\rho'_{ss}+\rho'_{ts})-\frac{1}{\sqrt{2}}\sin\theta\rho'_{rs}\right)$$
$$+\gamma_{13}\frac{\Delta_1}{\Omega_2}\exp(-i\omega_{31}t_0)\left(\frac{1}{\sqrt{32}}\sin\theta^3\cos\theta^2\rho'_{rs}+\frac{1}{2}\sin\theta^2\cos\theta\rho'_{ss}-\frac{1}{4}\sin\theta\cos\theta(1+\sin\theta^2)\rho'_{ts}\right),$$
$$\Psi_5(t_0) \to \gamma_{13}\exp(-i\omega_{31}t_0)\left(-\tfrac{1}{2}\cos\theta(\rho'_{st}+\rho'_{tt})+\frac{1}{\sqrt{2}}\sin\theta\rho'_{rt}\right)$$
$$+\gamma_{13}\frac{\Delta_1}{\Omega_2}\exp(-i\omega_{31}t_0)\left(\frac{1}{\sqrt{32}}\sin\theta\cos\theta^2\rho'_{rt}-\frac{1}{4}\sin\theta\cos\theta(1+\sin\theta^2)\rho'_{st}+\frac{1}{2}\sin\theta^3\cos\theta\rho'_{tt}\right),$$
$$\Psi_6(t_0) \to \gamma_{13}\frac{\Delta_1}{\Omega_2}\exp(-i\omega_{31}t_0)\left(-\sin\theta^3\cos\theta\rho'_{rs}+\frac{1}{\sqrt{2}}\sin\theta^2\cos\theta^2\rho'_{ss}+\frac{1}{\sqrt{2}}\sin\theta^2\cos\theta^2\rho'_{ts}\right),$$
$$\Psi_7(t_0) \to \gamma_{13}\exp(-i\omega_{31}t_0)\left(-\tfrac{1}{2}\cos\theta(\rho'_{sr}+\rho'_{tr})+\frac{1}{\sqrt{2}}\sin\theta\rho'_{rr}\right)$$
$$+\gamma_{13}\frac{\Delta_1}{\Omega_2}\exp(-i\omega_{31}t_0)\left(\frac{1}{\sqrt{32}}\sin\theta^2\cos\theta^2\rho'_{rr}-\frac{1}{4}\sin\theta\cos\theta(1+\sin\theta^2)\rho'_{sr}+\frac{1}{2}\sin\theta^3\cos\theta\rho'_{tr}\right),$$
$$\Psi_8(t_0) \to \gamma_{13}\exp(-i\omega_{31}t_0)\left(-\tfrac{1}{2}\cos\theta(\rho'_{ss}+\rho'_{ts})+\frac{1}{\sqrt{2}}\sin\theta\rho'_{rs}\right)$$
$$+\gamma_{13}\frac{\Delta_1}{\Omega_2}\exp(-i\omega_{31}t_0)\left(\frac{1}{\sqrt{32}}\sin\theta^2\cos\theta^2\rho'_{rs}-\frac{1}{4}\sin\theta\cos\theta(1+\sin\theta^2)\rho'_{ss}+\frac{1}{2}\sin\theta^3\cos\theta\rho'_{ts}\right).$$

Note that in the stationary limit the off-diagonal elements of $\rho'_{\mu\nu}$ vanish and the only nonzero elements are

$$\rho'_{ss}=\Psi_{4\infty}\quad \rho'_{tt}=\Psi_{5\infty}\,, \tag{2.337}$$

as given by Eq. (2.316). In this way, Eq. (2.334) becomes

$$\begin{aligned}
\Psi_1(t_0\to\infty) &= \gamma_{13}\exp(-i\omega_{31}t_0)\left(\frac{1}{2}\cos\theta-\frac{1}{4}\frac{\Delta_1}{\Omega_2}\sin\theta\cos\theta(1+\sin\theta^2)\right)\Psi_5(\infty)\,, \qquad (2.338)\\
\Psi_2(t_0\to\infty) &= -\gamma_{13}\exp(-i\omega_{31}t_0)\left(\frac{1}{\sqrt{2}}\sin\theta-\frac{1}{\sqrt{32}}\frac{\Delta_1}{\Omega_2}\sin\theta^2\cos\theta^2\right)(1-\Psi_4(\infty)-\Psi_5(\infty))\,,\\
\Psi_3(t_0\to\infty) &= \gamma_{13}\exp(-i\omega_{31}t_0)\frac{1}{\sqrt{2}}\frac{\Delta_1}{\Omega_2}\sin\theta^2\cos\theta^2\Psi_5(\infty)\,,\\
\Psi_4(t_0\to\infty) &= \gamma_{13}\exp(-i\omega_{31}t_0)\left(\frac{1}{2}\cos\theta+\frac{1}{2}\frac{\Delta_1}{\Omega_2}\sin\theta^2\cos\theta^2\right)\Psi_5(\infty)\,,
\end{aligned}$$

$$
\begin{aligned}
\Psi_5(t_0\to\infty) &= -\gamma_{13}\exp(-i\omega_{31}t_0)\left(\frac{1}{2}\cos\theta-\frac{1}{2}\frac{\Delta_1}{\Omega_2}\sin\theta^3\cos\theta\right)\Psi_5(\infty)\,,\\
\Psi_6(t_0\to\infty) &= \gamma_{13}\exp(-i\omega_{31}t_0)\frac{1}{\sqrt{2}}\frac{\Delta_1}{\Omega_2}\sin\theta^2\cos\theta^2\Psi_4(\infty)\,,\\
\Psi_7(t_0\to\infty) &= \gamma_{13}\exp(-i\omega_{31}t_0)\left(\frac{1}{\sqrt{2}}\sin\theta+\frac{1}{\sqrt{32}}\frac{\Delta_1}{\Omega_2}\sin\theta^2\cos\theta^2\right)(1-\Psi_4(\infty)-\Psi_5(\infty))\,,\\
\Psi_8(t_0\to\infty) &= -\gamma_{13}\exp(-i\omega_{31}t_0)\left(\frac{1}{2}\cos\theta+\frac{1}{4}\frac{\Delta_1}{\Omega_2}\sin\theta\cos\theta(1+\sin\theta^2)\right)\Psi_5(\infty)\,,
\end{aligned}
$$

in the first order of $1/\Omega_R$. The result of these manipulations is the correlation function

$$
\begin{aligned}
&\langle\hat{P}^{(-)}(z)P^{(+)}(\infty)\rangle = \tfrac{\gamma_{13}^2}{32z_1}[16(I_{\infty4}M_{44}+I_{\infty5}M_{45}-I_{\infty4}M_{54}-I_{\infty5}M_{55})\cos\theta \qquad (2.339)\\
+\;& 8z(M_{44}\Psi_4(\infty)-M_{54}\Psi_4(\infty)+M_{88}\Psi_4(\infty)+M_{11}\Psi_5(\infty)-M_{45}\Psi_5(\infty)+M_{55}\Psi_5(\infty))\cos\theta^2\\
-\;& 16(M_{22}+M_{77})z_1(-1+\Psi_4(\infty)+\Psi_5(\infty))\sin\theta^2]+\tfrac{\gamma_{13}^2}{32z_1}\{-8M_{54}z_1\Psi_4(\infty)\cos\theta^3\sin\theta^2\\
-\;& 8M_{11}z_1\Psi_5(\infty)\cos\theta^3\sin\theta^2+32[-1+I_{\infty4}(M_{44}+M_{54})+I_{\infty5}(M_{45}+M_{55})]\cos\theta\sin\theta^3\\
+\;& 4\cos\theta^2[M_{88}z_1\Psi_4(\infty)\sin\theta-M_{11}z_1\Psi_5(\infty)\sin\theta-z_1(M_{22}+(M_{11}+2M_{45})\Psi_5(\infty)\\
+\;& 2M_{77}(-1+\Psi_4(\infty)+\Psi_5(\infty)))\sin\theta^3+(8I_{\infty4}M_{44}+8I_{\infty5}M_{45}+M_{22}z_1(-1+\Psi_4(\infty)\\
+\;& \Psi_5(\infty)))\sin\theta^4]+(-4I_{\infty4}M_{54}-4I_{\infty5}M_{55}+2M_{44}z_1\Psi_4(\infty)-2M_{54}z_1\Psi_4(\infty)\\
+\;& 2M_{55}z_1\Psi_5(\infty)\cos\theta)\sin2\theta^2+z_1\sin\theta\sin2\theta^2[4M_{67}+M_{22}\Psi_4(\infty)+4M_{44}\Psi_4(\infty)+4M_{54}\Psi_4(\infty)\\
-\;& 4M_{67}\Psi_4(\infty)+4M_{76}\Psi_4(\infty)+M_{88}\Psi_4(\infty)+M_{22}\Psi_5(\infty)-4M_{23}\Psi_5(\infty)-6M_{55}\Psi_5(\infty)\\
-\;& 4M_{67}\Psi_5(\infty)+4M_{32}(-1+\Psi_4(\infty)+\Psi_5(\infty))+2(M_{44}\Psi_4(\infty)-M_{88}\Psi_4(\infty)\\
-\;& M_{45}\Psi_5(\infty))\sin2\theta]\}\frac{\Delta_1}{\Omega_2}+\mathscr{O}(\Delta_1)^2
\end{aligned}
$$

$$
\begin{aligned}
\langle\hat{P}^{(-)}(z)P^{(+)}(\infty)\rangle = {}& \tfrac{\gamma_{13}^2}{4}\cos^2\theta\Psi_\infty(M_{11}^0+M_{44}^0-M_{54}^0+M_{55}^0+M_{88}^0) \qquad (2.340)\\
&+\tfrac{\gamma_{13}^2}{4}\sin^2\theta(1-2\Psi_\infty)(M_{22}^0+M_{77}^0)\,.
\end{aligned}
$$

At this point we need to calculate the explicit expressions for the matrix elements M_{ij}^0. This task is made easy by the fact that the first and last blocks of the M_0 matrix are trivial, while the remaining three blocks have the generic form

$$
\begin{pmatrix} a & b\\ b & a\end{pmatrix}^{-1}\to\frac{1}{a^2-b^2}\begin{pmatrix} a & -b\\ -b & a\end{pmatrix}\,. \qquad (2.341)
$$

After a few simple calculations Eq. (2.340) becomes

$$
\begin{aligned}
&\langle\hat{P}^{(-)}(z)\hat{P}^{(+)}(\infty)\rangle = \tfrac{\gamma_{13}^2}{4}\cos^2\theta\Psi_\infty\left(\frac{1}{z_1-\gamma_1+2i\Omega_R}+\frac{2}{z_1-\gamma_4+\gamma_5}+\frac{1}{z_1-\gamma_1-2i\Omega_R}\right)\\
&+\tfrac{\gamma_{13}^2}{2}\sin^2\theta(1-2\Psi_\infty)\left(\frac{z_1-\gamma_2+i\Omega_R}{(z_1-\gamma_2+i\Omega_R)^2-\gamma_3^2}+\frac{z_1-\gamma_2-i\Omega_R}{(z_1-\gamma_2-i\Omega_R)^2-\gamma_3^2}\right)\,, \qquad (2.342)
\end{aligned}
$$

and the emission spectrum will be given by

$$
S(\omega)=Re\langle\hat{P}^{(-)}(z)\hat{P}^{(+)}(\infty)\rangle|_{z=i(\omega-\omega_{31})}\,. \qquad (2.343)
$$

We list the set of constants that are needed to discuss this result:

$$\begin{aligned}
&\Gamma_{stst} = \Gamma_{tsts} = \gamma_1 \,, \\
&\Gamma_{srsr} = \Gamma_{rtrt} = \Gamma_{rsrs} = \Gamma_{trtr} = \gamma_2 \,, \\
&\Gamma_{srrt} = \Gamma_{rtsr} = \Gamma_{rstr} = \Gamma_{trrs} = \gamma_3 \,, \\
&\Gamma_{ssss} - \Gamma_{ssrr} = \Gamma_{tttt} - \Gamma_{ttrr} = \gamma_4 \,, \\
&\Gamma_{sstt} - \Gamma_{ssrr} = \Gamma_{ttss} - \Gamma_{ttrr} = \gamma_5 \,,
\end{aligned} \tag{2.344}$$

with the γ-s given as

$$\begin{aligned}
\gamma_1 &= -\Gamma_{32}\tfrac{1}{4}\cos^2\theta(1+\cos^2\theta) - \Gamma_{31}\tfrac{3}{4}\cos^2\theta - \Gamma_{21}\tfrac{3}{4}\sin^2\theta \,, \\
\gamma_2 &= -\Gamma_{32}\tfrac{1}{4}[1+\sin^2\theta(1+2\cos^2\theta)] - \Gamma_{31}\tfrac{1}{4}(1+\sin^2\theta) - \Gamma_{21}\tfrac{1}{4}(1+\cos^2\theta) \,, \\
\gamma_3 &= -\Gamma_{32}\tfrac{1}{2}\sin^2\theta\cos^2\theta \,, \\
\gamma_4 &= -\Gamma_{32}(\tfrac{1}{4}\cos^2\theta + \tfrac{1}{4}\cos^4\theta + \tfrac{1}{2}\sin^4\theta) - \Gamma_{31}\tfrac{1}{4}(1+\sin^2\theta) - \Gamma_{21}\tfrac{1}{4}(1+\cos^2\theta) \,, \\
\gamma_5 &= \Gamma_{32}\tfrac{1}{2}\sin^2\theta(\tfrac{1}{2}\cos^2\theta - \sin^2\theta) + \Gamma_{31}(\tfrac{1}{4}\cos^2\theta - \tfrac{1}{2}\sin^2\theta) + \Gamma_{21}(\tfrac{1}{4}\sin^2\theta - \tfrac{1}{2}\cos^2\theta) \,.
\end{aligned} \tag{2.345}$$

The main features of the spectrum whose analytic representation is given by Eq. (2.343) can be summarized as follows: In general, the emission spectrum of the $3 \rightarrow 1$ transition is composed of five contributions. One is centered at the transition frequency ω_{31} and has a Lorentzian shape, and two sidebands are moved by an amount $\pm\Omega_R$ from the central peak. The outermost sidebands are the ones that also appear in the Mollow spectrum of a strongly driven two-level atom. The inner sidebands are instead a feature of the three-level system, although they disappear if the rate of decay of the $3 \rightarrow 2$ transition approaches zero because their weighting factor is proportional to Γ_{32}.

The peak heights of the central component and of the outer sidebands are given by

$$\begin{aligned}
&P(0) = \tfrac{\gamma_{13}^2}{4}\cos^2\theta\frac{2}{\gamma_5-\gamma_4}\Psi_\infty \,, \quad P(\pm\Omega_R) = \tfrac{\gamma_{13}^2}{2}\sin^2\theta(1-2\Psi_\infty)\frac{|\gamma_2|}{|\gamma_2^2-\gamma_3^2|} \,, \\
&P(\pm 2\Omega_R) = \tfrac{\gamma_{13}^2}{4}\cos^2\theta\frac{1}{|\gamma_1|}\Psi_\infty \,.
\end{aligned} \tag{2.346}$$

The full widths of the spectral features are given in an analytic representation by

$$\begin{aligned}
\Delta\omega(0) &= 2(\gamma_5-\gamma_4) = \Gamma_{32}\cos^2\theta + \Gamma_{31}\cos^2\theta + \Gamma_{21}\sin^2\theta \,, \\
\Delta\omega(\pm\Omega_R) &= 2\{[4\gamma_3^4 + (\gamma_2^2-\gamma_3^2)]^{1/2} - 2\gamma_3^2\}^{1/2} \,, \\
\Delta\omega(\pm 2\Omega_R) &= 2|\gamma_1| = \Gamma_{32}\tfrac{1}{2}\cos^2\theta(1+\cos^2\theta) + \Gamma_{31}\tfrac{3}{2}\cos^2\theta + \Gamma_{21}\tfrac{3}{2}\sin^2\theta \,.
\end{aligned} \tag{2.347}$$

Now, we consider only the emission process for the $2 \rightarrow 1$ transition so that

$$P^{(+)} = \gamma_{12}|1\rangle\langle 2| \,, \quad P^{(-)} = \gamma_{12}|2\rangle\langle 1| \,. \tag{2.348}$$

The single-time average is

$$\langle P^{(-)}(t_1)\rangle = \gamma_{12} Tr[\rho'(t_1)|2\rangle\langle 1|]\exp(i\omega_{21}t_1) \,. \tag{2.349}$$

In terms of dressed states we have

$$\begin{aligned}
|2\rangle\langle 1|r\rangle &= 0 \,, \\
|2\rangle\langle 1|s\rangle &= \frac{1}{2}\sin\theta(|s\rangle + |t\rangle) + \frac{1}{\sqrt{2}}\cos\theta|r\rangle \,, \\
|2\rangle\langle 1|t\rangle &= -\frac{1}{2}\sin\theta(|s\rangle + |t\rangle) - \frac{1}{\sqrt{2}}\cos\theta|r\rangle \,,
\end{aligned} \tag{2.350}$$

so that, in Laplace space, it follows that

$$\langle P^{(-)}(z)\rangle = \frac{\gamma_{12}}{2}\sin\theta(\hat{\Psi}_4(z_2)+\hat{\Psi}_1(z_2)-\hat{\Psi}_8(z_2)-\hat{\Psi}_5(z_2)) + \frac{\gamma_{12}}{\sqrt{2}}\cos\theta(\hat{\Psi}_2(z_2)-\hat{\Psi}_7(z_2))\,, \tag{2.351}$$

where $z_2 = z - i\omega_{21}$. After replacing $\hat{\Psi}_i(z_1)$ by the appropriate expressions in terms of $\Psi_i(t_0)$, we need to write the various $\Psi_i(t_0)$ in the form of expectation values and to carry out the standard replacements as required by the regression theorem. Thus, we have

$$\begin{aligned}
\Psi_1(t_0) &\rightarrow \gamma_{12}\exp(-i\omega_{21}t_0)\left(\tfrac{1}{2}\sin\theta(\rho'_{st}+\rho'_{tt})-\frac{1}{\sqrt{2}}\cos\theta\rho'_{rt}\right), \qquad (2.352)\\
\Psi_2(t_0) &\rightarrow \gamma_{12}\exp(-i\omega_{21}t_0)\left(\tfrac{1}{2}\sin\theta(\rho'_{sr}+\rho'_{tr})+\frac{1}{\sqrt{2}}\cos\theta\rho'_{rr}\right),\\
\Psi_3(t_0) &\rightarrow 0\,,\\
\Psi_4(t_0) &\rightarrow \gamma_{12}\exp(-i\omega_{21}t_0)\left(\tfrac{1}{2}\sin\theta(\rho'_{ss}+\rho'_{ts})+\frac{1}{\sqrt{2}}\cos\theta\rho'_{rs}\right),\\
\Psi_5(t_0) &\rightarrow -\gamma_{12}\exp(-i\omega_{21}t_0)\left(\tfrac{1}{2}\sin\theta(\rho'_{st}+\rho'_{tt})+\frac{1}{\sqrt{2}}\cos\theta\rho'_{rt}\right),\\
\Psi_6(t_0) &\rightarrow 0\,,\\
\Psi_7(t_0) &\rightarrow -\gamma_{12}\exp(-i\omega_{21}t_0)\left(\tfrac{1}{2}\sin\theta(\rho'_{sr}+\rho'_{tr})+\frac{1}{\sqrt{2}}\cos\theta\rho'_{rr}\right),\\
\Psi_8(t_0) &\rightarrow -\gamma_{12}\exp(-i\omega_{21}t_0)\left(\tfrac{1}{2}\sin\theta(\rho'_{ss}+\rho'_{ts})+\frac{1}{\sqrt{2}}\cos\theta\rho'_{rs}\right).
\end{aligned}$$

Similar expressions hold for the remaining components of $\Psi(t_0)$. Note that in the stationary limit, the off-diagonal elements of $\rho'_{\mu\nu}$ vanish and the only nonzero elements are

$$\rho'_{ss} = \rho'_{tt} = \Psi_\infty\,, \tag{2.353}$$

as given by Eq. (2.316). In this way, Eqs. (2.352) become

$$\begin{aligned}
\Psi_1(t_0\rightarrow\infty) &= \gamma_{12}\exp(-i\omega_{21}t_0)\tfrac{1}{2}\sin\theta\rho'_{tt}+\mathscr{O}(1/\Omega_R)\,, \qquad (2.354)\\
\Psi_2(t_0\rightarrow\infty) &= \gamma_{12}\exp(-i\omega_{21}t_0)\tfrac{1}{\sqrt{2}}\cos\theta\rho'_{rr}+\mathscr{O}(1/\Omega_R)\,,\\
\Psi_4(t_0\rightarrow\infty) &= \gamma_{12}\exp(-i\omega_{21}t_0)\tfrac{1}{2}\sin\theta\rho'_{ss}+\mathscr{O}(1/\Omega_R)\,,\\
\Psi_5(t_0\rightarrow\infty) &= \gamma_{12}\exp(-i\omega_{21}t_0)\tfrac{1}{2}\sin\theta\rho'_{tt}+\mathscr{O}(1/\Omega_R)\,,\\
\Psi_7(t_0\rightarrow\infty) &= -\gamma_{12}\exp(-i\omega_{21}t_0)\tfrac{1}{\sqrt{2}}\cos\theta\rho'_{rr}+\mathscr{O}(1/\Omega_R)\,,\\
\Psi_8(t_0\rightarrow\infty) &= -\gamma_{12}\exp(-i\omega_{21}t_0)\tfrac{1}{2}\sin\theta\rho'_{ss}+\mathscr{O}(1/\Omega_R)\,.
\end{aligned}$$

As a result, one obtains the correlation function

$$\begin{aligned}
\langle\hat{P}^{(-)}(z)\hat{P}^{(+)}(\infty)\rangle &= \tfrac{\gamma_{12}^2}{4}\sin^2\theta\Psi_\infty(M^0_{11}+M^0_{44}-M^0_{54}-M^0_{45}+M^0_{55}+M^0_{88}) \qquad (2.355)\\
&+ \tfrac{\gamma_{12}^2}{4}\cos^2\theta(1-2\Psi_\infty)(M^0_{22}+M^0_{77})\,.
\end{aligned}$$

After a few calculations, Eq. (2.355) becomes

$$\langle\hat{P}^{(-)}(z)\hat{P}^{(+)}(\infty)\rangle = \tfrac{\gamma_{12}^2}{4}\sin^2\theta\Psi_\infty\left(\frac{1}{z_2-\gamma_1+2i\Omega_R}+\frac{2}{z_2-\gamma_4+\gamma_5}+\frac{1}{z_2-\gamma_1-2i\Omega_R}\right)$$
$$+\tfrac{\gamma_{12}^2}{2}\cos^2\theta(1-2\Psi_\infty)\left(\frac{z_2-\gamma_2+i\Omega_R}{(z_2-\gamma_2+i\Omega_R)^2-\gamma_3^2}+\frac{z_2-\gamma_2-i\Omega_R}{(z_2-\gamma_2-i\Omega_R)^2-\gamma_3^2}\right). \tag{2.356}$$

and the emission spectrum is given by

$$S(\omega) = Re\langle \hat{P}^{(-)}(z)\hat{P}^{(+)}(\infty)\rangle|_{z=i(\omega-\omega_{21})}\,. \tag{2.357}$$

The emission spectrum of the $2 \rightarrow 1$ transition is in general composed of five contributions. One is centered at the transition frequency ω_{21} and has a Lorentzian shape, and two sidebands are moved by an amount of $\pm\Omega_R$ from the central peak. The peak heights of the central component and of the outer sidebands are given by

$$\begin{aligned} P(0) &= \tfrac{\gamma_{12}^2}{4}\sin^2\theta\frac{2}{\gamma_5-\gamma_4}\Psi_\infty\,, \quad P(\pm\Omega_R) = \tfrac{\gamma_{12}^2}{2}\cos^2\theta(1-2\Psi_\infty)\frac{|\gamma_2|}{|\gamma_2^2-\gamma_3^2|}\,, \\ P(\pm 2\Omega_R) &= \tfrac{\gamma_{12}^2}{4}\sin^2\theta\frac{1}{|\gamma_1|}\Psi_\infty\,, \end{aligned} \tag{2.358}$$

and the widths of the spectral features are as follows:

$$\begin{aligned} \Delta\omega(0) &= 2(\gamma_5-\gamma_4) = \Gamma_{32}\cos^2\theta + \Gamma_{31}\cos^2\theta + \Gamma_{21}\sin^2\theta\,, \\ \Delta\omega(\pm\Omega_R) &= 2\{[4\gamma_3^4 + (\gamma_2^2-\gamma_3^2)]^{1/2} - 2\gamma_3^2\}^{1/2}\,, \\ \Delta\omega(\pm 2\Omega_R) &= 2|\gamma_1| = \Gamma_{32}\tfrac{1}{2}\cos^2\theta(1+\cos^2\theta) + \Gamma_{31}\tfrac{3}{2}\cos^2\theta + \Gamma_{21}\tfrac{3}{2}\sin^2\theta\,. \end{aligned} \tag{2.359}$$

In the following, for completeness, we consider the Λ model (see Fig. 2.8 b)). The emission spectrum of the $3 \rightarrow 1$ transition is assigned by the correlation function

$$\begin{aligned} \hat{\Gamma}_{\Lambda 1}^{\rm incoh}(z) &= \tfrac{\gamma_{13}^2}{4}\cos^2\theta\Psi_\infty\left(\frac{1}{z_1-\gamma_1+2i\Omega_R} + \frac{2}{z_1-\gamma_4+\gamma_5} + \frac{1}{z_1-\gamma_1-2i\Omega_R}\right) \\ &+ \tfrac{\gamma_{13}^2}{2}\sin^2\theta\Psi_\infty\left(\frac{z_1-\gamma_2+i\Omega_R}{(z_1-\gamma_2+i\Omega_R)^2-\gamma_3^2} + \frac{z_1-\gamma_2-i\Omega_R}{(z_1-\gamma_2-i\Omega_R)^2-\gamma_3^2}\right)\,, \end{aligned} \tag{2.360}$$

and the one for the $3 \rightarrow 2$ transition by

$$\begin{aligned} \hat{\Gamma}_{\Lambda 2}^{\rm incoh}(z) &= \tfrac{\gamma_{12}^2}{4}\cos^2\theta\Psi_\infty\left(\frac{1}{z_2-\gamma_1+2i\Omega_R} + \frac{2}{z_2-\gamma_4+\gamma_5} + \frac{1}{z_2-\gamma_1-2i\Omega_R}\right) \\ &+ \tfrac{\gamma_{12}^2}{2}\sin^2\theta\Psi_\infty\left(\frac{z_2-\gamma_2+i\Omega_R}{(z_2-\gamma_2+i\Omega_R)^2-\gamma_3^2} + \frac{z_2-\gamma_2-i\Omega_R}{(z_2-\gamma_2-i\Omega_R)^2-\gamma_3^2}\right)\,, \end{aligned} \tag{2.361}$$

where

$$\Psi_\infty = \frac{\Gamma_{21}\cos^4\theta}{\Gamma_{21}(\sin^4\theta + 2\cos^4\theta) + \Gamma_{32}\cos^2\theta + \Gamma_{31}\sin^2\theta}\,, \tag{2.362}$$

and

$$\begin{aligned} \gamma_1 &= -\tfrac{1}{4}[\Gamma_{21}\sin^2\theta(1+\sin^2\theta) + \Gamma_{32}(2+\sin^2\theta) + \Gamma_{31}(2+\cos^2\theta)]\,, \\ \gamma_2 &= -\tfrac{1}{4}\{\Gamma_{21}[1+\cos^2\theta(1+2\sin^2\theta)] + \Gamma_{32} + \Gamma_{31}\}\,, \\ \gamma_3 &= -\tfrac{1}{2}\Gamma_{21}\cos^2\theta\sin^2\theta\,, \\ \gamma_4 &= -\tfrac{1}{4}\{\Gamma_{21}[\sin^2\theta(1+\sin^2\theta) + 2\cos^2\theta] + \Gamma_{32}(1+\cos^2\theta) + \Gamma_{31}(1+\sin^2\theta)\}\,, \\ \gamma_5 &= \tfrac{1}{4}[\Gamma_{21}(\cos^2\theta\sin^2\theta - 2\cos^4\theta) + \Gamma_{32}\sin^2\theta + \Gamma_{31}\cos^2\theta]\,. \end{aligned} \tag{2.363}$$

Both the $3 \rightarrow 1$ and $3 \rightarrow 2$ emission spectra consists of five well-resolved components. The central peak and the $\pm 2\Omega_R$ sidebands have Lorentzian shapes, while the $\pm\Omega_R$ sidebands have a slightly more

complicated structure. The full widths at half maximum of the central peak and the sidebands of $3 \to 1$ spectrum are identical to the corresponding widths of the $3 \to 2$ profiles and are given by

$$\begin{aligned} \Delta\omega(0) &= 2|\gamma_5 - \gamma_4| = \Gamma_{21}\sin^2\theta + \Gamma_{32} + \Gamma_{31}\,, \\ \Delta\omega(\pm\Omega_R) &= 2\{-2\gamma_3^2 + [4\gamma_3^4 + (\gamma_2^2 - \gamma_3^2)^2]^{1/2}\}^{1/2}\,, \\ \Delta\omega(\pm 2\Omega_R) &= 2|\gamma_1|\,. \end{aligned} \tag{2.364}$$

The peak heights of $3 \to 1$ emission spectrum are given by

$$\begin{aligned} &P(0) = \tfrac{\gamma_{13}^2}{4}\cos^2\theta \frac{2}{|\gamma_5 - \gamma_4|}\Psi_\infty\,, \quad P(\pm\Omega_R) = \tfrac{\gamma_{13}^2}{2}\sin^2\theta\left|\frac{\gamma_2}{\gamma_2^2 - \gamma_3^2}\right|\Psi_\infty\,, \\ &P(\pm 2\Omega_R) = \tfrac{\gamma_{13}^2}{4}\cos^2\theta\frac{1}{|\gamma_1|}\Psi_\infty\,. \end{aligned} \tag{2.365}$$

Those of the $3 \to 2$ spectrum are identical except for the replacements of $\sin\theta$ with $\cos\theta$, and vice versa, and γ_{13} with γ_{12}.

The formulas for the Ξ model (see Fig. 2.8 c)) are quite similar to those of the Λ, with some differences, however, it is necessary to summarize them separately. The emission spectrum of the $2 \to 1$ transition is given by the correlation function

$$\begin{aligned} \hat{\Gamma}^{\rm incoh}_{\Xi 1}(z) &= \tfrac{\gamma_{13}^2}{4}\cos^2\theta\Psi_\infty\left(\frac{1}{z_1 - \gamma_1 + 2i\Omega_R} + \frac{2}{z_1 - \gamma_4 + \gamma_5} + \frac{1}{z_1 - \gamma_1 - 2i\Omega_R}\right) \\ &+ \tfrac{\gamma_{13}^2}{2}\sin^2\theta\Psi_\infty\left(\frac{z_1 - \gamma_2 - i\Omega_R}{(z_1 - \gamma_2 - i\Omega_R)^2 - \gamma_3^2} + \frac{z_1 - \gamma_2 + i\Omega_R}{(z_1 - \gamma_2 + i\Omega_R)^2 - \gamma_3^2}\right). \end{aligned} \tag{2.366}$$

For the $3 \to 2$ decay we have instead

$$\begin{aligned} \hat{\Gamma}^{\rm incoh}_{\Xi 2}(z) &= \tfrac{\gamma_{12}^2}{4}\sin^2\theta\Psi_\infty\left(\frac{1}{z_2 - \gamma_1 + 2i\Omega_R} + \frac{2}{z_2 - \gamma_4 + \gamma_5} + \frac{1}{z_2 - \gamma_1 - 2i\Omega_R}\right) \\ &+ \tfrac{\gamma_{12}^2}{2}\cos^2\theta(1 - 2\Psi_\infty)\left(\frac{z_2 - \gamma_2 - i\Omega_R}{(z_2 - \gamma_2 - i\Omega_R)^2 - \gamma_3^2} + \frac{z_2 - \gamma_2 + i\Omega_R}{(z_2 - \gamma_2 + i\Omega_R)^2 - \gamma_3^2}\right), \end{aligned} \tag{2.367}$$

where

$$\Psi_\infty = \frac{\frac{1}{2}(\Gamma_{31}\cos^4\theta + \Gamma_{32}\cos^2\theta)}{\Gamma_{31}(\frac{1}{2}\sin^4\theta + \cos^4\theta) + \frac{1}{2}\Gamma_{21}\sin^2\theta + \Gamma_{32}\cos^2\theta}\,, \tag{2.368}$$

and

$$\begin{aligned} \gamma_1 &= -\tfrac{1}{4}[\Gamma_{31}\sin^2\theta(1 + \sin^2\theta) + 3\Gamma_{32}\sin^2\theta + \Gamma_{21}(2 + \cos^2\theta)]\,, \\ \gamma_2 &= -\tfrac{1}{4}\{\Gamma_{31}[1 + \cos^2\theta(1 + 2\sin^2\theta)] + \Gamma_{32}(1 + \cos^2\theta) + \Gamma_{21}\}\,, \\ \gamma_3 &= -\tfrac{1}{2}\Gamma_{31}\cos^2\theta\sin^2\theta\,, \\ \gamma_4 &= -\tfrac{1}{4}[\Gamma_{31}(\sin^2\theta + \sin^4\theta + 2\cos^4\theta) + \Gamma_{32}(1 + \cos^2\theta) + \Gamma_{21}(1 + \sin^2\theta)]\,, \\ \gamma_5 &= \tfrac{1}{4}[\Gamma_{31}\cos^2\theta(\sin^2\theta - 2\cos^2\theta) + \Gamma_{32}(\sin^2\theta - 2\cos^2\theta) + \Gamma_{21}\cos^2\theta]\,. \end{aligned} \tag{2.369}$$

Again, the $2 \to 1$ and $3 \to 2$ emission spectra consists of five symmetric components. The central peak and the outer sidebands have a Lorentzian shape and the inner sidebands are non-Lorentzian. The

full width at half maximum of these spectral components are the same for both the $2 \to 1$ and $3 \to 2$ fluorescence processes and they are given by

$$\begin{aligned} \Delta\omega(0) &= \Gamma_{31}\sin^2\theta + \Gamma_{32}\sin^2\theta + \Gamma_{21}\,, \\ \Delta\omega(\pm\Omega_R) &= 2\{-2\gamma_3^2 + [4\gamma_3^4 + (\gamma_2^2 - \gamma_3^2)^2]^{1/2}\}^{1/2}\,, \\ \Delta\omega(\pm 2\Omega_R) &= \tfrac{1}{2}[\Gamma_{31}\sin^2\theta(1+\sin^2\theta) + 3\Gamma_{32}\sin^2\theta + \Gamma_{21}(2+\cos^2\theta)]\,. \end{aligned} \tag{2.370}$$

Their peak heights are given by the expressions

$$\begin{aligned} &P_{21}(0) = \tfrac{\gamma_{13}^2}{4}\cos^2\theta\frac{2}{|\gamma_5-\gamma_4|}\Psi_\infty\,, \quad P_{21}(\pm\Omega_R) = \tfrac{\gamma_{13}^2}{2}\sin^2\theta\left|\frac{\gamma_2}{\gamma_2^2-\gamma_3^2}\right|\Psi_\infty\,, \\ &P_{21}(\pm 2\Omega_R) = \tfrac{\gamma_{13}^2}{4}\cos^2\theta\frac{1}{|\gamma_1|}\Psi_\infty\,, \quad P_{32}(0) = \tfrac{\gamma_{12}^2}{4}\sin^2\theta\frac{2}{|\gamma_5-\gamma_4|}\Psi_\infty\,, \\ &P_{32}(\pm\Omega_R) = \tfrac{\gamma_{12}^2}{2}\cos^2\theta(1-2\Psi_\infty)\left|\frac{\gamma_2}{\gamma_2^2-\gamma_3^2}\right|\,, \quad P_{32}(\pm 2\Omega_R) = \tfrac{\gamma_{12}^2}{4}\sin^2\theta\frac{1}{|\gamma_1|}\Psi_\infty\,. \end{aligned} \tag{2.371}$$

2.7 Total fluorescence and steady-state population

Now, we compute the total fluorescence of transition $1-3$ which is defined, following Ref. [KNS95], as

$$I_{13} = \int_{-\infty}^{\infty} d\omega S(\omega)\,. \tag{2.372}$$

From Eq. (2.342) and (2.343) we obtain

$$I_{13} = \frac{\gamma_{13}^2}{4}\cos^2\theta\Psi_\infty(\pi + 2\pi + \pi) + \frac{\gamma_{13}}{2}\sin^2\theta(1-2\Psi_\infty)(\pi+\pi)\,, \tag{2.373}$$

or, by using the expression (2.316) for the Ψ_∞, one may gets the following:

$$I_{13} = \frac{\gamma_{13^2}\pi}{2}\cos^2\frac{\Gamma_{32}\sin^2\theta + \Gamma_{31}\sin^2\theta + \Gamma_{21}\cos^2\theta}{\Gamma_{32}(\frac{1}{2}\cos^4\theta + \sin^4\theta) + \Gamma_{31}\sin^2\theta + \Gamma_{21}\cos^2\theta}\,. \tag{2.374}$$

In the case of the $1-2$ transition, starting with the formulas (2.356) and (2.357), and using the same procedure, we get

$$I_{12} = \frac{\gamma_{12}^2\pi}{2}\frac{\Gamma_{32}(\sin^6\theta + \cos^6\theta) + \Gamma_{31}\sin^4\theta + \Gamma_{21}\sin^2\theta\cos^2\theta}{\Gamma_{32}(\frac{1}{2}\cos^4\theta + \sin^4\theta) + \Gamma_{31}\sin^2\theta + \Gamma_{21}\cos^2\theta}\,. \tag{2.375}$$

Applying Eq. (2.313) and (2.305) it is easy to see that

$$\frac{I_{13}}{\rho_{33}} = \pi\gamma_{13}^2\,, \quad \frac{I_{12}}{\rho_{22}} = \pi\gamma_{12}^2\,. \tag{2.376}$$

2.8 High-precision metrology of highly charged ions via relativistic resonance fluorescence

2.9 High-precision metrology of highly charged ions

As an application of our relativistic formalism for describing resonance fluorescence in a three-level setting, we describe line narrowing phenomena obsevable in highly charged ions and its application for the accurate metrology of properties of highly charged ions.

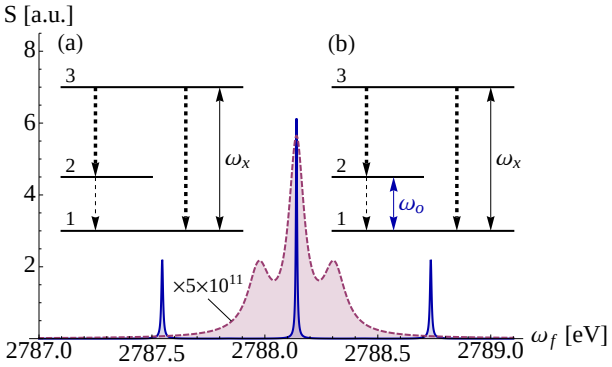

Figure 2.9: Fluorescence photon spectrum for the $2s \leftrightarrow 2p_{3/2}$ transition in Li-like ^{209}Bi as a function of the fluorescence photon frequency ω_f. (a) Dashed (red) curve: An x-ray laser ($I_x = 5 \times 10^{11}$ W/cm^2) is in resonance with the ionic electric dipole (E1) transition at $\omega_x = 2788.1$ eV between the hyperfine-split ground state 1 ($2s$ with $F = 4$, $M_F = 4$) and the uppermost state 3 ($2p_{3/2}$ with $F = 5$, $M_F = 5$). This curve is multiplied by a factor of 5×10^{11}. Thick (thin) dashed arrows represent fast E1 x-ray (slow M1 optical) decays. (b) Continuous (blue) curve: an additional optical driving ($I_o = 10^{14}$ W/cm^2) is applied on the $\omega_o = 0.797$ eV [SST$^+$98] M1 transition between the hyperfine-split magnetic sublevels 1 ($F = 4$, $M_F = 4$) and 2 ($F = 5$, $M_F = 5$). The inner sidebands are suppressed. See text for more details.

In Fig. 2.9 (a) we plot the power spectrum of resonance fluorescence for the case of the $2s \leftrightarrow 2p_{3/2}$ electric dipole transition in Li-like ^{209}Bi (Z=83) ions. The dynamic (AC) Stark shift leads to a splitting of the central peak, giving rise to a Mollow spectrum. Due to the long lifetime of the upper level of the hyperfine-split ground state, level 2, almost 100 % of the population is trapped in this level if only the $3 \leftrightarrow 1$ transition is driven coherently with an x-ray laser. The calculation yields for the population of the uppermost state a value of approx. $\Gamma_{21}/(\Gamma_{32} + 2\Gamma_{21}) \approx 10^{-12} \ll 1$, resulting in a negligibly small total x-ray fluorescence [1]. This undesirable effect may be reversed if additionally the $2 \leftrightarrow 1$ optical transition is coherently driven (see Fig. 2.9), leading to an efficient re-population of level 3.

Furthermore, the spectral lines become substantially narrower due to coherence and interference effects (see [NSO$^+$90] for the pioneering non-specific treatment). The width of the central peak and the outer sidebands are given, following our derivations in the previous sections, by $\Gamma_C = (\Gamma_{31} + \Gamma_{32} + \gamma_D)R + \Gamma_{21}(1 - R)$ and $\Gamma_{SB} = |\frac{3}{2}(\Gamma_{31} - \frac{1}{3}\gamma_D)R + \frac{1}{2}\Gamma_{32}(R + R^2) + \frac{3}{2}\Gamma_{21}(1 - R)|$, respectively, with the ratio R being $g_{31}^2/(g_{31}^2 + g_{21}^2)$. This effect is shown in Fig. 2.9 (b). Further increasing the intensity of the long-wavelength driving field and thus g_{21} could even assign the narrow linewidth of $7.7 \cdot 10^{-15}$ eV of the M1 hyperfine transition to the E1 x-ray transition of interest. The above line width formulas also imply that the dephasing width γ_D – typically on the order of 0.1 eV for XFELs [XFE] – does not hamper the observation of sub-natural linewidths in the x-ray regime as their contribution scales with the same factor R.

Transition lifetimes – and related quantities like the atomic dipole or multipole moments – are of great interest for astrophysical applications and for testing fundamental theories. Measurements of these quantities are particularly necessary since they are especially sensitive to the long-range behavior of atomic wave functions. Currently, even the best measurements do not exceed the 10^{-3} level of accuracy [LJC$^+$05]. In our scheme, the narrowed central and outer lines enable in principle an even more accurate determination of the atomic Rabi frequencies: the outer sideband peaks' distance is given by

[1] Our current discussion is valid in the secular limit $G = \sqrt{g_{31}^2 + g_{21}^2} \gg \max\{\Gamma_{31}, \Gamma_{32}, \Gamma_{21}\}$. If the effective Rabi frequency G can not be rendered high enough for a sufficient applicability of this approximation, one has to work with the more accurate and lengthy expressions of the spectral features.

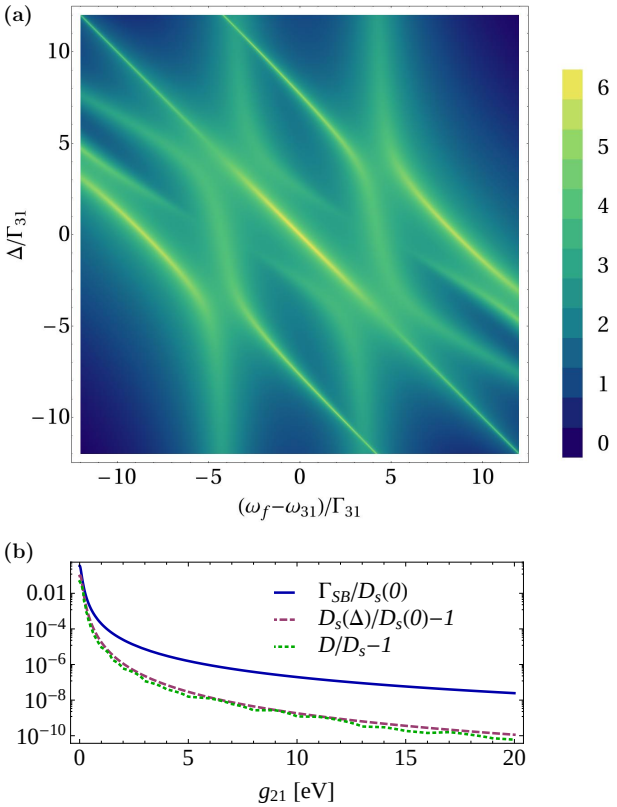

Figure 2.10: (a) Density plot of the fluorescence spectrum (logarithmic scale, arb. units) as a function of the fluorescence photon frequency ω_f with respect to the x-ray transition frequency ω_{31} (abscissa) and the laser detuning $\Delta = \omega_x - \omega_{31}$ (ordinate), with the frequencies normalized by the Γ_{31} rate. The parameters are for Bi as in Fig. 2.9. (b) Continuous (blue) curve: ratio of the interference-narrowed width Γ_{SB} of the outer sideband peaks to their distance $D_s(0) = 4G = 4\sqrt{g_{31}^2 + g_{21}^2}$ as a function of the optical Rabi frequency g_{21}, with further parameters for the Bi three-level system as given in the third line of Table 2.2. Dashed (red) curve: deviation of the sideband distance D_s, with $\Delta = \Gamma_{31}$. Dotted (green) curve: deviation of the exact sideband distance D from its value in the secular limit D_s.

$D_s(0) = 4G = 4\sqrt{g_{31}^2 + g_{21}^2}$ (in the secular limit and when the x-ray laser is on resonance, i.e. its detuning $\Delta = \omega_x - \omega_{31}$ from the transition frequency is 0). In this formula, the optical Rabi frequency g_{21} is usually known, therefore, determining its counterpart g_{31} for the x-ray transition is only limited by the accuracy of measuring the peak distance D. Fig. 2.10 (b) shows the ratio of the width of the narrowed outer lines to their distance $D_s(0)$. As shown, this ratio, characterizing the relative accuracy for the determination of atomic multipole moments, can be improved by several orders of magnitude for higher optical laser intensities.

Our calculation shows that the detuning dependence of the outer sideband distance is given by $D_s(\Delta) = 4G + \frac{G}{2}\left(4R - 3R^2\right)(\Delta/G)^2 + \mathcal{O}\left((\Delta/G)^4\right)$. This weak dependence is also illustrated in Fig. 2.10 (a). Hence, the experimental sensitivity on the potentially inaccurately known detuning may be reduced by orders of magnitude by increasing the optical intensity (Rabi frequency), as also shown on Fig. 2.10 (b). The multipole matrix elements of the ionic transitions can thus be determined in principle to a high accuracy on the order of 10^{-4}–10^{-6}, once the intensity of the driving field is accurately known. Conversely, the intensity may be measured to high accuracy if the multipole moments are reliably known from an independent experiment (e.g. lifetime measurements). At the same time, knowing the Rabi

Table 2.2: Parameters for $2s \leftrightarrow 2p_{3/2}$ transitions in the Li-like ions $^{203}Tl^{78+}$ (ω_{31}=2236.5 eV), $^{209}Bi^{80+}$ (2788.1 eV) and $^{235}U^{89+}$ (4459.4 eV). Optical transition energies (ω_{21}), natural line widths (Γ_{31}, Γ_{21}) and Rabi frequencies (g_{31}, g_{21}) as well as the interference-narrowed outer sideband width (Γ_{SB}) of the x-ray transition are given for the laser intensities I_x, I_o. $x(y)$ stands for $x \times 10^y$.

	ω_{21}	Γ_{31}	Γ_{SB}	Γ_{21}	g_{31}	g_{21}	I_x	I_o
	[meV]						[W/cm^2]	
Tl	499	6.6	7.1(-2)	1.1(-12)	1.8(2)	2.1(3)	1(12)	1(16)
			7.2(-4)		1.8(2)	2.1(4)	1(12)	1(18)
Bi	797	7.2(1)	9.7(-2)	7.7(-12)	8.3(1)	2.9(3)	5(11)	1(16)
			1.9(-1)		1.2(3)	2.9(4)	1(14)	1(18)
U	136	2.4(1)	3.7(-2)	3.7(-14)	7.7(1)	2.8(3)	5(11)	1(16)
			1.3		3.3(4)	1.9(5)	9(16)	5(19)

frequencies, the dependence of sideband positions on the x-ray detuning could allow to measure in principle the ionic x-ray transition energy in an independent way. Table 2.2 lists values for some elements and atomic transitions.

Our above results have been demonstrated on the example of highly charged ions with non-vanishing nuclear spins, i.e. when hyperfine splitting of the electronic ground state occurs. However, certainly, the results may be applied to further three-level configurations. For example, such configurations may also be prepared by applying (strong) external magnetic fields, which gives rise to a large Zeeman splitting of the ground-state level, addressable by long-wavelength coherent radiation such as masers (or even CO_2 lasers). Furthermore, the results can be generalized to other physical systems with high transition energies, such as electromagnetic transitions in nuclei. In this setting, nuclear multipole moments and transition energies may in principle be determined by an independent method.

2.10 Experimental aspects

Laser systems with photon energies of up to a few keV (in the range of Li-like transitions) are presently available [ABB$^+$06, LCL], allowing to excite elements as heavy as U and observing emission lines of sub-natural linewidths. In the following we briefly summarize the operational principles of free-electron lasers in the x-ray domain, and further devices such as electron beam ion traps and storage rings which are in principle capable of performing relativistic resonance fluorescence spectroscopy as put forward in this work.

A free-electron laser, or FEL, is a laser that shares the same optical properties as conventional lasers such as emitting a beam consisting of coherent electromagnetic radiation which can reach high power. Unlike gas, liquid, or solid-state lasers such as diode lasers, in which electrons are excited in bound atomic or molecular states, FELs use a relativistic electron beam as the lasing medium which moves freely through a magnetic structure. The free-electron laser has the widest frequency range of any laser type, and can be widely tunable, currently ranging in wavelength from microwaves, through terahertz radiation and infrared, to the visible spectrum, to ultraviolet and x-rays.

To create a FEL, a beam of electrons is accelerated to almost light velocity. The beam passes through an FEL oscillator in the form of a periodic, transverse magnetic field, produced by arranging magnets with alternating poles within a laser cavity along the beam path (see Fig.2.11). This array of magnets is called an undulator, or a "wiggler", because it forces the electrons in the beam to follow a sinusoidal

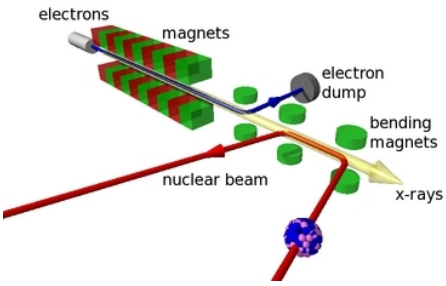

Figure 2.11: Scheme of a free electron laser. A fast electron beam is sent through the periodic, transverse magnetic field of the undulator, which creates coherent radiation.

path. The acceleration of the electrons along this path results in the release of photons (synchrotron radiation). Since the electron motion is in phase with the field of the light already emitted, the fields add together coherently. Whereas conventional undulators would cause the electrons to radiate independently, instabilities in the electron beam resulting from the interactions of the oscillations of electrons in the undulators and the radiation they emit leads to a bunching of the electrons, which continue to radiate in phase with each other. The wavelength of the light emitted can be readily tuned by adjusting the energy of the electron beam or the magnetic field strength of the undulators. Upcoming laser facilities are expected to increase the frequency limit to the order of tens of keVs (e.g. [XFE]), permitting to directly address the most relativistic heavy H-like systems or even nuclear transitions.

An electron beam ion trap (EBIT), see Fig. 2.12, is an electromagnetic trap that produces and confines highly charged ions. An EBIT uses an electron beam focused by means of a powerful magnetic field to ionize by repeated electron impact atoms injected into the apparatus to very high charge states. The vacuum device requires intense electron beam currents of tens up to hundreds of milliamps accelerated by means of high voltages (up to 200,000 V) applied to special electrodes. The positive – and, mostly, highly charged – ions produced in the region where the atoms intercept the electron beam are tightly confined in their motion by the strong attraction exerted by the negative charges flowing in the electron beam. Therefore, their paths orbit around the electron beam crossing it frequently, thus giving rise to further collisions and continued ionization. To keep their motion restricted in the direction of the electron beam axis, trapping electrodes carrying positive voltages with respect to the central electrode are used. The resulting ion trap can hold the ions for many seconds and even minutes, and conditions for reaching the highest charge states, up to bare uranium (U^{92+}) are achieved in this way. To avoid spoiling the produced ions by collisions with neutral atoms from which they can capture electrons, the vacuum in the apparatus is usually maintained at ultra high vacuum (UHV) levels.

EBITs are used to investigate the fundamental properties of highly charged ions e. g. by photon spectroscopy in particular in the context of relativistic atomic structure theory and quantum electrodynamics (QED). Their suitability to prepare and reproduce in a microscopic volume the conditions of high temperature astrophysical plasmas and magnetic confinement fusion plasmas make them very appropriate research tools. Fluorescence spectroscopy in the soft x-ray range has been already performed by employing ions trapped in an EBIT as described in Ref. [ECB$^+$07], suggesting that the schemes to manipulate x-ray resonance fluorescence as described in this thesis are feasible in the near future.

An other device to allow for experiments with highly charged ions is a storage ring, represented in Fig. 2.13, which is a type of circular particle accelerator in which a continuous or pulsed particle beam may be kept circulating for a long period of time, up to many hours. Technically speaking, a storage ring is a type

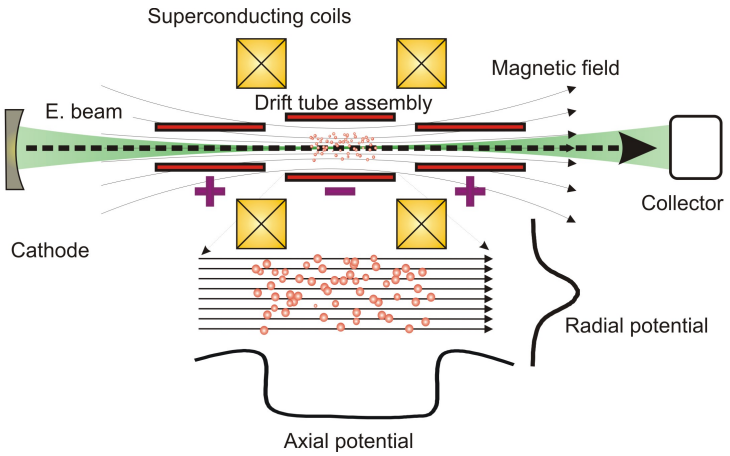

Figure 2.12: Logical scheme of an electron beam ion trap. See the text for a brief explanation of the EBIT operation.

of synchrotron. However, a conventional synchrotron serves to accelerate particles from a low to a high energy with the aid of radio-frequency accelerating cavities; a storage ring, as the name suggests, keeps particles stored at a constant energy, and radio-frequency cavities are only used to replace energy lost through synchrotron radiation and other processes. Emission spectroscopic studies with highly charged ions as heavy as uranium in the hard x-ray range has been performed at the Experimental Storage Ring (ESR) facility of the Gesellschaft für Schwerionenforschung (GSI) by Gumberidze et al. [GSB$^+$05], demonstrating that storage rings may serve as good candidates for performing resonance fluorescence experiments with x-ray lasers.

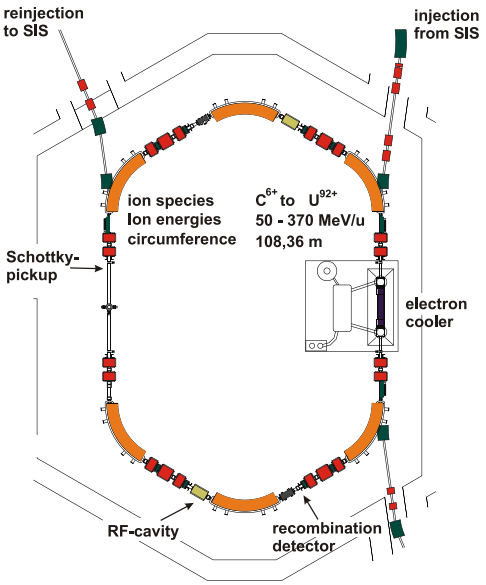

Figure 2.13: Scheme of the Experimental Storage Ring (ESR) of the GSI. See the text for a general summary of storage ring operation.

–III–

RELATIVISTIC LIGHT SHIFTS IN HYDROGENIC IONS

Energy shifts of atomic levels due to laser fields play an important role in high-precision laser spectroscopy. The dynamic Stark shift is one of the inherent systematic effects that shifts atomic energy levels in a laser spectroscopic experiment. In contrast to other shifting effects which may in principle be experimentally controllable, the dynamic Stark shift is due to the probing laser field itself and as such it cannot be eliminated. For this reason, it received considerable attention. The dynamic (AC) Stark shift is also present in laser-induced processes like ionization [SBF$^+$07, Cos07, KHK06, BK06]. Theoretical investigations so far apply nonrelativistic approaches and are restricted to electric dipole transitions.

In this Chapter we calculate light field shifts in a fully relativistic manner. This allows one to extend the field of investigations to stronger laser fields, higher frequencies – e.g., x-ray lasers [ECB$^+$07] –, and to the highest nuclear charges.

3.1 Dynamic shift by means of perturbation theory

Let us consider the effect of adding the interaction Hamiltonian $V(\epsilon, t)$ to the sum of relativistic hydrogen-like ion H_0:

$$\begin{aligned} H &= H_0 + V(\epsilon, t)\,, \\ H_0 &= c\boldsymbol{\alpha}\boldsymbol{p} + \boldsymbol{\beta} m_0 c^2 - \frac{Ze^2}{4\pi\epsilon_0 r}\,, \\ V(\epsilon, t) &= -\left(A_0 \boldsymbol{\alpha}\hat{\epsilon}_\nu e^{i\boldsymbol{k}\boldsymbol{r} - i\omega t} + c.c.\right) e^{\epsilon t}\,. \end{aligned} \tag{3.1}$$

Here, ϵ is an infinitesimal damping parameter [Sak94]. The introduction of an adiabatic damping parameter is a key element of time-dependent perturbation theory. In the interaction picture (denoted by the subscript I), the interaction V is represented by [BJ89]:

$$V_I(\epsilon, t) = e^{\frac{i}{\hbar} H_0 t} V(\epsilon, t) e^{-\frac{i}{\hbar} H_0 t}\,. \tag{3.2}$$

We calculate the time evolution operator U_I up to second order in V_I from the Dyson series:

$$\begin{aligned} U_I &= \lim_{t\to\infty} U_I(\epsilon, t)\,, \\ U_I(\epsilon, t) &= 1 - \frac{i}{\hbar}\int_{-\infty}^{t} dt' V_I(\epsilon, t) + \\ &\quad \left(-\frac{i}{\hbar}\right)^2 \int_{-\infty}^{t} dt' \int_{-\infty}^{t'} dt'' V_I(\epsilon, t') V_I(\epsilon, t")\,. \end{aligned} \tag{3.3}$$

Let Φ_n represent an eigenfunction of the unperturbed Hamiltonian H_0 with an eigenvalue E_n. We denote the complete set of eigenstates of H_0 by $\{|\Phi_n\rangle\}$. $|\Phi_I(t)\rangle$ is a time-dependent atomic state in the interaction picture. The state function before interaction is an eigenstate of H_0: $|\Phi_I(t=-\infty)\rangle = |\Phi_a\rangle$, where Φ_a is an eigenstate of the unperturbed Hamiltonian H_0. Thus the state function at any time can be constructed by applying the evolution operator as

$$|\Phi_I(t)\rangle = U_I(\epsilon,t)|\Phi_I(t=-\infty)\rangle = \sum_n c_n(t)|\Phi_n\rangle\,. \tag{3.4}$$

This condition is also true for the degenerate case [BJ89] without loss of generality. The time-dependent expansion coefficients $c_n(t)$ are given as the projections

$$c_n(t) = \langle\Phi_n|\Phi_I(t)\rangle\,. \tag{3.5}$$

For calculating the light shift of a given atomic state a, we are interested in the projection [Sak94]

$$c_a(t) = \langle\Phi_a|\Phi_I(t)\rangle = \langle\Phi_a|U_I(\epsilon,t)|\Phi_a\rangle\,. \tag{3.6}$$

The first-order perturbation $\langle\Phi_a|V|\Phi_a\rangle$ vanishes. Substituting $U_I(\epsilon,t)$ from Eq. (3.3), the leading order of the perturbation expansion is V^2 and the problem reduces to calculating the matrix element

$$\begin{aligned} M = &\int_{-\infty}^{t} dt' \int_{-\infty}^{t'} dt''\langle\Phi_a|V_I(\epsilon,t')V_I(\epsilon,t'')|\Phi_a\rangle = \\ &\sum_n \int_{-\infty}^{t} dt' \int_{-\infty}^{t'} dt''\langle\Phi_a|V_I(\epsilon,t')|\Phi_n\rangle\langle\Phi_n|V_I(\epsilon,t'')|\Phi_a\rangle\,. \end{aligned} \tag{3.7}$$

The index n counts all bound and continuum states of the unperturbed hydrogen-like ion. After carrying out the time integration, the matrix element is given as

$$\begin{aligned} M = -\frac{\hbar}{i}\sum_n \Bigg(& A_0^2 \frac{\langle\Phi_a|V_1|\Phi_n\rangle\langle\Phi_n|V_1|\Phi_a\rangle e^{2t(\epsilon-i\omega)}}{2(\epsilon-i\omega)(E_a-E_n+\hbar\omega-i\hbar\epsilon)} \\ &+|A_0|^2 \frac{\langle\Phi_a|V_2|\Phi_n\rangle\langle\Phi_n|V_1|\Phi_a\rangle}{2\epsilon(E_a-E_n-\hbar\omega-i\hbar\epsilon)} e^{2\epsilon t} \\ &+|A_0|^2 \frac{\langle\Phi_a|V_1|\Phi_n\rangle\langle\Phi_n|V_2|\Phi_a\rangle}{2\epsilon(E_a-E_n+\hbar\omega-i\hbar\epsilon)} e^{2\epsilon t} \\ &+(A_0^*)^2 \frac{\langle\Phi_a|V_2|\Phi_n\rangle\langle\Phi_n|V_2|\Phi_a\rangle e^{2t(\epsilon+i\omega)}}{2(\epsilon+i\omega)(E_a-E_n-\hbar\omega-i\hbar\epsilon)} \Bigg)\,. \end{aligned} \tag{3.8}$$

For simplicity the notation $V_1 = -\boldsymbol{\alpha}\hat{\epsilon}_\nu e^{i\boldsymbol{kr}}$ and $V_2 = -\boldsymbol{\alpha}^*\hat{\epsilon}_\nu^* e^{-i\boldsymbol{kr}}$ is introduced above. In the second order of perturbation theory one can write

$$c_a(t) = -\frac{i}{\hbar}M'(t)\,, \tag{3.9}$$

with $M' = -\frac{i}{\hbar}M$. Neglecting higher-order terms, the logarithmic derivative of the expansion coefficient is

$$\frac{d}{dt}\ln(c_a(t)) = -\frac{i}{\hbar}\frac{dM'}{dt}\,. \tag{3.10}$$

In the limit $\epsilon \to 0$, the time derivative of the matrix element is

$$\begin{aligned}\frac{dM'}{dt} &= \sum_n \left(A_0^2 \frac{\langle\Phi_a|V_1|\Phi_n\rangle\langle\Phi_n|V_1|\Phi_a\rangle}{E_a - E_n + \hbar\omega} e^{-2i\omega t} \right. \\ &+ |A_0|^2 \frac{\langle\Phi_a|V_2|\Phi_n\rangle\langle\Phi_n|V_1|\Phi_a\rangle}{E_a - E_n - \hbar\omega} \\ &+ |A_0|^2 \frac{\langle\Phi_a|V_1|\Phi_n\rangle\langle\Phi_n|V_2|\Phi_a\rangle}{E_a - E_n + \hbar\omega} \\ &+ \left. (A_0^*)^2 \frac{\langle\Phi_a|V_2|\Phi_n\rangle\langle\Phi_n|V_2|\Phi_a\rangle}{E_a - E_n - \hbar\omega} e^{2i\omega t} \right) . \end{aligned} \tag{3.11}$$

In the static limit $\omega \to 0$ of the electromagnetic field, this expression simplifies to

$$\begin{aligned}\frac{dM'_{(\omega=0)}}{dt} &= \sum_n \left(A_0^2 \frac{\langle\Phi_a|V_1|\Phi_n\rangle\langle\Phi_n|V_1|\Phi_a\rangle}{E_a - E_n} \right. \\ &+ |A_0|^2 \frac{\langle\Phi_a|V_2|\Phi_n\rangle\langle\Phi_n|V_1|\Phi_a\rangle}{E_a - E_n} \\ &+ |A_0|^2 \frac{\langle\Phi_a|V_1|\Phi_n\rangle\langle\Phi_n|V_2|\Phi_a\rangle}{E_a - E_n} \\ &+ \left. (A_0^*)^2 \frac{\langle\Phi_a|V_2|\Phi_n\rangle\langle\Phi_n|V_2|\Phi_a\rangle}{E_a - E_n} \right) . \end{aligned} \tag{3.12}$$

For $\omega \neq 0$ we use the property $e^{2i\omega t} = \frac{1}{2i\omega}\int_0^t dt' e^{2i\omega t'}$. Using relation (3.3) (see Ref. [Joh]) to form the Dyson series, we get

$$\begin{aligned}\frac{dM'_{\omega\neq 0}}{dt} &= \sum_n \left(|A_0|^2 \frac{\langle\Phi_a|V_2|\Phi_n\rangle\langle\Phi_n|V_1|\Phi_a\rangle}{E_a - E_n - \hbar\omega} \right. \\ &+ \left. |A_0|^2 \frac{\langle\Phi_a|V_1|\Phi_n\rangle\langle\Phi_n|V_2|\Phi_a\rangle}{E_a - E_n + \hbar\omega} \right) . \end{aligned} \tag{3.13}$$

Because $\frac{dM'_{\omega\neq 0}}{dt}$ and $\frac{dM'_{(\omega=0)}}{dt}$ are time independent, one can make the ansatz [Sak94]

$$\frac{\dot{c}_a}{c_a} = -\frac{i}{\hbar}\Delta_a^{AC} \tag{3.14}$$

and define the energy shift of the state a due to interaction with the light field as

$$\begin{aligned}\Delta_a^{AC} &= |A_0|^2 \sum_n \left(\frac{\langle\Phi_a|V_2|\Phi_n\rangle\langle\Phi_n|V_1|\Phi_a\rangle}{E_a - E_n - \hbar\omega} \right. \\ &+ \left. \frac{\langle\Phi_a|V_1|\Phi_n\rangle\langle\Phi_n|V_2|\Phi_a\rangle}{E_a - E_n + \hbar\omega} \right) . \end{aligned} \tag{3.15}$$

A_0 is given as $|A_0|^2 = \frac{|\boldsymbol{E}|^2 c^2}{\omega^2}$, with $\boldsymbol{E}$ being the electric field strength. On Fig. 3.1, the diagrams representing the two terms in the above equations are shown.

3.2 Evaluation of matrix elements

In this section we describe how the relativistic wave functions, the vector potential of the electromagnetic field and the interaction matrix elements in Eq. (3.15) are treated. Our description is fully relativistic and

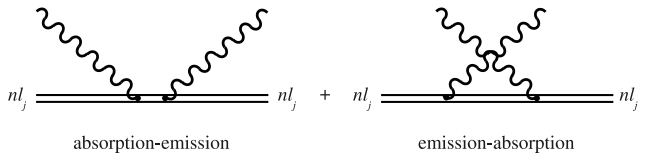

Figure 3.1: Diagrams representing the lowest-order perturbative light shift corrections. The Coulomb-dressed electron is depicted by a double line and the wavy lines represent photons.

accounts for spin and magnetic field effects. A similar description is used for the relativistic theoretical study of the spontaneous emission in Refs. ([Joh, BS88, Gra74, Gra06]).

The principal task in calculating the light shift is the evaluation of the matrix element

$$M = \sum_n \frac{\langle \Phi_a | \hat{\alpha}^* \hat{\epsilon}^*_\nu e^{-i\boldsymbol{kr}} | \Phi_n \rangle \langle \Phi_n | \hat{\alpha} \hat{\epsilon}_\nu e^{i\boldsymbol{kr}} | \Phi_a \rangle}{E_a - E_n - \hbar\omega} \,. \tag{3.16}$$

We apply the multipole decomposition of the transverse electromagnetic plane wave as

$$\hat{\alpha}\hat{\epsilon_\nu} e^{i\boldsymbol{kr}} = 4\pi\hat{\alpha} \sum_{lm} \sum_{\lambda=0}^{1} i^{l-\lambda} \left(\boldsymbol{Y}^{(\lambda)}_{lm}(\hat{k}) \cdot \hat{\epsilon}_\nu \right)^\dagger \boldsymbol{a}^{(\lambda)}_{lm}(\boldsymbol{r}) \,, \tag{3.17}$$

thus M becomes

$$\begin{aligned} M &= 16\pi^2 \sum_{nlm\lambda l'm'\lambda'} \langle \Phi_a | \hat{\alpha}^* i^{\lambda - l} (\hat{\epsilon_\nu} \boldsymbol{Y}^{(\lambda)}_{lm}(\hat{k})) \boldsymbol{a}^{(\lambda)\dagger}_{lm}(\boldsymbol{r}) | \Phi_n \rangle \\ &\times \frac{\langle \Phi_n | \hat{\alpha} (i^*)^{l' - \lambda'} (\boldsymbol{Y}^{(\lambda')}_{l'm'}(\hat{k}) \hat{\epsilon_\nu})^\dagger \boldsymbol{a}^{(\lambda')}_{l'm'}(\boldsymbol{r}) | \Phi_a \rangle}{E_a - E_n - \hbar\omega} \,. \end{aligned} \tag{3.18}$$

To obtain the level shift, a summation over polarization states and integration over photon directions has to be performed:

$$M = \frac{1}{2} \sum_\nu \frac{1}{4\pi} \int d\Omega_k M \,. \tag{3.19}$$

Using the orthogonality property

$$\sum_\nu \int d\Omega_k \left(\boldsymbol{Y}^{(\lambda')}_{l'm'}(\hat{k}) \hat{\epsilon}_\nu \right)^\dagger \left(\hat{\epsilon_\nu} \boldsymbol{Y}^{(\lambda)}_{lm}(\hat{k}) \right) = \delta_{ll'} \delta_{mm'} \delta_{\lambda\lambda'} \,, \tag{3.20}$$

the expression above simplifies to

$$M = 2\pi \sum_{nlm\lambda} \frac{\langle \Phi_a | \hat{\alpha}^* \boldsymbol{a}^{(\lambda)\dagger}_{lm}(\boldsymbol{r}) | \Phi_n \rangle \langle \Phi_n | \hat{\alpha} \boldsymbol{a}^{(\lambda)}_{lm}(\boldsymbol{r}) | \Phi_a \rangle}{E_a - E_n - \hbar\omega} \,. \tag{3.21}$$

Using the spectral representation of Green's function

$$G(\boldsymbol{r}, \boldsymbol{r}'; z) = \sum_n \frac{\Phi_n(\boldsymbol{r}) \Phi_n(\boldsymbol{r})^\dagger}{E_n - z} \,, \tag{3.22}$$

and splitting Eq. (3.21) into an electric ($\lambda = 1$) and a magnetic ($\lambda = 0$) part we get:

$$\begin{aligned} M &= -2\pi \sum_{lm} \int d\boldsymbol{r} d\boldsymbol{r}' \Phi_a^\dagger(\boldsymbol{r}) \hat{\alpha}^* \boldsymbol{a}_{lm}^{(0)\dagger}(\boldsymbol{r}) G(\boldsymbol{r}, \boldsymbol{r}'; z) \\ &\quad \times \hat{\alpha} \boldsymbol{a}_{lm}^{(0)}(\boldsymbol{r}) \Phi_a(\boldsymbol{r}') \\ &\quad -2\pi \sum_{lm} \int d\boldsymbol{r} d\boldsymbol{r}' \Phi_a^\dagger(\boldsymbol{r}) \hat{\alpha}^* \boldsymbol{a}_{lm}^{(1)\dagger}(\boldsymbol{r}) G(\boldsymbol{r}, \boldsymbol{r}'; z) \\ &\quad \times \hat{\alpha} \boldsymbol{a}_{lm}^{(1)}(\boldsymbol{r}) \Phi_a(\boldsymbol{r}') \,, \end{aligned} \tag{3.23}$$

where the energy variable is $z = E_a - \hbar\omega$.

We perform a gauge transformation of the matrix elements. The transformed multipole potential can be written as

$$\begin{aligned} \boldsymbol{a}_{JM}^{\lambda}(\hat{r}) &\longrightarrow \boldsymbol{a}_{JM}^{\lambda}(\hat{r}) + \nabla \chi_{JM}(\hat{r}) \,, \\ \Phi_{JM}(\hat{r}) &\longrightarrow i\omega \chi_{JM}(\hat{r}) \,. \end{aligned} \tag{3.24}$$

where the gauge function $\chi_{JM}(\hat{r})$ (and the multipole potential) is a solution to the Helmholtz equation. We choose the gauge function to be

$$\chi_{JM}(\hat{r}) = -\frac{1}{k} G_J j_J(kr) Y_{JM}(\hat{r}) \,. \tag{3.25}$$

With the choice of $G_J = \sqrt{J + 1/J}$, the so-called Babushkin gauge, i.e. a relativistic generalization of the length form interaction, is adopted [Gra74, Gra06, Bab62]. This transformation has no effect on the magnetic multipole potentials, but transforms electric potentials to the form

$$\begin{aligned} \boldsymbol{a}_{JM}^{(1)}(\hat{r}) &= -j_{J+1}(kr) \left(\boldsymbol{Y}_{JM}^{(1)}(\hat{r}) - \sqrt{\frac{J+1}{J}} \boldsymbol{Y}_{JM}^{(-1)}(\hat{r}) \right) \,, \\ \Phi_{JM}^{(1)}(\hat{r}) &= -ic \sqrt{\frac{J+1}{J}} j_J(kr) Y_{JM}(\hat{r}) \,. \end{aligned} \tag{3.26}$$

The electric multipole potentials can be rewritten as

$$\boldsymbol{a}_{JM}^{(1)}(\hat{r}) = -\sqrt{\frac{2J+1}{J}} \boldsymbol{a}_{JJ+1M}(\hat{r}) \,, \tag{3.27}$$

with $\boldsymbol{a}_{JJ+1M}(\hat{r})$ given by Eq. (B.7) in the Appendix.

Denoting with M^m the magnetic part and with M^e the electric part and after some algebraic manipula-

tions we obtain

$$
\begin{aligned}
M^m &= \frac{4\pi}{\hbar c}\sum_{lm\kappa_n}\Big\{(R_1^m+R_4^m)K^{\kappa_n-\kappa_a}_{JJM}K^{-\kappa_n\kappa_a}_{JJM} \\
&\quad -R_2^m\left(K^{-\kappa_n\kappa_a}_{JJM}\right)^2-R_3^m\left(K^{\kappa_n-\kappa_a}_{JJM}\right)^2\Big\}, \\
M^e &= \frac{4\pi}{\hbar c}\sum_{lm\kappa_n}\left\{\frac{2J+1}{J}\Big[(R_1^e+R_4^e)K^{\kappa_n-\kappa_a}_{JJ+1M}K^{-\kappa_n\kappa_a}_{JJ+1M}\right. \\
&\quad -R_2^e\left(K^{-\kappa_n\kappa_a}_{JJ+1M}\right)^2-R_3^e\left(K^{\kappa_n-\kappa_a}_{JJ+1M}\right)^2\Big] \\
&\quad -\frac{J+1}{J}\Big[R_{1'}^e\left(K^{\kappa_n\kappa_a}_{JM}\right)^2+\left(R_{2'}^e+R_{3'}^e\right)K^{\kappa_n\kappa_a}_{JM}K^{-\kappa_n-\kappa_a}_{JM} \\
&\quad \left.+R_{4'}^e\left(K^{-\kappa_n-\kappa_a}_{JM}\right)^2\Big]\right\}. \qquad (3.28)
\end{aligned}
$$

We shall refer to the K's as the angular matrix elements and to the R's as the radial matrix elements.

The matrix element

$$
M'=\sum_n\frac{\langle\Phi_a|\hat{\alpha}\hat{\epsilon}_\nu e^{i\boldsymbol{kr}}|\Phi_n\rangle\langle\Phi_n|\hat{\alpha}^*\hat{\epsilon}^*_\nu e^{-i\boldsymbol{kr}}|\Phi_a\rangle}{E_a-E_n+\hbar\omega} \qquad (3.29)
$$

can readily be found from Eq. (3.28) by the substitutions $K^{\kappa_n-\kappa_a}\to K^{-\kappa_a-\kappa_n}$, $K^{\kappa_n\kappa_a}\to K^{\kappa_a-\kappa_n}$, $K^{\kappa_n\kappa_a}\to K^{\kappa_a\kappa_n}$ and $K^{-\kappa_n-\kappa_a}\to K^{-\kappa_a-\kappa_n}$. In the radial part, the energy variable $z=E_a+\hbar\omega$ has to be substituted.

3.2.1 Radial matrix elements

The following notations are introduced for the two-dimensional radial integrals:

$$
\begin{aligned}
R_1^m &= \int drdr'r^2r'^2F_a(r)j_J(kr)g_{12}(r,r';E)j_J(kr')G_a(r'), \\
R_2^m &= \int drdr'r^2r'^2G_a(r)j_J(kr)g_{22}(r,r';E)j_J(kr')G_a(r'), \\
R_3^m &= \int drdr'r^2r'^2F_a(r)j_J(kr)g_{11}(r,r';E)j_J(kr')F_a(r'), \\
R_4^m &= \int drdr'r^2r'^2G_a(r)j_J(kr)g_{21}(r,r';E)j_J(kr')F_a(r'), \\
R_{1'}^e &= \int drdr'r^2r'^2G_a(r)j_J(kr)g_{11}(r,r';E)j_J(kr')G_a(r'), \\
R_{2'}^e &= \int drdr'r^2r'^2F_a(r)j_J(kr)g_{21}(r,r';E)j_J(kr')G_a(r'), \\
R_{3'}^e &= \int drdr'r^2r'^2G_a(r)j_J(kr)g_{12}(r,r';E)j_J(kr')F_a(r'), \\
R_{4'}^e &= \int drdr'r^2r'^2F_a(r)j_J(kr)g_{22}(r,r';E) \\
&\quad \times j_J(kr')F_a(r'). \qquad (3.30)
\end{aligned}
$$

In these integrals, $j_J(kr)$ is the spherical Bessel function [AS72] and the g_{ij} $(i,j=1,2)$ are the radial components of the Coulomb-Dirac Green's function.

All radial matrix elements can be evaluated analytically by the help of the substitution

$$j_l(kr) = \left(\frac{\pi}{2kr}\right)^{1/2} J_{l+1/2}(kr) \tag{3.31}$$

and the Taylor expansion of the Bessel functions $J_{l+1/2}$:

$$j_l(kr) = \sqrt{\frac{\pi}{2kr}} \sum_{n=0} \frac{(-1)^n}{2^{2n+l+1/2} n! \Gamma(n+l+3/2)} (kr)^{2n+l+1/2}\,. \tag{3.32}$$

The final results are as follows:

$$\begin{aligned} R_1^m = & \left(1 - \frac{E_a^2}{m^2c^4}\right)^{1/2} U_a^2 \frac{1}{2} (2\lambda_n)^{(2\gamma_n)} \sum_n \\ & \Bigg(- (\kappa_n + \nu/\epsilon_n) \frac{n!(I_{A_1J}^2 - I_{B_1J}^2)}{\Gamma(2\gamma_n + 1 + n)(n + \gamma_n + 1 - \nu)} \\ & -(\kappa_n - \nu/\epsilon_n) \frac{n!(I_{A_1J}^2 - I_{B_1J}^2)}{\Gamma(2\gamma_n + 1 + n)(n + \gamma_n - \nu)} \\ & - \frac{n!2}{\Gamma(2\gamma_n + n)(n + \gamma_n - \nu)} (I_{A_2J} I_{B_1J} - I_{A_1J} I_{B_2J}) \Bigg)\,, \end{aligned} \tag{3.33}$$

$$\begin{aligned} R_2^m = & \left(1 + \frac{E_a}{mc^2}\right) U_a^2 \frac{\varepsilon}{2} (2\lambda_n)^{(2\gamma_n)} \sum_n \\ & \Bigg((\kappa_n + \nu/\epsilon_n) \frac{n!'(I_{A_1J} - I_{B_1J})^2}{\Gamma(2\gamma_n + 1 + n)(n + \gamma_n + 1 - \nu)} - \\ & [(\kappa_n - \nu/\epsilon_n) - 2(\gamma_n + \nu)] \frac{n!(I_{A_1J} - I_{B_1J})^2}{\Gamma(2\gamma_n + 1 + n)(n + \gamma_n - \nu)} \\ & - \frac{n!2}{\Gamma(2\gamma_n + n)(n + \gamma_n - \nu)} \\ & \times (I_{A_2J} I_{A_1J} - I_{A_1J} I_{B_2J} - I_{A_2J} I_{B_1J} + I_{B_1J} I_{B_2J}) \Bigg)\,, \end{aligned} \tag{3.34}$$

$$\begin{aligned} R_3^m = & \left(1 - \frac{E_a}{mc^2}\right) U_a^2 \frac{1}{2\varepsilon} (2\lambda_n)^{(2\gamma_n)} \sum_n \\ & \Bigg((\kappa_n + \nu/\epsilon_n) \frac{n!(I_{A_1J} + I_{B_1J})^2}{\Gamma(2\gamma_n + 1 + n)(n + \gamma_n + 1 - \nu)} - \\ & [(\kappa_n - \nu/\epsilon_n) + 2(\gamma_n + \nu)] \frac{n!(I_{A_1J} + I_{B_1J})^2}{\Gamma(2\gamma_n + 1 + n)(n + \gamma_n - \nu)} \\ & + \frac{n!2}{\Gamma(2\gamma_n + n)(n + \gamma_n - \nu)} \\ & \times (I_{A_2J} I_{A_1J} + I_{A_1J} I_{B_2J} + I_{A_2J} I_{B_1J} + I_{B_1J} I_{B_2J}) \Bigg)\,, \end{aligned} \tag{3.35}$$

$$R_4^m = \left(1 - \frac{E_a^2}{m^2c^4}\right) U_a^2 \frac{1}{2} (2\lambda_n)^{(2\gamma_n)} \sum_n \tag{3.36}$$
$$\left(- (\kappa_n + \nu/\epsilon_n) \frac{n!(I_{A_1J}^2 - I_{B_1J}^2)}{\Gamma(2\gamma_n + 1 + n)(n + \gamma_n + 1 - \nu)} \right.$$
$$-(\kappa_n - \nu/\epsilon_n) \frac{n!(I_{A_1J}^2 - I_{B_1J}^2)}{\Gamma(2\gamma_n + 1 + n)(n + \gamma_n - \nu)}$$
$$\left. - \frac{n!2}{\Gamma(2\gamma_n + n)(n + \gamma_n - \nu)} (I_{A_2J} I_{B_1J} - I_{A_1J} I_{B_2J}) \right),$$

$$R_{1'}^e = \left(1 + \frac{E_a}{mc^2}\right) U_a^2 \frac{1}{2\varepsilon} (2\lambda_n)^{(2\gamma_n)} \sum_n \tag{3.37}$$
$$\left((\kappa_n + \nu/\epsilon_n) \frac{n!(I_{A_1J} - I_{B_1J})^2}{\Gamma(2\gamma_n + 1 + n)(n + \gamma_n + 1 - \nu)} - \right.$$
$$[(\kappa_n - \nu/\epsilon_n) + 2(\gamma_n + \nu)] \frac{n!(I_{A_1J} - I_{B_1J})^2}{\Gamma(2\gamma_n + 1 + n)(n + \gamma_n - \nu)}$$
$$+ \frac{n!2}{\Gamma(2\gamma_n + n)(n + \gamma_n - \nu)}$$
$$\left. \times (I_{A_2J} I_{A_1J} - I_{A_1J} I_{B_2J} - I_{A_2J} I_{B_1J} + I_{B_1J} I_{B_2J}) \right),$$

$$R_{2'}^e = \left(1 - \frac{E_a^2}{m^2c^4}\right)^{1/2} U_a^2 \frac{1}{2} (2\lambda_n)^{(2\gamma_n)} \sum_n \tag{3.38}$$
$$\left(- (\kappa_n + \nu/\epsilon_n) \frac{n!(I_{A_1J}^2 - I_{B_1J}^2)}{\Gamma(2\gamma_n + 1 + n)(n + \gamma_n + 1 - \nu)} \right.$$
$$-(\kappa_n - \nu/\epsilon_n) \frac{n!(I_{A_1J}^2 - I_{B_1J}^2)}{\Gamma(2\gamma_n + 1 + n)(n + \gamma_n - \nu)}$$
$$\left. + \frac{n!2}{\Gamma(2\gamma_n + n)(n + \gamma_n - \nu)} (I_{A_2J} I_{B_1J} - I_{A_1J} I_{B_2J}) \right),$$

$$R_{3'}^e = \left(1 - \frac{E_a^2}{m^2c^4}\right)^{1/2} U_a^2 \frac{1}{2} (2\lambda_n)^{(2\gamma_n)} \sum_n \tag{3.39}$$
$$\left(- (\kappa_n + \nu/\epsilon_n) \frac{n!(I_{A_1J}^2 - I_{B_1J}^2)}{\Gamma(2\gamma_n + 1 + n)(n + \gamma_n + 1 - \nu)} \right.$$
$$-(\kappa_n - \nu/\epsilon_n) \frac{n!(I_{A_1J}^2 - I_{B_1J}^2)}{\Gamma(2\gamma_n + 1 + n)(n + \gamma_n - \nu)}$$
$$\left. + \frac{n!2}{\Gamma(2\gamma_n + n)(n + \gamma_n - \nu)} (I_{A_2J} I_{B_1J} - I_{A_1J} I_{B_2J}) \right),$$

$$
\begin{aligned}
R^e_{4'} = & \left(1-\frac{E_a}{mc^2}\right) U_a^2 \frac{\varepsilon}{2} (2\lambda_n)^{(2\gamma_n)} \sum_n \\
& \left((\kappa_n + \nu/\epsilon_n) \frac{n!(I_{A_1J}+I_{B_1J})^2}{\Gamma(2\gamma_n+1+n)(n+\gamma_n+1-\nu)} - \right. \\
& [(\kappa_n - \nu/\epsilon_n) - 2(\gamma_n+\nu)] \frac{n!(I_{A_1J}+I_{B_1J})^2}{\Gamma(2\gamma_n+1+n)(n+\gamma_n-\nu)} \\
& - \frac{n!2}{\Gamma(2\gamma_n+n)(n+\gamma_n-\nu)} \\
\times \quad & \left. (I_{A_2J}I_{A_1J} + I_{A_1J}I_{B_2J} + I_{A_2J}I_{B_1J} + I_{B_1J}I_{B_2J}) \right) .
\end{aligned} \tag{3.40}
$$

For the one-dimensional radial integrals we obtain the following analytical results:

$$
\begin{aligned}
I_{A_1J} = & \left(\frac{\pi}{2k}\right) \sum_{\alpha,p} \frac{a_r(-1)^\alpha}{\alpha!\Gamma(\alpha+l+3/2)} \frac{(-a_r+1)_p}{(2\gamma_a+1)_p} \\
& \times \frac{\Gamma(\gamma_{an}+l+2\alpha+p+1)\Gamma(2\gamma_n+n+1)}{n!\Gamma(2\gamma_n+1)} \\
& \times \left(\frac{k}{2}\right)^{2\alpha+l+1/2} \frac{(2\lambda_a)^{p+\gamma_a-1}}{p!} \lambda_{an}^{-(\gamma_{an}+p+2)} \\
& \times {}_2F_1(-n, \gamma_{an}+l+2\alpha+p+1, 2\gamma_n+1, \frac{2\lambda_n}{\lambda_{an}}) ,
\end{aligned} \tag{3.41}
$$

$$
\begin{aligned}
I_{A_2J} = & \left(\frac{\pi}{2k}\right) \sum_{\alpha,p} \frac{a_r(-1)^\alpha}{\alpha!\Gamma(\alpha+l+3/2)} \frac{(-a_r+1)_p}{(2\gamma_a+1)_p} \\
& \times \frac{\Gamma(\gamma_{an}+l+2\alpha+p+1)\Gamma(2\gamma_n+n)}{n!\Gamma(2\gamma_n)} \\
& \times \left(\frac{k}{2}\right)^{2\alpha+l+1/2} \frac{(2\lambda_a)^{p+\gamma_a-1}}{p!} \lambda_{an}^{-(\gamma_{an}+p+2)} \\
& \times {}_2F_1(-n, \gamma_{an}+l+2\alpha+p+1, 2\gamma_n, \frac{2\lambda_n}{\lambda_{an}}) ,
\end{aligned} \tag{3.42}
$$

$$
\begin{aligned}
I_{B_1J} = & \left(\frac{\pi}{2k}\right) \sum_{\alpha,p} \frac{(N_a-\kappa_a)(-1)^\alpha}{\alpha!\Gamma(\alpha+l+3/2)} \frac{(-a_r)_p}{(2\gamma_a+1)_p} \\
& \times \frac{\Gamma(\gamma_{an}+l+2\alpha+p+1)\Gamma(2\gamma_n+n+1)}{n!\Gamma(2\gamma_n+1)} \\
& \times \left(\frac{k}{2}\right)^{2\alpha+l+1/2} \frac{(2\lambda_a)^{p+\gamma_a-1}}{p!} \lambda_{an}^{-(\gamma_{an}+p+2)} \\
& \times {}_2F_1(-n, \gamma_{an}+l+2\alpha+p+1, 2\gamma_n+1, \frac{2\lambda_n}{\lambda_{an}}) ,
\end{aligned} \tag{3.43}
$$

$$
\begin{aligned}
I_{B_2 J} &= \Big(\frac{\pi}{2k}\Big) \sum_{\alpha,p} \frac{(N_a-\kappa_a)(-1)^\alpha}{\alpha!\Gamma(\alpha+l+3/2)} \frac{(-a_r)_p}{(2\gamma_a+1)_p} \\
&\times \frac{\Gamma(\gamma_{an}+l+2\alpha+p+1)\Gamma(2\gamma_n+n)}{n!\Gamma(2\gamma_n)} \\
&\times \left(\frac{k}{2}\right)^{2\alpha+l+1/2} \frac{(2\lambda_a)^{p+\gamma_a-1}}{p!} \lambda_{an}^{-(\gamma_{an}+p+2)} \\
&\times {}_2F_1(-n, \gamma_{an}+l+2\alpha+p+1, 2\gamma_n, \frac{2\lambda_n}{\lambda_{an}}) \,. \qquad (3.44)
\end{aligned}
$$

Here we introduced the notations $\lambda_{an} = \lambda_a + \lambda_n$ and $\gamma_{an} = \gamma_a + \gamma_n$ for simplicity. The remaining radial matrix elements can be calculated from the ones given in Eq. (3.33-3.36) by the substitutions $R_i^e = R_i^m(J \to J+1)$ for all $i \in \{1,2,3,4\}$.

3.2.2 Angular matrix elements

The equations (3.28) contain angular integrals of the form

$$
K_{JkM}^{\kappa_n \kappa_a} = \int do_r \Omega_{\kappa_n}^\dagger(\hat{r}) \hat{\sigma} \boldsymbol{Y}_{JkM}(\hat{r}) \Omega_{\kappa_a}(\hat{r}) \,. \qquad (3.45)
$$

The direct product of the spin operator $\hat{\sigma}$ and the vector spherical harmonic is a spherical tensor operator and thus its matrix element can be rewritten as

$$
K_{JkM}^{\kappa_n \kappa_a} = \langle l_n \frac{1}{2} j_n | T_J(Y_k \sigma_1) | l_a \frac{1}{2} j_a \rangle \,. \qquad (3.46)
$$

The reduced matrix elements of the tensor T can be calculated using the formula

$$
\begin{aligned}
&\langle l_1 \frac{1}{2} j || T_K(C_k \sigma_1) || l_1' \frac{1}{2} j' \rangle = \\
&= a_K (-1)^{J'-K-1/2} (2j'+1)^{1/2} \begin{pmatrix} j & j' & K \\ \frac{1}{2} & -\frac{1}{2} & 0 \end{pmatrix} , \qquad (3.47)
\end{aligned}
$$

where the coefficients are [BS02]

$$
\begin{aligned}
a_k &= (\kappa - \kappa')/\sqrt{k(k+1)} \,, \\
a_{k-1} &= -(k+\kappa+\kappa')/\sqrt{2k(k+1)} \,, \\
a_{k+1} &= (k+1-\kappa-\kappa')/\sqrt{(k+1)(2k+1)} \,. \qquad (3.48)
\end{aligned}
$$

These formulas are derived in detail in the Appendix. For the integrals containing the scalar spherical harmonics,

$$
\begin{aligned}
K_{JM}^{\kappa_n \kappa_a} &= \int do_r \Omega_{\kappa_n}^\dagger(\hat{r}) Y_{JM}(\hat{r}) \Omega_{\kappa_a}(\hat{r}) \\
&= \langle l_n \frac{1}{2} j_n | Y_{JM} | l_a \frac{1}{2} j_a \rangle \,, \qquad (3.49)
\end{aligned}
$$

one can compute the reduced matrix elements as [BS02]

$$
\begin{aligned}
&\langle l_1 \frac{1}{2} j || C_K || l_1' \frac{1}{2} j' \rangle = \\
&= (-1)^{j'-K-1/2} (2j'+1)^{1/2} \begin{pmatrix} j & j' & K \\ \frac{1}{2} & -\frac{1}{2} & 0 \end{pmatrix} . \qquad (3.50)
\end{aligned}
$$

Table 3.1: Comparision of non-relativistic (NR) and relativistic (R) light shifts for K and L shell states in hydrogenic ions, at an optical laser frequency. E_b denotes the binding energy of the orbital and ΔE stands for the light shift contribution.

		$Z = 54$		$Z = 92$	
		E_b	ΔE	E_b	ΔE
NR	$1s$	-39674.2	$-1.02586(-4)$	-115159	$-1.21763(-5)$
R	$1s_{1/2}$	-41347.0	$-8.17337(-5)$	-132280	$-5.63212(-6)$
NR	$2s$	-9918.55	$-2.73564(-3)$	-28789.6	$-3.24700(-4)$
R	$2s_{1/2}$	-10443.5	$-4.94986(-2)$	-34215.5	$-1.40870(-3)$
NR	$2p$	-9918.55	$-4.92415(-3)$	-28789.6	$-5.84460(-4)$
R	$2p_{1/2}$	-10443.5	$-3.17409(-3)$	-34215.5	$-2.17374(-4)$
R	$2p_{3/2}$	-10016.7	$+4.31087(-2)$	-29649.8	$+7.88416(-4)$

3.3 Numerical results

To start our discussion on relativistic results of light shifts, we present results for an atom in a laser field at an infrared frequency ($\lambda = 1054$ nm, $\hbar\omega = 1.176$ eV) and with the widely accessible intensity of $I = 10^{18}$ W/cm^2. We calculate the light shifts in eV, both in relativistic and nonrelativistic treatments, for some heavy elements ($Z = 54, 92$, i.e. Xe and U). Results are shown in Table 3.1. As it is well known, the AC stark shifts, calculated in a non-relativistic way, follow an exact $\propto Z^{-4}$ scaling. It is also intuitively understandable that external field effects in general have a smaller effect if the electrons are bound by stronger central potentials. Still, even for elements as heavy as Xe and U, and for orbitals of the L shell, the light shift exceeds or approaches to the meV range. This is anticipated to be noticeable in near-future experiments. For measurements with lighter elements, the effects are certainly more pronounced.

As the table also clearly shows, the relativistic and nonrelativistic results greatly differ. For these relativistic systems, the non-relativistic calculation can only serve as an order-of-magnitude approximation, since not even the first digits of the results calculated in the two different approaches agree. In some cases, e.g. for the $2p_{3/2}$ state, even the sign of the shift is different, which is originated in the different level structure as described by the relativistic theory.

For soft x-ray frequencies ($\hbar\omega = 50$ eV), for the same intensity, we display the shifts for the elements $Z = 10, 54$ and 92 in Table 3.2. At the heaviest system studied, namely, for U, these results almost coincide with the light shifts calculated with optical laser frequencies. This illustrates that retardation effects are only relevant when the photon energy is comparable to the atomic binding energy: in the case of U, where the binding energies exceed the 10 keV-range, even a photon frequency of 50 eV is negligible in the description of the dynamic Stark shift. However, for lighter systems such as Xe ($Z = 54$), the difference between the optical and the soft x-ray light field is noticeable. This is especially the case for excited states.

In order to avoid a discussion about the intensity I and for a better comparison with existing non-relativistic literature data, in the following we introduce the dynamic Stark shift coefficient β:

$$\Delta_a^{AC} = h\beta_a I, \tag{3.51}$$

where Δ_a^{AC} is the Stark shift of the atomic level $|\Phi_a\rangle$. In Tables 3.3, 3.4 and 3.5, the nonrelativistic and relativistic Stark shift coefficients β_{NR} and β_R are compared for $1s - ns$ two-photon resonance

Table 3.2: Comparison of nonrelativistic (NR) and relativistic (R) light shifts for K and L shell states in hydrogenic ions at a soft x-ray laser frequency. Notations as in Table 3.1.

	$Z=10$		$Z=54$		$Z=92$	
	E_b	ΔE	E_b	ΔE	E_b	ΔE
$1s$	-1360.57	$-8.74042(-2)$	-39674.2	$-1.02587(-4)$	-115159	$-1.21763(-5)$
$1s_{1/2}$	-1362.39	$-8.6767(-2)$	-41347.0	$-8.17339(-5)$	-132280	$-5.63212(-6)$
$2s$	-340.142	-2.47409	-9918.55	$-2.73583(-3)$	-28789.6	$-3.24703(-4)$
$2s_{1/2}$	-340.710	-2.33842	-10443.5	$-5.01577(-2)$	-34215.5	$-1.40885(-3)$
$2p$	-340.142	-4.47426	-9918.55	$-4.92452(-3)$	-28789.6	$-5.84465(-4)$
$2p_{1/2}$	-340.710	-3.61534	-10443.5	$-3.17429(-3)$	-34215.5	$-2.17375(-4)$
$2p_{3/2}$	-340.256	-4.16667	-10016.7	$+4.37674(-2)$	-29649.8	$+7.88564(-4)$

Table 3.3: Comparison of nonrelativistic (NR) and relativistic (R) light shifts for $1s$–ns two-photon transitions for Z=1.

$Z=1$	$\beta_{\rm NR}$ [Hz(W/m^2)$^{-1}$]	$\beta_{\rm R}$ [Hz(W/m^2)$^{-1}$]
	$1s-ns$	$1s_{1/2}-ns_{1/2}$
$1s-2s$	$-2.67827(-5)$	$-2.67808(-5)$
$1s-3s$	$-3.02104(-5)$	$-3.02082(-5)$
$1s-4s$	$-3.18301(-5)$	$-3.18278(-5)$
$1s-5s$	$-3.26801(-5)$	$-3.26778(-5)$
$1s-6s$	$-3.31724(-5)$	$-3.31701(-5)$
$1s-7s$	$-3.34805(-5)$	$-3.34781(-5)$
$1s-8s$	$-3.36851(-5)$	$-3.36827(-5)$
$1s-9s$	$-3.38277(-5)$	$-3.38252(-5)$

transitions for nuclear charge numbers $Z=1, 10$ and 54. The light shift calculated in the non-relativistic limit of the formulas derived in this thesis agree perfectly with the calculations of Haas et al. [HJK$^+$06]. Also, they show an exact $\propto Z^{-4}$ scaling with the atomic number Z. However, for the relativistic results, a clear deviation from this law is observable, especially for the highest atomic charge numbers. These tables also illustrate that the light shifts are most relevant for highly excited, weakly bound states, i.e. for Rydberg levels.

As we can see from the Eqs. (3.23,3.26), in the final expression of dipole light shifts we have the following possible combinations of electromagnetic potentials: matrix elements of scalar-scalar, vector-vector and scalar-vector potentials. Because of the selection rules incorporated in the angular matrix elements, the scalar-vector part is zero. In the following tables we give some values of the dynamic Stark shift coefficient β for scalar-scalar and vector-vector parts and for the interaction with the magnetic field component of the laser field, including the retardation contribution caused by the dependence on the photons frequency. If we calculate the Stark shifts with the $\boldsymbol{rE}$ potential, we get for the scalar-scalar part the same results as in Eq. (3.2) for dipole approximation, without including the frequency-dependent retardation. The tables shows that the scalar-scalar contribution is by far the dominant part of the interaction. Thus we can conclude that the $\boldsymbol{rE}$ form is a rather good approximation of the total relativistic interaction operator. At high nuclear charges and frequencies, the dependence of the scalar-scalar term on the photon

Table 3.4: Comparison of nonrelativistic (NR) and relativistic (R) light shifts for $1s$–ns two-photon transitions for Z=10.

$Z = 10$	$\beta_{\rm NR}$ [Hz(W/m^2)$^{-1}$]	$\beta_{\rm R}$ [Hz(W/m^2)$^{-1}$]
	$1s - ns$	$1s_{1/2} - ns_{1/2}$
$1s - 2s$	$-2.67827(-9)$	$-2.65885(-9)$
$1s - 3s$	$-3.02104(-9)$	$-2.99941(-9)$
$1s - 4s$	$-3.18301(-9)$	$-3.16030(-9)$
$1s - 5s$	$-3.26801(-9)$	$-3.24471(-9)$
$1s - 6s$	$-3.31724(-9)$	$-3.29360(-9)$
$1s - 7s$	$-3.34805(-9)$	$-3.32418(-9)$
$1s - 8s$	$-3.36851(-9)$	$-3.34449(-9)$
$1s - 9s$	$-3.38277(-9)$	$-3.35863(-9)$

Table 3.5: Comparison of nonrelativistic (NR) and relativistic (R) light shifts for $1s$–ns two-photon transitions for Z=54.

$Z = 54$	$\beta_{\rm NR}$ [Hz(W/m^2)$^{-1}$]	$\beta_{\rm R}$ [Hz(W/m^2)$^{-1}$]
	$1s - ns$	$1s_{1/2} - ns_{1/2}$
$1s - 2s$	$-3.14978(-12)$	$-2.51398(-12)$
$1s - 3s$	$-3.55288(-12)$	$-2.84491(-12)$
$1s - 4s$	$-3.74337(-12)$	$-3.00038(-12)$
$1s - 5s$	$-3.84334(-12)$	$-3.08132(-12)$
$1s - 6s$	$-3.90124(-12)$	$-3.12789(-12)$
$1s - 7s$	$-3.93747(-12)$	$-3.15688(-12)$
$1s - 8s$	$-3.96153(-12)$	$-3.17606(-12)$
$1s - 9s$	$-3.97829(-12)$	$-3.18937(-12)$

Table 3.6: Different relativistic electric dipole (E1) contributions to the light shift for $1s$-ns two-photon transitions: scalar-scalar (s-s), vector-vector (v-v), and magnetic field contributions, with or without frequency-dependent retardation (ret.) contributions. The results are given for $Z = 10$.

$Z = 10$	s-s	s-s, ret.	v-v	v-v, ret.	Mag.	Mag., ret.
$1s - 2s$	$-2.6588(-9)$	$-2.6579(-9)$	$-6.7879(-16)$	$-6.7848(-16)$	$-9.2665(-13)$	$-9.2635(-13)$
$1s - 3s$	$-2.9994(-9)$	$-2.9978(-9)$	$-1.0200(-15)$	$-1.0193(-15)$	$-1.0973(-12)$	$-1.0968(-12)$
$1s - 4s$	$-3.1603(-9)$	$-3.1584(-9)$	$-1.1667(-15)$	$-1.1658(-15)$	$-1.1753(-12)$	$-1.1746(-12)$
$1s - 5s$	$-3.2447(-9)$	$-3.2427(-9)$	$-1.2402(-15)$	$-1.2393(-15)$	$-1.2156(-12)$	$-1.2149(-12)$
$1s - 6s$	$-3.2936(-9)$	$-3.2915(-9)$	$-1.2818(-15)$	$-1.2808(-15)$	$-1.2387(-12)$	$-1.2380(-12)$
$1s - 7s$	$-3.3241(-9)$	$-3.3220(-9)$	$-1.3075(-15)$	$-1.3064(-15)$	$-1.2531(-12)$	$-1.2524(-12)$
$1s - 8s$	$-3.3444(-9)$	$-3.3423(-9)$	$-1.3243(-15)$	$-1.3233(-15)$	$-1.2627(-12)$	$-1.2619(-12)$
$1s - 9s$	$-3.3586(-9)$	$-3.3564(-9)$	$-1.3360(-15)$	$-1.3349(-15)$	$-1.2693(-12)$	$-1.2685(-12)$

Table 3.7: Different relativistic electric dipole (E1) contributions to the light shift for $1s$-ns two-photon transitions: scalar-scalar (s-s), vector-vector (v-v), and magnetic field contributions, with or without frequency-dependent retardation (ret.) contributions. The results are given for $Z = 54$.

$Z = 54$	s-s	s-s, ret.	v-v	v-v, ret.	Mag.	Mag., ret.
$1s - 2s$	$-2.5139(-12)$	$-2.4873(-12)$	$-6.2890(-16)$	$-6.2032(-16)$	$-2.8362(-14)$	$-2.8093(-14)$
$1s - 3s$	$-2.8449(-12)$	$-2.8013(-12)$	$-9.5338(-16)$	$-9.3473(-16)$	$-3.3758(-14)$	$-3.3284(-14)$
$1s - 4s$	$-3.0003(-12)$	$-2.9488(-12)$	$-1.0922(-15)$	$-1.0683(-15)$	$-3.6223(-14)$	$-3.5646(-14)$
$1s - 5s$	$-3.0813(-12)$	$-3.0255(-12)$	$-1.1615(-15)$	$-1.1347(-15)$	$-3.7490(-14)$	$-3.6859(-14)$
$1s - 6s$	$-3.1278(-12)$	$-3.0697(-12)$	$-1.2004(-15)$	$-1.1720(-15)$	$-3.8214(-14)$	$-3.7552(-14)$
$1s - 7s$	$-3.1568(-12)$	$-3.0972(-12)$	$-1.2243(-15)$	$-1.1949(-15)$	$-3.8664(-14)$	$-3.7982(-14)$
$1s - 8s$	$-3.1760(-12)$	$-3.1153(-12)$	$-1.2400(-15)$	$-1.2099(-15)$	$-3.8960(-14)$	$-3.8266(-14)$
$1s - 9s$	$-3.1893(-12)$	$-3.1280(-12)$	$-1.2508(-15)$	$-1.2202(-15)$	$-3.9166(-14)$	$-3.8462(-14)$

frequency starts to show up; however, the vector-vector and magnetic terms are still orders of magnitude smaller.

For completeness, in the Tables 3.8-3.9 we present values for the quadrupole contributions to the level shift. These terms are also approx. 3 orders of magnitude weaker than the dominant electric dipole interaction. However, with the improvement of experimental accuracy, the thorough understanding of relativistic light shift effects becomes increasingly stringent.

Table 3.8: Different relativistic electric quadrupole (E2) contributions to the light shift for $1s$-ns two-photon transitions: scalar-scalar (s-s), vector-vector (v-v), and magnetic field contributions, with or without frequency-dependent retardation (ret.) contributions. The results are given for $Z = 10$.

$Z = 10$	s-s	s-s, ret.	v-v	v-v, ret.	Mag.	Mag., ret.
$1s - 2s$	$-7.4262(-14)$	$-7.4227(-14)$	$-2.2189(-20)$	$-2.2178(-20)$	$-2.6903(-17)$	$-2.6891(-17)$
$1s - 3s$	$-1.1060(-13)$	$-1.1053(-13)$	$-4.7669(-20)$	$-4.7635(-20)$	$-4.4819(-17)$	$-4.4790(-17)$
$1s - 4s$	$-1.2604(-13)$	$-1.2594(-13)$	$-6.1152(-20)$	$-6.1104(-20)$	$-5.3336(-17)$	$-5.3298(-17)$
$1s - 5s$	$-1.3374(-13)$	$-1.3363(-13)$	$-6.8463(-20)$	$-6.8406(-20)$	$-5.7793(-17)$	$-5.7749(-17)$
$1s - 6s$	$-1.3808(-13)$	$-1.3797(-13)$	$-7.2755(-20)$	$-7.2693(-20)$	$-6.0368(-17)$	$-6.0320(-17)$
$1s - 7s$	$-1.4075(-13)$	$-1.4064(-13)$	$-7.5459(-20)$	$-7.5394(-20)$	$-6.1975(-17)$	$-6.1926(-17)$
$1s - 8s$	$-1.4251(-13)$	$-1.4239(-13)$	$-7.7263(-20)$	$-7.7195(-20)$	$-6.3042(-17)$	$-6.2991(-17)$
$1s - 9s$	$-1.4372(-13)$	$-1.4360(-13)$	$-7.8522(-20)$	$-7.8452(-20)$	$-6.3784(-17)$	$-6.3732(-17)$

Table 3.9: Different relativistic electric quadrupole (E2) contributions to the light shift for $1s$-ns two-photon transitions: scalar-scalar (s-s), vector-vector (v-v), and magnetic field contributions, with or without frequency-dependent retardation (ret.) contributions. The results are given for $Z = 54$.

$Z = 10$	s-s	s-s, ret.	v-v	v-v, ret.	Mag.	Mag., ret.
$1s - 2s$	$-2.1019(-15)$	$-2.0727(-15)$	$-6.0334(-19)$	$-5.9420(-19)$	$-2.4280(-17)$	$-2.3956(-17)$
$1s - 3s$	$-3.1586(-15)$	$-3.0960(-15)$	$-1.3122(-18)$	$-1.2840(-18)$	$-4.0816(-17)$	$-4.0029(-17)$
$1s - 4s$	$-3.6054(-15)$	$-3.5255(-15)$	$-1.6853(-18)$	$-1.6449(-18)$	$-4.8642(-17)$	$-4.7588(-17)$
$1s - 5s$	$-3.8269(-15)$	$-3.7378(-15)$	$-1.8859(-18)$	$-1.8384(-18)$	$-5.2707(-17)$	$-5.1505(-17)$
$1s - 6s$	$-3.9511(-15)$	$-3.8566(-15)$	$-2.0028(-18)$	$-1.9511(-18)$	$-5.5040(-17)$	$-5.3750(-17)$
$1s - 7s$	$-4.0272(-15)$	$-3.9294(-15)$	$-2.0761(-18)$	$-2.0217(-18)$	$-5.6489(-17)$	$-5.5144(-17)$
$1s - 8s$	$-4.0771(-15)$	$-3.9770(-15)$	$-2.1248(-18)$	$-2.0686(-18)$	$-5.7447(-17)$	$-5.6065(-17)$
$1s - 9s$	$-4.1115(-15)$	$-4.0099(-15)$	$-2.1587(-18)$	$-2.1012(-18)$	$-5.8112(-17)$	$-5.6704(-17)$

–IV–

HIGHER-ORDER RESONANT RECOMBINATION PROCESSES

In the dielectronic recombination process involving two interacting electrons, as sketched in Fig. 4.1, the kinetic energy of the recombined electron is transferred to a single bound electron by a radiationless excitation to an intermediate autoionizing state. The recombination is completed by its radiative stabilization. For the case of highly charged ions (HCIs), radiative transition probabilities are high, and the competition of radiative deexcitation and Auger decay of the intermediate state is biased towards the first mechanism.

Beyond the well-known DR, resonant recombination processes involving higher-order correlations are relevant, too. Here, as displayed in Fig. 4.1, two or even three bound electrons can be simultaneously excited by the resonantly captured electron in trielectronic or even quadruelectronic recombination (TR and QR, respectively). The higher-order recombination mechanisms can be summarized by the equation

$$A^{q+} + e^- \rightarrow \left[A^{(q-1)+}\right]^{(n+1)*} \rightarrow A^{(q-1)+} + \text{photons}\,, \tag{4.1}$$

where n represents the number of simultaneously excited bound electrons, respectively the order of the resonant capture process.

Resonant mechanisms are highly efficient in either ionizing or recombining ions and hence already DR is of paramount importance for the physics of outer planetary atmospheres and interstellar clouds as well as an important radiative cooling mechanism in astrophysical and laboratory high-temperature plasmas [MB42,Bur64,CWP$^+$90]. DR often represents the dominant pathway for populating excited states in plasmas and, consequently, for inducing easily observable x-ray lines which are used as diagnostic tools for fusion plasmas (whereby Kr as well as Ar were chosen as ideal candidates) [CCH$^+$90, WBD$^+$95], triggering a range of DR studies with highly charged Kr ions [BHB$^+$93, FBR98, RBF$^+$00]. From a more fundamental point of view, the selectivity of DR [BKM$^+$03] allows testing stringently sophisticated atomic structure and dynamics calculations, in particular of relativistic and quantum electrodynamic (QED) effects in bound electronic systems.

Investigating HCIs with DR offers additional important advantages including large cross sections and the magnification of relativistic and QED contributions by several orders of magnitude. These have been exploited in experiments both at electron beam ion traps (EBITs) (see, e.g., [KBC$^+$95, GCB$^+$05, GCB$^+$06, HTA$^+$06, ZCU03, N$^+$08]) and in storage rings (SRs). The $2s_{1/2} - 2p_{1/2}$ splitting in lithiumlike ions was determined in a SR with an accuracy capable of testing second-order QED corrections [BKM$^+$03]. Direct EBIT spectroscopic measurements have achieved even higher precision [BCTT05]. Similarly,

using DR in an ultra-cold electron target at a SR, the same splitting in Li-like Sc^{18+} has been indirectly determined with a precision of 4.6 ppm [LLO+08]. DR measurements have recently become sensitive to isotopic shifts in Li-like ^{142,150}Nd [BKH+08] and to the contribution of the generalized Breit interaction [N+08].

It is important to mention that in general TR and QR offer new photorecombination channels and their contribution to the radiative cooling of plasmas needs to be considered in the theoretical modeling. However, very scarce experimental data are available. At interaction energies of less than 52 eV, intra-shell TR resonances involving L-shell electrons of Cl^{13+} ions were observed at the TSR [SGB+03]. Contributions of roughly 10% to the total photorecombination rate at temperatures $T_e \approx 1$ to 100 eV (a range interesting for astrophysical photoionized plasmas) were found.

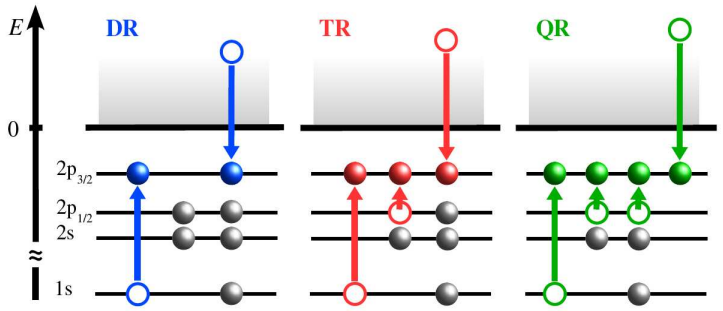

Figure 4.1: Scheme of correlated resonant electron recombination processes: In dielectronic recombination (blue) one bound electron is excited by the captured electron, in trielectronic recombination (red) two and in quadruelectronic recombination (green) three electrons are promoted to higher states by the captured electron (K-LL, KL-LLL and KLL-LLLL processes, respectively, where the initial and final shells of the bound and active electrons are specified).

4.1 Total cross section for resonant recombination processes

Cross section formulas for dielectronic recombination have been derived in the framework of several formalisms, including non-relativistic [Hah85] and relativistic [Zim96, Sha02] approaches. These results can be generalized to describe the higher-order correlated processes of trielectronic, quadruelectronic etc. processes as well. One can express the differential cross section in the solid angle Ω_k of the emitted photon as

$$\frac{d\sigma_{i\to f}}{d\Omega_k} = \frac{2\pi}{F_i} \sum_{dd'} \frac{\langle \Phi_f | H_{er} | \Phi_d \rangle \langle \Phi_d | V_{capt} | \Phi_i \rangle}{E - E_d + i\Gamma_d/2} \frac{\langle \Phi_f | H_{er} | \Phi'_d \rangle^* \langle \Phi'_d | V_{capt} | \Phi_i \rangle^*}{E - E_{d'} - i\Gamma_{d'}/2} \rho_f \,, \tag{4.2}$$

with H_{er} being the electron-radiation field interaction Hamiltonian and V_{capt} being the sum of the Coulomb and Breit interactions. In the above formula, E is the total initial energy of the system, and Φ_i, Φ_d and Φ_f (just as their counterparts with primed indices) denote the initial, intermediate and final states of a given recombination channel. E_d denotes the energy of the intermediate state including radiative corrections, and Γ_d is total decay width of that state. F_i and ρ_f stand for the incoming electron flux and the density of final photonic states, respectively. In the isolated resonances – or two-level – approximation the non-diagonal elements of the double sum above are neglected, thus the differential cross section

simplifies to

$$\frac{d\sigma_{i\to f}}{d\Omega_k} = \frac{2\pi}{F_i}\sum_d \frac{|\langle\Phi_f|H_{er}|\Phi_d\rangle|^2|\langle\Phi_d|V_{capt}|\Phi_i\rangle|^2}{(E-E_d)^2+\Gamma_d^2/4}\rho_f\,, \tag{4.3}$$

For evaluating the total cross section, this expression has to be averaged over the initial states and summed over the final states. This includes an averaging over the magnetic sub-states M_i of the target ion and over the two spin projections m_s of the incoming electron. One has to sum over the magnetic sub-states M_f of the final state ion, integrate over the directions Ω_k and sum over the polarizations λ of the outgoing photon. The total cross section does not depend on the direction of the electron to be captured, so an extra averaging over the electron solid angle can be performed. This results in a simple formula for the total cross section [Hah85]

$$\sigma_{i\to f}^{DR} = \frac{2\pi^2}{p^2}\frac{A_r}{\Gamma_d}L_d(E-E_d-\Delta E_d)V_a\,, \tag{4.4}$$

with the radiative decay rate from the intermediate state d to f

$$A_r = \frac{2\pi}{2J_d+1}\sum_{M_f\lambda}\sum_{M_d}\int d\Omega_k|\langle\Psi_f;J_fM_f,\mathbf{k},\lambda|H_{er}|\Psi_d;J_dM_d\rangle|^2\rho_f\,, \tag{4.5}$$

where the total angular momentum of the intermediate state, J_d was introduced, and the normalized Lorentz resonance profile

$$L_d(E-E_d) = \frac{\Gamma_d/2\pi}{(E-E_d)^2+\Gamma_d^2/4}\,. \tag{4.6}$$

The rate of resonant capture into the state d is given by

$$V_a = \frac{p^2}{4\pi^2F_i}\frac{1}{2(2J_i+1)}\sum_{M_im_sM_d}\int d\Omega_p|\langle\Psi_d;J_dM_d|V_{capt}|\Psi_i;J_iM_i,\mathbf{p}m_s\rangle|^2\,, \tag{4.7}$$

with the initial state total angular momentum J_i, and it is connected to its time-reversed analogue, the Auger (autoionization) rate A_a, by the principle of detailed balance

$$V_a = \frac{2J_d+1}{2(2J_i+1)}A_a\,. \tag{4.8}$$

The Auger rate is defined as

$$A_a = \frac{2\pi}{2J_d+1}\sum_{M_im_sM_d}\int d\Omega_p|\langle\Psi_d;J_dM_d|V_{capt}|\Psi_i;J_iM_i,\mathbf{p}m_s\rangle|^2\rho_i\,. \tag{4.9}$$

Here, we have made use of the relation $F_i\rho_i = p^2/(2\pi)^3$.

The appearance of higher-order processes, i.e. the trielectronic and quadruelectronic recombination channels with more than two active electrons can be understood as follows: Let us consider recombination with an initially C-like ion in its ground state, labeled by the dominant $|1s^22s^22p_{1/2}^2\rangle$ configuration. When describing TR, the autoionizing state can be approximated as a minimal linear combination of two configurations sharing total angular momentum and parity, $|\mathrm{TR}\rangle = c_1|1s2s^22p_{1/2}2p_{3/2}^3\rangle + c_2|1s2s^22p_{1/2}^22p_{3/2}^2\rangle$. Here, the first term is the dominant one, as represented in the simplified scheme of Fig. 4.1. The neglect of the second term, i.e. the independent-particle (e.g. Hartree-Fock) approximation, would in the first order lead to a vanishing transition amplitude, $\langle 1s2s^22p_{1/2}2p_{3/2}^3|V_{Coul}|1s^22s^22p_{1/2}^2\rangle = 0$. Only the inclusion of configuration mixing, a means of accounting for all-order electron correlation,

leads to a non-vanishing amplitude $\langle \mathrm{TR}|V_{Coul}|1s^2 2s^2 2p_{1/2}^2\rangle = c_2\langle 1s2s^2 2p_{1/2}^2 2p_{3/2}^2|V_{Coul}|1s^2 2s^2 2p_{1/2}^2\rangle$. Thus higher-order processes appear only if correlation effects are taken into account and their measurement can benchmark more thoroughly their theoretical description both in terms of structure and dynamics. In spite of their relevance, the exact quantitative description of such correlations and their scaling with the number of involved electrons remains an open theoretical problem.

The resonance strength, which is defined as the integrated area under the peak for a given resonance, can be expressed as follows – provided the fluorescence x-rays are observed at 90° to the incoming electron beam as in case of a typical EBIT experiment:

$$S_{idf}^{DR} = \frac{\pi\hbar^3}{2p^2}\left(1 - \frac{\beta_{df}}{2}\right)\frac{2J_d+1}{2(2J_i+1)}\frac{A_r^{df}A_a^{di}}{\sum_f A_r^{df} + A_a^{di}}\,. \tag{4.10}$$

In Eq. (4.10), the dipole angular distribution factor for photon detection perpendicular to the electron beam direction was taken into account by means of the anisotropy parameter β_{df} [GGS98].

4.2 Description of the relativistic many-body system: the multiconfiguration Dirac-Fock method

In the following, we present a brief overview of the MCDF approximation for the calculation of atomic states, level energies and transition data. We use the GRASP suite of codes (General Relativistic Atomic Structure Package) for the generation of these many-electron wave functions [DGJ$^+$89]. Atomic units with $e = \hbar = m_e = 1; \alpha = 1/c$, where e is the charge of photon, $\hbar$ is the reduced Planck's constant, m_e is the electron's rest mass, α is the fine-structure constant, and c is the speed of light in vacuum, will be used throughout.

4.2.1 Relativistic one-particle orbitals

A relativistic (or Dirac) orbital $\Phi \to |n\kappa m\rangle$ is an eigenfunction of the angular-momentum operators $\hat{\mathbf{j}}^2$ ($\hat{\mathbf{j}} = \hat{\mathbf{l}} + \hat{\mathbf{s}}$) and $\hat{j}_z$,

$$\hat{\mathbf{j}}^2\Phi = j(j+1)\Phi, \quad \hat{j}_z\Phi = m\Phi, \quad m = -j, ..., j, \tag{4.11}$$

and of the relativistic parity operator $\hat{p} = \beta\hat{\pi}$ ($\hat{\pi}$ is the usual parity operator; the matrix β will be defined in Eq. (4.24))

$$\hat{p}\Phi = (-1)^l\Phi \tag{4.12}$$

In (4.11) and (4.12) we have n the principal quantum number, and κ the relativistic angular quantum number, $\kappa = \pm(j + \frac{1}{2})$ for $l = j \pm \frac{1}{2}$; thus $j = |\kappa| - \frac{1}{2}$.

Each of the $\leq 2j+1$ orbitals with the same $(n\kappa)$ but differing m quantum numbers (referred to as a subshell) are assumed to have the same radial form. An explicit representation in spherical coordinates is

$$\Phi(\mathbf{r}) = \frac{1}{r}\begin{pmatrix} G_{n\kappa}(r)\Omega_{\kappa M}(\hat{r}) \\ iF_{n\kappa}(r)\Omega_{-\kappa M}(\hat{r}) \end{pmatrix} \tag{4.13}$$

Here, $G_{n\kappa}(r)$ and $F_{n\kappa}(r)$ are, respectively, the large and small component radial wavefunctions, and the functions $\Omega_{\kappa M}(\hat{r})$ are the spinor spherical harmonics

$$\begin{aligned}
\Omega_{\kappa M}(\hat{r}) &= \sum_{m=-l}^{l} \sum_{\mu=\pm 1/2} C\left(l\tfrac{1}{2}j; m\mu M\right) Y_{lm}(\theta,\phi)\chi_{\mu}, \qquad (4.14)\\
\hat{\mathbf{j}}^2\Omega_{\kappa M}(\hat{r}) &= j(j+1)\Omega_{\kappa M}(\hat{r}),\\
\hat{j}_z\Omega_{\kappa M}(\hat{r}) &= m\Omega_{\kappa M},\\
\hat{\mathbf{l}}^2\Omega_{\kappa M}(\hat{r}) &= l(l+1)\Omega_{\kappa M}(\hat{r}),\\
\hat{\mathbf{s}}^2\Omega_{\kappa M}(\hat{r}) &= \tfrac{3}{4}\Omega_{\kappa M}(\hat{r}),\\
\hat{\pi}\Omega_{\kappa M}(\hat{r}) &= (-1)^l\Omega_{\kappa M}(\hat{r}),
\end{aligned}$$

where $C\left(l\frac{1}{2}j; m\mu M\right)$ is a Clebsch-Gordon coefficient, $Y_{lm}(\theta,\phi)$ is a spherical harmonic, and χ_{μ} denotes the usual two-component Pauli spinors:

$$\chi_{1/2} = \begin{pmatrix} 1 \\ 0 \end{pmatrix}, \quad \chi_{-1/2} = \begin{pmatrix} 0 \\ 1 \end{pmatrix}.$$

The angular-momentum algebra is simplest when the orbitals are chosen to form an orthonormal set,

$$\int d\mathbf{r}\Phi_a(\mathbf{r})\Phi_b(\mathbf{r}) = \delta_{ab} \qquad (4.15)$$

hence it is necessary to impose

$$\begin{aligned}
N(ab) &= \begin{cases} 0, & \text{when } a \neq b \text{ but } \kappa_a = \kappa_b, \\ 1, & \text{when } a = b, \end{cases} \qquad (4.16)\\
N(ab) &\equiv \int_0^{\infty} dr\left(G_{n_a\kappa_a}(r)G_{n_b\kappa_b}(r) + F_{n_a\kappa_a}(r)F_{n_b\kappa_b}(r)\right).
\end{aligned}$$

4.2.2 Configuration state functions

A configuration state function (CSF), $|\gamma PJM\rangle$, of an N-electron system is formed by taking linear combinations of Slater determinants of order N constructed from the orbitals (4.13) so as to obtain normalized ($\langle\gamma PJM|\gamma PJM\rangle = 1$) eigenfunction of parity operator $\hat{P}$, and total angular-momentum operators $\hat{\mathbf{J}}^2$ and $\hat{J}_z$:

$$\begin{aligned}
\hat{P}|\gamma PJM\rangle &= P|\gamma PJM\rangle, \qquad (4.17)\\
\hat{\mathbf{j}}^2|\gamma PJM\rangle &= J(J+1)|\gamma PJM\rangle\\
\hat{j}_z|\gamma PJM\rangle &= M|\gamma PJM\rangle,\ M = -J, ..., J.
\end{aligned}$$

The label γ represent all information such as orbital occupation numbers, subshell orbital couplings, etc., required to define the CSF uniquely. The standard coupling scheme for a CFS is defined as follows. Firstly, the electrons are assigned to subshells by specifying the orbital occupation numbers, $q(a) \leq 2j_a + 1$. For each shell a the electrons are jj-coupled to give a seniority, v_a, and angular momentum, j_a, M_a,

$$\left|(j_a)^{q(a)} v_a J_a M_a\right\rangle. \qquad (4.18)$$

Table D.1 in the Appendix lists the allowed values of the quantum numbers v and J for given occupations j^q. Next, subshell angular momenta J_1 and J_2 are coupled to give an intermediate angular momentum, X_1, which in turn is coupled to J_3 to give an X_2 and so on until all shells have been coupled to give a total angular momentum J:

$$(...((J_1J_2)X_1J_3)X_2...)J. \tag{4.19}$$

CFSs formed by redistributing electrons among the subshells and changing the coupling sequence are orthogonal.

4.2.3 Atomic state functions

Atomic state functions (ASFs) are linear combinations of CFSs sharing common values of P, J, and M,

$$|\Gamma PJM\rangle = \sum_{r=1}^{n_c} c_{r\Gamma}|\gamma_r PJM\rangle. \tag{4.20}$$

The mixing coefficients, $c_{r\Gamma}$, may be combined in a column vector, $\mathbf{c}_\Gamma \equiv \{c_{r\Gamma}, r = 1, ..., n_c\}$, the representation of the atomic state $|\Gamma PJM\rangle$ with respect to the CSF basis set $|\gamma_r PJM\rangle, r = 1, ..., n_c$. The ASFs will be chosen to be orthogonal, so that

$$(\mathbf{c}_{\Gamma_i})^\dagger \mathbf{c}_{\Gamma_j} = \delta_{ij}; \tag{4.21}$$

the dagger denotes the Hermitian conjugate.

4.2.4 The Dirac-Coulomb Hamiltonian

All the dominant interactions in an N-electron atom or ion are included in the Dirac-Coulomb Hamiltonian,

$$\hat{H}^{\rm DC} = \sum_{i=1}^{N} \hat{H}_i + \sum_{i=1}^{N-1} \sum_{j=i+1}^{N} |\hat{\mathbf{r}}_i - \hat{\mathbf{r}}_j|^{-1}. \tag{4.22}$$

In the first term,

$$\hat{H} = c\sum_{i=1}^{3} \alpha_i \hat{p}_i + (\beta - 1)c^2 + V_{\rm nuc}(\hat{r})\,, \tag{4.23}$$

is the one-body contribution for an electron due to its kinetic energy and interaction with the nucleus - the rest energy, c^2, has been subtracted out. The nuclear potential, $V_{\rm nuc}(r)$, has been discussed in Chapter 2 already. In the standard representation the Dirac matrices, α_i, β, are given as

$$\alpha_i = \begin{pmatrix} 0 & \sigma_i \\ \sigma_i & 0 \end{pmatrix}, \quad i = 1, ..., 3, \quad \beta = \begin{pmatrix} 1 & 0 \\ 0 & -1 \end{pmatrix}, \tag{4.24}$$

where the σ_i are the usual Pauli matrices. The two-body instantaneous Coulomb interactions between the electrons comprise the second term in (4.22). Higher-order (QED) modifications to (4.22) and (4.23) due to the transverse electromagnetic interaction and the radiative corrections are treated via perturbation theory.

The matrix of the Hamiltonian (4.22) with respect to a basis of CSFs plays a central role in all relativistic atomic structure calculations. Making use of the expansion (4.20), in this approximation the energy of the atomic state Γ is

$$E_\Gamma^{\rm DC} = \langle \Gamma PJM | \hat{H}^{\rm DC} | \Gamma PJM \rangle \equiv \left(\mathbf{c}_\Gamma^{\rm DC}\right)^\dagger \mathbf{H}^{\rm DC} \mathbf{c}_\Gamma^{\rm DC} \,. \tag{4.25}$$

The Hamiltonian matrix, $\mathbf{H}^{\rm DC}$, has the elements

$$H_{rs}^{\rm DC} = \langle \gamma_r PJM | \hat{H}^{\rm DC} | \gamma_s PJM \rangle. \tag{4.26}$$

Requiring $E_\Gamma^{\rm DC}$ (4.25) to be stationary with respect to variations in the mixing coefficient subject to (4.21) leads to the eigenvalue problem for the mixing coefficients:

$$(\mathbf{H}^{\rm DC} - E_\Gamma^{\rm DC}\mathbf{1})\mathbf{c}_\Gamma^{\rm DC} = 0. \tag{4.27}$$

Here, $\mathbf{1}$ is the $n_c \times n_c$ unit matrix.

4.2.5 Elements of the Hamiltonian matrix

The matrix elements (4.26) can be expressed in terms of angular coefficients and radial integrals [Gra70]. One-body interactions give rise to the $I(ab)$ integrals,

$$\begin{aligned} I(ab) &= \delta_{\kappa_a\kappa_b} \int_0^\infty dr \left[c\left(Q_{n_a\kappa_a}(r) P'_{n_b\kappa_b}(r) - P_{n_a\kappa_a}(r) Q'_{n_b\kappa_b}(r)\right)\right. \\ &- 2c^2 Q_{n_a\kappa_a}(r) Q_{n_b\kappa_b}(r) + \frac{c\kappa_b}{r}\left(P_{n_a\kappa_a}(r) Q_{n_b\kappa_b}(r) + Q_{n_a\kappa_a}(r) P_{n_b\kappa_b}(r)\right) \\ &+ \left. V_{\rm nuc}(r)\left(P_{n_a\kappa_a}(r) P_{n_b\kappa_b}(r) + Q_{n_a\kappa_a}(r) Q_{n_b\kappa_b}(r)\right)\right], \end{aligned} \tag{4.28}$$

where $f' \equiv df/dr$; two-body interactions yield relativistic Slater integrals,

$$R^k(abcd) = \int_0^\infty dr \left[\left(P_{n_a\kappa_a}(r) P_{n_c\kappa_c}(r) + Q_{n_a\kappa_a}(r) Q_{n_c\kappa_c}(r)\right) \frac{1}{r} Y^k(bd;r) \right]; \tag{4.29}$$

the relativistic Hartree Y-functions are defined by the equation

$$Y^k(ab;r) = r \int_0^\infty ds \frac{r_<^k}{r_>^{k+1}} \left(P_{n_a\kappa_a}(s) P_{n_b\kappa_b}(s) + Q_{n_a\kappa_a}(s) Q_{n_b\kappa_b}(s)\right). \tag{4.30}$$

Here $r_>$ ($r_<$) denotes the greater (lesser) of the radial variables r and s.

A diagonal contribution to the Hamiltonian matrix can be written as

$$H_{rr}^{DC} = \sum_{a=1}^{n_w} \left(q_r(a) I(aa) + \sum_{b\geq a}^{n_w} \sum_{k=0,2,\ldots}^{k_0} f_r^k(ab) F^k(ab) + \sum_{b>a}^{n_w} \sum_{k=k_1,k_1+2,\ldots}^{k_2} g_r^k(ab) G^k(ab) \right). \tag{4.31}$$

In this expression $F^k(ab)$ and $G^k(ab)$ are special case of (4.29):

$$F^k(ab) = R^k(abab), \quad G^k(ab) = R^k(abba)\,. \tag{4.32}$$

$q_r(a)$ is the occupation number of orbital a in the CSF r, and the summation limits k_0, k_1, and k_2 are given by

$$\begin{aligned} k_0 &= (2j_a - 1)\delta_{ab}; \\ k_1 &= \begin{cases} |j_a - j_b|, & \text{if} \quad \kappa_a\kappa_b > 0, \\ |j_a - j_b| + 1, & \text{if} \quad \kappa_a\kappa_b < 0; \end{cases} \\ k_2 &= \begin{cases} j_a + j_b, & \text{if} \quad j_a + j_b - k_1 \text{ is even}, \\ j_a + j_b - 1, & \text{otherwise}. \end{cases} \end{aligned} \tag{4.33}$$

The angular coefficients $f_r^k(ab)$ and $g_r^k(ab)$ have the form

$$f_r^0(aa) = \tfrac{1}{2}q_r(a)(q_r(a) - 1), \quad f_r^0(ab) = q_r(a)q_r(b), \tag{4.34}$$

always, whereas for $k > 0$ and $q_r(a) = 2j_a + 1$ or $q_r(b) = 2j_b + 1$,

$$\begin{aligned} &f_r^k(ab) = -\tfrac{1}{2}(q_r(a)C(a,k,a))^2\delta_{ab}, \qquad g_r^k(ab) = -q_r(a)q_r(b)C^2(a,k,b), \\ &C(a,k,b) = \begin{pmatrix} j_a & k & j_b \\ \frac{1}{2} & 0 & -\frac{1}{2} \end{pmatrix}. \end{aligned} \tag{4.35}$$

If $k > 0$ and $q_r(a) < 2j_a + 1$ and $q_r(b) < 2j_b + 1$, one has

$$f_r^k(ab) = V_{rr}^k(abab), \qquad g_r^k(ab) = V_{rr}^k(abba). \tag{4.36}$$

Off-diagonal ($r \neq s$) matrix elements are obtained as

$$H_{rs}^{DC} = \sum_{abcd}\sum_k V_{rs}^k(abcd)R^k(abcd) + \sum_{ab} T_{rs}(ab)I(ab). \tag{4.37}$$

The configuration coupling coefficients $V_{rs}^k(abcd)$ and $T_{rs}(ab)$ are discussed further.

4.2.6 Generation of the radial functions

A pair of bound-state radial wavefunctions $G_{n_a\kappa_a}(r)$, $F_{n_a\kappa_a}(r)$, for a subshell a may be obtained, in general, by solving a pair of radial Dirac equations,

$$\begin{aligned} \left(\frac{d}{dr} + \frac{\kappa_a}{r}\right) G_{n_a\kappa_a}(r) - \left(2c - \frac{\epsilon_a}{c} + \frac{Y_a(r)}{cr}\right) F_{n_a\kappa_a}(r) &= -\frac{\chi_a^{(G)}(r)}{r}, \\ \left(\frac{d}{dr} - \frac{\kappa_a}{r}\right) F_{n_a\kappa_a}(r) + \left(-\frac{\epsilon_a}{c} + \frac{Y_a(r)}{cr}\right) G_{n_a\kappa_a}(r) &= \frac{\chi_a^{(F)}(r)}{r}, \end{aligned} \tag{4.38}$$

with $\epsilon_a > 0$ subject to boundary conditions

$$\begin{aligned} Gn_a\kappa_a(r = 0) &= 0, \quad Fn_a\kappa_a(r = 0) = 0, \\ Gn_a\kappa_a(r \to \infty) &\to 0, \quad Fn_a\kappa_a(r \to \infty) \to 0, \\ G'n_a\kappa_a(r \to 0) &> 0\,. \end{aligned} \tag{4.39}$$

and the orthonormalization condition (4.16). The asymptotic form of, and the relation between, the large and small-component functions near the origin are dependent upon the behavior of the potential

energy functions, $Y_a(r)$, which dominates the inhomogeneous terms $\chi_a^{(G)}(r)$, and $\chi_a^{(F)}(r)$ in this neighborhood [GQ87].

The equation (4.38) along with its boundary conditions (4.39) define an eigenvalue problem for the orbitals $G_{n_a\kappa_a}(r)$, $F_{n_a\kappa_a}(r)$, and the energies $\epsilon_a,\ a = 1, ..., n_w$ when $Y_a(r) = Y_{\kappa_a}(r)$ (i.e. orbitals with the same angular quantum number, κ are generated in the same potential), and $\chi_a^{(G)}(r)$, $\chi_a^{(F)}(r) \equiv 0$. We treat three simple, but important, cases of this general nature.

(i) In the instance where $Y_{\kappa_a}(r) = Z$, the Coulomb central field, the solution may be obtained analytically. Such solutions have been presented in the previous chapters of this thesis. Screened Coulomb functions are obtained by using $Z^{\text{eff}} = Z - \sigma$ in place of the actual atomic number, Z, of the system under consideration. If different screening numbers, σ_a, are used for different subshells, (4.16) will not be satisfied in general. In such instances, the Gram-Schmidt orthogonalization procedure,

$$\begin{pmatrix} G_{n_a\kappa_a}(r) \\ F_{n_a\kappa_a}(r) \end{pmatrix} \to \begin{pmatrix} G_{n_a\kappa_a}(r) \\ F_{n_a\kappa_a}(r) \end{pmatrix} - \sum_{b<a} \delta_{\kappa_a\kappa_b} N(ab) \begin{pmatrix} G_{n_b\kappa_b}(r) \\ F_{n_b\kappa_b}(r) \end{pmatrix}, \tag{4.40}$$

by normalization performed after each subtraction, may be used to obtain an orthonormal set of basis functions.

(ii) In many cases, orbitals calculated in a potential based upon the nonrelativistic Thomas-Fermi theory,

$$\begin{aligned} &Y_{\kappa_a}(r) \to Y^{TF}(r) = Z_\infty - (rV_{\text{nuc}}(r) + Z_\infty) f^2(x), \\ &Z_\infty = Z + 1 - \sum_{a=1}^{n_w} q_{\text{av}}(a), \\ &f(x) = \frac{0.60112x^2 + 1.181061x + 1}{0.04793x^5 + 0.21465x^4 + 0.77112x^3 + 1.39515x^2 + 1.81061x + 1}, \\ &x = \left[\frac{(Z - Z_\infty)^{1/3} r}{0.8853} \right]^{1/2}, \end{aligned} \tag{4.41}$$

where the average occupation number $q_{\text{av}}(a)$ is defined by

$$q_{\text{av}}(a) = \sum_{r=1}^{n_c} (2J_r + 1) q_r(a) \Bigg/ \sum_{r=1}^{n_c} (2J_r + 1)\ , \tag{4.42}$$

are better estimates than screened Coulomb functions. This is because the Thomas-Fermi potential provides an estimate of the radial variation of screening of the nuclear field.

(iii) Calculations based on density-functional theory may be considered to be the next level in sophistication, as they include an estimate of certain exchange and correlation effects. Now the potential $Y_{\kappa_a}(r)$ includes a term that is also a function of the spherically-average particle density, $\rho(r)$,

$$Y_{\kappa_a}(r) \to Y_{\kappa_a}(r) - Y_{\kappa_a}^{\text{xc}}(\rho; r), \quad \rho(r) = \frac{1}{4\pi r^2} \sum_{a=1}^{n_w} q_{\text{av}} \left(G_{n_a\kappa_a}^2(r) + F_{n_a\kappa_a}^2(r) \right). \tag{4.43}$$

The Slater exchange approximation consists in setting $Y_{\kappa_a}^{\text{xc}}(\rho(r); r) \approx Y^{\text{Six}}(\rho; r)$,

$$Y^{\text{Six}}(\rho; r) = \frac{3}{2} \left(\frac{3}{\pi} \rho(r) \right)^{1/3}. \tag{4.44}$$

Unlike the form of (4.38) for cases (i) and (ii), the dependence of $Y_{\kappa_a}(r)$ on $G_{\kappa_b\kappa_b}(r)$, $F_{\kappa_b\kappa_b}(r)$, $b = 1, ..., n_w$ renders (4.38) nonlinear in case (iii). Such systems are solved by a self-consistent-field (SCF) procedure:

1. The potential $Y_{\kappa_a}(r)$ is calculated from an estimated set of radial functions $G^{\rm est}_{\kappa_b\kappa_b}(r)$, $F^{\rm est}_{\kappa_b\kappa_b}(r)$, $b = 1, ..., n_w$.

2. Equations (4.38) are solved using this potential to obtain a new set of radial functions $G^{\rm new}_{\kappa_b\kappa_b}(r)$, $F^{\rm new}_{\kappa_b\kappa_b}(r)$, $b = 1, ..., n_w$.

3. An improved estimated set of radial functions is obtained from

$$\begin{pmatrix} G^{\rm est}_{n_b\kappa_b}(r) \\ F^{\rm est}_{n_b\kappa_b}(r) \end{pmatrix} \rightarrow (1-\eta_b) \begin{pmatrix} G^{\rm new}_{n_b\kappa_b}(r) \\ F^{\rm new}_{n_b\kappa_b}(r) \end{pmatrix} + \eta_b \begin{pmatrix} G^{\rm est}_{n_b\kappa_b}(r) \\ F^{\rm est}_{n_b\kappa_b}(r) \end{pmatrix}. \tag{4.45}$$

where $0 \leq \eta_b < 1$ are damping or accelerating factors. If the improved estimated set agrees to within a specified tolerance with the original estimated set, convergence has been achieved. If not, steps 1-3 are executed again.

When different orbitals with the same angular quantum number are generated in different potentials, we no longer have an eigenvalue problem: condition (4.16) is enforced by introducing the inhomogeneous terms

$$\chi_a \begin{pmatrix} G \\ F \end{pmatrix}(r) = \frac{r}{cq_{\rm av}(a)} \sum_{b\neq a} \delta_{\kappa_a\kappa_b}\epsilon_{ab} \begin{pmatrix} G_{n_b\kappa_b} \\ F_{n_b\kappa_b} \end{pmatrix}(r), \tag{4.46}$$

and the required Lagrange multipliers ϵ_{ab} are determined from either of

$$\begin{aligned} \frac{\epsilon_{ab}}{q_{\rm av}(a)} &= \int_0^\infty \frac{dr}{r} \left(Y_a(r) + rV_{\rm nuc(r)}\right)\left(G_{n_b\kappa_b(r)}G_{n_a\kappa_a(r)} + F_{n_b\kappa_b(r)}F_{n_a\kappa_a(r)}\right) - I(ab), \\ \frac{\epsilon_{ab}}{q_{\rm av}(b)} &= \int_0^\infty \frac{dr}{r} \left(Y_b(r) + rV_{\rm nuc(r)}\right)\left(G_{n_b\kappa_b(r)}G_{n_a\kappa_a(r)} + F_{n_b\kappa_b(r)}F_{n_a\kappa_a(r)}\right) - I(ab), \end{aligned} \tag{4.47}$$

or their difference or sum.

Koopmans has shown [Koo33], quite generally, that Lagrange multipliers need to be included only between pairs of orbitals (a, b) that vary subject to (4.16) if either $\bar{q}(a) < 2j_a + 1$ or $\bar{q}(b) < 2j_b + 1$. (For pairs involving one fixed orbital Lagrange multipliers must always be included. Pairs in which both orbitals are fixed are assumed orthogonal.)

It is now necessary to calculate the inhomogeneous term (4.46) also in step one of SCF procedure given above. This is applicable also to the forms of (4.38) discussed below.

The most general form of (4.38) arises when such equations are derived from a variational principle. Consider the energy functional

$$W^{\rm DC} = \sum_{r,s=1}^{n_c} d_{rs}H^{\rm DC}_{rs} + \sum_{a=1}^{n_w} \bar{q}(a)\epsilon_a N(aa) + \sum_{a=1}^{n_w-1}\sum_{b=a+1}^{n_w} \delta_{\kappa_a\kappa_b}\epsilon_{ab}N(ab), \tag{4.48}$$

with generalized weights,

$$d_{rs} = \sum_{i=1}^{n_L}(2J_i+1)c_{r\Gamma_i}c_{s\Gamma_i} \Big/ \sum_{i=1}^{n_L}(2J_i+1). \tag{4.49}$$

This is simply equivalent to

$$W^{\rm DC} = \sum_{i=1}^{n_L} (2J_i+1) E^{\rm DC}_{\Gamma_i} \Big/ \sum_{i=1}^{n_L} (2J_i+1), \tag{4.50}$$

a weighted sum over a certain subset of atomic levels with Lagrange multipliers ϵ_a and ϵ_{ab} introduced to enforce the restriction (4.16). The generalized occupation numbers, $\bar{q}(a)$, are defined in terms of the diagonal coefficients

$$\bar{q}(a) = \sum_{r=1}^{n_c} d_{rr} q_r(a). \tag{4.51}$$

The requirement that $W^{\rm DC}$ be stationary with respect to variations in the functions $G_{n_a\kappa_a}(r)$, $F_{n_a\kappa_a}(r)$ leads to equations of the form (4.38), with the direct potential $Y_a(r)$,

$$\begin{aligned} Y_a(r) &= -rV_{\rm nuc}(r) - \sum_k \left(\sum_{b=1}^{n_w} y^k(ab) Y^k(aa;r) - \sum_{b,d} y^k(abad) Y^k(bd;r) \right), \qquad (4.52) \\ y^k(ab) &= \left(\frac{1+\delta_{ab}}{\bar{q}(a)} \right) \sum_{r=1}^{n_c} d_{rr} f^k_r(ab), \quad y^k(abad) = \frac{1}{\bar{q}(a)} \sum_{r,s} d_{rs} V^k_{rs}(abad), \end{aligned}$$

and the inhomogeneous terms

$$\chi_a \begin{pmatrix} G \\ F \end{pmatrix}(r) = X_a \begin{pmatrix} G \\ F \end{pmatrix}(r) + \frac{r}{c\bar{q}(a)} \sum_{b\neq a} \delta_{\kappa_a\kappa_b} \epsilon_{ab} \begin{pmatrix} G_{n_b\kappa_b} \\ F_{n_b\kappa_b} \end{pmatrix}(r), \tag{4.53}$$

$$\begin{aligned} cX_a \begin{pmatrix} G \\ F \end{pmatrix}(r) &= \sum_k \left(\sum_{b\neq a} x^k(ab) Y^k(ab;r) \begin{pmatrix} G_{n_b\kappa_b} \\ F_{n_b\kappa_b} \end{pmatrix}(r) - \sum_{b,c,d;c\neq a} x^k(abcd) Y^k(bd;r) \begin{pmatrix} G_{n_c\kappa_c} \\ F_{n_c\kappa_c} \end{pmatrix}(r) \right), \\ x^k(ab) &= \frac{1}{\bar{q}(a)} \sum_{r=1}^{n_c} d_{rr} g^k_r(ab), \quad x^k(abcd) = \frac{1}{\bar{q}(a)} \sum_{r,s} d_{rs} V^k_{rs}(abcd). \end{aligned}$$

The second term in the equation for $\chi_a \begin{pmatrix} G \\ F \end{pmatrix}(r)$ is similar to right-hand side of (4.46), and also arises from the introduction of Lagrange multipliers to enforce (4.16). The Lagrange multipliers are determined from either of

$$\begin{aligned} \frac{\epsilon_{ab}}{\bar{q}(a)} &= c \int_0^\infty \frac{dr}{r} \left(G_{n_b\kappa_b}(r) X^{(F)}_a(r) - F_{n_b\kappa_b}(r) X^{(G)}_a(r) \right) \qquad (4.54) \\ &+ \int_0^\infty \frac{dr}{r} \left(Y_a(r) + rV_{\rm nuc}(r) \right) \left(G_{n_b\kappa_b}(r) G_{n_a\kappa_a}(r) + F_{n_b\kappa_b}(r) F_{n_a\kappa_a}(r) \right) - I(ab), \\ \frac{\epsilon_{ab}}{\bar{q}(a)} &= c \int_0^\infty \frac{dr}{r} \left(G_{n_a\kappa_a}(r) X^{(F)}_b(r) - F_{n_a\kappa_a}(r) X^{(G)}_b(r) \right) \\ &+ \int_0^\infty \frac{dr}{r} \left(Y_b(r) + rV_{\rm nuc}(r) \right) \left(G_{n_b\kappa_b}(r) G_{n_a\kappa_a}(r) + F_{n_b\kappa_b}(r) F_{n_a\kappa_a}(r) \right) - I(ab), \end{aligned}$$

or their difference or sum.

The choice (4.49) yields the optimal-level (OL) [GMP76] formalism when $n_L = 1$, and an extended-optimal-level (EOL) calculation when $n_L > 1$. The freedom in choosing the n_L ASFs which contribute to the energy functional in EOL calculations can be considerable advantage in certain situations. However, the user should be aware that the optimization applies only to the n_L ASFs involved, so that the orbitals cannot be assumed to be of equal quality in evaluating quantities connected with the other $(n_c - n_L)$ ASFs generated by the Hamiltonian matrix eigenvectors. Simultaneous solution of (4.27) and (4.38) must be achieved, requiring three more steps (numbered 0, 4, and 5) in the SCF procedure described above:

4. The coefficients d_{rs} are calculated from an estimated set of mixing-coefficient vectors $\mathbf{c}_\Gamma^{\rm est}$, $i = 1, ..., n_L$.

5. Equation (4.27) is solved using the Hamiltonian obtained with the improved estimated radial functions to calculate a new estimated set of mixing-coefficient vectors $\mathbf{c}_{\Gamma_i}^{\rm new}$, ,$1 = i, ..., n_L$.

6. An improved estimated set of mixing coefficient vectors is obtained from

$$\mathbf{c}_{\Gamma_i}^{\rm est} \rightarrow (1 - \xi_i)\mathbf{c}_{\Gamma_i}^{\rm new} + \xi_i \mathbf{c}_{\Gamma_i}^{\rm est} \tag{4.55}$$

where $0 \leq \xi_i < 1$ are also damping or accelerating factors. If the improved estimated set agrees to within a specified tolerance with the original estimated set, convergence has been achieved. If not, steps 0-5 are executed again.

Convergence for E/OL calculations is often difficult to achieved, and is invariably computationally expensive when compared with the straightforward alternative, more approximate, method described in the next paragraph.

The average-level (AL) [GMP76] formalism obviates the need to obtain the coefficients d_{rs} iteratively by setting

$$d_{rs} = \begin{cases} (2J_r + 1)/\sum_{t=1}^{n_c}(2J_t + 1), & \text{if} \quad r = s, \\ 1, \quad \text{otherwise} \end{cases} \tag{4.56}$$

(whence $\bar{q}(a) \rightarrow q_{\rm av}(a)$). An extended-average-level (EAL) calculation differs from the AL case in that weights chosen by the user replace $(2J_r + 1)$ in (4.56). Steps 0, 4, and 5 of the iterative procedure are once again unnecessary. The object of the E/AL options is to determine a set of orbitals which are optimal for average energy of a set of CFSs.

4.2.7 The transverse electromagnetic interaction

The lowest-order correction to Coulomb interaction between two electrons, labelled 1 and 2, due to exchange of a single transverse photon, is given by

$$\hat{H}^{\rm Transv} = -\sum_{i,j=1}^{3} \alpha_{1i}\alpha_{2j}\left(\delta_{ij}\frac{\cos(\omega R)}{R} + \frac{\delta^2}{\delta R_{1i}\delta R_{2j}}\frac{\cos(\omega R) - 1}{\omega^2 R}\right), \tag{4.57}$$

where $R = |\mathbf{r}_1 - \mathbf{r}_2|$ and $\omega = |\epsilon_1 - \epsilon_2|/c$. This interaction is sometimes referred to as the generalized Breit interaction, as in the long-wavelength limit $(\omega \rightarrow 0)$ it reduces to the well-known Breit interaction. In the context of MCDF theory, this contributes the matrix elements [GM80, GP76, MJ71]

$$H_{rs}^{\rm Transv} = \sum_{abcd}\sum_{k\tau} V_{rs}^{k\tau}(abcd)S^{k\tau}(abcd), \tag{4.58}$$

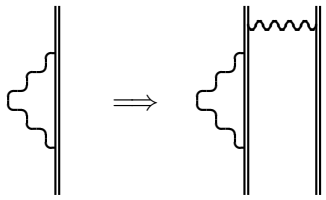

Figure 4.2: Self-energy and self-energy screening diagrams in many-electron systems. The double lines represent Furry-picture electronic wave functions or propagators for Dirac particles moving in a Coulomb field. Wavy lines represent (virtual) photons. In the case of the screening contribution, the electronic wave function is perturbed by interaction with other electrons, which is mediated by the exchange of virtual photons.

where the index τ which takes the values $1, ..., 6$, enumerates the six types of radials integrals $S^{kr}(abcd)$ that occur. The integrals can all be expressed as combinations of two integrals, $\bar{R}^k(abcd;\omega)$ and $\bar{S}^k(abcd;\omega)$:

$$\bar{R}^k(abcd;\omega) = \int_0^\infty dr \left[\rho_{bd}(r)\Phi_k(\omega r)\frac{1}{r}\bar{Y}^k(ac;\Phi_k;\omega;r)\right],$$
$$\bar{S}^k(abcd;\omega) = \Sigma_1^k(abcd;\omega) - \Sigma_2^k(abcd;\omega),$$
$$\Sigma_1^k(abcd;\omega) = \int_0^\infty dr \left[\rho_{bd}(r)\left(\frac{2k+1}{\omega r}\right)^2\frac{1}{r}\left(\bar{Y}^{k-1}(ac;1;1;r) - \Phi_{k+1}(\omega r)\bar{Y}^{k-1}(ac;\Phi_{k-1};\omega;r)\right)\right],$$
$$\Sigma_2^k(abcd;\omega) = \int_0^\infty dr \left[\rho_{ac}(r)\frac{\omega^2 r^2}{(2k+3)(2k-1)}\Phi_{k-1}(\omega r)\bar{Y}^{k+1}(bd;\Phi_{k+1};\omega;r)\right],$$
$$\bar{Y}^k(ab;f;\omega;r) = \int_0^r ds \left[\rho_{ab}(s)\left(\frac{s}{r}\right)^k f(\omega s)\right],$$
$$\rho_{ab}(r) = G_{n_a\kappa_a}(r)F_{n_b\kappa_b}(r), \quad \Phi_k(z) = \frac{(2k+1)!!}{z^k}j_k(z), \quad \Psi_k(z) = -\frac{z^{k+1}}{(2k-1)!!}y_k(z).$$

We have adopted the conventions of Ref. [AS72] for the spherical Bessel functions, $j_k(z)$, $y_k(z)$, of the first and second kind, respectively. The calculation of the angular coefficients $V_{rs}^{kr}(abcd)$ will be discussed in subsection 4.2.9.

4.2.8 Quantum electrodynamic radiative corrections

The inclusion of interactions due to fluctuation in the electron-positron and electromagnetic fields produces the radiative corrections of QED. The Furry-picture Feynman diagrams of the self-energy and vacuum polarization contributions is shown on Fig. 4.2 and 4.3, respectively.

Known simply as the self-energy, the dominant radiative correction to the energy arises from the lowest-order modification to an electron's interaction with the quantized ambient electromagnetic field when in the presence of the field due to the nucleus and the other atomic electrons. In terms of a function $M_{n\kappa}(Z/c)$ that varies slowly with respect to its argument, the self-energy in hydrogenlike systems in given by

$$E_{n\kappa}^{\mathrm{SE}}(Z/c) = \frac{Z^4}{\pi c^3 n^3}M_{n\kappa}(Z/c). \tag{4.59}$$

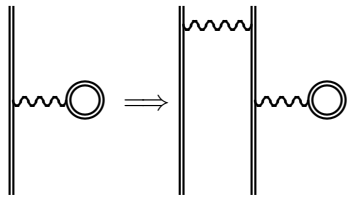

Figure 4.3: Vacuum polarization and vacuum polarization screening diagrams in many-electron systems. Notations as for the previous figure.

Tabulations of $M_{n\kappa}(Z/c)$ for the $1s$, $2s$, $2p_{1/2}$, and $2p_{3/2}$ states in these one-electron system are given in the literature [Moh92, JS85]. We obtain an estimate of the screened self-energy by setting

$$H_{rr}^{\rm SE} = \sum_{a=1}^{n_w} q_r(a) E_{n_a\kappa_a}^{\rm SE}, \tag{4.60}$$

$$E_{n_a\kappa_a}^{\rm SE} = \frac{\left(Z_a^{\rm eff}\right)^4}{\pi c^3 n^3} \begin{cases} M_{n_a\kappa_a}\left(Z_a^{\rm eff}/c\right), & \text{for } 1s,\ 2s,\ 2p_{1/2}, \text{ and } 2p_{3/2} \text{ orbitals,} \\ M_{2\kappa_a}\left(Z_a^{\rm eff}/c\right), & \text{for } ns,,\ np_{1/2}, \text{ and } np_{3/2} \text{ orbitals,} \\ 0, & \text{otherwise.} \end{cases}$$

The use of $Z^{\rm eff}$ to roughly correct for electron screening is an expedient intended for inner shells where the orbitals are most likely to be nearly hydrogenic. It is likely to be increasingly less realistic as n increases. Calculations based more rigorously on QED are those of Johnson and coworkers [CJ76, DJ71]. A fully rigorous practical computational scheme for taking screening effects on the self-energy into account is one of the major unsolved challenges in atomic structure theory.

Next in order of importance is vacuum polarization correction. To lowest order, this is the short-range modification of the nuclear field due to screening by virtual electron-positron pairs. Expressions for the second-order perturbation potential – also known as the Uehling potential [Ueh35] – and the fourth-order potential that take finite nuclear size into account have been given in the literature, for example in Ref. [FR76]. The diagonal contributions,

$$H_{rr}^{\rm VP} = \sum_{a=1}^{n_w} q_r(a) \int_0^\infty dr V^{\rm VP}(r) \left(G_{n_a\kappa_a}^2(r) + F_{n_a\kappa_a}^2(r)\right) , \tag{4.61}$$

from these potentials have been included in our calculations.

4.2.9 The angular coefficients

The configuration coupling coefficients, $V_{rs}^k(abcd)$ of (4.36) and (4.37), for the Coulomb interaction have the general form

$$\sum (-1)^P S \cdot R \cdot C \cdot X^k. \tag{4.62}$$

The factor $(-1)^P$ S arises from the operation of Pauli's exclusion principle, and depends entirely on subshell occupation number $q_r(a)$. R represents an angular momentum recoupling coefficient which appears when integration over polar angles in the matrix element are performed, and which contains all

the information on the angular momentum coupling structure of the participating CSF. C is a product of four-one-electron coefficients of fractional parentage. X^k is a quantity which depends on the orbital labels appearing in the associated radial integral and a parameter k. The latter arises from the standard expansion of $|\mathbf{r}_1 - \mathbf{r}_2|^{-1}$ in terms of Legendre polynomials, each term of which is a scalar product of irreducible tensor operators of rank k. The summation goes over all possible parent states which may contribute when the "active" electrons, whose labels appear in the radial matrix element, are removed from the CSFs $|\gamma_r PJM\rangle$ and $|\gamma_s PJM\rangle$.

The structure of the coefficient $V_{rs}^{k\tau}(abcd)$ is very similar, differing only in the replacement of X^k by more complex expressions.

Operators of the type $\sum_i \hat{f}^k(\mathbf{r}_i)$, where $\hat{f}^k(\mathbf{r})$ is a rank-k irreducible one-body tensor operator, have matrix elements with respect to $|\gamma_r P_{JM}\rangle$ and $|\gamma_s P'J'M'\rangle$ which can, in general, be written

$$\langle \gamma_r PJM| \sum_i \hat{f}^k(\mathbf{r}_i)|\gamma_s P'J'M'\rangle = \sum T_{rs}^k(ab)(n_a\kappa_a|\hat{f}^k(r)|n_b\kappa_b)(-1)^{J-M} \begin{pmatrix} J & k & J' \\ M & q & -M' \end{pmatrix},$$

where $(n_a\kappa_a|\hat{f}^k(r)|n_b\kappa_b)$ is a radial matrix element between orbitals a and b. The $T_{rs}(ab)$ coefficients of (4.37) are special cases with $k = 0$, appropriate to scalar operators.

4.3 Evaluation of Coulomb-Dirac continuum wave functions

The initial state of the recombination process can be represented by an antisymmetrized product of the bound many-particle wave function and the continuum state

$$\Psi(\gamma_i J_i M_i \mathbf{p} m_s) = \mathscr{A}[\Psi(\gamma_i J_i M_i) \otimes \psi_{\mathbf{p}m_s}(\mathbf{r})]\,. \tag{4.63}$$

Here, $\Psi(\gamma_i J_i M_i)$ denotes the wave function of the bound electrons of the ion, and $\psi_{\mathbf{p}m_s}(\mathbf{r})$ is the wave function of the incoming electron. The symbol γ_i summarizes all information necessary to specify the orbital occupation and the coupling.

The continuum solutions can not be given in a closed form. One can use a partial wave expansion for the electron with asymptotic momentum $\mathbf{p}$ and the spin projection m_s [EM95]

$$\psi_{\mathbf{p}m_s}(\mathbf{r}) = \sum_{\kappa\mu} i^l e^{i\Delta_\kappa} \sum_{m_l} Y_l^{m_l *}(\hat{p}) C(l\tfrac{1}{2}j; m_l m_s \mu)\psi_{p\kappa\mu}(\mathbf{r})\,. \tag{4.64}$$

Here, the phases Δ_κ ensure that the wave function satisfies the boundary condition of an incoming plane wave and an outgoing spherical wave.

The Dirac bispinor $\psi_{p\kappa\mu}(\mathbf{r})$ is calculated numerically by solving the Dirac equation with the nuclear potential screened by the bound electrons in the initial state. This procedure is referred to as the frozen orbital approximation, in which the ionic states are assumed to be weakly influenced by the continuum electron. In the case of highly charged ions studied in this thesis, this is a valid assumption. The continuum radial functions $F_{p\kappa_p}(r)$ and $G_{p\kappa_p}(r)$ will be generated by integrating the radial Dirac equations with the screened potential Y_p and with the positive continuum energy ϵ_p

$$\begin{aligned} \left(\frac{d}{dr} + \frac{\kappa_p}{r}\right) F_{p\kappa_p}(r) - \left(2c + \frac{\epsilon_p}{c} + \frac{Y_p(r)}{cr}\right) G_{p\kappa_p}(r) &= 0\,, \\ \left(\frac{d}{dr} - \frac{\kappa_p}{r}\right) G_{p\kappa_p}(r) + \left(\frac{\epsilon_p}{c} + \frac{Y_p(r)}{cr}\right) F_{p\kappa_p}(r) &= 0\,, \end{aligned} \tag{4.65}$$

and imposing the boundary conditions

$$F_{p\kappa_p}(0) = 0\,, \quad G_{p\kappa_p}(0) = 0\,. \tag{4.66}$$

The solutions also have to satisfy the following normalization condition:

$$\int_0^\infty dr \left(G_{p\kappa_p}(r) G_{p'\kappa'_p}(r) + F_{p\kappa_p}(r) F_{p'\kappa'_p}(r) \right) = \delta_{\kappa_p \kappa'_p} \delta(E - E')\,. \tag{4.67}$$

4.4 Calculation of Auger rates

The Auger decay rate of the autoionizing intermediate state d is, as defined previously,

$$A_a = \frac{2\pi}{2J_d + 1} \sum_{M_i m_s M_d} \int d\Omega_p |\langle \Psi_d; J_d M_d | V_{capt.} | \Psi_i; J_i M_i, \mathbf{p} m_s \rangle|^2 \rho_i\,, \tag{4.68}$$

with the capture operator being the sum of the Coulomb and Breit interactions. For the coordinate representation of the initial state $|\Psi_i; J_i M_i, \mathbf{p} m_s\rangle$, after substituting the partial wave expansion (4.64) of the continuum orbital we get

$$\begin{aligned} \Psi(\gamma_i J_i M_i \mathbf{p} m_s) = \sum_{\kappa\mu} i^l e^{i\Delta_\kappa} \sum_{m_l} Y_l^{m_l *}(\hat{p}) C(l \tfrac{1}{2} j; m_l m_s \mu) \\ \times \sum_{JM} C(J_i j J; M_i \mu M) \Psi(\gamma_i J_i M_i, p\kappa; JM)\,. \end{aligned} \tag{4.69}$$

Here, the configuration state function $\Psi(\gamma_i J_i M_i, p\kappa; JM)$ differs from the CSFs for bound states by the replacement of a bound orbital by one belonging to the continuous spectrum. After carrying out the reduction of (4.68), we arrive to the following simpler formula for the Auger rate:

$$A_a = 2\pi \sum_\kappa |\langle \Psi_d; J_d || V_{capt} || \Psi_i; J_i, p\kappa; J_d \rangle|^2\,. \tag{4.70}$$

Here we have made use the fact that for energy-normalized wave functions $\rho_i = 1$. The reduced matrix element $\langle \Psi_d; J_d || V_{capt} || \Psi_i; J_i, p\kappa; J_d \rangle$, which does not depend on the magnetic quantum numbers of the states by definition, is defined as in Ref. [BS02]. The numerical evaluation of these matrix elements are performed by an adopted version of the AUGR module [Zim92], which is an extension module of the GRASP 1.0 suite of codes [DGJ$^+$89].

The matrix elements of the Coulomb and Breit interactions contain angular and radial integrals. The former can be calculated algebraically by means of the Racah algebra, resulting in angular coefficients. The matrix element of the Coulomb interaction between two CSFs has the form [DGJ$^+$89]

$$\langle \gamma_r J_r | \sum_{i<j} \frac{1}{|\mathbf{r}_i - \mathbf{r}_j|} | \gamma_s J_s \rangle = \sum_{abcd} \sum_k V_{rs}^k(abcd) R^k(abcd)\,, \tag{4.71}$$

where the first sum goes over the orbitals occupied in the configuration r and s. The radial integrals read

$$R^k(abcd) = \int_0^\infty dr \left[(F_{n_a\kappa_a}(r) F_{n_c\kappa_c}(r) + G_{n_a\kappa_a}(r) G_{n_c\kappa_c}(r)) \frac{1}{r} Y^k(bd; r) \right]\,. \tag{4.72}$$

Here, the relativistic Hartree Y-functions are defined as

$$Y^k(ac; r) = r \int_0^\infty ds \frac{r_<^k}{r_>^{k+1}} [F_{n_a\kappa_a}(r) F_{n_c\kappa_c}(r) + G_{n_a\kappa_a}(r) G_{n_c\kappa_c}(r)]\,. \tag{4.73}$$

The angular coefficients $V_{rs}^{k}(abcd)$ are calculated by the program MCP by Grant [Gra76].

Similarly to the Coulomb matrix elements, the matrix elements of the generalized Breit interaction operator between two electrons with indices 1 and 2,

$$V_{\rm Breit}(1,2) = -\boldsymbol{\alpha}_1\boldsymbol{\alpha}_2\frac{\cos(\omega R)}{R} + (\boldsymbol{\alpha}_1\nabla_1)(\boldsymbol{\alpha}_2\nabla_2)\frac{\cos(\omega R)-1}{\omega^2 R}\,, \tag{4.74}$$

where ω is the frequency of the exchanged photon and $R = |\mathbf{r}_1 - \mathbf{r}_2|$, can be expressed as a sum over products of angular coefficients and radial integrals

$$\langle\gamma_r J_r|\sum_{i<j} V_{Breit}(i,j)|\gamma_s J_s\rangle = \sum_{abcd}\sum_{k\tau} V_{rs}^{k\tau}(abcd)S^{k\tau}(abcd)\,. \tag{4.75}$$

The angular coefficients $V_{rs}^{k\tau}$ are evaluated with the MCBP code [GMN$^+$80]. The index τ differentiates six types of integrals appearing in the calculation of matrix elements. These expressions for the radial integrals $S^{k\tau}(abcd)$ can be taken from Ref. [DGJ$^+$89]. They are solved by the program module BENA [GMN$^+$80] numerically, using a finite differences method. Corrections of the Breit interaction to the energy levels are included in a perturbative approximation.

4.5 Radiative transitions between many-electron states

In this section we briefly outline the calculation of radiative transition probabilities between many-electron states as described by MCDF state vectors. This can be regarded as a straightforward generalization of the calculation of radiative rates involving single-electron states as derived in Chapter 2. The electromagnetic transition probability from the intermediate state d to the final state f by the emission of a photon with all possible wave number vectors $\mathbf{k}$ and polarizations λ was introduced in section 4.1 as

$$A_r^{d\to f} = \frac{2\pi}{2J_d+1}\sum_{M_d}\sum_{M_f\lambda}\int d\Omega_k|\langle\Gamma_f J_f M_f;\mathbf{k},\lambda|H_{er}|\Gamma_d J_d M_d;0\rangle|^2\rho_f\,. \tag{4.76}$$

H_{er} is the Hamiltonian describing the interaction of the electrons with photons. The matrix element between the two atomic state functions d and f is

$$\langle\Gamma_f J_f M_f;\mathbf{k},\lambda|H_{er}|\Gamma_d J_d M_d;0\rangle = \sum_{r,s=1}^{n_c} c^*_{r\Gamma_f}c_{s\Gamma_d}\langle\gamma_r J_r M_r;\mathbf{k},\lambda|H_{er}|\gamma_s J_s M_s;0\rangle\,, \tag{4.77}$$

where for the ASFs we applied the series expansion into configuration state functions. The matrix element $\langle\gamma_r J_r M_r;\mathbf{k},\lambda|H_{er}|\gamma_s J_s M_s;0\rangle$ is evaluated with the CSFs r and s.

For evaluating these matrix elements of H_{er}, the electromagnetic radiation is expanded in multipole waves. Thus, the emission operator is decomposed in a sum of multipole operators $\mathbf{a}^{(0)}_{LM}(r)$ and $\mathbf{a}^{(1)}_{LM}(r)$ describing electric (1) and magnetic (0) multipole radiation. This results in

$$\begin{aligned}\langle\gamma_r J_r M_r;\mathbf{k},\lambda|H_{er}|\gamma_s J_s M_s;0\rangle &= \sqrt{\frac{2\pi c^2}{\omega_{\mathbf{k}}V}}\sum_L\sum_M\sqrt{2\pi}(-i)^L\sqrt{2L+1}D^L_{M,-\lambda}(\hat{k}) \\ &\times \left[\langle\gamma_r J_r M_r|\boldsymbol{\alpha}\mathbf{a}^{(0)}_{LM}(r) + i\lambda\boldsymbol{\alpha}\mathbf{a}^{(1)}_{LM}(r)|\gamma_s J_s M_s\rangle\right]\,.\end{aligned} \tag{4.78}$$

Here, $D^L_{M,-\lambda}(\hat{k})$ is a rotation matrix as defined in [Ros67]. The reduced matrix elements between configuration state functions can be expressed as a sum of single-electron reduced matrix elements using

$$\langle \gamma_r J_r M_r || O^{(L)} || \gamma_s J_s M_s \rangle = \sum_{ab} d^L_{ab}(rs) \langle n_a \kappa_a || O^{(L)} || n_b \kappa_b \rangle \,, \tag{4.79}$$

where the angular re-coupling coefficients $d^L_{ab}(rs)$ are given in Ref. [PGB78]. $O^{(L)}$ denotes a spherical tensor operator of rank L, and M, to be used later, is the corresponding magnetic quantum number. The magnetic and electric one-particle matrix elements are given by [Gra06]

$$\begin{aligned} \langle f || \boldsymbol{\alpha} \mathbf{a}^{(0)}_{LM} || i \rangle &= i(-1)^{j_i + L + 1/2} \sqrt{\frac{(2j_i+1)(2L+1)}{4\pi L(L+1)}} \\ &\times \begin{pmatrix} j_f & j_i & L \\ \frac{1}{2} & -\frac{1}{2} & 0 \end{pmatrix} (\kappa_f + \kappa_i) \left[\int dr (F_f(r) G_i(r) + F_i(r) G_f(r)) j_L(kr) \right] , \end{aligned} \tag{4.80}$$

$$\begin{aligned} \langle f || \boldsymbol{\alpha} \mathbf{a}^{(1)}_{LM} || i \rangle &= i(-1)^{j_i + L + 1/2} \sqrt{\frac{2j_i+1}{4\pi}} \begin{pmatrix} j_f & j_i & L \\ \frac{1}{2} & -\frac{1}{2} & 0 \end{pmatrix} \\ &\times \left[\sqrt{\frac{L+1}{L(2L+1)}} \left(L I^-_{L-1} - (\kappa_f - \kappa_i) I^+_{L-1} \right) \right. \\ &+ \left. \sqrt{\frac{L}{(L+1)(2L+1)}} \left((L+1) I^-_{L+1} + (\kappa_f - \kappa_i) I^+_{L+1} \right) \right] , \end{aligned} \tag{4.81}$$

with the radial integrals defined as

$$I^{\pm} = \int dr \left(F_f(r) G_i(r) \pm F_i(r) G_f(r) \right) j_L(kr) \,. \tag{4.82}$$

The evaluation of these integrals with the radial orbital functions $F_i(r)$, $G_i(r)$, $F_f(r)$ and $G_f(r)$, stemming from the MCDF variational procedure, is performed numerically.

The oscillator strength for the transition from ASF Γ_i to ASF Γ_j induced by a multipole radiation field operator $\hat{\mathbf{O}}^{(L)}_M$ of order L is [Gra74]

$$f_{i \to j} = \frac{\pi c}{(2L+1)\omega^2} \left| \langle \Gamma_i P_i J_i || \hat{\mathbf{O}}^{(L)} || \Gamma_j P_j J_j \rangle \right|^2 , \tag{4.83}$$

where we use the Brink and Satchler [BS02] definition of reduced matrix element. This in turn, can be expressed in terms of CSF matrix elements by

$$\langle \Gamma_i P_i J_i || \hat{\mathbf{O}}^{(L)} || \Gamma_j P_j J_j \rangle = \sum_{r,s} c_{r\Gamma_i} c_{s\Gamma_j} \langle \gamma_r P_r J_r || \hat{\mathbf{O}}^{(L)} || \gamma_s P_s J_s \rangle, \tag{4.84}$$

and this, in turn as a sum of single-electron transition integrals using

$$\langle \gamma_r P_r J_r || \hat{\mathbf{O}}^{(L)} || \gamma_s P_s J_s \rangle = \sum_{a,b} d^L_{ab}(rs) \langle n_a \kappa_a || \hat{\mathbf{O}}^{(L)} || n_b \kappa_b \rangle, \tag{4.85}$$

where the coefficients $d^L_{ab}(rs)$ are described in subsection 4.2.9 below. Allowing for the fact that we are now using Brink-and-Satchler type reduced matrix elements, we have

$$\langle n_a \kappa_a || \hat{\mathbf{O}}^{(L)} || n_b \kappa_b \rangle = \left(\frac{(2j_b+1)\omega}{\pi c} \right)^{1/2} (-1)^{j_a - 1/2} \begin{pmatrix} j_a & L & j_b \\ \frac{1}{2} & 0 & -\frac{1}{2} \end{pmatrix} \bar{M}_{ab}, \tag{4.86}$$

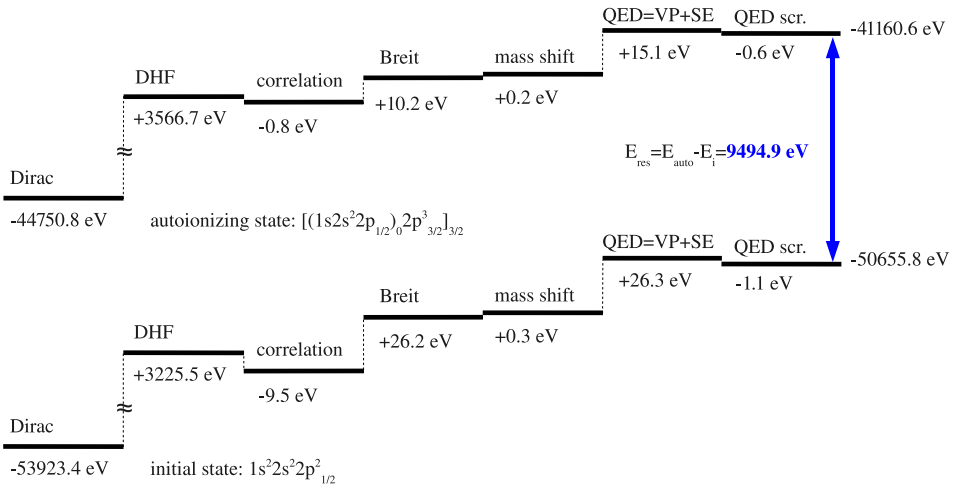

Figure 4.4: Different contributions to the energy of the ground state and the excited autoionizing state of a given transition in C-like Kr, as calculated with the methods presented in the previous sections.

where $\bar{M}_{ab}$ is one of the radiative transition integrals defined by Grant [Gra74]

$$
\begin{aligned}
\bar{M}_{ab} &= \begin{cases} \bar{M}^e_{ab} + G\bar{M}^l_{ab}, & \text{for electric multipole transitions,} \\ \bar{M}^m_{ab}, & \text{for magnetic multipole transitions,} \end{cases} \\
\bar{M}^e_{ab} &= -i^L \left[\left(\frac{L}{L+1} \right)^{1/2} [(\kappa_a - \kappa_b) I^+_{L+1} + (L+1) I^-_{L+1}] - \left(\frac{L+1}{L} \right)^{1/2} [(\kappa_a - \kappa_b) I^+_{L-1} - L I^-_{L-1}] \right], \\
\bar{M}^l_{ab} &= -i^L \{ [(\kappa_- \kappa_b) I^+_{L+1} + (L+1) I^-_{L+1}] + [(\kappa_a - \kappa_b) I^+_{L-1} - L I^-_{L-1}] - (2L+1) J_L \}, \\
\bar{M}^m_{ab} &= -i^{L+1} \frac{(2L+1)}{[L(L+1)]^{1/2}} (\kappa_a + \kappa_b) I^+_L, \\
I^\pm_L &= \int_0^\infty dr j_L(\omega r/c) \left(G_{n_a\kappa_a}(r) F_{n_b\kappa_b}(r) \pm F_{n_a\kappa_a}(r) G_{n_b\kappa_b}(r) \right), \\
J_L &= \int_0^\infty dr j_L(\omega r/c) \left(G_{n_a\kappa_a}(r) G_{n_b\kappa_b}(r) + F_{n_a\kappa_a}(r) F_{n_b\kappa_b}(r) \right).
\end{aligned}
$$

Here G is the gauge parameter; it takes the value 0 in the Coulomb gauge and $[(L+1)/L]^{1/2}$ in the Babushkin gauge. In the nonrelativistic limit $G = 0$ gives the velocity form of radiation matrix elements whilst $G = [(L+1)/L]^{1/2}$ gives the length form [Gra74].

4.6 Comparision of theoretical and experimental results

Once the bound-state wave functions and energies, and the radiative and Auger transition rates have been calculated, the cross section and related quantites like the resonance strength can be evaluated. Fig. 4.4 illustrates the magnitude of contributions to the transition energy of a trielectronic resonance in the C-like krypton ion. Such calculations have been performed to all possible transitions in the relevant K-LL energy range for He-, Li-, Be-, B-, C-, N-, and O-like Ar, Fe, and Kr ions, however, we do not list all numbers here. In Figs. 4.5 and 4.6 we show total theoretical cross sections for resonance recombination in highly charged Ar- and Fe-ions, respectively, as a function of the electron beam energy.

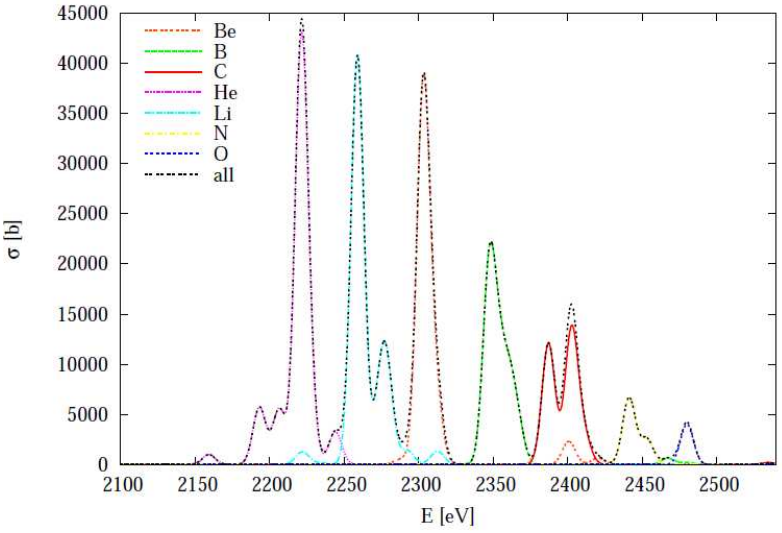

Figure 4.5: Total calculated cross section for resonant recombination, involving DR, TR and QR channels, for few-electron Ar ions. The electron energy range of the K-LL resonances is shown. The Lorentzian peaks have been convoluted with a Gaussian line shape with a FWHM of 10 eV for better comparision with experiments.

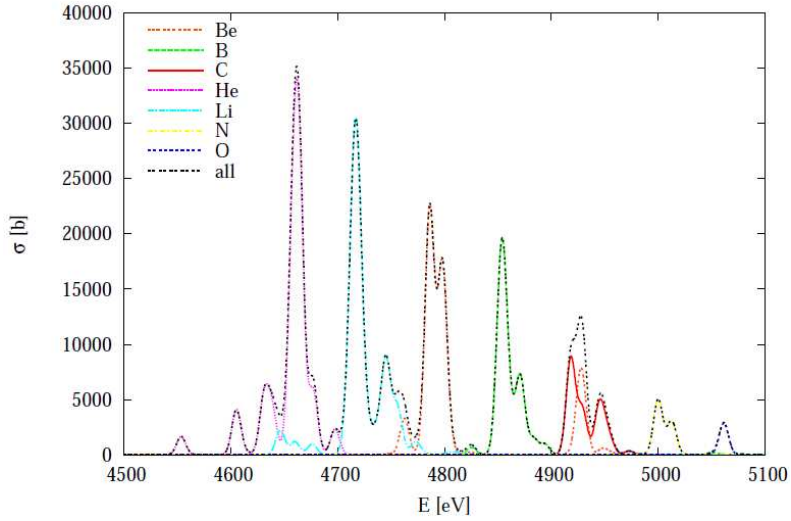

Figure 4.6: Total calculated cross section for resonant recombination, involving DR, TR and QR channels, for few-electon Fe ions. The electron energy range of the K-LL resonances is shown.

Fig. 4.7 shows the relative strength of certain TR transitions as compared to the dominant DR process in some few-electron charge states.

The experiment was performed at the Heidelberg EBIT [CDMU99] where highly charged Kr, Fe and Ar ions were produced and radially trapped by an electron beam, as explained at the end of Chapter 2. A magnetic field of 8 T compresses the beam to a radius of $\approx$ 22 μm. The ions were axially confined by electrostatic potentials applied to a set of drift tubes. The electron beam energy was swept over

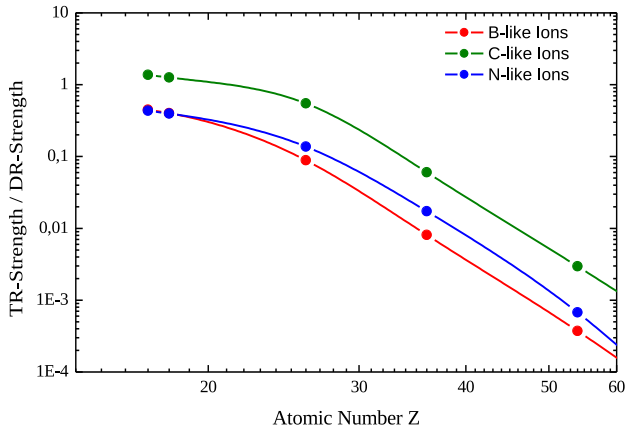

Figure 4.7: Ratio of trielectronic to dielectronic recombination resonance strengths for elements with different atomic numbers Z for certain transitions involving the B-, C- and N-like charge states. As expected, the relative weight of the TR process which is due to higher-order electron correlation decreases for stronger central Coulomb fields.

the expected range of resonance energies. Photons emitted as signature of the direct and indirect photorecombination and their cascades were detected with a high-purity germanium x-ray detector having a resolution of about 350 eV viewing the trap in a direction perpendicular to the exciting beam. The photons counted are represented in a two-dimensional intensity plot as a function of the electron beam energy. Bright spots at well-defined electron and photon energies reveal the recombination resonances in the illustration in Fig. 4.8. Projecting the counts within a certain photon energy region around the energy difference of the K and L shell (about 13 keV) onto the beam energy axis yields the energy-differential cross section of the photorecombination under perpendicular observation. An excellent electron energy resolution of about 13 eV FWHM at 10 keV was accomplished in the EBIT and actually was prerequisite to resolve the weak peaks corresponding to inter-shell TR and separate them from the roughly twenty times stronger DR features.

Fig. 4.8 presents an example of resonances appearing in the electron energy region of C- to O-like K-LL DR. Well-resolved DR and TR resonances of C- to O-like Kr ions are found. Close to their theoretically expected positions, signatures of C- and Be-like inter-shell QR resonances are indicated as well. The experimental resonance energies for inter-shell TR as well as the signatures of QR are compared to the theoretical values in Table 4.1. Our predictions agree very well within error bars with the inter-shell TR results and reasonably with the weaker QR signatures.

In Fig. 4.8 the theoretical resonance strengths were also normalized to the earlier mentioned C-like DR resonance line for Be-like, B-like and C-like Kr and to the first corresponding DR line for N-like and O-like ions. These values also show a good agreement with our predictions, thus further confirming the identification of the features as inter-shell TR resonances.

An overview on the calculated and measured DR, TR and QR resonance strengths is shown on Fig. 4.9. The DR strength decreases monotonically with a growing number of L electrons. For inter-shell TR, the possible range of ion charge states spans from the Li- to the N-like isoelectronic sequence. It is noteworthy that the predicted KL-LLL TR strength vanishes for initially Be-like ions due to parity rea-

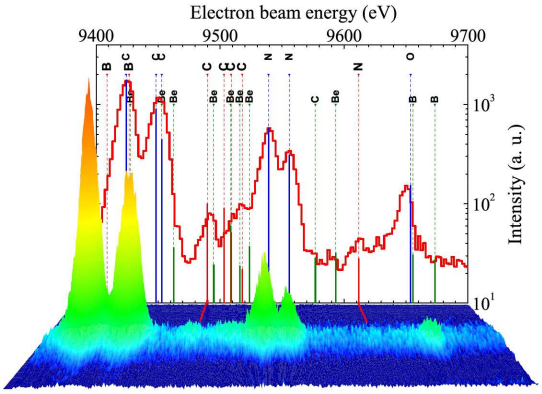

Figure 4.8: DR and TR resonances in the K-LL DR region of C- to O-like Kr ions as a projection and in three-dimensional illustration (photon intensity against electron beam energy and photon energy). Predictions (this work) for DR, TR and QR resonances and their strength are marked by blue, red and green lines, respectively. At the top the calculated resonances (color coded) for differently charged ion species are indicated.

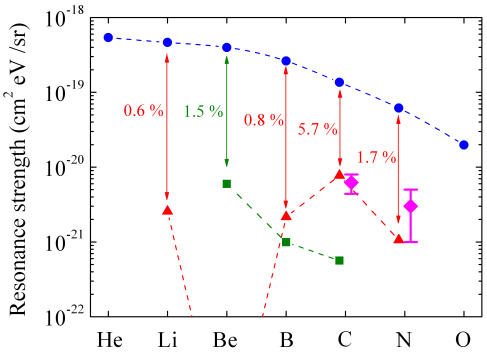

Figure 4.9: DR, TR and QR resonances strengths for He- to O-like Kr ions. Theory: DR, blue circles; TR, red triangles; QR, green squares. Measured TR strength: magenta diamonds. The relative strengths of the higher-order recombination processes with respect to total DR are indicated.

sons: while the TR resonances should necessarily be described by $|1s2s2p^3\rangle$ configurations possessing negative parity, the nearby K-LL DR configurations $|1s2s^22p^2\rangle$ are of positive parity, forbidding the requested admixtures. For this case, QR is the dominant higher-order recombination process. Interestingly, the ratio of inter-shell TR to the *total* DR resonance strength reaches values of up to 6% for C-like Kr^{30+}. This demonstrates that higher-order recombination processes of such mid-Z HCI contribute in the $1-10\,\%$ range to the total resonant photorecombination at interaction energies as high as 10 keV, which are relevant in the temperature range from $T_e = 500\,\mathrm{eV}$ upwards. The measured values confirm this statement. Experimental total TR resonance strengths of $(6.2\pm1.8)\times10^{-21}$ cm^2 eV sr^{-1} for C-like and $(3\pm2)\times10^{-21}$ cm^2 eV sr^{-1} for N-like ions agree reasonably well with theoretical values, as seen on Fig. 4.9. Moreover, they are remarkably large for a higher-order process in an inter-shell reaction involving a K-shell excitation. Studying HCIs at lower and higher Z values and, therefore, shifting from the nonrelativistic to the relativistic regime helps quantifying these contributions for the benefit of fundamental aspects and of plasma physics applications.

Table 4.1: Predicted and measured energies of selected dielectronic (TR), trielectronic (TR) and quadruelectronic (QR) resonances for Be-like to O-like Kr ions. The autoionizing configurations are given in the jj coupling notation; subscripts following round brackets denote the angular momentum of coupled subshells and subscripts following square brackets stand for the total angular momentum of the level. The experimental errors correspond to statistical uncertainties.

Process	charge state	intermediate state	E_{exp} (eV)	E_{theo} (eV)
DR	C	$[1s2s^22p_{1/2}^2(2p_{3/2}^2)_2]_{5/2}$	9429.0(2)	9429(5)
DR	C	$\left\{ \begin{array}{l} [1s2s^22p_{1/2}^2(2p_{3/2}^2)_2]_{3/2} \\ [1s2s^22p_{1/2}^2(2p_{3/2}^2)_0]_{1/2} \end{array} \right\}$	9455.0(3)	9455(5)
DR	N	$[1s2s^22p_{1/2}^2 2p_{3/2}^3]_2$	9543.9(3)	9543(6)
DR	N	$[1s2s^22p_{1/2}^2 2p_{3/2}^3]_1$	9561.6(4)	9560(6)
DR	O	$[1s2s^22p_{1/2}^2 2p_{3/2}^4]_{1/2}$	9653.8(4)	9653(7)
TR	C	$[(1s2s^22p_{1/2})_0 2p_{3/2}^3]_{3/2}$	9496.3(3)	9495(4)
TR	C	(blend)	9514.3(3)	9514(5)
TR	N	$[(1s2s^22p_{1/2})_1 2p_{3/2}^4]_1$	9617.5(7)	9616(6)
QR	Be	$[1s2p_{3/2}^4]_{1/2}$	9594(2)	9598(4)
QR	C	$[1s2s^22p_{3/2}^4]_{1/2}$	9576(2)	9582(4)

These considerations lead to the EBIT measurement of resonant recombination cross sections with the somewhat lighter Fe ions. Fig. 4.10 shows an experimental spectrum for this case. Beyond the TR peaks observed just as in the case of Kr, by the help of our theoretical calculations QR peaks have been unambiguously identified for the first time. They appear in the spectral range of the C- and Be-like Fe ions.

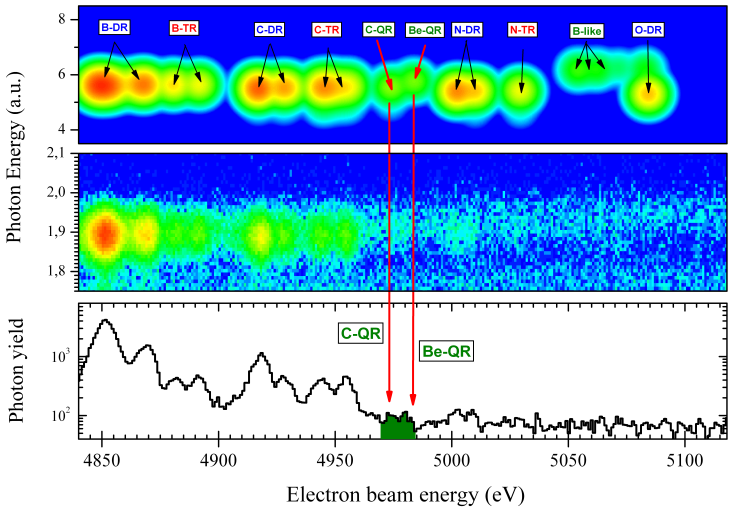

Figure 4.10: Theoretical (uppermost panel) and experimental (middle panel) intensity (arbitrary units) of x-ray emission as a function of the x-ray photon energy and the electron beam energy, for B- to O-like Fe ions [Bei]. Also, the photon yield integrated over the x-ray energies is shown in the bottom panel. The light spots correspond to DR, TR and QR resonances. QR resonances, indicated by the long red arrows and the green area, have been observed for the first time.

–V–

CONCLUSIONS AND OUTLOOK

5.1 Conclusions

In this thesis we theoretically investigated relativistic processes in highly charged ions, where strong electromagnetic fields play a decisive role.

In Chapter 2 we developed a fully relativistic ab initio theory of the bound dynamics of atomic systems in laser fields ranging to the x-ray domain. This study completes and extends a number of earlier investigations on the response of three-level atoms to external driving fields. It has been known from some time that multilevel atoms can display a much broader range of effects than their two-level counterparts as a result of the coherence induced among the states by the radiation, and the interference effects that can produce unexpected and sometime counterintuitive behaviors (e.q., coherent population trapping). In this work we have focused mainly on the properties of spontaneous emission from a V-model atom. The most interesting consequence of the presence of two fields is the structure acquired by the spontaneous emission spectra, and specially the influence of the spontaneous decay rates in setting the strength of the emitted intensity and the width of each of the spectral components.

As relativistic effects on the bound electronic wave function increase rapidly with the nuclear charge number Z, one needs to formulate a fully relativistic theory of coherent laser-atom interaction. The bare atomic states are constructed from solutions of the Dirac equation. This approach allows for exploiting the sensitivity of inner-shell electrons to relativistic electron correlation, QED and nuclear effects in strong Coulomb fields. Also the description of the theory beyond dipole approximation allowed us to describe forbidden transitions such as $M1$ transitions. As a demonstrative example, a means to determine ionic transition multipole moments and frequencies via a three-level configuration driven by an x-ray and an optical field has been put forward. Current or near-future laser systems are expected to increase the accuracy of multipole moment determinations from the current 10^{-3} level (via lifetime measurements) to the 10^{-4} range or better. Furthermore, the undesirable trapping of atomic population in a long-lived metastable state – naturally occurring in certain three-level systems – can be reversed by the scheme presented here. Other scenarios developed for the quantum control of non-relativistic resonance fluorescence emission [ZS96b, ZS96a, PK98, SZ98, Kei99] are anticipated to yield further improvement of detection and accuracy.

The inner-shell electrons in highly charged ions have a large overlap with the nuclear matter. Also, the relative simplicity of electronic shell structure in such few-electron ions allows for the accurate theoretical extraction of nuclear proton distribution parameters from isotope shift data, as shown in the first half of Chapter 2. Here, we have investigated isotope shifts measurements and we have extracted in-

formation on heavy nuclei via resonance fluorescence of a two-level atomic configuration driven by a short-wavelength laser field.

For the case of ions or atoms driven by lasers with off-resonant frequencies, shifts of hydrogenic energy levels were calculated in Chapter 3 in an analytical way. Interaction with the monofrequent laser field is treated by second-order time-dependent perturbation theory. Our formalism goes beyond the Stark long-wavelength dipole approximation and takes into account non-dipole effects of retardation and interaction with the magnetic field components of the laser beam. The technics is based on the adiabatically damped Babushkin gauge interaction. This procedure is based on using the unperturbed Hamiltonian, and treating the interaction $\boldsymbol{\alpha} \cdot \boldsymbol{A}$ as the perturbation. This interaction gives rise to a dynamic Stark shift. The procedure gives a time-dependent energy shift which depends on a constant of integration. If the duration of the measurements is short compared with the period of the electromagnetic field, the time-dependent AC Stark shift must be time averaged. When a time average is taken, the terms involving the constant of integration cancel. In order to calculate the matrix elements, we used the fully relativistic wavefunction, solutions of the Dirac-Coulomb equation. Because the transition is off-resonant, a Green function representing an infinite sum over virtual bound states and integration over all virtual continuum states is involved. The computation takes advantage of an expansion over a Sturmian basis of the first-order Dirac-Coulomb Green function.

At high laser intensities, the light shifts are found to be sizable, especially for excited states with lower binding energies. These results are relevant in current and near-future spectroscopic experiments, especially for experiments employing advanced light sources in the x-ray regime. This opens interesting perspectives regarding the possibility to address the difficult problem of the simulation of the response of heavy atoms or ions in the presence of an intense, high frequency, radiation field. The result of our calculations show that, for two-photon bound-bound transitions, relativistic contributions can be significant. In comparison to the usual nonrelativistic dipole treatment, the influence of relativity is to decrease the magnitude of the transition matrix element in two-photon processes. Such an influence is opposite to the one observed in the case on single-photon bound-free transitions, where relativistic effects tend to increase the cross sections. It appears also that retardation effects cannot be neglected. In fact, the magnitude of these corrections depends crucially on the final state of the two-photon transition. However, no significant cancellations take place when adding up the contributions of retardation and relativity, meaning that the nonrelativistic dipole result loses its accuracy by several percent already for $Z \approx 20$. For higher nuclear charge and corresponding shorter wavelength of radiation, relativistic calculations are clearly mandatory. We saw also that the dipole approximation is a reasonable approximation in most cases, where just the retardation effects should be added.

A further central point of this work has been the process of dielectronic (DR), trielectronic (TR) and quadruelectronic (QR) recombination via the KLL resonant channels. We have analyzed various effects which contribute to the resonance energies observed in DR, TR and QR into He-, Li-, Be-, B-, C-, N-, and O-like Ar, Fe, and Kr ions. We applied the multiconfiguration Dirac-Fock method to determine atomic state functions and energies. Our calculations include Coulomb and Breit correlation contributions, approximations for the many-electron QED terms as well as finite nuclear size effects. The comparison of our theoretical values with the experimental data shows a good overall agreement.

Due to the complex nature of the physical problem, results in many-body theories are commonly provided without error estimates in the literature. In our work we assigned theoretical uncertainties to the transition energies. On the theoretical side, the largest error bars are due to QED screening effects and electron correlation contributions. As electron interaction terms to DR, TR and QR energies beyond the no-pair approximation may not be negligible in the case of heavy ions, the calculation of such terms is necessary in the future to improve the accuracy of theoretical results.

The previously unobserved processes of TR and QR have been unambiguously identified in EBIT measurements performed at the Max Planck Institute for Nuclear Physics [BPA$^+$09], involving for the first time a K-shell electron as one of the actors. By investigating the electronic rearrangements taking place in such multiple excitations, new access to the study of dynamic correlations of bound electrons is presented. In the case of Kr ions, the inclusion of these hitherto unexplored contributions raises the total resonant photorecombination x-ray yield by up to 6% at temperatures in the $T_e > 500\,\mathrm{eV}$ range, an effect which has to be considered in the quantitative modeling of fusion and other hot, e. g. , astrophysical plasmas. Future improvements experimental in resolution – e.g. by means of the forced evaporative cooling technique [BPA$^+$09] to decrease Doppler broadening due to ionic motion – may even enable A A.detailed studies of the hyperfine structure as well as of isotopic shifts.

5.2 Outlook

In this thesis, a versatile fully relativistic theory of correlated electronic dynamics in strong Coulomb and laser fields has been developed. Beyond the dynamic processes and level shifts investigated in this work, a range of other phenomena may be theoretically studied using the same framework.

As seen in Chapter 2, the resonance fluorescence spectrum bears the signature of the driving process. For monochromatic x-ray light, the spectrum exhibits sidebands with positions determined by the Rabi frequency. By superimposing a second color, e.g., an optical laser, an efficient manipulation of the fluorescence spectrum could be achieved, e.g., in a V-type system the spectral line widths can be narrowed by several orders of magnitude. For future investigations, one may think of other schemes in which an x-ray transition is strongly driven and the fluorescence spectrum is manipulated with optical light. This should imprint a clear signature on the fluorescence spectrum as seen in our V-type system. Specifically, one may ask the question what effect an optical twin pulse or a frequency comb have on the fluorescence spectrum. To this end, the formalism of Chapter 2 needs to be extended to describe the dynamics in the time domain. This may offer the opportunity for novel frequency combs at x-ray wavelengths, a finer control over the comb and novel spectroscopic methods. A potential application is a more accurate spectroscopy of highly charged ions.

Diffraction of x rays represents a salutary method to learn about ionic structure since the photons that are irradiated and scattered interact only weakly with other ions or electrons in the interaction volume. This is particularly beneficial for the spectroscopy of highly charged ions. In this context, one may investigate Raman scattering (Stokes and anti-Stokes processes) of highly charged ions with transitions in the x-ray range. A high x-ray flux from free electron lasers [LCL, XFE] appears to be necessary to compensate for the somewhat lower cross sections.

The perturbative description of non-resonant light shifts, described in Chapter 3, may be employed with little modifications to further two-photon processes: excitation, ionization and electron-positron (or, in general, fermion-antifermion) pair creation. These processes are illustrated in Fig. 5.1. In case of excitation, the second-order electrodynamic process promotes a bound electron initially in the ground state to an excited bound state. For ionization, this final state is replaced by an electronic wave function belonging to the continuous part of the spectrum with an electron energy above $+mc^2$. Pair creation in a Coulomb field occurs when the initial electronic state has an energy below $-mc^2$ („Dirac sea“), and then photon absorption promotes the fermion into a bound or positive continuum state (bound-free and free-free pair production, respectively).

These processes are not only interesting from an academic point of view but they also have important experimental applications. The theoretical understanding of relativistic two-photon excitation is required

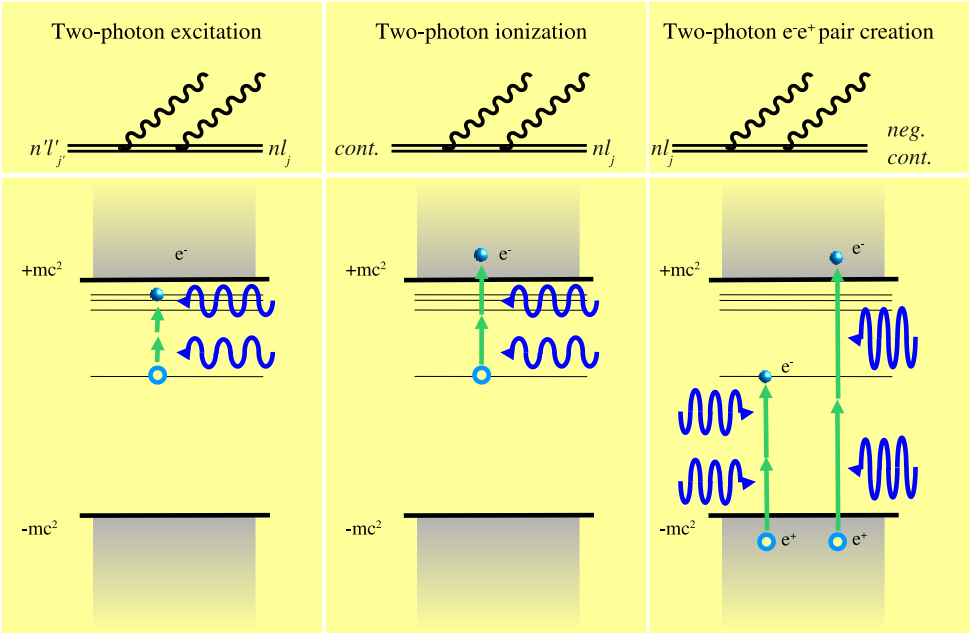

Figure 5.1: Two-photon processes involving highly charged ions: excitation, ionization, and free-free and bound-free electron-positron pair creation, respectively. The panels in the upper row show the Feynman diagrams of the corresponding processes, while the panels in the lower row show the level structures involved. See text for further details.

to conceive Doppler-free two-photon spectroscopic experiments with trapped ions, especially for highly charged ions where a relativistic treatment is mandatory. Our treatment applies for a broad range of transition energies, also allowing to perform studies in the x-ray range. The scheme of such experiments, allowing for the determination of ionic transition energies with accuracies much higher than presently possible, is shown in Fig. 5.2. As the laser intensities required for two-photon excitation are anticipated to be rather high, the levels involved in the transition are shifted by the polarization effects discussed in Chapter 3, therefore, the light shift effect calculated in the present work plays an important role in the interpretation and analysis of such experiments.

The two-photon ionization of highly charged ions is anticipated to become feasible by the use of upcoming intense x-ray free electron lasers such us the LCLS [LCL] and XFEL [XFE] facilities, equipped with transportable EBITs providing the trapped ions as targets. Experiments of this type are planned by the Max Planck Institute for Nuclear Physics, therefore, thorough theoretical investigation are necessary. The perturbative treatment developed for the calculation of light shift of energy levels (Chapter 3) can be extended to bound-continuum transitions in a straightforward way. Also, the inclusion of resonance pathways (resonant excitation-ionization) is feasible by means of a density operator approach such as that applied for relativistic resonance fluorescence in Chapter 2.

The direct production of electron-positron or even the heavier muon-antimuon pairs by two-photon absorption from a high-frequency laser wave colliding with an atomic nucleus has been investigated recently [MDK08]. The process is sensitive to the nuclear form factor, i.e. electrodynamic nuclear properties such as charge radii and other parameters of the protonic charge distribution. It could be realized experimentally by combining radiation from upcoming x-ray free electron or high harmonic generation [Mül09] laser sources with an ultra-relativistic ion beam from the present accelerator generation.

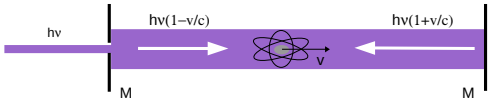

Figure 5.2: Scheme of a Doppler-free spectroscopic experiment with two-photon excitation. The atomic transition corresponds to two times the photon energy $h\nu$. The incoming laser light is split into two counter-propagating beams by the use of two parallel planar mirrors (M). The atoms (or ions), trapped in the interaction region between the mirrors, move with a random thermal velocity v. In the reference frame of the ion, the photons arriving from the two different directions have slightly Doppler-shifted frequencies; however, as the shifts have different signs in the dominant linear order in v/c, the blue and red shifts largely cancel. As a consequence, all ions (possessing different velocities) can absorb two laser photons and emit fluorescence photons.

In Ref. [MDK08], the strong field approximation has been employed, i.e. the created fermionic pair was described by Volkov wave functions accounting for interaction with the intense laser field but fully neglecting interaction with the nucleus. This description may be refined by our formalism described in Chapter 3, taking into account the nuclear potential to all orders. In the case of $\mu^+\mu^-$ pairs, the wave functions and the analytic Sturmian basis set corresponding to a pointlike nucleus have to be substituted with their counterparts integrated in the potential of an extended nucleus.

–APPENDIX A–

COULOMB-DIRAC GREEN'S FUNCTION IN THE STURMIAN REPRESENTATION

Given a Hermitian operator H, the corresponding resolvent or Green operator $G(z)$ is defined by

$$(H - z)G(z) = 1, \tag{A.1}$$

where z, referred to later on as the *energy variable*, is a complex number. Let us assume that H possesses a complete set of eigenfunctions Φ_n corresponding to eigenvalues E:

$$(H - E_n)\Phi_n = 0\,, \tag{A.2}$$

$$\sum_n \Phi_n \Phi_n^\dagger = 1\,. \tag{A.3}$$

In the spectral representation, $G(z)$ is formally given by

$$G(z) = -\sum_n \frac{\Phi_n \Phi_n^\dagger}{z - E_n}\,. \tag{A.4}$$

Generally, the summation is performed over a discrete and a continuous spectrum of eigenfunctions.

If H is represented by a differential operator H_r acting on a Hilbert space of functions on R^3, $G(z)$ is itself represented by a function $G(\boldsymbol{r_1}, \boldsymbol{r_2}; z)$ on $R^3 \times R^3$ which satisfies the equation

$$(H_{\boldsymbol{r_1}} - z)G(\boldsymbol{r_1}, \boldsymbol{r_2}; z) = \delta(\boldsymbol{r_1} - \boldsymbol{r_2})\,. \tag{A.5}$$

For a certain class of Hamiltonians, the Green's function can be given analytically, without explicitly carrying out the summation over a complete spectrum. The Green's function associated with the Dirac-Coulomb Hamiltonian can be decomposed into radial and angular parts as

$$G(\boldsymbol{r}_1, \boldsymbol{r}_2; E_n) = \frac{1}{c\hbar} \begin{pmatrix} G^{11} & G^{12} \\ G^{21} & G^{22} \end{pmatrix}\,, \tag{A.6}$$

where in the components G^{ij}, $i, j \in \{1, 2\}$, which are 2×2 matrices, we omitted the coordinate and

energy arguments for brevity. They can be decomposed as

$$\begin{aligned} G^{11} &= \sum_{\kappa_n m_n} g^{11}_{\kappa_n}(r_1, r_2; E_n)\Omega_{\kappa_n m_n}(\hat{r})\Omega^*_{\kappa_n m_n}(\hat{r'})\,, \\ G^{12} &= \sum_{\kappa_n m_n} -ig^{12}_{\kappa_n}(r_1, r_2; E_n)\Omega_{\kappa_n m_n}(\hat{r})\Omega^*_{-\kappa_n m_n}(\hat{r'})\,, \\ G^{21} &= \sum_{\kappa_n m_n} ig^{21}_{\kappa_n}(r_1, r_2; E_n)\Omega_{-\kappa_n m_n}(\hat{r})\Omega^*_{\kappa_n m_n}(\hat{r'})\,, \\ G^{22} &= \sum_{\kappa_n m_n} g^{22}_{\kappa_n}(r_1, r_2; E_n)\Omega_{-\kappa_n m_n}(\hat{r})\Omega^*_{-\kappa_n m_n}(\hat{r'})\,. \end{aligned} \tag{A.7}$$

The radial components g^{ij} can be represented as an expansion involving Laguerre polynomials:

$$\begin{aligned} g^{11}_{\kappa_n} &= \frac{1}{2\varepsilon}(2\lambda_n)^{2\gamma_n}(rr')^{\gamma_n-1}e^{-\lambda_n(r+r')}\sum_{n=0}^{\infty}\Bigg((\kappa_n+\nu/\epsilon_n)\frac{n!}{\Gamma(2\gamma_n+1+n)}\frac{L_n^{2\gamma_n}(2\lambda_n r)L_n^{2\gamma_n}(2\lambda_n r')}{n+\gamma_n+1-\nu} \\ &- [(\kappa_n-\nu/\epsilon_n)+2(\gamma_n+\nu)]\frac{n!}{\Gamma(2\gamma_n+1+n)}\frac{L_n^{2\gamma_n}(2\lambda_n r)L_n^{2\gamma_n}(2\lambda_n r')}{n+\gamma_n-\nu} \\ &+ \frac{n!}{\Gamma(2\gamma_n+n)}\frac{L_n^{2\gamma_n-1}(2\lambda_n r)L_n^{2\gamma_n}(2\lambda_n r')+L_n^{2\gamma_n}(2\lambda_n r)L_n^{2\gamma_n-1}(2\lambda_n r')}{n+\gamma_n-\nu}\Bigg)\,, \end{aligned} \tag{A.8}$$

$$\begin{aligned} g^{12}_{\kappa_n} &= \frac{1}{2}(2\lambda_n)^{2\gamma_n}(rr')^{\gamma_n-1}e^{-\lambda_n(r+r')}\sum_{n=0}^{\infty}\Bigg((\kappa_n+\nu/\epsilon_n)\frac{n!}{\Gamma(2\gamma_n+1+n)}\frac{L_n^{2\gamma_n}(2\lambda_n r)L_n^{2\gamma_n}(2\lambda_n r')}{n+\gamma_n+1-\nu} \\ &+ (\kappa_n-\nu/\epsilon_n)\frac{n!}{\Gamma(2\gamma_n+1+n)}\frac{L_n^{2\gamma_n}(2\lambda_n r)L_n^{2\gamma_n}(2\lambda_n r')}{n+\gamma_n-\nu} \\ &- \frac{n!}{\Gamma(2\gamma_n+n)}\frac{L_n^{2\gamma_n-1}(2\lambda_n r)L_n^{2\gamma_n}(2\lambda_n r')-L_n^{2\gamma_n}(2\lambda_n r)L_n^{2\gamma_n-1}(2\lambda_n r')}{n+\gamma_n-\nu}\Bigg)\,, \end{aligned} \tag{A.9}$$

$$g^{21}_{\kappa_n} = g^{12}_{\kappa_n}(r \leftrightarrow r')\,, \tag{A.10}$$

$$\begin{aligned} g^{22}_{\kappa_n} &= \frac{\varepsilon}{2}(2\lambda_n)^{2\gamma_n}(rr')^{\gamma_n-1}e^{-\lambda_n(r+r')}\sum_{n=0}^{\infty}\Bigg((\kappa_n+\nu/\epsilon_n)\frac{n!}{\Gamma(2\gamma_n+1+n)}\frac{L_n^{2\gamma_n}(2\lambda_n r)L_n^{2\gamma_n}(2\lambda_n r')}{n+\gamma_n+1-\nu} \\ &- [(\kappa_n-\nu/\epsilon_n)-2(\gamma_n+\nu)]\frac{n!}{\Gamma(2\gamma_n+1+n)}\frac{L_n^{2\gamma_n}(2\lambda_n r)L_n^{2\gamma_n}(2\lambda_n r')}{n+\gamma_n-\nu} \\ &- \frac{n!}{\Gamma(2\gamma_n+n)}\frac{L_n^{2\gamma_n-1}(2\lambda_n r)L_n^{2\gamma_n}(2\lambda_n r')+L_n^{2\gamma_n}(2\lambda_n r)L_n^{2\gamma_n-1}(2\lambda_n r')}{n+\gamma_n-\nu}\Bigg)\,. \end{aligned} \tag{A.11}$$

Here, we introduced the notations

$$\varepsilon = \sqrt{\frac{mc^2-E}{mc^2+E}}\,, \epsilon = \frac{E}{mc^2}\,, \nu = \frac{\alpha Z\epsilon}{\sqrt{1-\epsilon^2}}\,. \tag{A.12}$$

–APPENDIX B–

ELECTROMAGNETIC MULTIPOLES

In the following, we systematize the decomposition of the first-order transition amplitude into multipole components (electric and magnetic dipole, electric and magnetic quadrupole etc.). The transition matrix element is defined as

$$T_{an} = \int d^3r \phi_a^\dagger(\mathbf{r}) \boldsymbol{\alpha} \mathbf{A}(\mathbf{r},\omega) \phi_n(\mathbf{r}) \,, \tag{B.1}$$

where $\boldsymbol{A}(\boldsymbol{r},\omega)$ is the transverse-gauge vector potential [Joh]:

$$\boldsymbol{A}(\boldsymbol{r},\omega) = \hat{\epsilon} e^{i\boldsymbol{kr}}. \tag{B.2}$$

As a first step of the multipole decomposition, we expand the vector potential $\boldsymbol{A}(\boldsymbol{r},\omega)$ in a series of vector spherical harmonics [Joh] as

$$\boldsymbol{A}(\boldsymbol{r},\omega) = \sum_{JLM} A_{JLM} \boldsymbol{Y}_{JLM}(\hat{r}) \,. \tag{B.3}$$

The expansion coefficients are given by

$$A_{JLM} = \int d\Omega (\boldsymbol{Y}_{JLM}(\hat{r}) \cdot \hat{\epsilon})^\dagger e^{i\boldsymbol{kr}} \,. \tag{B.4}$$

Using the expansion of a plane wave in terms of spherical Bessel functions $j_l(kr)$ [AS72], namely,

$$e^{i\boldsymbol{kr}} = 4\pi \sum_{lm} i^l j_l(kr) Y^*_{lm}(\hat{k}) Y_{lm}(\hat{r}) \,, \tag{B.5}$$

and carrying out the angular integration in Eq. (B.4), we can rewrite the vector potential in the form

$$\boldsymbol{A}(\boldsymbol{r},\omega) = 4\pi \sum_{JLM} i^L (\boldsymbol{Y}_{JLM}(\hat{k}) \cdot \hat{\epsilon}) \boldsymbol{a}_{JLM}(\boldsymbol{r}) \,, \tag{B.6}$$

with

$$\boldsymbol{a}_{JLM}(\boldsymbol{r}) = j_L(kr) \boldsymbol{Y}_{JLM}(\hat{r}) \,. \tag{B.7}$$

For compactness, we introduce the notation $\boldsymbol{Y}^{(\lambda)}_{JM}(\hat{r})$, which is related to the vector spherical harmonics as

$$\begin{aligned}
\boldsymbol{Y}_{JJ-1M}(\hat{r}) &= \sqrt{\frac{J}{2J+1}} \boldsymbol{Y}^{(-1)}_{JM}(\hat{r}) + \sqrt{\frac{J+1}{2J+1}} \boldsymbol{Y}^{(1)}_{JM}(\hat{r}) \,, \\
\boldsymbol{Y}_{JJM}(\hat{r}) &= \boldsymbol{Y}^{(0)}_{JM}(\hat{r}) \,, \\
\boldsymbol{Y}_{JJ+1M}(\hat{r}) &= -\sqrt{\frac{J+1}{2J+1}} \boldsymbol{Y}^{(-1)}_{JM}(\hat{r}) + \sqrt{\frac{J}{2J+1}} \boldsymbol{Y}^{(1)}_{JM}(\hat{r}) \,.
\end{aligned} \tag{B.8}$$

This transformation leads immediately to the multipole expansion of the vector potential,

$$\boldsymbol{A}(\boldsymbol{r},\omega) = 4\pi \sum_{JM\lambda} i^{J-\lambda} (\boldsymbol{Y}^{(\lambda)}_{JM}(\hat{k}) \cdot \hat{\epsilon})^{\dagger} \boldsymbol{a}^{(\lambda)}_{JM}(\boldsymbol{r})\,. \tag{B.9}$$

The vector functions $\boldsymbol{a}^{(\lambda)}_{JM}$ are referred to as the multipole potentials. They are given by

$$\begin{aligned} \boldsymbol{a}^{(0)}_{JM}(\boldsymbol{r}) &= \boldsymbol{a}_{JJM}(\boldsymbol{r})\,, \\ \boldsymbol{a}^{(1)}_{JM}(\boldsymbol{r}) &= \sqrt{\frac{J+1}{2J+1}}\boldsymbol{a}_{JJ-1M}(\boldsymbol{r}) - \sqrt{\frac{J}{2J+1}}\boldsymbol{a}_{JJ+1M}(\boldsymbol{r})\,. \end{aligned} \tag{B.10}$$

Only terms with $\lambda = 0$ and $\lambda = 1$ contribute to this multipole expansion, since $\boldsymbol{Y}^{(-1)}_{JM}(\hat{k}) = \hat{k} Y_{JM}(\hat{k})$ is orthogonal to $\hat{k}$.

A gauge transformation leaves the transition amplitudes invariant, provided the energy difference between the initial and final states equals the energy carried off by the photon. The transformed multipole potential can be written as

$$\begin{aligned} \boldsymbol{a}^{\lambda}_{JM}(\hat{r}) &\longrightarrow \boldsymbol{a}^{\lambda}_{JM}(\hat{r}) + \nabla \chi_{JM}(\hat{r})\,, \\ \Phi_{JM}(\hat{r}) &\longrightarrow i\omega \chi_{JM}(\hat{r})\,, \end{aligned} \tag{B.11}$$

where the gauge function $\chi_{JM}(\hat{r})$ is a solution to the Helmholtz equation. We choose the gauge function to be

$$\chi_{JM}(\hat{r}) = -\frac{1}{k}\sqrt{\frac{J+1}{J}} j_J(kr) Y_{JM}(\hat{r}), \tag{B.12}$$

to cancel the contribution that is of lowest order in powers of kr. The resulting transformation has no effect on the magnetic multipoles, but transforms electric multipole potentials to the form

$$\begin{aligned} \boldsymbol{a}^{(1)}_{JM}(\hat{r}) &= -j_{J+1}(kr)\left(\boldsymbol{Y}^{(1)}_{JM}(\hat{r}) - \sqrt{\frac{J+1}{J}}\boldsymbol{Y}^{(-1)}_{JM}(\hat{r})\right)\,, \\ \Phi^{(1)}_{JM}(\hat{r}) &= -ic\sqrt{\frac{J+1}{J}} j_J(kr) Y_{JM}(\hat{r})\,. \end{aligned} \tag{B.13}$$

The resulting potentials reduce to the *length form* potentials in the nonrelativistic limit [Gra06, Gra74].

–APPENDIX C–

REDUCTION OF ANGULAR MATRIX ELEMENTS

We collect some formulas which will be important in the calculation of the angular part. In a general two-component system like a Dirac wave function possessing an orbital and a spin part, with the tensor $R_{k_1}(1)$ acting only on the first part and $S_{k_2}(2)$ only on the second component, a tensor acting on the composite system can be written as [BS02]

$$\begin{aligned} &T_{KQ}(k_1 k_2) = \\ &= \sum_{q_1 q_2} R_{k_1 q_1}(1) S_{k_2 q_2}(2) C(k_1 k_2 K; q_1 q_2 Q)\,, \end{aligned} \tag{C.1}$$

with the $C(k_1 k_2 K; q_1 q_2 Q)$ being the Clebsch-Gordan coefficients. The reduced matrix element of the spherical tensor operator can be written as [BS02]

$$\begin{aligned} &\langle j_1 j_2 j || T_K(k_1 k_2) || j_1' j_2' j' \rangle = \\ &= [(2j'+1)(2K+1)(2j_1+1)(2j_2+1)]^{1/2} \\ &\times \left\{ \begin{array}{ccc} j & j' & K \\ j_1 & j_1' & k_1 \\ j_2 & j_2' & k_2 \end{array} \right\} \langle j_1 || R_{k_1} || j_1' \rangle \langle j_2 || S_{k_2} || j_2' \rangle\,. \end{aligned} \tag{C.2}$$

Here, the $9j$ symbol was introduced in its usual notation. We apply this general theorem to an electron, i.e. a particle with its spin equal to $1/2$, coupled with the orbital angular momentum l (l') to the quantum number j (j') (i.e. we substitute in the above equation $j_1 = l_1$, $j_1' = l_1'$, and $j_2 = j_2' = 1/2$):

$$\begin{aligned} &\langle l_1 \frac{1}{2} j || T_K(C_{k_1} \sigma_1) || l_1' \frac{1}{2} j' \rangle = \\ &= [(2j'+1)(2K+1)(2l_1+1)2]^{1/2} \\ &\times \left\{ \begin{array}{ccc} j & j' & K \\ l_1 & l_1' & k_1 \\ \frac{1}{2} & \frac{1}{2} & 1 \end{array} \right\} \langle l_1 || C_{k_1} || l_1' \rangle \langle \frac{1}{2} || \sigma_1 || \frac{1}{2} \rangle\,. \end{aligned} \tag{C.3}$$

Using the matrix elements

$$\langle l_1 || C_{k_1} || l_1' \rangle = (2l_1'+1)^{1/2} (-1)^{l_1} \left(\begin{array}{ccc} l_1 & k_1 & l_1' \\ 0 & 0 & 0 \end{array} \right) \tag{C.4}$$

and

$$\langle \frac{1}{2} || \sigma_1 || \frac{1}{2} \rangle = 2 \langle \frac{1}{2} || \boldsymbol{S} || \frac{1}{2} \rangle = \sqrt{3}\,, \tag{C.5}$$

we get

$$\langle l_1 \frac{1}{2} j || T_K(C_{k_1}\sigma_1) || l_1' \frac{1}{2} j' \rangle =$$
$$= \sqrt{(2j'+1)(2K+1)(2l_1+1)6} \left\{ \begin{array}{ccc} j & j' & K \\ l_1 & l_1' & k_1 \\ \frac{1}{2} & \frac{1}{2} & 1 \end{array} \right\}$$
$$\times (2l_1'+1)^{1/2} (-1)^{l_1} \left(\begin{array}{ccc} l_1 & k_1 & l_1' \\ 0 & 0 & 0 \end{array} \right), \tag{C.6}$$

where $\boldsymbol{S}$ is the spin operator.

In the case of $k_1 = K$, the expression relating the $9j$-symbol to the Racah W-coefficient simplifies to [BS02]

$$\left\{ \begin{array}{ccc} j & j' & K \\ l_1 & l_1' & K \\ \frac{1}{2} & \frac{1}{2} & 1 \end{array} \right\} =$$
$$= \frac{j(j+1) - l_1(l_1+1) - j'(j'+1) + l_1'(l_1'+1)}{[6K(K+1)(2K+1)]^{1/2}}$$
$$\times (-1)^{K+1/2-j-l_1'} W\left(jj'l_1l_1'; K1/2\right). \tag{C.7}$$

Thus, the reduced matrix element can be rewritten as

$$\langle l_1 \frac{1}{2} j || T_K(C_K\sigma_1) || l_1' \frac{1}{2} j' \rangle =$$
$$= \frac{j(j+1) - l_1(l_1+1) - j'(j'+1) + l_1'(l_1'+1)}{\sqrt{K(K+1)}}$$
$$\times (-1)^{K+1/2-j-l_1'+l_1} \sqrt{(2j'+1)(2l_1+1)(2l_1'+1)}$$
$$\times W\left(jj'l_1l_1'; K1/2\right) \left(\begin{array}{ccc} l_1 & k_1 & l_1' \\ 0 & 0 & 0 \end{array} \right). \tag{C.8}$$

Let us pay attention to the product of the Racah coefficient and the $3j$ symbol. The $6j$ symbol is invariant under the interchange of any two columns, and also for interchange of the upper and lower arguments in each of any two columns. Thus the following relation holds: $W\left(abcd; e1/2\right) = W\left(dcba; e1/2\right)$. If $a+b+e$ is even, a special case is

$$W\left(abcd; e\frac{1}{2}\right) \left(\begin{array}{ccc} a & b & e \\ 0 & 0 & 0 \end{array} \right) = \tag{C.9}$$
$$= -\frac{1}{[(2a+1)(2b+1)]^{1/2}} \left(\begin{array}{ccc} c & d & e \\ -\frac{1}{2} & \frac{1}{2} & 0 \end{array} \right).$$

In our case the corresponding expression is as follows:

$$W\left(l_1'l_1j'j; K\frac{1}{2}\right) \left(\begin{array}{ccc} K & l_1 & l_1' \\ 0 & 0 & 0 \end{array} \right) = \tag{C.10}$$
$$= -(-1)^{K+l_1+l_1'} \frac{1}{[(2l_1'+1)(2l_1+1)]^{1/2}} \left(\begin{array}{ccc} j' & j & K \\ -\frac{1}{2} & \frac{1}{2} & 0 \end{array} \right).$$

The reduced matrix element thus becomes

$$\begin{aligned}
&\langle l_1 \frac{1}{2} j || T_K(C_K \sigma_1) || l_1' \frac{1}{2} j' \rangle = \\
&= \frac{j(j+1) - l_1(l_1+1) - j'(j'+1) + l_1'(l_1'+1)}{[K(K+1)]^{1/2}} \\
&\times (-1)^{j'-K-1/2} (2j'+1)^{1/2} \begin{pmatrix} j & j' & K \\ \frac{1}{2} & -\frac{1}{2} & 0 \end{pmatrix} .
\end{aligned} \tag{C.11}$$

Using the relation $j(j+1) - l_1(l_1+1) - j'(j'+1) + l_1'(l_1'+1) = \kappa - \kappa'$, we arrive to

$$\begin{aligned}
&\langle l_1 \frac{1}{2} j || T_K(C_K \sigma_1) || l_1' \frac{1}{2} j' \rangle = \frac{\kappa - \kappa'}{[K(K+1)]^{1/2}} \\
&\times (-1)^{j'-K-1/2} (2j'+1)^{1/2} \begin{pmatrix} j & j' & K \\ \frac{1}{2} & -\frac{1}{2} & 0 \end{pmatrix} .
\end{aligned} \tag{C.12}$$

In the case of $k_1 = K+1$, the reduced matrix element of the spherical tensor operator can be written as

$$\begin{aligned}
&\langle l_1 \frac{1}{2} j || T_K(C_{K+1} \sigma_1) || l_1' \frac{1}{2} j' \rangle = \\
&= [(2j'+1)(2K+1)(2l_1+1)6]^{1/2} \begin{Bmatrix} j & j' & K \\ l_1 & l_1' & K+1 \\ \frac{1}{2} & \frac{1}{2} & 1 \end{Bmatrix} \\
&\times (2l_1'+1)^{1/2} (-1)^{-K-1-l_1'} \begin{pmatrix} K+1 & l_1 & l_1' \\ 0 & 0 & 0 \end{pmatrix} .
\end{aligned} \tag{C.13}$$

If $c+d+e$ is odd, the following relation holds:

$$\begin{aligned}
&\begin{pmatrix} c+1 & d & e \\ 0 & 0 & 0 \end{pmatrix} \begin{Bmatrix} a & b & c \\ d & e & c+1 \\ \frac{1}{2} & \frac{1}{2} & 1 \end{Bmatrix} = \\
&= \frac{(d-a)(2a+1) + (e-b)(2b+1) + c + 1}{[6(c+1)(2c+1)(2c+3)(2d+1)(2e+1)]^{1/2}} \\
&\times (-1)^{b+e+1/2} \begin{pmatrix} a & b & c \\ \frac{1}{2} & -\frac{1}{2} & 0 \end{pmatrix} ,
\end{aligned} \tag{C.14}$$

thus the product of the $3j$ and $9j$ symbols in our case can be written as

$$\begin{aligned}
&\begin{pmatrix} K+1 & l_1 & l_1' \\ 0 & 0 & 0 \end{pmatrix} \begin{Bmatrix} j & j' & K \\ l_1 & l_1' & K+1 \\ \frac{1}{2} & \frac{1}{2} & 1 \end{Bmatrix} = \\
&= \frac{(l_1 - j)(2j+1) + (l_1' - j')(2j'+1) + K + 1}{[6(K+1)(2K+1)(2K+3)(2l_1+1)(2l_1'+1)]^{1/2}} \\
&\times (-1)^{j'+l_1'+1/2} \begin{pmatrix} j & j' & K \\ \frac{1}{2} & -\frac{1}{2} & 0 \end{pmatrix} .
\end{aligned} \tag{C.15}$$

Using the formula $\kappa = (l_1 - j)(2j + 1)$, this can be further simplified to

$$\begin{aligned}
&\langle l_1 \frac{1}{2} j || T_K(C_{K+1}\sigma_1) || l_1' \frac{1}{2} j' \rangle = \\
&= -\frac{\kappa + \kappa' + K + 1}{[(K+1)(2K+3)]^{1/2}} (-1)^{j'-K-1/2} \\
&\times (2j'+1)^{1/2} \begin{pmatrix} j & j' & K \\ \frac{1}{2} & -\frac{1}{2} & 0 \end{pmatrix} .
\end{aligned} \tag{C.16}$$

Finally, in the case of $k_1 = K - 1$, the reduced matrix element is given as

$$\begin{aligned}
&\langle l_1 \frac{1}{2} j || T_K(C_{K+1}\sigma_1) || l_1' \frac{1}{2} j' \rangle = \\
&= [(2j'+1)(2K+1)(2l_1+1)6]^{1/2} \begin{Bmatrix} j & j' & K \\ l_1 & l_1' & K-1 \\ \frac{1}{2} & \frac{1}{2} & 1 \end{Bmatrix} \\
&\times (2l_1'+1)^{1/2} (-1)^{-K-1-l_1'} \begin{pmatrix} K-1 & l_1 & l_1' \\ 0 & 0 & 0 \end{pmatrix} .
\end{aligned} \tag{C.17}$$

When the sum $c + d + e$ is odd, the product of the algebraic symbols can be written as

$$\begin{aligned}
&\begin{pmatrix} c+1 & d & e \\ 0 & 0 & 0 \end{pmatrix} \begin{Bmatrix} a & b & c \\ d & e & c-1 \\ \frac{1}{2} & \frac{1}{2} & 1 \end{Bmatrix} = \\
&= \frac{(d-a)(2a+1) + (e-b)(2b+1) - c}{[6c(2c+1)(2c-1)(2d+1)(2e+1)]^{1/2}} \\
&\times (-1)^{b+e+1/2} \begin{pmatrix} a & b & c \\ \frac{1}{2} & -\frac{1}{2} & 0 \end{pmatrix} .
\end{aligned} \tag{C.18}$$

Applying this relation to the case of interest,

$$\begin{aligned}
&\begin{pmatrix} K-1 & l_1 & l_1' \\ 0 & 0 & 0 \end{pmatrix} \begin{Bmatrix} j & j' & K \\ l_1 & l_1' & K-1 \\ \frac{1}{2} & \frac{1}{2} & 1 \end{Bmatrix} = \\
&= \frac{(l_1 - j)(2j+1) + (l_1' - j')(2j'+1) - K}{[6K(2K+1)(2K-K)(2l_1+1)(2l_1'+1)]^{1/2}} \\
&\times (-1)^{j'+l_1'+1/2} \begin{pmatrix} j & j' & K \\ \frac{1}{2} & -\frac{1}{2} & 0 \end{pmatrix} ,
\end{aligned} \tag{C.19}$$

and applying again the formula $\kappa = (l_1 - j)(2j + 1)$, one arrives to

$$\begin{aligned}
&\langle l_1 \frac{1}{2} j || T_K(C_{K+1}\sigma_1) || l_1' \frac{1}{2} j' \rangle = \\
&= \frac{\kappa + \kappa' - K}{[K(2K-1)]^{1/2}} (-1)^{j'-K-1/2} \\
&\times (2j'+1)^{1/2} \begin{pmatrix} j & j' & K \\ \frac{1}{2} & -\frac{1}{2} & 0 \end{pmatrix}
\end{aligned} \tag{C.20}$$

The results in Eq. (C.11), (C.16) and (C.20) can be summarized as

$$\begin{aligned}
&\langle l_1 \frac{1}{2} j || T_K(C_k\sigma_1) || l_1' \frac{1}{2} j' \rangle = \\
&= a_K (-1)^{j'-K-1/2} (2j'+1)^{1/2} \begin{pmatrix} j & j' & K \\ \frac{1}{2} & -\frac{1}{2} & 0 \end{pmatrix} ,
\end{aligned} \tag{C.21}$$

with the factors

$$\begin{aligned} a_k &= (\kappa - \kappa')/\sqrt{k(k+1)}\,, \\ a_{k-1} &= -(k + \kappa + \kappa')/\sqrt{2k(k+1)}\,, \\ a_{k+1} &= (k + 1 - \kappa - \kappa')/\sqrt{(k+1)(2k+1)}\,. \end{aligned} \tag{C.22}$$

–APPENDIX D–

ALLOWED COUPLINGS OF SUBSHELL ANGULAR MOMENTA IN RELATIVISTIC ATOMIC STATES

	q	v	J
$j=\frac{1}{2}$	0,2	0	0
	1	1	$\frac{1}{2}$
$j=\frac{3}{2}$	0,4	0	0
	1,3	1	$\frac{3}{2}$
	2	0	0
		2	2
$j=\frac{5}{2}$	0,6	0	0
	1,5	1	$\frac{5}{2}$
	2,4	0	0
		2	2,4
	3	1	$\frac{5}{2}$
		3	$\frac{3}{2},\frac{9}{2}$
$j=\frac{7}{2}$	0,8	0	0
	1,7	1	$\frac{7}{2}$
	2,6	0	0
		2	2,4,6
	3,5	1	$\frac{7}{2}$
		3	$\frac{3}{2},\frac{5}{2},\frac{9}{2},\frac{11}{2},\frac{15}{2}$
	4	0	0
		2	2,4,6
		4	2,4,5,8
$j=\frac{9}{2}$	0,10	0	0
	1,9	1	$\frac{9}{2}$
	2,8	0	0
		2	2,4,6,8
	3,7	1	$\frac{9}{2}$
		3	$\frac{3}{2},\frac{5}{2},\frac{7}{2},\frac{9}{2},\frac{11}{2},\frac{13}{2},\frac{15}{2},\frac{17}{2},\frac{21}{2}$
	4,6	0	0
		2	2,4,6,8

	q	v	J
$j=\frac{9}{2}$		4	0,2,3,4^2,5,6^2,7,8,9,10,12
	5	1	$\frac{9}{2}$
		3	$\frac{3}{2},\frac{5}{2},\frac{7}{2},\frac{9}{2},\frac{11}{2},\frac{13}{2},\frac{15}{2},\frac{17}{2},\frac{21}{2}$
		5	$\frac{1}{2},\frac{5}{2},\frac{7}{2},\frac{9}{2},\frac{11}{2},\frac{13}{2},\frac{15}{2},\frac{17}{2},\frac{19}{2},\frac{25}{2}$

Table D.1: Allowed coupling of states j^q for $j=\frac{1}{2}-\frac{9}{2}$.The seniority of the coupling and the subshell angular momentum are denoted, respectively, by v and J. The superscript 2 that follows $J=4,6$ for $j^q=\left(\frac{9}{2}\right)^{4,6}$, $v=4$ indicates a two-fold degeneracy with respect to this classification scheme.

Bibliography

[ABB+06] V. Ayvazyan, N. Baboi, J. Bahr, V. Balandin, B. Beutner, A. Brandt, I. Bohnet, A. Bolzmann, R. Brinkmann, O. I. Brovko, J. P. Carneiro, S. Casalbuoni, M. Castellano, P. Castro, L. Catani, E. Chiadroni, S. Choroba, A. Cianchi, H. Delsim-Hashemi, G. Di Pirro, M. Dohlus, S. Dusterer, H. T. Edwards, B. Faatz, A. A. Fateev, J. Feldhaus, K. Flottmann, J. Frisch, L. Frohlich, T. Garvey, U. Gensch, N. Golubeva, H. J. Grabosch, B. Grigoryan, O. Grimm, U. Hahn, J. H. Han, M .V. Hartrott, K. Honkavaara, M. Huning, R. Ischebeck, E. Jaeschke, M. Jablonka, R. Kammering, V. Katalev, B. Keitel, S. Khodyachykh, Y. Kim, V. Kocharyan, M. Korfer, M. Kollewe, D. Kostin, D. Kramer, M. Krassilnikov, G. Kube, L. Lilje, T. Limberg, D. Lipka, F. Lohl, M. Luong, C. Magne, J. Menzel, P. Michelato, V. Miltchev, M. Minty, W. D. Moller, L. Monaco, W. Muller, M. Nagl, O. Napoly, P. Nicolosi, D. Nolle, T. Nunez, A. Oppelt, C. Pagani, R. Paparella, B. Petersen, B. Petrosyan, J. Pfluger, P. Piot, E. Plonjes, L. Poletto, D. Proch, D. Pugachov, K. Rehlich, D. Richter, S. Riemann, M. Ross, J. Rossbach, M. Sachwitz, E. L. Saldin, W. Sandner, H. Schlarb, B. Schmidt, M. Schmitz, P. Schmuser, J. R. Schneider, E. A. Schneidmiller, H. J. Schreiber, S. Schreiber, A. V. Shabunov, D. Sertore, S. Setzer, S. Simrock, E. Sombrowski, L. Staykov, B. Steffen, F. Stephan, F. Stulle, KP. Sytchev, H. Thom, K. Tiedtke, M. Tischer, R. Treusch, D. Trines, I. Tsakov, A. Vardanyan, R. Wanzenberg, T. Weiland, H. Weise, M. Wendt, I. Will, A. Winter, K. Wittenburg, M. V. Yurkov, I. Zagorodnov, P. Zambolin, and K Zapfe. First operation of a free-electron laser generating GW power radiation at 32 nm wavelength. *Eur. Phys. J. D*, 37:297, 2006.

[AS72] M. Abramowitz and I. A. Stegun. *Handbook of mathematical functions*. National Bureau of Standards, 1972.

[Bab62] F. A. Babushkin. A relativistic treatment of radiation transitions. *Opt. Spectr.*, 13:77, 1962.

[BCTT05] P. Beiersdorfer, H. Chen, D. B. Thorn, and E. Träbert. Measurement of the two-loop lamb shift in Lithiumlike U^{89+}. *Phys. Rev. Lett.*, 95:233003, 2005.

[Bei] C. Beilmann. Measurement of higher-order resonant recombination processes. in preparation.

[BHB+93] M. Bitter, H. Hsuan, C. Bush, S. Cohen, C. J. Cummings, B. Grek, K. W. Hill, J. Schivell, M. Zarnstorff, P. Beiersdorfer, A. Osterheld, A. Smith, and B. Fraenkel. Spectra of Heliumlike Krypton from Tokamak fusion test reactor plasmas. *Phys. Rev. Lett.*, 71:1007, 1993.

[BJ89] B. M. Brandsen and C. J. Joachain. *Introduction to Quantum Mechanics*. Longman, 1989.

[BK06] D. Bauer and P. Koval. Qprop: A Schrödinger-solver for intense laseratom interaction. *Comput. Phys. Comm.*, 174:396, 2006.

[BKH+08] C. Brandau, C. Kozhuharov, Z. Harman, A. Müller, S. Schippers, Y. S. Kozhedub, D. Bernhardt, S. Böhm, J. Jacobi, E. W. Schmidt, P. H. Mokler, F. Bosch, H.-J. Kluge, Th. Stöhlker, K. Beckert, P. Beller, F. Nolden, M. Steck, A. Gumberidze, R. Reuschl, U. Spillmann, F. J. Currell, I. I. Tupitsyn, V. M. Shabaev, U. D. Jentschura, C. H. Keitel, A. Wolf, and Z. Stachura. Isotope shifts in the dielectronic recombination of three-electron $^{A}Nd^{57+}$. *Phys. Rev. Lett.*, 100:073201, 2008.

[BKM+03] C. Brandau, C. Kozhuharov, A. Müller, W. Shi, S. Schippers, T. Bartsch, S. Böhm, C. Böhme, A. Hoffknecht, H. Knopp, N. Grün, W. Scheid, T. Steih, F. Bosch, B. Franzke, P. H. Mokler, F. Nolden, M. Steck, T. Stöhlker, and Z. Stachura. Precise determination of the $2s_{1/2} - 2p_{1/2}$ splitting in very heavy Lithiumlike ions utilizing dielectronic recombination. *Phys. Rev. Lett.*, 91:073202, 2003.

[BPA+09] C. Beilmann, O. Postavaru, L. H. Arntzen, R. Ginzel, C. H. Keitel, V. Mäckel, P. H. Mokler, M. C. Simon, H. Tawara, I. I. Tupitsyn, J. Ullrich, J. R. Crespo López-Urrutia, and Z. Harman. Intershell trielectronic recombination with K-shell excitation in Kr^{30+}. *Phys. Rev. A*, 80:050702(R), 2009.

[BS88] A. O. Barut and Y. I. Salamin. Relativistic theory of spontaneous emission. *Phys. Rev. A*, 37:2284, 1988.

[BS02] D. M. Brink and G. R. Satchler. *Angular Momentum*. Oxford Science Publications, 2002.

[Bur64] A. Burgess. A general formula for the estimation of dielectronic recombination coefficients in low-density plasmas. *Astr. Jour.*, 139:886, 1964.

[CCH+90] J. Cummings, S.A. Cohen, R. Hulse, D.E. Post, M.H. Redi, and J. Perkins. Power radiated from ITER by impurities. *Jour. Nucl. Mater.*, 176 & 177:916, 1990.

[CDMU99] J. R. Crespo López-Urrutia, A. Dorn, R. Moshammer, and J. Ullrich. The Freiburg electron beam ion trap/source project FreEBIT. *Phys. Scr.*, T80:502, 1999.

[cHSG04] R. Şchiopu, Z. Harman, W. Scheid, and N. Grün. Isotope shifts of dielectronic resonances for heavy few-electron ions. *Eur. Phys. J. D.*, 31:21, 2004.

[CJ76] K.-T. Cheng and W. R. Johnson. Self-energy corrections to the K-electron binding in heavy and superheavy atoms. *Phys. Rev. A*, 14:1943, 1976.

[Coo06] N. D. Cook. *Models of the Atomic Nucleus*. Springer, Berlin, Heidelberg, New York, 2006.

[Cos07] J. T. Costello. Photoionization experiments with the ultrafast EUV laser 'FLASH' free electron laser in Hamburg. *J. Phys.: Conf. Ser.*, 88:012057, 2007.

[CWP+90] S. A. Cohen, K.A. Werley, D.E. Posta, B.J. Braams, J.L. Perkins, and D. Pearlstein. Two-dimensional fluid simulations of the ITER SOL plasma. *Jour. Nucl. Mater.*, 176 & 177:909, 1990.

[DGJ+89] K. G. Dyall, I. P. Grant, C. T. Johnson, F. A. Parpia, and E. P. Plummer. Grasp: A general-purpose relativistic atomic structure program. *Comput. Phys. Commun.*, 55:425, 1989.

[Dir28] P.A.M. Dirac. The quantum theory of the electron. *P. Roy. Soc. Lond. A Mat.*, 117:610, 1928.

[DJ71] A. M. Desiderio and W. R. Johnson. Lamb shift and binding energies of K electrons in heavy atoms. *Phys. Rev. A*, 3:1267, 1971.

[EBC96] S.R. Elliott, P. Beiersdorfer, and M.H. Chen. Trapped-ion technique for measuring the nuclear charge radii of highly charged radioactive isotopes. *Phys. Rev. Lett.*, 76:1031, 1996.

[ECB+07] S. W. Epp, J. R. Crespo López-Urrutia, G. Brenner, V. Mäckel, P. H. Mokler, R. Treusch, M. Kuhlmann, M. V. Yurkov, J. Feldhaus, J. R. Schneider, M. Wellhöfer, M. Martins, W. Wurth, and J. Ullrich. Soft X-Ray laser spectroscopy on trapped highly charged iones at FLASH. *Phys. Rev. Lett.*, 98:183001, 2007.

[EM95] J. Eichler and W.E. Meyerhof. *Relativistic Atomic Collisions*. Academic Press San Diego, 1995.

[FBH+95] G. Fricke, C. Bernhardt, K. Heilig, L.A. Schellenberg, E.B. Shera, and C.W. Dejager. Nuclear ground state charge radii from electromagnetic interactions. *At. Data. Nucl. Data. Tables 60*, 2:177, 1995.

[FBR98] T. Fuchs, C. Biedermann, and R. Radtke. Channel-specific dielectronic recombination of highly charged Krypton. *Phys. Rev. A*, 58:4518, 1998.

[FR76] L. W. Fullerton and G. A. Rinker. Accurate and efficient methods for the evaluation of vacuum-polarization potentials of order $Z\alpha$ and $Z\alpha^2$. *Phys. Rev. A*, 13:1283, 1976.

[GCB+05] A. J. González Martínez, J. R. Crespo López-Urrutia, J. Braun, G. Brenner, H. Bruhns, A. Lapierre, V. Mironov, R. Soria Orts, H. Tawara, M. Trinczek, and J. Ullrich. State-selective quantum interference observed in the recombination of highly charged $Hg^{75+-78+}$ Mercury ions in an electron beam ion trap. *Phys. Rev. Lett.*, 94:203201, 2005.

[GCB+06] A. J. González Martínez, J. R. Crespo López-Urrutia, J. Braun, G. Brenner, H. Bruhns, A. Lapierre, V. Mironov, R. Soria Orts, H. Tawara, M. Trinczek, J. Ullrich, A. N. Artemyev, Z. Harman, U. D. Jentschura, C. H. Keitel, J. H. Scofield, and I. I. Tupitsyn. Benchmarking high-field few-electron correlation and QED contributions in Hg^{75+} to Hg^{78+} ions. i. experiment. *Phys. Rev. A*, 73:052710, 2006.

[GGS98] M. Gail, N. Grün, and W. Scheid. Angular distribution of radiation emitted after resonant transfer and excitation. *J. Phys. B: At. Mol. Opt. Phys.*, 31:4645, 1998.

[GM80] I. P. Grant and B. J. McKenzie. The transverse electron-electron interaction in atomic structure calculations. *J. Phys. B*, 13:1671, 1980.

[GMN+80] I. P. Grant, B.J. McKenzie, P. H. Norrington, D. F. Mayer, and N. C. Pyper. An atomic multiconfigurational Dirac-Fock package. *Comput. Phys. Commun.*, 21:233, 1980.

[GMP76] I. P. Grant, D. F. Mayers, and N. C. Pyper. Studies in multiconfiguration Dirac-Fock theory. I. the low-lying spectrum of Hf III. *J. Phys. B: At. Mol. Phys.*, 9:2777, 1976.

[GNA+08] W. Geithner, T. Neff, G. Audi, K. Blaum, P. Delahaye, H. Feldmeier, S. George, C. Guénaut, F. Herfurth, A. Herlert, S. Kappertz, M. Keim, A. Kellerbauer, H.-J. Kluge, M. Kowalaska, P. Livens, D. Lunney, K. Marinova, R. Neugart, L. Schweikhard, S. Wibert, and C. Yazidjian. Masses and charge radii of $^{17-22}$Ne and the two-proton-halo candidate ^{17}Ne. *Phys. Rev. Lett.*, 101:252502, 2008.

[GP76] I. P. Grant and N. C. Pyper. Breit interaction in multi-configuration relativistic atomic calculations. *J. Phys. B*, 9:761, 1976.

[GQ87] I. P. Grant and H. M. Quiney. Foundations of the relativistic theory of atomic and molecular structure. *Adv. At. Mol. Phys.*, 23:37, 1987.

[Gra70] I. P. Grant. Relativistic calculation of atomic structures. *Adv. Phys.*, 19:747, 1970.

[Gra74] I. P. Grant. Gauge invariance and relativistic radiative transitions. *J. Phys. B*, 7:1458, 1974.

[Gra76] I. P. Grant. A program to calculate angular momentum coefficients in relativistic atomic structure - revised version. *Comput. Phys. Commun.*, 11:397, 1976.

[Gra06] I. P. Grant. *Relativistic Quantum Theory of Atoms and Molecules*. Springer, Berlin, Germany, 2006.

[GSB+05] A. Gumberidze, Th. Stöhlker, D. Banaś, K. Beckert, P. Beller, H. F. Beyer, F. Bosch, S. Hagmann, C. Kozhuharov, D. Liesen, F. Nolden, X. Ma, P. H. Mokler, M. Steck, D. Sierpowski, and S. Tashenov. Quantum electrodynamics in strong electric fields: The ground-state Lamb shift in Hydrogenlike Uranium. *Phys. Rev. Lett.*, 94:223001, 2005.

[Hah85] Y. Hahn. Theory of dielectronic recombination. *Adv. At. Mol. Phys.*, 21:123, 1985.

[HJK+06] M. Haas, U. D. Jentschura, C. H. Keitel, N. Kolachevsky, M. Herrmann, P. Fendel, M. Fischer, Th. Udem, R. Holzwarth, T. W. Hänsch, M. O. Scully, and G. S. Agarwal. Two-photon excitation dynamics in bound two-body Coulomb systems including ac Stark shift and ionization. *Phys. Rev. A*, 73:052501, 2006.

[HK09] H. G. Hetzheim and C. H. Keitel. Ionization dynamics versus laser intensity in laser-driven multiply charged ions. *Phys. Rev. Lett.*, 102:083003, 2009.

[HTA+06] Z. Harman, I. I. Tupitsyn, A. N. Artemyev, U. D. Jentschura, C. H. Keitel, J. R. Crespo López-Urrutia, A. J. González Martínez, H. Tawara, and J. Ullrich. Benchmarking high-field few-electron correlation and QED contributions in Hg$^{75+\ldots78+}$ ions. II. theory. *Phys. Rev. A*, 73:052711, 2006.

[Joh] W. R. Johnson. Atomic physics. lecture notes, see `http://www.nd.edu/~johnson/Publications/book.pdf`.

[JS85] W. R. Johnson and G. Soff. The Lamb shift in Hydrogen-like atoms. *At. Data Nucl. Data Tables*, 33:405, 1985.

[KBC+95] A. D. Knapp, P. Beiersdorfer, M. H. Chen, J. H. Scofield, and D. Schneider. Observation of interference between dielectronic recombination and radiative recombination in highly charged Uranium Ions. *Phys. Rev. Lett.*, 74:54, 1995.

[Kei99] C. H. Keitel. Narrowing spontaneous emission without intensity reduction. *Phys. Rev. Lett.*, 83:1307, 1999.

[KHK06] M. Klaiber, K. Z. Hatsagortsyan, and C. H. Keitel. Gauge-invariant relativistic strong-field approximation. *Phys. Rev. A*, 73:053411, 2006.

[KNS95] C. H. Keitel, L. M. Narducci, and M. O. Scully. Origin of the sub-natural line-narrowing effect in resonance fluorescence. *Phys. Rev. B*, 60:153, 1995.

[Koo33] T. Koopmans. Ordering of wave functions and eigenenergies to the individual electrons of an atom. *Physica*, 1:104, 1933.

[LCL] Stanford LCLS Specifications, https://slacportal.slac.stanford.edu/sites/lcls_public/Instruments/SXR/Pages/Specifications.aspx.

[LJC+05] A. Lapierre, U. D. Jentschura, J. R. Crespo López–Urrutia, J. Braun, G. Brenner, H. Bruhns, D. Fischer, A. J. González Martínez, Z. Harman, W. R. Johnson, C. H. Keitel, V. Mironov, C. J. Osborne, G. Sikler, R. Soria Orts, V. Shabaev, H. Tawara, I. I. Tupitsyn, J. Ullrich, and A. Volotka. Relativistic electron correlation, quantum electrodynamics, and the lifetime of the $1s^2 2s^2 2p\ ^2P^o_{3/2}$ level in Boronlike Argon. *Phys. Rev. Lett.*, 95:183001, 2005.

[LL91] L. D. Landau and E. M. Lifshitz. *Quantum Mechanics, non-relativistic theory*. Pergamon Press, 1991.

[LLO+08] M. Lestinsky, E Lindroth, D.A. Orlov, E.W. Schmidt, S. Schippers, S. Böhm S, C. Brandau, F. Sprenger, A.S. Terekhov, A. Müller, and A. Wolf. Screened radiative corrections from hyperfine-split dielectronic resonances in Lithiumlike Scandium. *Phys. Rev. Lett.*, 100(3):033001, 2008.

[MB42] H. S. W. Massey and R. R. Bates. The properties of neutral and ionized atomic Oxygen and their influence on the upper atmosphere. *Rep. Prog. Phys.*, 9:62, 1942.

[MDK08] C. Müller, C. Deneke, and C. H. Keitel. Muon-pair creation by two X-Ray laser photons in the field of an atomic nucleus. *Phys. Rev. Lett.*, 101:060402, 2008.

[MDLMNO91] A. S. Manka, H. M. Doss, P. Ru L. M. Narducci, and G.-L. Oppo. Spontaneous emission and absorption properties of a driven three-level system. ii. the and cascade models. *Phys. Rev. A*, 43:3748, 1991.

[MJ71] J. B. Mann and W. R. Johnson. Breit interaction in multielectron atoms. *Phys. Rev. A*, 4:41, 1971.

[Moh92] P. J. Mohr. Self-energy correction to one-electron energy levels in a strong Coulomb field. *Phys. Rev. A*, 46:4421–4424, 1992.

[Mül09] C. Müller. Nonlinear Bethe-Heitler pair creation with attosecond laser pulses at the LHC. *Phys. Lett. B*, 672:56, 2009.

[N+08] N. Nakamura et al. Evidence for strong Breit interaction in dielectronic recombination of highly charged heavy ions. *Phys. Rev. Lett.*, 100(7):073203, 2008.

[NSO+90] L. M. Narducci, M. O. Scully, G.-L. Oppo, P. Ru, and J. R. Tredicce. Spontaneous emission and absorption properties of a driven three-level system. *Phys. Rev. A*, 42:1630, 1990.

[Pal87] C. W. P. Palmer. Reformulation of the theory of the mass shift. *J. Phys. B*, 20:5987, 1987.

[PGB78] N. C. Pyper, I. P. Grant, and N. Beatham. A new program for calculating matrix elements of one-particle operators in jj-coupling. *Comput. Phys. Commun.*, 15:387, 1978.

[PK98] E. Paspalakis and P. L. Knight. Phase control of spontaneous emission. *Phys. Rev. Lett.*, 81:293, 1998.

[RBF+00] R. Radtke, C. Biedermann, T. Fuchs, G Fussmann, and P. Beiersdorfer. Measurement of the radiative cooling rates for high-ionization species of Krypton using an electron beam ion trap. *Phys. Rev. E*, 61:1966, 2000.

[Ros67] M. E. Rose. *Elementary Theory of Angular Momentum*. John Wiley & Sons, 1967.

[SA95] V. M. Shabaev and A. N. Artemyev. Relativistic nuclear recoil corrections to the energy levels of multicharged ions. *J. Phys. B*, 27:1307, 1995.

[Sak94] J. J. Sakurai. *Modern Quantum Mechanics*. Addison-Wesley Publishing Company, Inc., 1994.

[SBF+07] A. A. Sorokin, S. V. Bobashev, T. Feigl, K. Tiedtke, H. Wabnitz, and M. Richter. Photoelectric effect at ultrahigh intensities. *Phys. Rev. Lett.*, 99:213002, 2007.

[SGB+03] M. Schnell, G. Gwinner, N. R. Badnell, M. E. Bannister, S. Böhm, J. Colgan, S. Kieslich, S. D. Loch, D. Mitnik, A. M̈ller, M. S. Pindzola, S. Schippers, D. Schwalm, W. Shi, A.Wolf, and S.-G. Zhou. Observation of trielectronic recombination in Be-like Cl Ions. *Phys. Rev. Lett.*, 91:043001, 2003.

[Sha98] V. M. Shabaev. QED theory of nuclear recoil effects in atoms. *Phys. Rev. A*, 57:59, 1998.

[Sha02] V. M. Shabaev. Two-time Green function method in the quantum electrodynamics of high-Z few-electron atoms. *Phys. Rep.*, 356:119, 2002.

[SHC+06] R. Soria Orts, Z. Harman, J. R. Crespo López-Urrutia, A. N. Artemyev, H. Bruhns, A. J. González Martínez, U. D. Jentschura, C. H. Keitel, A. Lapierre, V. Mironov, V. M. Shabaev, H. Tawara, I. I. Tupitsyn, J. Ullrich, and A. V. Volotka. Exploring relativistic many-body recoil effects in highly charged ions. *Phys. Rev. Lett.*, 97:103002, 2006.

[SNE+06] R. Sánchez, W. Nörtershäuser, G. Ewald, D. Albers, J. Behr, P. Bricault, B. A. Bushaw, A. Dax, J. Dilling, M. Dombsky, G. W. F. Drake, S. Götte, R. Kirchner, H.-J. Kluge, Th. Kühl, J. Lassen, C. D. P. Levy, M. R. Pearson, E. J. Prime, V. Ryjkov, A. Wojtaszek, Z.-C. Yan, and C. Zimmerrmann. Nuclear charge radii of ^{9,11}Li: The influence of halo neutrons. *Phys. Rev. Lett.*, 96:033002, 2006.

[SST+98] V. M. Shabaev, M. B. Shabaeva, I. I. Tupitsyn, V. A. Yerokhin, A. N. Artemyev, T. Kühl, M. Tomaselli, and O. M. Zherebtsov. Transition energy and lifetime for the ground-state hyperfine splitting of high-Z Lithiumlike ions. *Phys. Rev. A*, 57:149, 1998.

[SZ98] M. O. Scully and S.-Y. Zhu. Quantum control of the inevitable. *Science*, 281:1973, 1998.

[Ueh35] E. A. Uehling. Polarization effects in the positron theory. *Phys. Rev.*, 48:55, 1935.

[WBD+95] K. Widmann, P. Beiersdorfer, V. Decaux, S.R. Elliott, D. Knapp, A. Osterheld, M. Bitter, and A. Smith. Studies of He-like Krypton for use in determining electron and ion temperatures in very-high-temperature plasmas. *Rev. Sci. Instrum.*, 66:761, 1995.

[XFE] European XFEL Project, http://xfel.desy.de/technical_information/photon_beam_parameter/.

[ZCU03] Y. Zou, J. R. Crespo López-Urrutia, and J. Ullrich. Observation of dielectronic recombination through two-electron one-photon correlative stabilization in an electron-beam ion trap. *Phys. Rev. A*, 67:042703, 2003.

[Zim92] P. Zimmerer. *Relativistische Theorie für die dielektronische Rekombination bei sehr schweren hochgeladenen Ionen*. PhD thesis, Justus-Liebig-Universität Giessen, 1992.

[Zim96] M. Zimmermann. *Photo-Rekombination bei sehr schweren hochgeladenen Ionen*. PhD thesis, Justus-Liebig-Universität Giessen, 1996.

[ZS96a] P. Zhou and S. Swain. Ultranarrow spectral lines via quantum interference. *Phys. Rev. Lett.*, 77:3995, 1996.

[ZS96b] S.-Y. Zhu and M. O. Scully. Spectral line elimination and spontaneous emission cancellation via quantum interference. *Phys. Rev. Lett.*, 76:388, 1996.

[ZST+84] J.D. Zumbro, E.B. Shera, Y. Tanaka, C.E. Bemis, Jr., R.A. Naumann, M.V. Hoehn, W. Reuter, and R.M. Steffen. E2 and E4 deformation in ^{233,234,235,238}U. *Phys. Rev. Lett.*, 53:1888, 1984.

ACKNOWLEDGMENTS

Firstly, I must thank my two supervisors Prof. Dr. Christoph H. Keitel and Dr. Zoltán Harman who have kept me on the right track throughout my research.

I express my gratitude to my parents, Dan and Raica, and my brother Silviu, who have been a constant support to me through my whole life.

To my friends Benjamin Galow, Dr. Mihai Macovei and Dr. Bennaceur Najjari, thank you for teaching me something new each day. I hope we will work on interesting things together in the future.

I thank my previous advisors, Prof. Dr. Sorin Ciulli and Prof. Dr. Adrian Costescu, whose help and advice was invaluable for my scientifical career.

I extend my aknowledgments to my colleagues from the EBIT group of MPIK: Christian Beilmann, PD Dr. José R. Crespo López-Urrutia, Dr. Volkhard Mäckel, Prof. Dr. Paul Mokler and Prof. Dr. Hiroyuki Tawara for such a nice collaboration.

At not last, I would like to say thanks to Sven Bernitt, PD Dr. Jörg Evers, Mircea Girju, Markus Kohler, Dr. Adriana Pálffy, Dr. Sergey Popruzhenko, Prof. Dr. Yousef Salamin, Dr. Andrey Surzhykov, Qurrat-ul-Ain and Dr. Jacek Zatorski for helpful conversations.